

OPTIMUM RECEIVER DESIGN AND PERFORMANCE ANALYSIS
FOR WIRELESS COMMUNICATION

A Dissertation
presented to
the Faculty of the Graduate School
University of Missouri-Columbia

In Partial Fulfillment
of the Requirements for the Degree

Doctor of Philosophy

by
JINGXIAN WU

Dr. Chengshan Xiao, Dissertation Supervisor

JULY 2005

The undersigned, appointed by the Dean of the Graduate School, have examined the dissertation entitled

OPTIMUM RECEIVER DESIGN AND PERFORMANCE ANALYSIS
FOR WIRELESS COMMUNICATION

presented by Jingxian Wu

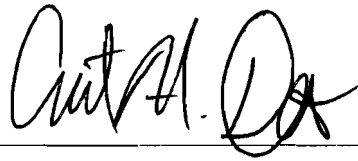
a candidate for the degree of Doctor of Philosophy

and hereby certify that in their opinion it is worth acceptance.

Dr. Chengshan Xiao



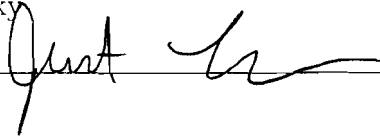
Dr. Curt H. Davis



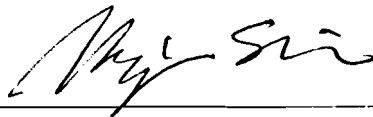
Dr. Dominic K.C. Ho



Dr. Justin J. Legarsky



Dr. Hongchi Shi



In memory of my mother, Furong Yao,
and to my father, Weizhong Wu, and my wife, Yu Ning.

Acknowledgments

During the course of this dissertation work, I received enormous supports from many people to whom I would like to express my thanks.

First, I would like to thank my dissertation adviser, Dr. Chengshan Xiao, for introducing me to the wonderful world of wireless communication, for guiding me through the challenging yet rewarding path leading to the fulfillment of this dissertation, for cultivating my independent research abilities, and for providing me with full supports in both my research and my life. His broad expertise and superb intuition have been my constant source of inspirations during the pursuit of my Ph.D. degree. His meticulous attitude towards research, his strict requirements on the perfection of the research results, and his detailed comments to my research work have greatly influenced my research style and my technical writing. I'm greatly indebted to him for his incomparable help during the past four years.

I'm also grateful to my other dissertation committee members, Dr. Curt Davis, Dr. Dominic Ho, Dr. Justin Legarsky, and Dr. Hongchi Shi, for taking time from their busy schedules serving in my dissertation committee, for providing me with insightful suggestions and criticisms to help improve the quality of the dissertation.

I would like to express my gratitude to Dr. Jin Zhang of Mitsubishi Electric Research Lab (MERL) for providing me the opportunity to work as an Internship Engineer at her research group at MERL, twice. During that period of time, I had the opportunity to get familiar with the industry research environment, and get in touch with many exciting research topics.

I'm grateful to Dr. Neelesh B. Mehta of MERL for closely working with me during my internship at MERL. He provided me with numerous valuable suggestions which significantly benefit the system-level research results presented in this dissertation. His detailed comments and criticisms of my work on the system level simulator project helped me greatly improve my programming skills. I would like to thank Dr. Henry Horng of Samsung Electronic Inc., who granted me his supports and his trust during my first internship term at MERL.

I would express my thanks to Dr. Norman Beaulieu and Dr. Khaled Letaief for spending their valuable time working with me on several of my research projects, for their insightful suggestions which help me improve the quality of my papers.

I'm thankful to my current and previous group-mates: Dr. Yahong R. Zheng, Dr. Sang-Yick Leong, Dr. Liang Hong, Dr. Jianfei Cai, Dr. Lei Cao, Mr. Min Wu, Mr. Yunhong Li, Ms. Xiaoning Lu, for their help and their priceless friendship. I would also like to thank all my other friends at Columbia, Missouri, too many to be listed here, who had made my life at University of Missouri- Columbia such an enjoyable experience.

Last, but certainly not the least, I offer my heartfelt thanks to the support and the sacrifice of my family. My parents instilled me with the importance of honesty and knowledge when I was a small kid, and helped me growing up an accountable person. My wife, Yu Ning, has always been standing by my side, providing me with everything she can render to assist my work. I would like to designate this dissertation to them to express my utmost gratitude. Without their help, it's impossible for me to reach this stage.

Contents

ACKNOWLEDGMENTS	ii
LIST OF TABLES	viii
LIST OF FIGURES	ix
LIST OF ABBREVIATIONS	xv
ABSTRACT	xvii
1 Introduction	1
1.1 Background and Motivation	1
1.2 Objectives	4
1.3 Dissertation Outline	5
2 A Discrete-time model for spatio-temporally correlated MIMO WS- SUS multipath channels	8
2.1 Introduction	8
2.2 MIMO Channel Description and Assumptions	10
2.2.1 MIMO Channel Description	10
2.2.2 MIMO Channel Assumptions	12
2.3 The Discrete-time MIMO Channel Model	14
2.3.1 The Discrete-Time Channel Model	14
2.3.2 Statistical Properties of the Discrete-Time Channel	16
2.3.3 Generation of the Discrete-Time MIMO Channel Fading	19
2.3.4 Computational Complexity	21

2.4	Simulation Experiments	23
2.4.1	Spatial-Temporal Statistics	23
2.4.2	Bit Error Rate Comparison	25
2.4.3	MIMO Channel Capacity	28
2.5	Conclusions	31
3	Multuser Channel Estimation for CDMA Systems over Doubly Selective Fading Channels	34
3.1	Introduction	34
3.2	Discrete-time System Model	37
3.3	Multuser Channel Estimation	42
3.4	MMSE-parameter Estimation	45
3.4.1	Estimation of the Additive Noise Variance N_0	45
3.4.2	Joint Estimation of \mathbf{R}_h and \mathbf{I}_m	49
3.5	Simulation Results	51
3.5.1	System Configurations	52
3.5.2	Performance Evaluation	53
3.6	Conclusions	60
4	Optimal Diversity Combining based on Noisy Channel Estimation	63
4.1	Introduction	63
4.2	System and Channel Models	65
4.3	Optimal Diversity Receiver with Noisy Channel Estimation	67
4.4	Error Performance Analyses	69
4.4.1	Conditional Error Probability	70
4.4.2	Error Probability in Rayleigh Fading Channels	72
4.4.3	Error Probability in Ricean Fading Channels	74
4.5	Numerical Examples	76
4.6	Conclusion	80

5	On the Performance of Wireless Systems with Doubly Selective Rayleigh Fading	82
	5.1 Introduction	82
	5.2 Discrete-time System Model	84
	5.3 Equivalent System Representation	87
	5.4 Error Performance Analysis	90
	5.4.1 Optimum Combining	90
	5.4.2 Conditional Error Probabilities	93
	5.4.3 Symbol Error Rate	96
	5.5 Numerical Examples	100
	5.6 Conclusions	107
6	Receiver Timing Phase Sensitivity of Systems with Frequency Selective Rayleigh Fading Channels	109
	6.1 Introduction	109
	6.2 System Model	112
	6.3 Error Performance of System with Timing Phase Offset	115
	6.3.1 Statistical Properties of SNR	115
	6.3.2 Error Performance Bound	118
	6.4 Case Studies	120
	6.4.1 Case 1: T_{sym} -spaced Receiver ($\mu = 1$), Arbitrary PDP $\varphi(t)$.	121
	6.4.2 Case 2: T_{sym} -spaced Receiver ($\mu = 1$), PDP $\varphi(t) = \sum_{l=0}^{L-1} \varphi_l \delta(t-lT_s)$	124
	6.4.3 Case 3: $T_{sym}/2$ -spaced Receiver ($\mu = 2$).	127
	6.5 Numerical Examples	130
	6.6 Conclusions	134
7	Flexible Lognormal Sum Approximation based on Gauss-Hermite Expansion of Moment Generating Function	137
	7.1 Introduction	137
	7.2 Comparison of Various Lognormal Sum Approximation Methods	139

7.3	Lognormal Sum Approximation Using Gauss-Hermite Expansion of MGF	142
7.3.1	Motivation	142
7.3.2	MGF-based Lognormal Sum Approximation	142
7.4	Numerical Examples	145
7.5	Conclusions	149
8	Spectral Efficiency Analysis of Multiuser Cellular System with Channel Aware Schedulers	150
8.1	Introduction	150
8.2	System Model	152
8.3	Spectral Efficiency of Round Robin Scheduler	154
8.3.1	Statistical Properties of Post Detection SINR	156
8.3.2	Average Spectral Efficiency for Single User	158
8.4	Spectral Efficiency of Max-SINR Scheduler	161
8.4.1	Statistical Properties of Post Detection SINR	161
8.4.2	Spectral Efficiency Analysis	163
8.5	Spectral Efficiency in Composite Fading Shadowing Environment	165
8.5.1	Statistical Properties of Post Detection SIR	166
8.5.2	Spectral Efficiency Analysis	169
8.6	Numerical Examples	170
8.6.1	Effects of CCI	170
8.6.2	Effects of Schedulers	171
8.6.3	Effects of Limit on Modulation Constellation Size	172
8.6.4	Effects of Cell Sectorization	173
8.6.5	Effects of Shadowing	174
8.7	Conclusions	175
9	Conclusions	178
9.1	Contributions	178
9.2	Future Works	180

Bibliography	182
A Subspace-based Channel Estimation with Pilot Symbols	196
B Proof of Proposition 4.1	198
C Derivation of Eqn. (5.37)	200
VITA	201

List of Tables

2.1	The computational complexity ratio of the proposed Discrete-time model to the conventional continuous-time model	23
2.2	The matrix \mathbf{C}_{ISI} for the exponential delay power profile	24
2.3	The matrix \mathbf{C}_{ISI} for the reduced 6-path Typical Urban profile	27
5.1	Parameters of the Unified Error Probability Expressions for Linearly Modulated Systems	96

List of Figures

1.1	A typical wireless propagation environment	2
2.1	A conventional continuous-time baseband MIMO channel model.	11
2.2	The equivalent discrete-time MIMO channel model.	16
2.3	The antenna placement of the 2×2 MIMO system.	24
2.4	Comparison of the theoretically calculated and empirically simulated auto-correlation of $h_{1,1}(k, 1)$, cross-correlation of $h_{1,1}(k, 0)$ and $h_{1,1}(k, 1)$, and cross-correlation of $h_{1,1}(k, 0)$ and $h_{2,1}(k, 1)$	26
2.5	Comparison of BER performance with discrete-time model and continuous-time model for EDGE mobile system under Typical Urban delay power profile.	27
2.6	The capacities of MIMO channels with different spatial correlation coefficients and $M = N$. Dash dot lines stand for $r = 1$, dash lines for $r = 0.5$, and solid lines for $r = 0$. Observation: The channel capacity is linearly scaling with M when $r \leq 0.5$, and the scaling rate is depending on the value of r	30
2.7	The capacities of MIMO channels with different delay power profiles, M -to- N ratio being constant, and $r = 0.5$. Observation: The channel capacity is linearly scaling with M	31
2.8	The capacities of MIMO channels with N being fixed. Dash dot lines stand for flat fading, solid lines for Vehicular Channel A profile. Observation: The channel capacity is approximately linearly scaling with $\log_2 M$ when $M \geq N$	32

2.9	The capacities of MIMO channels with M being fixed. Dash dot lines stand for flat fading, solid lines for Vehicular Channel A profile. Observation: The channel capacity is linearly scaling with $\log_2 N$ when $N \leq M$.	33
3.1	The l th delayed version of the transmitted symbols.	39
3.2	The slot structure to be utilized for simulations.	52
3.3	Vehicular A propagation profile. The differential delays between multiple paths are non-integer of the chip period T_c .	53
3.4	Comparison of the estimated noise variance and its corresponding actual noise variance at different level of E_b/N_0 .	54
3.5	BER performance comparison of the system which employs our multiuser channel estimation algorithm and the ideally perfect channel estimation.	55
3.6	BER performance comparison of the system which employs our multiuser channel estimation algorithm and the pilot assisted subspace-based channel estimation.	57
3.7	BER comparison for the effect of the estimated tap delay index vector \mathbf{l}_m and ideally known tap delay index vector on system performance. Note: all the curves are based on estimated \mathbf{R}_h using the proposed algorithm.	58
3.8	The normalized MSE performance of the system which uses the proposed algorithm, the LS-based method, and the pilot assisted subspace-based method.	60
3.9	BER performance comparison of the system which employs our multiuser channel estimation algorithm and the ideally perfect channel estimation, where the power delay profile is a continuous-time exponentially decaying function.	61
4.1	The decision region for MPSK modulation.	70
4.2	The a) SCER λ and b) covariance coefficient ρ vs. the Ricean factor K .	77
4.3	The SER of BPSK systems with polynomial interpolation channel estimation.	78

4.4	The SER of 8PSK systems with polynomial interpolation channel estimation.	78
4.5	The effect of SCER on system performance for Rayleigh fading channels.	79
4.6	The effect of SCER on system performance for Ricean fading channels. .	80
4.7	The system performance for different constellation sizes and diversity orders.	81
5.1	The block diagrams of the SISO system and its equivalent SIMO system representation.	88
5.2	the decision region for MASK symbol	95
5.3	Comparison of performance bounds of systems with two ray equal gain channel profile. Decoding length for the equalizers: 1024 symbols.	101
5.4	Performances of systems with Typical Urban profile. ν : oversampling factor. τ_0 : sampling timing offset. Decoding length of the equalizers: 1024 symbols.	102
5.5	The effects of sampler timing offset on system performance for two ray equal gain profile. ν : oversampling factor. τ_0 : sampler timing offset. α : roll-off factor of the root raised cosine filter.	103
5.6	The effects of sampler timing offset on system performance for Typical Urban profile. ν : oversampling factor. τ_0 : sampling timing offset. α : roll-off factor of the root raised cosine filter.	105
5.7	The effects of sampler timing offset on system performance for Exponential Decaying profile. ν : oversampling factor. τ_0 : sampling timing offset. α : roll-off factor of the root raised cosine filter.	106
6.1	The variations of eigenvalues and performance bound with respect to timing phase offset for systems with two path equal gain profile. α : roll-off factor of the RRC filter.	122
6.2	The overlapped power spectrum of the received signal samples for systems with two path equal gain profile. μ : oversampling factor. τ_0 : receiver timing phase offset. α : roll-off factor of the RRC filter.	123

6.3	The SER performance bounds for two path equal gain channels with different values of timing phase offset. μ : oversampling factor. τ_0 : receiver timing phase offset. α : roll-off factor of the RRC filter.	124
6.4	Comparison of the performances of ISI-free systems with fixed receive filter and statistical receive filter. $\mu = 2$: oversampling factor. $\alpha = 0.5$: roll-off factor of the RRC filter.	129
6.5	Comparison of performance bounds with simulation results of systems with Typical Urban channel profile. Decoding length for the MAP equalizers: 1024 symbols. μ : oversampling factor. τ_0 : receiver timing phase offset. α : roll-off factor of the RRC filter.	131
6.6	The variations of non-zero eigenvalues λ_l of the eigensystem (6.17) with respect to the timing phase offset. Exponentially decaying profile with $\tau_{\max} = 3T_{sym}$. α : roll-off factor of the RRC filter.	132
6.7	The effects of receiver timing phase and excessive bandwidth on the error performance of system with Exponentially Decaying profile with $\tau_{\max} = 3T_{sym}$. μ : oversampling factor. α : roll-off factor of the RRC filter.	133
6.8	The effects of timing phase offset and maximum delay spread on the error performance of system with two path equal gain channel profile. τ_{\max} : the relative delay between the two channel paths. μ : oversampling factor. τ_0 : receiver timing phase offset. α : roll-off factor of the RRC filter.	134
6.9	The SER performance of systems with two path equal gain profile with respect to the maximum delay spread of the channel (or the relative delay between the two channel paths). μ : oversampling factor. τ_0 : receiver timing phase offset. α : roll-off factor of the RRC filter.	135
7.1	Weight functions employed by F-W, S-Y, and MGF methods	144
7.2	$\widehat{\Psi}_x(s; \mu, \sigma)$ as a function of s for different Hermite integration orders, N ($\mu = 0$ and $\sigma = 8$ dB)	145
7.3	Cellular layout with up to two rings of downlink co-channel interferers . .	146
7.4	cdf of co-channel interference from first-tier interferers ($K = 6$) for $\sigma = 8$ dB	146

7.5	ccdf of co-channel interference from first-tier interferers ($N = 6$) for $\sigma = 8$ dB	147
7.6	cdf as a function of σ ($K = 6, s_1 = 1, s_2 = 100$)	148
7.7	cdf of co-channel interference from both first and second-tier interferers ($K = 18$) for $\sigma = 12$ dB	149
8.1	The spectral efficiencies of systems with Max-SINR scheduler with different number of cochannel interferers. Number of MS: $N = 10$. Number of sectors per cell: 1.	171
8.2	Spectral efficiencies of systems with Max-SINR scheduler and RR scheduler. SNR at cell corner: $\mu = 10$ dB. Number of sectors per cell: 1.	172
8.3	Spectral efficiencies of systems with different modulation constellation size limits. 7-cell system. SNR at cell corner: $\mu = 15$ dB. Number of MS: $N = 5$. Number of sectors per cell: 1.	174
8.4	The single user spectral efficiency at various positions inside the center cell. 7-cell system. SNR at cell corner: $\mu = 15$ dB. Number of sectors per cell: 6.	175
8.5	The spectral efficiency of the center cell with RR scheduler and various sectorization schemes. The MS are uniformly distributed inside the center cell	176
8.6	The spectral efficiency of the center cell undergoing fading and shadowing.	177

List of Abbreviations

8PSK:	8-ary Phase Shift Keying
AWGN:	Additive White Gaussian Noise
BPSK:	Binary Phase Shift Keying
BS:	Base Station
ccdf:	Complementary Cumulative Distribution Function
CCI:	Cochannel Interference
cdf:	Cumulative Distribution Function
CDMA:	Code Division Multiple Access
CEP:	Conditional Error Probability
CGRV:	Complex Gaussian Random Variable
CHF:	Characteristic Function
CIR:	Channel Impulse Response
CSI:	Channel State Information
DTFT:	Discrete Time Fourier Transform
EDGE:	Enhanced Data Rate for Global Evolution
EGC:	Equal Gain Combining
EVD:	Eigenvalue Decomposition
FT:	Fourier Transform
GPS:	Global Positioning System
GSM:	Global System for Mobile Communication
HT:	Hilly Terrain
IIR:	Infinite Impulse Response
ISI:	Intersymbol Interference

MASK:	M-ary Amplitude Shift Keying
MGF:	Moment Generating Function
MIMO:	Multiple Input Multiple Output
MLSE:	Maximum Likelihood Sequence Estimation
MMSE:	Minimum Mean Square Error
MPSK:	M-ary Phase Shift Keying
MQAM:	M-ary Quadrature Amplitude Modulation
MRC:	Maximal Ratio Combining
MS:	Mobile Station
MSE:	Mean Square Error
MUI:	Multiuser Interference
PSAM:	Pilot Symbol Assisted Modulation
pdf:	Probability Density Function
PDP:	Power Delay Profile
PSD:	Power Spectral Density
QPSK:	Quadrature Phase Shift Keying
RRC:	Root Raised Cosine
SCER:	Signal to Channel Estimation Error Ratio
SER:	Symbol Error Rate
SIMO:	Single Input Multiple Output
SINR:	Signal to Interference plus Noise Ratio
SISO:	Single Input Single Output
SNR:	Signal to Noise Ratio
TDMA:	Time Division Multiple Access
TU:	Typical Urban
UMTS:	Universal Mobile Telecommunication System
WSS:	Wide Sense Stationary
WSSUS:	Wide Sense Stationary Uncorrelated Scattering

Optimum Receiver Design and Performance Analysis for Wireless Communication

Jingxian Wu

Dr. Chengshan Xiao, Dissertation Supervisor

ABSTRACT

This dissertation is devoted to the optimum receiver design and theoretical performance analysis of wireless communication systems operated over fading channels, and this objective is incarnated by means of design, analysis and simulation of a broad range of wireless communication systems under various practical system configurations. First, a statistical discrete-time system model is proposed for wireless communication systems operated in wideband doubly selective (both time-selective and frequency-selective) fading environment, and it provides a generic analysis and simulation framework for the design and evaluation of wireless communication systems. Based on the statistical properties of the discrete-time model, we next develop a multiuser channel estimation algorithm for quasi-synchronous CDMA systems operated over doubly selective Rayleigh fadings to compensate the impairments of multipath fading. Then an optimum diversity receiver is proposed for systems with channel estimation error, and theoretical error probability expressions are derived for such receiver operated in time-selective flat Rayleigh and Ricean fading channels to investigate the effects of noisy channel estimation on system performance. By employing a new single-input multiple-output (SIMO) equivalent system method, we next analyze the theoretical error performance of systems with doubly selective fading channels to identify the relationship between system performance and fundamental system parameters such as Doppler spread, delay spread, and receiver timing phase offset, and closed-form error probability expressions are derived as tight performance low bounds for M-ary phase-shift-keying (MPSK), M-ary amplitude-shift-keying (MASK) and square M-ary quadrature-amplitude-modulation (MQAM) systems operated in doubly selective Rayleigh fadings. Moreover, with the help of frequency-domain analysis, the effects of receiver timing phase offset and receiver oversampling are explicitly expressed in the statistical representation of the post-detection signal to noise

ratio (SNR), which is further quantified in the error probability expressions, and some interesting results about receiver timing phase sensitivity are obtained from the analytical results. Finally, spectral efficiency analysis are carried out for multiuser multi-user cellular mobile radio systems, where the primary performance limiting factor is cochannel interference (CCI) from neighboring cells due to frequency reuse. To facilitate the analysis of the statistical properties of CCI in a wireless environment suffering from both short-scale fading and large-scale shadowing, a flexible lognormal sum approximation is proposed based on the Gauss-Hermite expansion of the moment generating function (MGF). By analyzing the statistical behaviors of the post-detection signal to noise plus interference ratio (SINR), we derive expressions for the system spectral efficiency and outage probability, with which the joint effects of CCI, multipath fading, shadowing, additive noise and cell sectorization on system performance are analyzed.

The theoretical performance expressions presented in this dissertation provide a set of analytical tools for communication system design and evaluation. In addition, all of the analytical results presented in this dissertation are rigorously verified through extensive numerical simulations, and excellent agreements are observed between the simulation results and theoretical expressions.

Chapter 1

Introduction

1.1 Background and Motivation

With the ever-increasing worldwide demand for mobile and personal portable communications, the next generation wireless communication systems are required to be capable of providing high quality reliable voice services as well as broadband data services with communication quality and data rates far beyond the limitations of current wireless systems. This objective, once achieved, will provide incomparable conveniences to our everyday life; at the mean time, the hostile nature of the mobile radio channels poses enormous challenges on the road leading to the fulfillment of this demanding yet intriguing quest.

One of the primary performance-limiting factors inherent in wireless channels is multipath fading, which is resulted from the reflection, diffraction or refraction of the transmitted waveforms through different propagation paths. A typical propagation environment between a base station and a mobile station is illustrated in Fig. 1.1. The superimposed multipath radio waves could add up either constructively or destructively at the receiver owing to their phase differences, and this will result in power fluctuation and phase distortion of the received signals, or, multipath fading.

Doppler spread and delay spread are two fundamental parameters characterize the behaviors of multipath fading. Doppler spread is introduced by the relative motion between

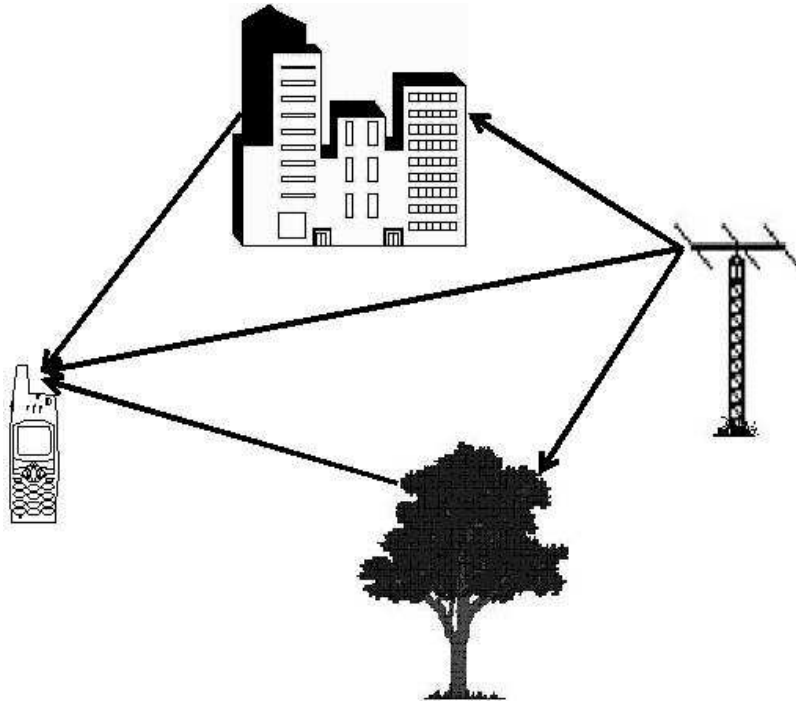


Figure 1.1: A typical wireless propagation environment

the base station and mobile stations, signals; while delay spread is a result of the relative propagation delays among the multipath radio waves. Doppler spread and delay spread can be equivalently represented by channel coherence time and channel coherence bandwidth, respectively. Coherence time (bandwidth) is defined as the time (frequency) range over which the statistical fadings are correlated. If the channel coherence time is less than the system symbol period, the channel is classified as time-selective; likewise, a smaller coherence bandwidth compared to the signal bandwidth will lead to frequency-selective fading in that different frequency components of the transmitted signals are subject to different attenuation and phase shifts. Time-selective fading lead to time variation of the amplitude and phase distortions of the transmitted signals, and the direct consequence of frequency-selective fading is intersymbol interference (ISI). The term doubly selective is used in this dissertation to describe multipath fading that is both time-selective and frequency-selective.

Multipath fading is a double-edged sword for wireless communication system: the uncertainties and ISI introduced by doubly selective fading are detrimental to system performance; however, if properly handled, the time selectivity and frequency selectivity could also be utilized to facilitate system design since they provide extra degrees of freedom in the time domain and/or frequency domain. As discussed before, signals transmitted in doubly selective fading channels at different time and/or frequency are undergoing statistically independent fading, thus the probabilities that all the signal components are deeply faded simultaneously is much smaller compared to the non-selective case. This selective property will provide extra order of diversity in the time and/or frequency domain, which will eventually benefit system performance. It is well known that the uncertainties of time-varying multipath fading can be compensated by adaptive channel estimation and diversity techniques, and the effects of ISI induced by frequency-selective fading can be effectively mitigated by equalization algorithms. However, how to quantify and utilize the benefits contributed by the doubly selective fading still remains an interesting question.

Another performance constraining factor that distinguishes wireless system from its wireline counterpart is cochannel interference (CCI), which is a byproduct of frequency reuse, the key feature adopted by cellular mobile radio systems to capitalize the scarce and precious spectral resources. To increase the overall system spectral efficiency, which is defined as the maximum data rate supported by unit bandwidth, the coverage area of the mobile radio system is divided into cells with the same frequency channels being reused in cells spatially separated. Inevitably, CCI is introduced due to the fact that the same frequency resources are shared among different cells. CCI will ultimately limit the link quality thus system capacity of the mobile radio network. Therefore, the proper identification of the relationship between system spectral efficiency and CCI will greatly benefit the system design.

To combat the hostile wireless environment as well as to explore the potential provided by mobile radio channel, we in this dissertation focus on the optimum receiver design as well as theoretical performance analysis of wireless communication systems operated

over fading channels. By exploring the system structure and statistical properties of the wireless channel, optimum receivers and performance enhancement algorithms can effectively mitigate or compensate the impairments caused by the wireless channel, thus improve the communication link quality and system spectral efficiency. Likewise, theoretical system performance analysis enables in depth analysis and investigation of the fundamental relationship among system performance criteria (error probability, spectral efficiency), system parameters (Doppler spread, delay spread, CCI, channel estimation error, etc.), along with various performance enhancement techniques (channel estimation, diversity reception, etc.). Moreover, the theoretical performance results provide a set of analytical tools which can be in turn used to guide the design and development of communication systems.

1.2 Objectives

The dissertation objectives lie in two aspects. First, to develop optimum receiver and performance enhancement algorithms which are capable of combating the impairments caused by multipath fading by exploring the properties unique to mobile radio channels, thus to improve the overall system performance. Second, to develop generic analytical frameworks for the investigation and evaluation of wireless communication systems, and to provide theoretical system performance expressions that can be applied to evaluate the performance of existent systems or to guide the development or planning of new systems. These two objectives are incarnated throughout this dissertation by means of practical design, theoretical analysis and extensive simulations of a broad range of wireless communication systems under various system configurations. Specifically, special attentions are given to quantitatively identify the influences of practical system parameters, such as channel estimation error, receiver timing phase offset, on system performance, so that the results obtained here will be of practical values to the design and analysis of actual systems.

1.3 Dissertation Outline

Chapter 2: In this chapter, a generic statistical discrete-time model is proposed to provide an analysis and simulation framework for systems with wideband multiple-input multiple-output (MIMO) fading channels which are doubly selective due to Doppler spread and delay spread. The new discrete-time MIMO channel model includes the combined effects of the transmit filter, physical MIMO multipath fading and receive filter, and it leads to very efficient analysis and simulation of physical continuous-time MIMO channels.

Chapter 3: Based on the statistical properties of the discrete-time channel model presented in Chapter 2, a pilot assisted minimum mean square error (MMSE) multiuser channel estimation algorithm is proposed for quasi-synchronous CDMA systems that undergo doubly selective fading. The multiuser fading channel is represented as a symbol-wise time-varying chip-spaced tapped delay line filter with *correlated* filter taps. In the development of the estimation algorithm, the channel inter-tap correlation matrix is deemed as an essential factor, and a novel iterative method is proposed for the joint estimation of the channel inter-tap correlation and filter tap timing based on the received pilot samples.

Chapter 4: In this chapter, the design and performances of coherent diversity receivers with channel estimation error are investigated. The optimal diversity receiver for coherent reception with noisy channel state information is derived. and expressions for the average error probability of optimal diversity MPSK with noisy channel estimation are derived for Rayleigh and Ricean fading channels.

Chapter 5: Theoretical error performance analysis of wireless communication systems suffering doubly selective Rayleigh fadings are carried out to identify the relationship between system performance and fundamental system parameters such as Doppler spread and delay spread. The single-input single-output (SISO) systems with doubly selective fading channels are equivalently represented as discrete-time single-input multiple-output (SIMO) systems with *correlated* frequency-flat fading channels, with the correlation information being determined by the combined effects of sampler timing phase,

maximum Doppler spread, and delay spread of the physical fading as discussed in Chapter 2. Based on the equivalent SIMO system representation, closed-form error probability expressions are derived as tight lower bounds for linearly modulated systems with fractionally spaced equalizers.

Chapter 6: we investigate the effects of timing phase offset, which is defined as the phase difference between the transmitter clock and receiver clock, on wireless system performance. With frequency domain analysis, the instantaneous SNR observed by the communication receiver is expressed as an explicit function of system timing phase offset and receiver oversampling. A tight performance low bound is then derived for system experiencing frequency selective Rayleigh fading by examining the statistical properties of the receiver SNR. From the analytical results, it is observed that, if the receiver sampling rate is less than the Nyquist rate of the received signal, then the system error probability is a periodic function of the timing phase offset; on the other hand, the performance of oversampled system is independent of timing phase offset.

Chapter 7: A simple and novel method is presented to approximate the sum of independent, but not necessarily identical, lognormal random variables, which are used to model the effects of large-scale shadowing in a wireless cellular system. With the help of a short Gauss-Hermite expansion of the moment generation function, the lognormal sum is approximated by a single lognormal random variable. Observations and comparisons are made between the proposed method and the ones available in the literature such as the Fenton-Wilkinson method, Schwartz-Yeh method, the recently proposed Beaulieu-Xie method, and others. The proposed method can accurately approximate different portions of the lognormal sum probability distribution function, and provides the parametric flexibility to handle the inevitable trade-off that needs to be made in approximating both the head and tail portions of the lognormal sum probability distribution function.

Chapter 8: This chapter is devoted to analyze the theoretical spectral efficiency of multiuser cellular mobile radio systems with practical resource scheduling algorithms. Co-channel interferences are modeled as independent, but non-identically, distributed random process, with the channel power determined by the geometric layout of the

cellular system. By analyzing the statistical properties of the post-detection signal to interference plus noise ratio (SINR), spectral efficiency expressions are derived for system with Max-SINR scheduler and Round Robin scheduler. The effects of modulation alphabet size limit on system performance are quantified in the analytical expressions. Excellent agreements are observed between the analytical expressions and the simulation results.

Chapter 9: Conclusion remarks are drawn in this chapter. The major contributions of this dissertation is summarized, and future work is discussed.

Chapter 2

A Discrete-time model for spatio-temporally correlated MIMO WSSUS multipath channels

2.1 Introduction

The Multiple-input multiple-output (MIMO) communication architecture has recently emerged as a new paradigm for high data rate wireless cellular communications in rich multipath environments. Using multiple-element antenna arrays at both the transmitter and receiver, which effectively exploits the spatial dimension in addition to time and frequency dimensions, this architecture shows channel capacity potential far beyond that of traditional techniques. In quasi-static, independent and identically distributed (i.i.d.), frequency flat Rayleigh fading channels, the MIMO capacity scales linearly with the number of antennas under some conditions [1], [2]. However, in practice, subchannels of a MIMO system are usually **space-selective** (caused by angle spread at the transmitter and/or receiver), **time-selective** (caused by Doppler spread), and **frequency-selective** (caused by delay spread), which are referred to as *triple selective* MIMO channels in this thesis. These selectivities may substantially affect the MIMO performance [3], [4]. Further work in this field necessitates a realistic and efficient MIMO channel simulation model to investigate, evaluate and test new algorithms and performance of MIMO

wireless systems under triply selective fading scenarios.

The topic of MIMO channel modeling has received great interests recently [5]- [12]. Among them, frequency-selective Rayleigh fading channels were discussed in [5] and [6] with certain assumptions, while flat Rayleigh fading channels were explored in [12]. Physical channel models which include antenna polarization and/or angular information were discussed in [7]- [11]. But, all of these previous models are special cases of triply selective fading, and they are continuous-time based models. When the number of multiple delayed fading paths is large and/or the differential delay between paths is small, which are usually true for wideband systems in practice, then a significant amount of computational effort is required in simulations with continuous-time channel models [13]. The discrete-time channel model was first presented by Forney [14], and simulation models in discrete-time domain were discussed in [15]- [17] for single-input single-output (SISO) wireless channels. These papers [15]- [17] qualitatively showed the computational efficiency in favor of the discrete-time models, however, simulation results showed that these discrete-time models are not statistically equivalent to their continuous-time counterparts. For example, the bit error rate (BER) performance from these discrete-time models of a mobile communication system is different from that of the corresponding continuous-time models. This significantly reduces the practical value of these simulation models in [15]- [17]. Therefore, an accurate discrete-time model for both SISO and MIMO channels is highly desirable.

The main objective of this chapter is to establish a discrete-time MIMO channel model, which is statistically accurate and computationally efficient to characterize the continuous-time MIMO Rayleigh fading channel that is triply selective. The discrete-time MIMO channel model will translate the effects of transmit filter, physical MIMO channel fading and receive filter into the receiver's sampling-period spaced stochastic channel coefficients. No oversampling is needed to handle multiple fractionally-delayed fading paths or to approximate channels with possible continuous-delayed paths. The simulation of a MIMO system is carried out in a pure discrete manner, which leads to a higher computational efficiency and possible better statistical accuracy.

This chapter is organized as follows. Section 2.2 describes the continuous-time MIMO Rayleigh fading channel which includes the transmit filter, physical MIMO fading channel and receive filter. Two assumptions on the physical MIMO channel are also stated in this section. Section 2.3 proposes a discrete-time MIMO channel model which is statistically equivalent to the continuous-time MIMO channel model. The statistical properties of the discrete-time MIMO Rayleigh fading channel are analyzed in detail, and further used to generate the stochastic channel coefficients for simulation purposes. Simulation experiments are shown in Section 2.4 to demonstrate the statistical accuracy, computational efficiency and applications of the discrete-time MIMO channel model, including the evaluation of MIMO channel capacity under triply selective fading scenarios. Finally, Section 2.5 concludes this chapter.

2.2 MIMO Channel Description and Assumptions

2.2.1 MIMO Channel Description

We consider a wideband MIMO wireless channel which contains N transmit antennas and M receive antennas. Let $p_T(t)$ and $p_R(t)$ be the time-invariant impulse responses of the transmit filter and the receive filter, respectively, and both are normalized with energy of unity. Let $g_{m,n}(t, \tau)$ be the time-varying impulse response of the (m, n) th-subchannel connecting the n th-transmit antenna and the m th-receive antenna, where $g_{m,n}(t, \tau)$ is defined as the response at time t to an impulse applied to the subchannel at time $t - \tau$ [18]. The block diagram of this MIMO channel is depicted in Figure 2.1, where $\{s_n(k)\}$ is a sequence of complex symbols transmitted by the n th-transmit antenna with symbol period of T_{sym} , $y_m(t)$ is the received signal at the m th-receive antenna, and $y_m(k)$ is the sampled version of $y_m(t)$ with sampling period of $T_s = T_{sym}/\eta$, and η is an integer number. If $\eta = 1$, then the sampling rate at the receiver is the same as the symbol rate at the transmitter.

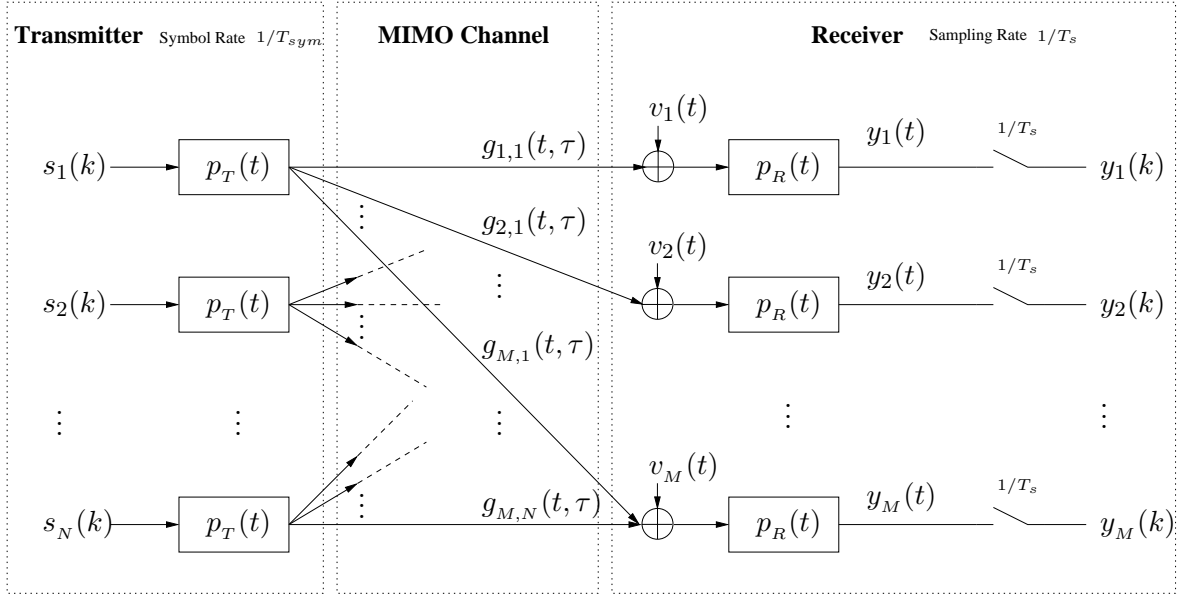


Figure 2.1: A conventional continuous-time baseband MIMO channel model.

We define the combined impulse response of the (m, n) th-subchannel as follows:

$$h_{m,n}(t, \tau) = p_R(\tau) \odot g_{m,n}(t, \tau) \odot p_T(\tau), \quad (2.1)$$

where $a(\tau) \odot b(t, \tau) = \int b(t, \alpha)a(\tau - \alpha)d\alpha$ represents the convolution operation. Therefore, the received signal $y_m(t) = \int h_{m,n}(t, \tau)s_n(t - \tau)d\tau$ can be expressed by

$$y_m(t) = \sum_{n=1}^N \sum_{k=-\infty}^{\infty} s_n(k)h_{m,n}(t, t - kT_{sym}) + z_m(t), \quad m = 1, 2, \dots, M, \quad (2.2)$$

where $z_m(t)$ is the additive noise given by

$$z_m(t) = v_m(t) \otimes p_R(t) \quad (2.3)$$

and $v_m(t)$ is the zero-mean complex-valued white Gaussian noise with a two-sided power spectral density N_0 . The sampled version of the received signal at the m th-receive antenna is given by

$$y_m(kT_s) = \sum_{n=1}^N \sum_{l=-\infty}^{\infty} s_n(l)h_{m,n}(kT_s, kT_s - lT_s) + z_m(kT_s), \quad m = 1, 2, \dots, M. \quad (2.4)$$

If we oversample the transmitted sequence $\{s_n(k)\}$ by inserting $(\nu - 1)$ zeros between each symbol $s_n(k)$, then the oversampled sequence denoted by $\{x_n(k)\}$ can be defined as follows:

$$x_n(k) = \begin{cases} s_n(k/\nu), & \text{if } k/\nu \text{ is integer,} \\ 0, & \text{otherwise.} \end{cases} \quad (2.5)$$

Replacing $s_n(k)$ in (2.4) by $x_n(k)$, we obtain the following equation with a single data rate of $1/T_s$:

$$y_m(k) = \sum_{n=1}^N \sum_{l=-\infty}^{\infty} x_n(k-l)h_{m,n}(k,l) + z_m(k), \quad m = 1, 2, \dots, M, \quad (2.6)$$

where $h_{m,n}(k,l) = h_{m,n}(kT_s, lT_s)$ is the T_s -space sampled version of $h_{m,n}(t, \tau)$, and $z_m(k) = z_m(kT_s)$ is the T_s -space sampled version of $z(t)$.

With the statistical properties of the discrete-time channel coefficients $h_{m,n}(k,l)$ and the additive noises $z_m(k)$, the MIMO channel input-output can be fully characterized in the discrete-time domain with high computational efficiency and no loss of information. Details are given in Section 2.3.

2.2.2 MIMO Channel Assumptions

We have two assumptions on the continuous-time physical channel of wideband MIMO wireless systems.

Assumption 2.1: The (m, n) th-subchannel, $g_{m,n}(t, \tau)$, of a MIMO system is a wide-sense stationary uncorrelated scattering (WSSUS) [18], [19] Rayleigh fading channel with a zero mean and autocorrelation given by

$$\mathbb{E} \{g_{m,n}(t, \tau) \cdot g_{m,n}^*(t - \xi, \tau')\} = J_0(2\pi f_d \xi) \cdot G(\tau) \cdot \delta(\tau - \tau'), \quad \forall m, n, \quad (2.7)$$

where $(\cdot)^*$ is the conjugate operator, f_d is the maximum Doppler frequency, and $G(\tau)$ is the power delay profile with $\int_{-\infty}^{\infty} G(\tau)d\tau = 1$.

It is important to note that this assumption is commonly employed for SISO channels in the literature [13], [15]- [17], and in wireless standards documents [22], [23] for both TDMA-based GSM (Global System for Mobile communications), EDGE (Enhanced Data rate for Global Evolution) systems, and CDMA-based UMTS (Universal Mobile Telecommunications System) and cdma2000 systems. Moreover, the power delay profile $G(\tau)$ is often assumed to be discrete and is given by

$$G(\tau) = \sum_{i=1}^K \sigma_i^2 \delta(\tau - \tau_i), \quad (2.8)$$

where K is the number of total resolvable paths, σ_i^2 is the power of the i th path with delay τ_i . For example, the Typical Urban (TU), Hilly Terrain (HT) and Equalization test (EQ) profiles for GSM and EDGE systems [22], the Pedestrian and Vehicular profiles for Channel A and Channel B of cdma2000 and UMTS systems [23] have all been defined as discrete delayed Rayleigh fading paths, and almost all the path delays τ_i are not an integer-multiple of their system's symbol period T_{sym} (or chip period T_c for CDMA systems).

This assumption implies that the fades of all the subchannels are identically distributed. However, it does not require them to be statistically independent. This implies that the subchannels are not necessarily i.i.d., which was commonly assumed in the literature for MIMO channels.

Assumption 2.2: The space selectivity or (spatial correlation) between the (m, n) th-subchannel $g_{m,n}(t, \tau)$ and the (p, q) th-subchannel $g_{p,q}(t, \tau)$ is given by

$$\mathbb{E} \{ g_{m,n}(t, \tau) \cdot g_{p,q}^*(t - \xi, \tau') \} = \rho_{Rx}^{(m,p)} \cdot \rho_{Tx}^{(n,q)} \cdot J_0(2\pi f_d \xi) \cdot G(\tau) \cdot \delta(\tau - \tau'), \quad (2.9)$$

where $\rho_{Rx}^{(m,p)}$ is the receive correlation coefficient between receive antennas m and p with $0 \leq |\rho_{Rx}^{(m,p)}| \leq \rho_{Rx}^{(m,m)} = 1$, and $\rho_{Tx}^{(n,q)}$ is the transmit correlation coefficient between transmit antennas n and q with $0 \leq |\rho_{Tx}^{(n,q)}| \leq \rho_{Tx}^{(n,n)} = 1$.

Assumption 2.2 is a straightforward extension of the MIMO Rayleigh flat fading case in [24] to the MIMO WSSUS multipath Rayleigh fading case. It implies three sub-assumptions as explained in [24] and cited as follows: 1) the transmit correlation between

the fading from transmit antennas n and q to the same receive antenna does not depend on the receive antenna; 2) the receive correlation between the fading from a transmit antenna to receive antennas m and p does not depend on the transmit antenna; and 3) the correlation between the fading of two distinct transmit-receive antenna pairs is the product of the corresponding transmit correlation and receive correlation. These three sub-assumptions are actually the “Kronecker correlation” assumption used in the literature, and they are quite accurate and commonly used for MIMO Rayleigh fading channels [4], [25]. However, it should be pointed out that the third sub-assumption may not be extended to Ricean fading MIMO channels [26].

It is noted here that the spatial correlation coefficients $\rho_{R_x}^{(m,p)}$ and $\rho_{T_x}^{(n,q)}$ are determined by the spatial arrangements of the transmit and receive antennas, and the angle of arrival, the angular spread, etc. They can be calculated by mathematical formulas [4], [25] or obtained from experimental data.

2.3 The Discrete-time MIMO Channel Model

In this section, we present a discrete-time model for triply selective MIMO Rayleigh fading channels, then we investigate the statistical properties of this MIMO channel in the discrete-time domain. These statistics are further used to build a computationally efficient discrete-time MIMO channel simulator, which is equivalent to its counterpart in the continuous-time domain in terms of various statistic measures.

2.3.1 The Discrete-Time Channel Model

It is known that the total number of T_s -spaced discrete-time channel coefficients, $h_{m,n}(k, l)$, is determined by the maximum delay spread of the physical fading channel $g_{m,n}(t, \tau)$, and the time durations of the transmit filter and receive filter, which are usually infinite in theory to maintain limited frequency bandwidth. Therefore, $h_{m,n}(k, l)$ is normally a

time-varying non-causal filter with infinite impulse response (IIR).¹ However, in practice, the time-domain tails of the transmit and receive filters are designed to fall off rapidly. Thus, the amplitudes of the channel coefficients $h_{m,n}(k, l)$ will decrease quickly with increasing $|l|$. When the power (or squared amplitude) of a coefficient is smaller than a pre-defined threshold, for example, 0.01% of the total power of its corresponding subchannel, it has very little impact on the output signal, and thus can be discarded. Therefore, the time-varying non-causal IIR channel can be truncated to a finite impulse response (FIR) channel. Without loss of generality, we assume that the coefficient index, l , is in the range of $[-L_1, L_2]$, where L_1 and L_2 are non-negative integers, and the total number of coefficients for the truncated FIR channel $h_{m,n}(k, l)$ is L with $L \leq L_1 + L_2 + 1$, where the equality is held if there are no discarded coefficients within the coefficient index range of $[-L_1, L_2]$.

Based on the above discussion and Eqn. (2.6), we can now describe the input-output relationship of the MIMO channel in the discrete-time domain as follows:

$$\mathbf{y}(k) = \sum_{l=-L_1}^{L_2} \mathbf{H}_l(k) \cdot \mathbf{x}(k-l) + \mathbf{z}(k), \quad (2.10)$$

where $\mathbf{x}(k) = [x_1(k), x_2(k), \dots, x_N(k)]^t$, $\mathbf{z}(k) = [z_1(k), z_2(k), \dots, z_M(k)]^t$ and $\mathbf{y}(k) = [y_1(k), y_2(k), \dots, y_M(k)]^t$ are the input vector, noise vector and output vector at time instant k , respectively, with $(\cdot)^t$ being the transpose operator; $\mathbf{H}_l(k)$ is the lT_s delayed channel matrix at time instant k , and defined by

$$\mathbf{H}_l(k) = \begin{bmatrix} h_{1,1}(k, l) & \cdots & h_{1,N}(k, l) \\ \vdots & \ddots & \vdots \\ h_{M,1}(k, l) & \cdots & h_{M,N}(k, l) \end{bmatrix}. \quad (2.11)$$

The block diagram of this discrete-time MIMO channel model is shown in Figure 2.2.

It is noted that there are (MNL) stochastic channel coefficients, and an M -element random noise vector in this MIMO Rayleigh fading model (2.10). Since all of them are complex-valued Gaussian random variables, the first-order and second-order statistics

¹It should be noted that the non-causality of $h_{m,n}(k, l)$ is induced by the effects of the transmit filter and receive filter, while the physical CIR $g_{m,n}(t, \tau)$ is always causal.

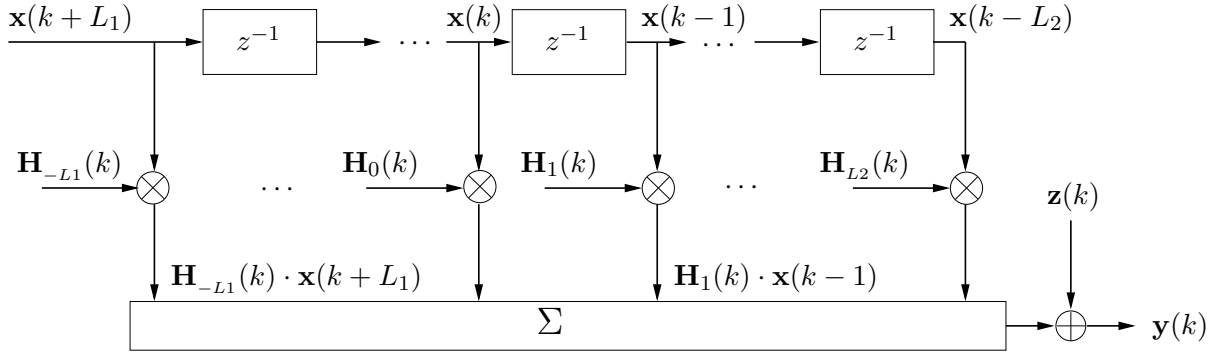


Figure 2.2: The equivalent discrete-time MIMO channel model.

of the channel coefficients and the noise vector will be sufficient to fully characterize the MIMO channel. For the convenience of discussion, we define the MIMO channel coefficient vector $\mathbf{h}_{vec}(k)$ as follows:

$$\mathbf{h}_{vec}(k) = [\mathbf{h}_{1,1}(k), \dots, \mathbf{h}_{1,N}(k) \mid \dots \mid \mathbf{h}_{M,1}(k), \dots, \mathbf{h}_{M,N}(k)]^t, \quad (2.12)$$

where $\mathbf{h}_{m,n}(k)$ is the (m, n) th-subchannel's FIR coefficients at time k , and given by

$$\mathbf{h}_{m,n}(k) = \begin{bmatrix} h_{m,n}(k, -L_1) & \dots & h_{m,n}(k, L_2) \end{bmatrix}. \quad (2.13)$$

We are now ready to discuss the statistical properties of the MIMO channel.

2.3.2 Statistical Properties of the Discrete-Time Channel

Proposition 2.1: The noise vector $\mathbf{z}(k)$ is zero-mean Gaussian distributed with auto-covariance matrix $\mathbf{R}_{\mathbf{z}\mathbf{z}}(k_1 - k_2)$ given by

$$\mathbf{R}_{\mathbf{z}\mathbf{z}}(k_1 - k_2) = \mathbb{E} [\mathbf{z}(k_1) \cdot \mathbf{z}^h(k_2)] = N_0 \cdot R_{p_R p_R} [(k_1 - k_2)T_s] \cdot \mathbf{I}_M, \quad (2.14)$$

where $(\cdot)^H$ stands for the Hermitian of a complex-valued vector or matrix, $R_{p_R p_R}(\xi)$ is the auto-correlation function of the receive filter $p_R(t)$, N_0 is the two sided power spectral density of the complex-valued additive white Gaussian noise (AWGN) $v_m(t)$, and \mathbf{I}_M is an $M \times M$ identity matrix.

Proof: Since $z_m(t)$ is the output of a time-invariant linear filter with the input of zero-mean AWGN $v_m(t)$, $z_m(t)$ and its sampled version $z_m(kT_s)$ are both zero-mean Gaussian random variables. Noting that the zero-mean AWGN $v_m(t)$ is independent from time to time and from antenna to antenna (i.e., $\mathbb{E}[v_{m_1}(t_1)v_{m_2}^*(t_2)] = N_0\delta(m_1 - m_2)\delta(t_1 - t_2)$), we can immediately get (2.14). \blacksquare

If the autocorrelation function of the receive filter, $p_R(t)$, satisfies the following condition

$$R_{p_R p_R}(kT_s) = 0, \quad k \neq 0, \quad (2.15)$$

then the discrete-time Gaussian noise $z_m(k)$ is still white, from sample to sample and from antenna to antenna, with variance of N_0 due to the receive filter being normalized to have energy of unity (i.e., $R_{p_R p_R}(0) = 1$).

Proposition 2.2: The channel coefficients $h_{m,n}(k, l)$ and $h_{p,q}(k, l)$ are zero-mean Gaussian random variables, and their covariance function is given by

$$\mathbb{E}[h_{m,n}(k_1, l_1) \cdot h_{p,q}^*(k_2, l_2)] = \rho_{R_x}^{(m,p)} \cdot \rho_{T_x}^{(n,q)} \cdot c(l_1, l_2) \cdot J_0[2\pi f_d(k_1 - k_2)T_s], \quad (2.16)$$

where

$$c(l_1, l_2) = \begin{cases} \int_{-\infty}^{+\infty} \bar{R}_{p_T p_R}(l_1 T_s - \tau) \bar{R}_{p_T p_R}^*(l_2 T_s - \tau) G(\tau) d\tau, & \text{if } G(\tau) \text{ is continuous} \\ \sum_{i=1}^K \sigma_i^2 \bar{R}_{p_T p_R}(l_1 T_s - \tau_i) \bar{R}_{p_T p_R}^*(l_2 T_s - \tau_i), & \text{if } G(\tau) \text{ is given by (2.8),} \end{cases} \quad (2.17)$$

with $\bar{R}_{p_T p_R}(\xi)$ being the convolution function of the transmit filter and receive filter.

Proof: Based on Eqn. (2.1) and $g_{m,n}(t, \tau)$ being zero-mean Gaussian process, it is easy to conclude that $h_{m,n}(k, l)$ and $h_{p,q}(k, l)$ are zero-mean Gaussian random variables. Since $h_{m,n}(k, l)$ is the sampled version of $h_{m,n}(t, \tau)$, we have

$$h_{m,n}(k, l) = \int_{-\infty}^{+\infty} \bar{R}_{p_T p_R}(lT_s - \tau) g_{m,n}(kT_s, \tau) d\tau. \quad (2.18)$$

According to Assumption 2.2, we can obtain

$$\begin{aligned} \mathbb{E} [h_{m,n}(k_1, l_1)h_{p,q}^*(k_2, l_2)] &= \rho_{Rx}^{(m,p)} \cdot \rho_{Tx}^{(n,q)} \cdot J_0 [2\pi f_d(k_1 - k_2)T_s] \times \\ &\quad \int_{-\infty}^{+\infty} \int_{-\infty}^{+\infty} \bar{R}_{p_T p_R}(l_1 T_s - \tau) \bar{R}_{p_T p_R}^*(l_2 T_s - \mu) G(\tau) \delta(\tau - \mu) d\tau d\mu \\ &= \rho_{Rx}^{(m,p)} \cdot \rho_{Tx}^{(n,q)} \cdot J_0 [2\pi f_d(k_1 - k_2)T_s] \cdot c(l_1, l_2), \end{aligned} \quad (2.19)$$

where $c(l_1, l_2)$ is given by (2.17). Thus the proof is complete. \blacksquare

We are now in a position to present the statistical property of the channel coefficient vector $\mathbf{h}_{vec}(k)$ with the following theorem.

Theorem 2.1: The channel coefficient column vector $\mathbf{h}_{vec}(k)$ is zero-mean Gaussian distributed, its covariance matrix $\mathbf{C}_h(k_1 - k_2) = \mathbb{E} \{ \mathbf{h}_{vec}(k_1) \cdot \mathbf{h}_{vec}^H(k_2) \}$ is given by

$$\mathbf{C}_h(k_1 - k_2) = (\Psi_{Rx} \otimes \Psi_{Tx} \otimes \mathbf{C}_{ISI}) \cdot J_0 [2\pi f_d(k_1 - k_2)T_s], \quad (2.20)$$

where \otimes denotes the Kronecker product [27] and \mathbf{C}_{ISI} is the covariance matrix of the intersymbol interference (ISI) filter tap vector $\mathbf{h}_{m,n}(k)$. Likewise, Ψ_{Rx} , Ψ_{Tx} and \mathbf{C}_{ISI} are given by

$$\Psi_{Rx} = \begin{bmatrix} \rho_{Rx}^{(1,1)} & \cdots & \rho_{Rx}^{(1,M)} \\ \vdots & \ddots & \vdots \\ \rho_{Rx}^{(M,1)} & \cdots & \rho_{Rx}^{(M,M)} \end{bmatrix}, \quad \Psi_{Tx} = \begin{bmatrix} \rho_{Tx}^{(1,1)} & \cdots & \rho_{Tx}^{(1,N)} \\ \vdots & \ddots & \vdots \\ \rho_{Tx}^{(N,1)} & \cdots & \rho_{Tx}^{(N,N)} \end{bmatrix}, \quad (2.21)$$

$$\mathbf{C}_{ISI} = \begin{bmatrix} c(-L_1, -L_1) & \cdots & c(-L_1, L_2) \\ \vdots & \ddots & \vdots \\ c(L_2, -L_1) & \cdots & c(L_2, L_2) \end{bmatrix}, \quad (2.22)$$

with $c(l_1, l_2)$ being determined by (2.17).

Proof: Based on (2.13), (2.16) and (2.17), we can immediately get

$$\mathbb{E} [\mathbf{h}_{m,n}^t(k_1) \cdot \mathbf{h}_{p,q}^*(k_2)] = \rho_{Rx}^{(m,p)} \cdot \rho_{Tx}^{(n,q)} \cdot \mathbf{C}_{ISI} \cdot J_0 [2\pi f_d(k_1 - k_2)T_s]. \quad (2.23)$$

According to expression (2.12) of the column vector $\mathbf{h}_{vec}(k)$, we can further get its covariance matrix as follows

$$\begin{aligned}
\mathbf{C}_h(k_1 - k_2) &= \begin{bmatrix} \rho_{Rx}^{(1,1)} \rho_{Tx}^{(1,1)} \mathbf{C}_{ISI} & \cdots & \rho_{Rx}^{(1,1)} \rho_{Tx}^{(1,N)} \mathbf{C}_{ISI} & & \rho_{Rx}^{(1,M)} \rho_{Tx}^{(1,1)} \mathbf{C}_{ISI} & \cdots & \rho_{Rx}^{(1,M)} \rho_{Tx}^{(1,N)} \mathbf{C}_{ISI} \\ \vdots & & \vdots & & \vdots & & \vdots \\ \rho_{Rx}^{(1,1)} \rho_{Tx}^{(N,1)} \mathbf{C}_{ISI} & \cdots & \rho_{Rx}^{(1,1)} \rho_{Tx}^{(N,N)} \mathbf{C}_{ISI} & & \rho_{Rx}^{(1,M)} \rho_{Tx}^{(N,1)} \mathbf{C}_{ISI} & \cdots & \rho_{Rx}^{(1,M)} \rho_{Tx}^{(N,N)} \mathbf{C}_{ISI} \\ & & \ddots & & & & \ddots \\ \rho_{Rx}^{(M,1)} \rho_{Tx}^{(1,1)} \mathbf{C}_{ISI} & \cdots & \rho_{Rx}^{(M,1)} \rho_{Tx}^{(1,N)} \mathbf{C}_{ISI} & & \rho_{Rx}^{(M,M)} \rho_{Tx}^{(1,1)} \mathbf{C}_{ISI} & \cdots & \rho_{Rx}^{(M,M)} \rho_{Tx}^{(1,N)} \mathbf{C}_{ISI} \\ \vdots & & \vdots & & \vdots & & \vdots \\ \rho_{Rx}^{(M,1)} \rho_{Tx}^{(N,1)} \mathbf{C}_{ISI} & \cdots & \rho_{Rx}^{(M,1)} \rho_{Tx}^{(N,N)} \mathbf{C}_{ISI} & & \rho_{Rx}^{(M,M)} \rho_{Tx}^{(N,1)} \mathbf{C}_{ISI} & \cdots & \rho_{Rx}^{(M,M)} \rho_{Tx}^{(N,N)} \mathbf{C}_{ISI} \end{bmatrix} \\
&\times J_0 [2\pi f_d(k_1 - k_2)T_s] \\
&= \begin{bmatrix} \rho_{Rx}^{(1,1)} \Psi_{Tx} & \cdots & \rho_{Rx}^{(1,M)} \Psi_{Tx} \\ \vdots & & \vdots \\ \rho_{Rx}^{(M,1)} \Psi_{Tx} & \cdots & \rho_{Rx}^{(M,M)} \Psi_{Tx} \end{bmatrix} \otimes \mathbf{C}_{ISI} \cdot J_0 [2\pi f_d(k_1 - k_2)T_s] \\
&= (\Psi_{Rx} \otimes \Psi_{Tx} \otimes \mathbf{C}_{ISI}) \cdot J_0 [2\pi f_d(k_1 - k_2)T_s]. \tag{2.24}
\end{aligned}$$

This completes the proof of the theorem. ■

2.3.3 Generation of the Discrete-Time MIMO Channel Fading

Having analyzed the statistical properties of the discrete-time MIMO channel model, we can generate the stochastic fading channel coefficients represented by the channel vector $\mathbf{h}_{vec}(k)$, whose covariance matrix matches the theoretical one given by Theorem 2.1, for computer simulations of MIMO systems.

Theorem 2.2: The zero-mean time-varying Rayleigh fading channel vector $\mathbf{h}_{vec}(k)$ can be generated by

$$\mathbf{h}_{vec}(k) = \mathbf{C}_h^{1/2}(0) \cdot \Phi(k) = (\Psi_{Rx}^{1/2} \otimes \Psi_{Tx}^{1/2} \otimes \mathbf{C}_{ISI}^{1/2}) \cdot \Phi(k), \tag{2.25}$$

where $\mathbf{X}^{1/2}$ is the square root of matrix $\mathbf{X} = \mathbf{X}^{1/2} \cdot (\mathbf{X}^{1/2})^H$, which can be obtained by a few methods shown in [28]; $\Phi(k)$ is an $(MNL) \times 1$ vector, whose elements are uncorrelated Rayleigh flat fading, and $\mathbb{E} [\Phi(k_1) \cdot \Phi^H(k_2)] = J_0 [2\pi f_d(k_1 - k_2)T_s] \cdot \mathbf{I}_{MNL \times MNL}$.

Proof: This theorem can be proved by using two identities of matrices [27]: $[A \otimes B][C \otimes D] = [AC] \otimes [BD]$ and $[A \otimes B]^H = A^H \otimes B^H$, where the matrices have appropriate dimensions. Details are omitted here for brevity. ■

The significance of Theorem 2.2 is that it indicates that the generation of the stochastic channel coefficients of a MIMO system can be done through the Kronecker product of the square roots of three small matrices in the sizes of $M \times M$, $N \times N$ and $L \times L$, rather than the square root of a very large matrix $\mathbf{C}_h(0)$ in the size of $(MNL) \times (MNL)$. The number of operations required for the square root decomposition of $\mathbf{C}_h(0)$ is approximately $6M^3N^3L^3$ [28]. Alternatively, the number of operations required to decompose three smaller matrices is approximately $6(M^3 + N^3 + L^3)$, and the Kronecker product of the three matrices requires about $(M^2N^2L^2)/2$ operations. Therefore, the ratio between the number of operations of decomposing one large matrix and the number of operations to decompose three smaller matrices can be approximated by $\frac{12M^3N^3L^3}{12(M^3+N^3+L^3)+M^2N^2L^2}$. It is apparent that significant amount of computations will be saved by this method, and it will additionally leads to much better numerical computation accuracy.

The generation of multiple uncorrelated Rayleigh flat fades is a classic topic with new challenges for the number (MNL) of multiple fades being large. It has been commonly postulated in the literature [6], [16], [17], that it can be done by Jakes' original simulator [29]. Unfortunately, there are two problems in the original Jakes' simulator. First, Jakes' simulator is a deterministic model, it has difficulty [30] to directly generate three or more uncorrelated Rayleigh flat fading waveforms. Secondly, and more importantly, it was shown in [31] that Jakes' simulator is even not stationary in the wide sense, and an improved Jakes' simulator was proposed in [31] to remove the stationarity problem. However, the improved Jakes' simulator along with the original Jakes' simulator have statistic deficiencies as pointed out in [32], and these statistic deficiencies were finally removed by new Rayleigh fading models developed in [33] and [34]. These new models can be employed for the generation of the multiple uncorrelated Rayleigh flat fading vector $\Phi(k)$. Here, we present another Rayleigh fading simulation model which can also

accurately generate the $(MNL) \times 1$ vector $\Phi(k)$ as follows.

$$\Phi(k) = \left[\Phi_1(k) \quad \Phi_2(k) \quad \cdots \quad \Phi_{MNL}(k) \right]^t \quad (2.26)$$

with

$$\begin{aligned} \Phi_q(k) = & \sqrt{\frac{2}{K_s}} \left\{ \sum_{p=1}^{K_s} \cos(\psi_{p,q}) \cdot \sin \left[2\pi f_d k T_s \cos \left(\frac{2\pi p - \pi + \theta_q}{4K_s} \right) + \phi_{p,q} \right] \right. \\ & \left. + j \sum_{p=1}^{K_s} \sin(\psi_{p,q}) \cdot \sin \left[2\pi f_d k T_s \cos \left(\frac{2\pi p - \pi + \theta_q}{4K_s} \right) + \phi_{p,q} \right] \right\}. \quad (2.27) \end{aligned}$$

It can be proved that $\Phi(k)$ defined above is a zero mean Gaussian process with auto-covariance matrix given by

$$\mathbb{E} [\Phi(k_1) \cdot \Phi^H(k_2)] = J_0 [2\pi f_d (k_1 - k_2) T_s] \cdot \mathbf{I}_{MNL \times MNL}, \quad (2.28)$$

where K_s is chosen to be no less than 8, $q = 1, 2, \dots, (MNL)$, the random phases θ_q , $\psi_{p,q}$ and $\phi_{p,q}$ are mutually independent and uniformly distributed on $[-\pi, \pi)$ for all p and q .

The physical meaning of eqn. (2.27) is that each flat Rayleigh fading waveform is made up of a number of sinusoids which have random path gain $\exp(\psi_{p,q})$, random initial phase $\phi_{p,q}$, and random Doppler frequency $f_d \cos[(2\pi p - \pi + \theta_q)/(4K_s)]$. The random path gains assure that fades Φ_q and Φ_n are statistically uncorrelated when $q \neq n$. The random initial phase assures that Φ_q will be stationary in the wide sense. The random Doppler frequency assures that the Rayleigh fading Φ_q has the correct power spectrum density.

2.3.4 Computational Complexity

Theorems 2.1–2.2 imply that our discrete-time MIMO channel model is statistically equivalent to the conventional continuous-time channel model. In this subsection, we will show that the computational complexity of our proposed discrete-time MIMO channel simulation model is much lower than that of the conventional continuous-time simulation model, based on the following three aspects.

First, the sampling rate of the discrete-time model is $1/T_s$, which is equal to ν/T_{sym} with ν being a small positive integer. However, for the conventional continuous-time model, when the differential delay of multiple fading paths is very small compared to the symbol period T_{sym} , the sampling rate for simulation needs to be very high to implement the multiple fading paths. Let ν_c/T_{sym} be the sampling rate for the continuous-time model, then the sampling computational complexity ratio of the discrete-time model to the continuous-time models is given by

$$\zeta_\nu = \frac{\nu}{\nu_c} \times 100\%. \quad (2.29)$$

Since ν_c is usually much larger than ν , the ratio ζ_ν is usually very small. For channels with continuous power delay profile, such as the exponential power delay profile [13], a much higher ν_c is required for continuous-time model, which will lead to a even smaller ζ_ν .

Second, the number of uncorrelated fades used in the discrete-time model, L_d , is not larger than the number of uncorrelated fades used in the continuous-time model, L_c . Thus the ratio $\zeta_L = \frac{L_d}{L_c} \times 100\%$ is not larger than 1.

Third, for the discrete-time model, the effects of the transmit and receive filters are incorporated in the statistical channel coefficients with no additional filtering calculations involved. However, the simulation of the continuous-time model must pass the input signals through the transmit and receive filters with extra computations. Moreover, to represent the small differential delay of multiple fading paths, the continuous-time model has to use high sampling rate which makes the transmit and receive filters have large number of taps. This makes the computational complexity of the continuous-time model even higher than that of the discrete-time model. Unfortunately, an explicit ratio between these two models is unlikely to obtain.

Combining the aforementioned three facts, we can obtain the total computational complexity ratio of the discrete-time model to the continuous-time model as follows

$$\zeta < \zeta_\nu \zeta_L. \quad (2.30)$$

For convenient comparison, Table 2.1 shows the computational complexity ratios for TU,

Table 2.1: The computational complexity ratio of the proposed Discrete-time model to the conventional continuous-time model

Profiles	TU	HT	EQ	PedA	PedB	VehA	VehB
ζ_ν	2.7%	2.7%	2.7%	3.8%	7.7%	3.8%	7.7%
ζ_L	66.7%	83.3%	100%	50%	100%	83.3%	100%
$\zeta < \zeta_\nu \zeta_L$	1.8%	2.3%	2.7%	1.9%	7.7%	3.2%	7.7%

HT and EQ propagation profiles of EDGE system, and Pedestrian A (PedA), Pedestrian B (PedB), Vehicular A (VehA) and Vehicular B (VehB) propagation profiles of cdma2000 and UMTS systems. It is noted that these profiles are commonly used simulation test cases for wireless system evaluation. As can be seen from the table, the newly proposed discrete-time MIMO channel model has much smaller computational complexity compared to the conventional continuous-time MIMO channel model.

2.4 Simulation Experiments

In this section, we are going to evaluate the discrete-time MIMO channel model by simulation in three different criteria. First, we assess the statistic accuracy of the model compared to its theoretically calculated statistics. Second, we demonstrate the statistical equivalence between the proposed discrete-time model and the conventional continuous-time model through BER comparison. Third, we present the application of the model for MIMO channel capacity evaluation of a system which experiences triply selective Rayleigh fading.

2.4.1 Spatial-Temporal Statistics

Consider a MIMO system consisting of 2 antennas at the base station as the transmitter and 2 antennas at the mobile station as the receiver, then the correlation coefficient matrices Ψ_{Tx} and Ψ_{Rx} can be calculated by the formulas derived in [4] under certain spatial parameters. For example, if the BS and MS antennas are spaced by 12λ and 0.5λ , respectively, where λ is the wavelength, the angle of arrival is 90° and the angular

spread is 10° as shown in Figure 2.3, then we get the two matrices as follows:

$$\Psi_{Tx} = \begin{bmatrix} 1.0000 & 0.2154 \\ 0.2154 & 1.0000 \end{bmatrix}, \quad \Psi_{Rx} = \begin{bmatrix} 1.0000 & -0.3042 \\ -0.3042 & 1.0000 \end{bmatrix}. \quad (2.31)$$

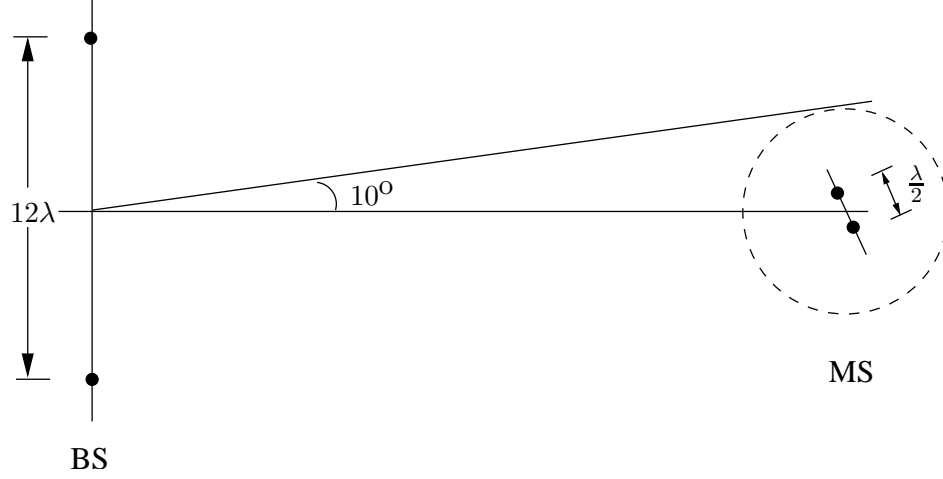


Figure 2.3: The antenna placement of the 2×2 MIMO system.

If the power delay profile is exponentially decaying [13], [17] and given by $G(\tau) = A \cdot \exp(\tau/\mu s)$ for $0 \leq \tau \leq 5\mu s$, and $G(\tau) = 0$ otherwise. Likewise, if the transmit filter is a linearized Gaussian filter with a time-bandwidth product 0.3 [35], the receive filter is a square root raised cosine (RRC) filter with a roll-off factor 0.3, and the sampling period T_s is $3.69\mu s$, then the elements $c(l_1, l_2)$ of the matrix \mathbf{C}_{ISI} obtained by (2.17) are shown in Table 2.2.

Table 2.2: The matrix \mathbf{C}_{ISI} for the exponential delay power profile

$c(l_1, l_2)$	$l_2 = -1$	$l_2 = 0$	$l_2 = 1$	$l_2 = 2$
$l_1 = -1$	0.0091	0.0426	0.0178	-0.0016
$l_1 = 0$	0.0426	0.3664	0.3407	0.0367
$l_1 = 1$	0.0178	0.3407	0.5583	0.1414
$l_1 = 2$	-0.0016	0.0367	0.1414	0.0602

Having obtained the above three matrices, we can now compare the theoretical statistics as defined in (2.20) of the discrete-time MIMO fading channel coefficients with

their corresponding empirical correlations obtained from simulations. For illustration purpose, we only show three of the comparisons here for the sake of brevity. Based on Theorem 2.1, the theoretical autocorrelation (same as the auto-covariance for a zero mean random variable) function of the channel coefficient $h_{1,1}(k, 1)$ is given by $0.5583 \times J_0[2\pi f_d(k_1 - k_2)T_s]$, the theoretical cross-correlation function of the channel coefficients $h_{1,1}(k, 0)$ and $h_{1,1}(k, 1)$ is given by $0.3407 \times J_0[2\pi f_d(k_1 - k_2)T_s]$, and the theoretical cross-correlation function of the channel coefficients $h_{1,1}(k, 0)$ and $h_{2,1}(k, 1)$ is given by $-0.1036 \times J_0[2\pi f_d(k_1 - k_2)T_s]$. Using the procedure described in Subsection 2.3.3, we have generated a set of the time-varying random channel coefficients for $h_{1,1}(k, 0)$, $h_{1,1}(k, 1)$ and $h_{2,1}(k, 1)$. Then, their correlation statistics obtained from the simulation are compared to their corresponding theoretical ones and depicted in Figure 2.4. As can be seen, the spatio-temporal statistics of the MIMO channel simulation model match the theoretical results very well. We have also compared the correlation statistics of all other channel coefficients to their theoretical ones, finding good agreement in all cases. Therefore, the statistical accuracy of the the discrete-time MIMO channel model is confirmed.

We conclude this subsection with two remarks. First, the non-zero cross-correlations between $h_{1,1}(k, 0)$ and $h_{1,1}(k, 1)$, and between $h_{1,1}(k, 0)$ and $h_{2,1}(k, 1)$ indicate that the fading coefficients from different subchannels with different delays can be statistically correlated (or even significantly correlated sometimes). This is quite different from the commonly used independence assumption in the literature [6], [36], [37], where the transmit and receive filters were not taken into consideration. Second, the conventional continuous-time channel model needs a very high oversampling rate [13] to approximately simulate this continuous power delay profile $G(\tau)$, but our discrete-time channel model can efficiently and accurately simulate the continuous delay power profile as shown above.

2.4.2 Bit Error Rate Comparison

The statistical equivalence of the discrete-time channel model to the conventional continuous-time channel model can be demonstrated by comparing their BER performances. We

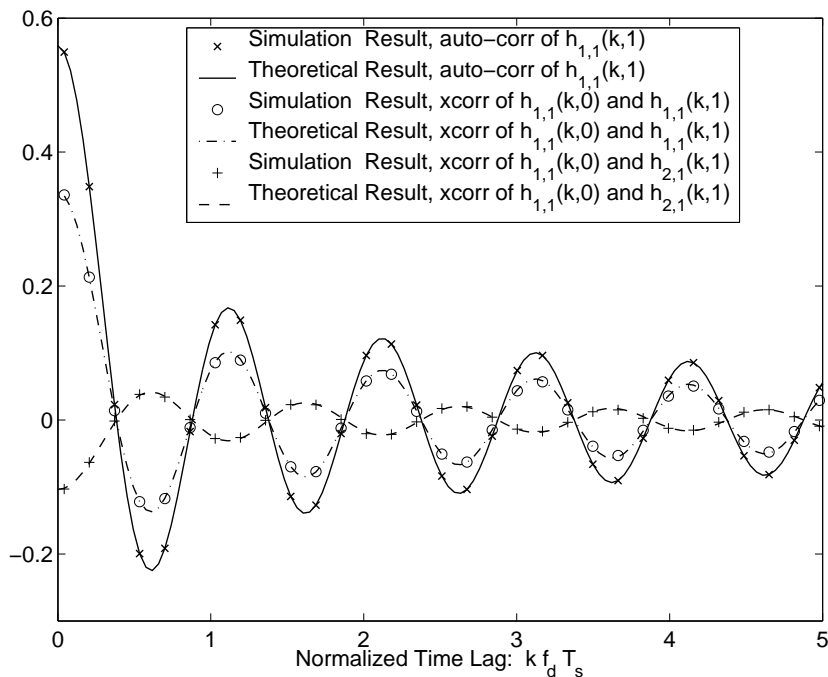


Figure 2.4: Comparison of the theoretically calculated and empirically simulated auto-correlation of $h_{1,1}(k, 1)$, cross-correlation of $h_{1,1}(k, 0)$ and $h_{1,1}(k, 1)$, and cross-correlation of $h_{1,1}(k, 0)$ and $h_{2,1}(k, 1)$.

choose the EDGE system [22], [35], as an example in this subsection. The power delay profile $G(\tau)$ used here is the reduced 6-path Typical Urban (TU) profile provided in [22], all the 6 paths characterized by uncorrelated Rayleigh flat fading as specified in [22]. The transmit filter, receiver filter and sampling period are the same as those used in the last subsection. The matrix \mathbf{C}_{ISI} is given in Table 2.3. It should be pointed out from this table that the power of this discrete-time channel is mainly concentrated on $h(k, 0)$ and $h(k, 1)$ corresponding to the values of $c(0, 0)$ and $c(1, 1)$, respectively. The total power of this truncated discrete-time channel is, given by the trace of \mathbf{C}_{ISI} , 0.9975, which is slightly less than unity as expected.

It is also noted that the RRC receive filter satisfies (2.15), so the additive noise in the discrete-time channel is still AWGN and can be directly generated by computer simulations. Assuming perfect channel estimation at the receiver for both the discrete-time channel model and continuous-time channel model, and by employing MLSE with

Table 2.3: The matrix \mathbf{C}_{ISI} for the reduced 6-path Typical Urban profile

$c(l_1, l_2)$	$l_2 = -1$	$l_2 = 0$	$l_2 = 1$	$l_2 = 2$	$l_2 = 3$
$l_1 = -1$	0.0481	0.1799	0.0678	-0.0030	0.0029
$l_1 = 0$	0.1799	0.7401	0.3253	-0.0073	0.0121
$l_1 = 1$	0.0678	0.3253	0.1957	0.0168	0.0052
$l_1 = 2$	-0.0030	-0.0073	0.0168	0.0133	-0.0002
$l_1 = 3$	0.0029	0.0121	0.0052	-0.0002	0.0002

the Viterbi algorithm for channel equalization with truncated channel memory length 4, we have obtained the uncoded BER vs E_b/N_0 shown in Figure 2.5.

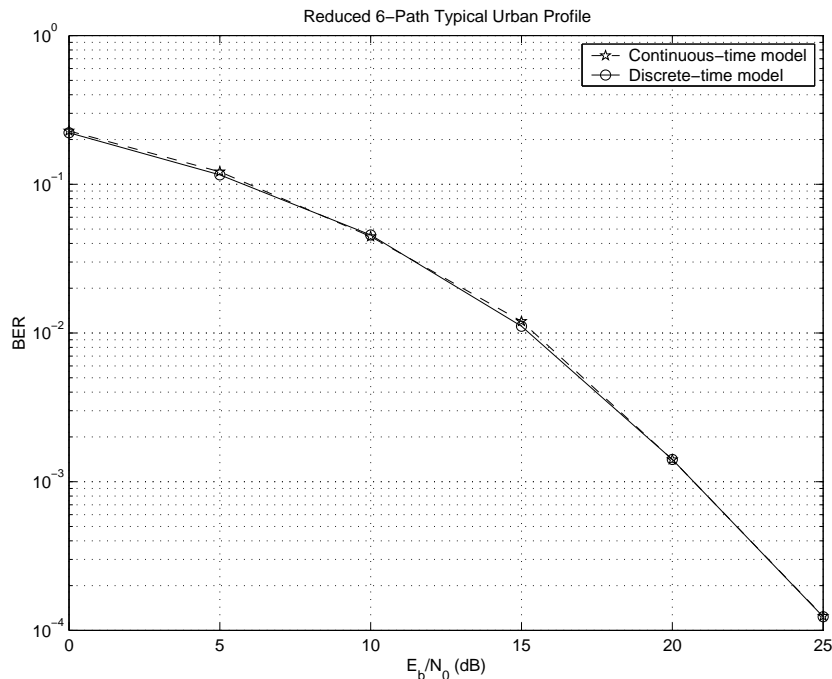


Figure 2.5: Comparison of BER performance with discrete-time model and continuous-time model for EDGE mobile system under Typical Urban delay power profile.

Apparently, the BER performance of the discrete-time channel model is almost identical to that of the continuous-time channel model. This demonstrates that the discrete-time channel model is statistically equivalent to the continuous-time channel model. However, according to Table 2.1, the discrete-time model needs only about 1.8% computations of the continuous-time model to generate the statistical fading channel coefficients in this

SISO example. This computational saving is very significant for discrete-time MIMO channels, where the computational burden for the generation of MIMO channel fading is a big issue.

2.4.3 MIMO Channel Capacity

In this subsection, the MIMO channel capacity is evaluated, using our discrete-time channel model, for triply selective Rayleigh fading channels to indicate the effects of spatial correlations, multipaths and number of antennas on the channel capacity.

When the MIMO channel is known to the receiver but unknown to the transmitter and assuming that the available power is uniformly distributed over all the transmit antennas, then the capacity of a spatially correlated MIMO WSSUS multipath Rayleigh channel with fixed total transmission power P_T is given by [38]:

$$C = \frac{1}{2W} \int_{-W}^W \log_2 \det \left[\mathbf{I}_M + \frac{\beta}{N} \cdot \mathbf{H}(k, f) \cdot \mathbf{H}^H(k, f) \right] df, \quad \text{bps/Hz}, \quad (2.32)$$

where W is the one-sided bandwidth of the baseband signal, β is the average SNR at each receiver branch, and $\mathbf{H}(k, f)$ is the time-varying frequency-dependent transfer function matrix given by

$$\mathbf{H}(k, f) = \sum_{l=-L_1}^{L_2} \mathbf{H}_l(k) z^{-l} \Bigg|_{z=\exp(j2\pi f T_s)}. \quad (2.33)$$

Obviously, the channel capacity C is a function of $\mathbf{H}(k, f)$, which is random for each channel realization. Hence, C can be treated as a random variable. The outage capacity, which is defined as the probability that a specified value of C cannot be achieved, is used to evaluate the capacity of the channel. It can be represented by the complementary cumulative distribution function (ccdf) of the random capacity C .

We take the UMTS system as an example. The power delay profile is chosen to be the Vehicular Channel A profile specified in [23]. The transmit and receive filters are RRC filters with roll-off factor 0.22, and the sampling period is the same as the chip period $0.26042\mu s$ [23]. The matrix \mathbf{C}_{ISI} can be calculated based on (2.22) but details are omitted here for brevity. For the convenience of illustration purpose, the elements

of the correlation coefficient matrices Ψ_{Tx} and Ψ_{Rx} are simply chosen to be exponential correlation matrix [39] as follows

$$\rho_{Rx}^{(m,p)} = r^{|m-p|}, \quad \rho_{Tx}^{(n,q)} = r^{|n-q|}, \quad |r| \leq 1. \quad (2.34)$$

The capacity cdf's of MIMO channels under different correlation coefficients $r = 0, 0.5, 1.0$, and different number of antennas with $M = N$ are shown in Figure 2.6, where the SISO flat fading channel is included for comparison purposes. It is noted that the number of receive antennas M and the number of transmit antennas N are indicated by (M, N) in the figure's legend. As can be seen, when $M = N$, the MIMO channel capacity is linearly growing with M when $r \leq 0.5$, and the growing rate depends on the value of r (the smaller r is, the larger the growth rate). This shows that the spatial correlation of the MIMO channel has a strong impact on the channel capacity. This observation for a frequency selective channel is in good agreement with the results presented in [24] for Rayleigh flat fading.

The capacity cdf's of flat fading channels, and the Vehicular A profile with M -to- N ratio being constant and $r = 0.5$ are plotted in Figure 2.7 to compare the flat fading and frequency selective fading's impact on the channel capacity. As can be seen, for 10% or less outage capacity, *i.e.*, the probability(capacity > abscissa) ≥ 0.9 , the frequency selective fading channels always have a larger capacity than the flat fading channels. This supports the view point that the rich scattering environment (multipaths) provides higher channel capacity [38]. It is also observed that when $M \neq N$ but M/N is constant, the MIMO channel capacity is still linearly growing with M for both flat fading and frequency selective fading.

The capacity cdf's of the flat fading channel, and Vehicular Channel A profile with N being fixed and M being fixed are plotted in Figures 2.8 and 2.9, respectively. It can be observed from Figure 2.8 that the channel capacity is approximately linearly changing with $\log_2 M$ when $M \geq N$ and N is fixed. It can also be concluded from Figure 2.9 that the channel capacity is linearly changing with $\log_2 N$ when $N \leq M$ and M is fixed. It should be pointed out that the MIMO channel capacity results reported in [1], [2], and [40] are only for i.i.d. flat Rayleigh fading channels. Hence, our simulation results

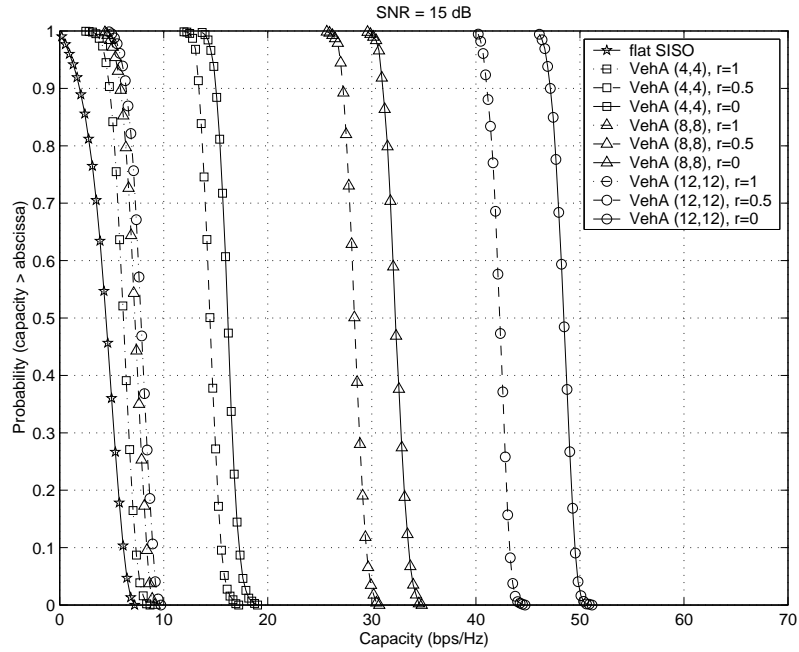


Figure 2.6: The capacities of MIMO channels with different spatial correlation coefficients and $M = N$. Dash dot lines stand for $r = 1$, dash lines for $r = 0.5$, and solid lines for $r = 0$. Observation: The channel capacity is linearly scaling with M when $r \leq 0.5$, and the scaling rate is depending on the value of r .

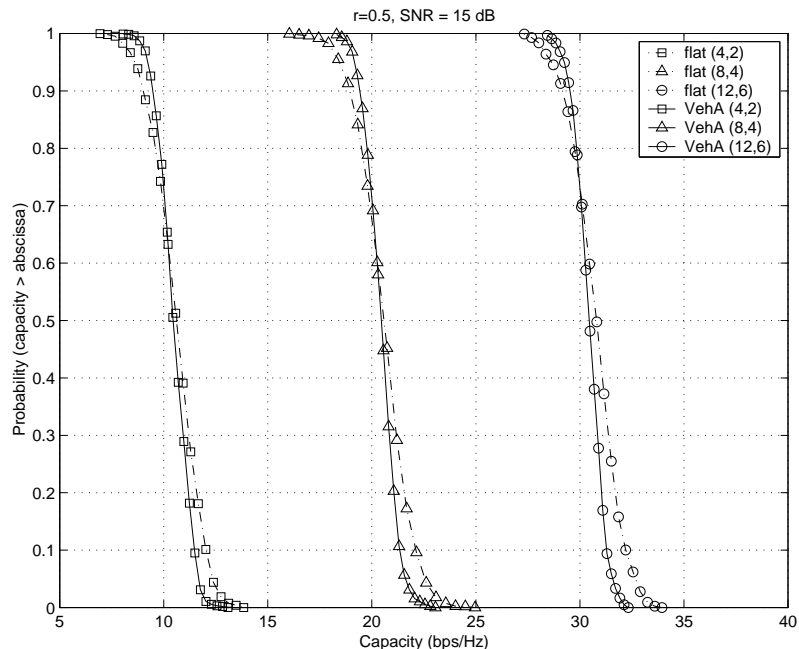


Figure 2.7: The capacities of MIMO channels with different delay power profiles, M -to- N ratio being constant, and $r = 0.5$. Observation: The channel capacity is linearly scaling with M .

are valuable observations for triply selective MIMO Rayleigh fading channels.

Finally, it is noted that the MIMO channel capacity with continuous-time models have also been performed by extensive simulations, and the results are all nearly identical to those obtained with the discrete-time model. This further verifies the statistical equivalence of the discrete-time and continuous-time channel models. However, with the discrete-time MIMO channel model, the outage capacity for the MIMO channel can be easier and more efficiently evaluated.

2.5 Conclusions

We have proposed a new discrete-time channel model for MIMO systems over space-selective (or spatially correlated), time-selective (or time-varying), and frequency-selective Rayleigh fading channels, which are referred to as triply selective Rayleigh fading channels. The stochastic channel coefficients of the new MIMO channel model have the same

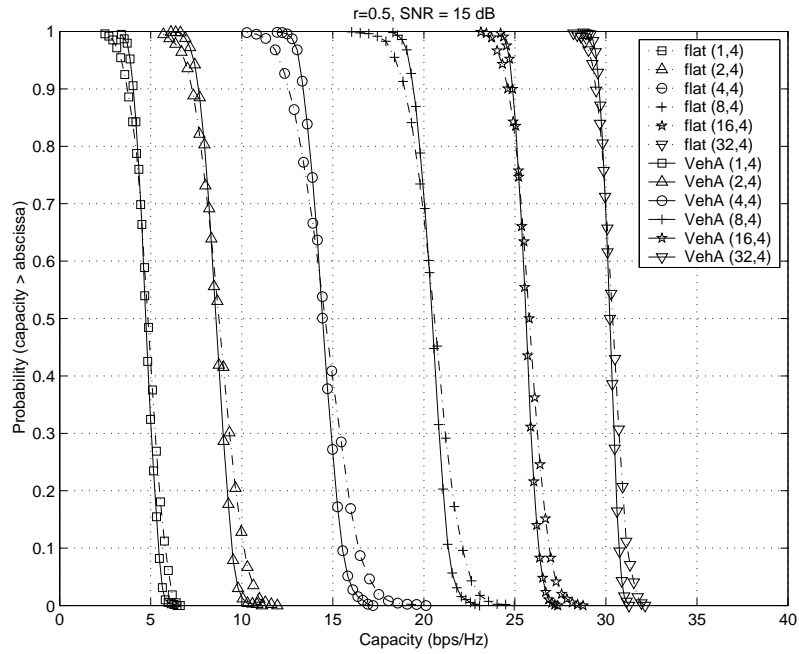


Figure 2.8: The capacities of MIMO channels with N being fixed. Dash dot lines stand for flat fading, solid lines for Vehicular Channel A profile. Observation: The channel capacity is approximately linearly scaling with $\log_2 M$ when $M \geq N$.

sampling period as that of the MIMO receiver, and they can be efficiently generated from a new method, presented in this chapter. The proposed approach combines the effects of the transmit filter, the physical MIMO channel multipath fading, and the receive filter. The new model is computationally efficient to describe the input-output of MIMO channels, because it does not need to oversample the fractionally delayed multipath channel fading, the transmit filter, and the receive filter. It is shown through analysis and simulation that the discrete-time stochastic channel coefficients of different individual subchannels with different delays are generally *statistically correlated* even if the physical channels have WSSUS multipath fading. The knowledge of this correlation may be used for improving the channel estimation of MIMO systems. The statistical accuracy of the discrete-time channel model is rigorously confirmed by extensive simulations in terms of second-order statistics and BER performance of a system that uses the model. The discrete-time MIMO channel model is further used to evaluate the MIMO channel capacity under a triply selective Rayleigh fading environment. For the high

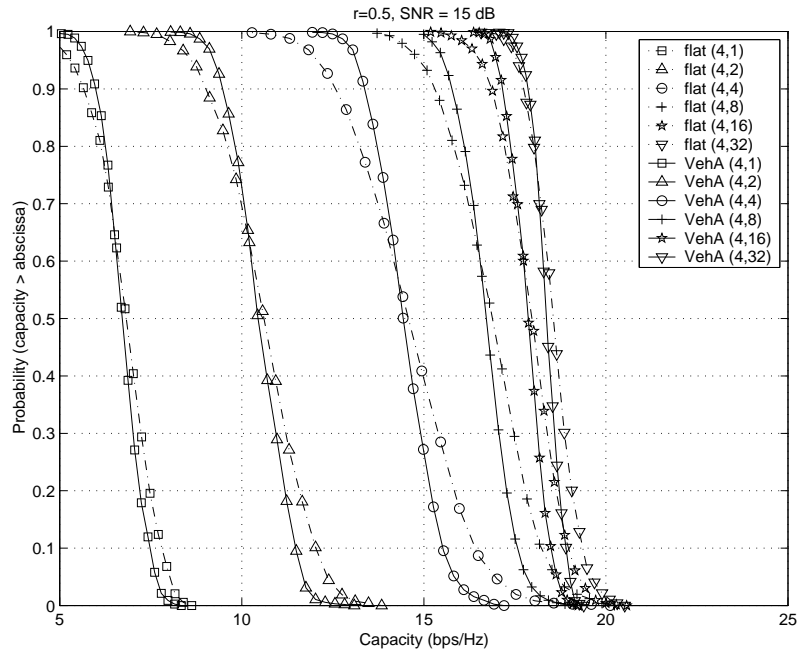


Figure 2.9: The capacities of MIMO channels with M being fixed. Dash dot lines stand for flat fading, solid lines for Vehicular Channel A profile. Observation: The channel capacity is linearly scaling with $\log_2 N$ when $N \leq M$.

SNR scenario, from the simulation experiments, we have three observations: 1) when the number of receive antennas M is the same as the number of transmit antennas N , or when M/N is constant, the MIMO channel capacity vary in a linear fashion with M ; 2) when N is fixed, the MIMO channel capacity increases approximately linearly with $\log_2 M$ when $M \geq N$; 3) when M is fixed, the MIMO channel capacity is linearly scaling with $\log_2 N$ when $N \leq M$. However, the scaling rates for all the three cases are dependent on the spatial correlation coefficients (the less correlation, the larger the scaling rate). Our observations are therefore valuable extensions to the capacity results of triply selective MIMO Rayleigh fading channels from the special case of quasi-static, i.i.d., flat Rayleigh fading MIMO channels.

Chapter 3

Multuser Channel Estimation for CDMA Systems over Doubly Selective Fading Channels

3.1 Introduction

In a code division multiple access (CDMA) communication system, multiple users can access a given frequency bandwidth simultaneously with different pre-assigned spreading codes, which may lead to multi-user interference (MUI) due to the non-perfect orthogonality of the spreading codes. Multiuser detectors [41], [42] can mitigate this problem by exploiting the information of all users present in the system, and substantial performance gain can be obtained over single-user detectors. Most of the works on multiuser detectors require knowledge of the multiuser channel states information, and this necessitates the research of multiuser channel estimation.

The topic of channel estimation for CDMA systems has received considerable attentions in [43]- [60]. Among them, the subspace-based blind channel estimation methods were proposed in the literature [43]- [45], [53], [59] to obtain channel parameters by exploiting the orthogonality of the signal and noise subspaces. The maximum-likelihood (ML)-based techniques were discussed in [47], [50], [51] and [58] for single-user channel and/or multiuser channel estimation with training symbols or pilots. The Kalman filter-based

methods were considered in [49] and [57] to estimate and track time-varying channels, where a relatively long training sequence is required to ensure the proper identification of the Kalman filter parameters. The minimum mean square error methods were employed in [56] and [60] to estimate fading channels by using training sequences.

All the aforementioned algorithms appeared to work fine under certain assumptions on the fading channels to be estimated. Specifically, it was assumed in [43]- [47], [50], [51], [53]- [56] that the fading channels are *time-invariant* frequency selective during the entire estimation block. In [49] and [52], the fading channels were assumed to be symbol-wise time-varying (*i.e.*, channel varies from symbol to symbol and keeps constant within one symbol period) but *frequency flat*. In [60], both time-varying and frequency selective channel was considered under the assumption that the delay spread and Doppler spread are known to the receiver. Moreover, most of the existing algorithms assumed that the transmit pulse shaping filter and receive matched filter are rectangular waveforms with a single chip duration. This is quite different from the bandwidth-limited root-raised cosine pulses adopted by the current and emerging CDMA wireless systems such as IS-95, cdma2000 [61] and UMTS [23]. The rectangular shaping pulse assumption certainly leads to simple system models to explore new algorithms for channel estimation, but it implies unlimited bandwidth, which is not the case in practice. Additionally, it is commonly assumed that, for a wide-sense stationary uncorrelated scattering (WSSUS) channel, the uncorrelated multipaths are chip spaced [36], which is generally not common in practice due to the random nature of multipaths. This assumption leads the fading channels to be represented as tapped delay line filters whose taps are statistically uncorrelated [56], [57] and [36]. However, it was shown in Chapter 2 that when fractionally spaced WSSUS multipaths pass through the bandwidth-limited and/or time-limited receive filter and the chip-rate sampling (or any other rate sampling after the matched filter), the equivalent discrete-time time-varying channel taps are generally correlated. This inter-tap correlation can affect the system performance dramatically if it is not carefully taken.

In this chapter, we focus on the multiuser channel estimation for quasi-synchronous

CDMA (QS-CDMA)¹ systems under a time-varying and frequency selective fading environment. The composite fading channel response, which combines the effects of the transmit filter, the physical frequency selective fading channel and the receive filter of each user in the QS-CDMA system, is represented as a tapped delay line filter with *correlated* tap coefficients, which is different from the system models presented in [56], [57], [36], where uncorrelated tap coefficients were employed. Moreover, we will show that the channel inter-tap correlation is critical to the performance of the channel estimation. Utilizing the channel inter-tap correlation information, we propose a minimum mean square error (MMSE) multiuser channel estimation algorithm, with the knowledge of the pilot symbols and spreading code of each user. In the development of the algorithm, the channel inter-tap correlation is treated as an essential factor, and efforts are put to preserve this information in the estimated channels. An iterative method is proposed for the joint estimation of the channel inter-tap correlation and the channel tap timing based on the received samples, and these parameters are used to form the MMSE algorithm. Simulation results show that the bit error rate (BER) performance of a CDMA system with our proposed multiuser channel estimation algorithm is close to that of a CDMA system with perfect multiuser channel knowledge.

The rest of this chapter is organized as follows. Section 3.2 presents a discrete-time representation of the multiuser CDMA system with correlated channel taps. In Section 3.3, multiuser channel estimation algorithms are summarized for a CDMA system with pilot symbol assisted modulation. Section 3.4 discusses the estimation of the channel statistics required by the MMSE algorithm, and a novel iterative method is presented for the joint estimation of the channel inter-tap correlation and channel tap timing information. Simulation results are given in Section 3.5, and Section 3.6 concludes the chapter.

¹In a QS-CDMA system, the uncertainty of the relative transmission delay of each user is limited to a few chip periods, which can be achieved with the use of a GPS receiver at the base station and mobile stations, [57], [63], [64].

3.2 Discrete-time System Model

Based on the general discrete-time MIMO channel model presented in Chapter 2, a discrete-time model of the multiuser CDMA system is described in this section. We consider the up-link of a multiuser CDMA system consisting of M users. The transmitted signal $s_m(t)$ of the m th user is given by

$$s_m(t) = \sqrt{\frac{P_m}{N}} \sum_{i=-\infty}^{+\infty} \sum_{k=0}^{N-1} b_m(i) \cdot c_m(k) \cdot p_T(t - iT_s - kT_c), \quad (3.1)$$

where P_m is the average transmit power of the m th user, N is the processing gain, T_c is the chip period, $T_s = NT_c$ is the symbol period, $\mathbf{c}_m = [c_m(0), c_m(1), \dots, c_m(N-1)]^T \in \mathbb{C}^{N \times 1}$ is the m th user's spreading code² with $(\cdot)^T$ denoting matrix transpose, $b_m(i)$ is the i th transmit data (or pilot) symbol, and $p_T(t)$ is the normalized root raised cosine (RRC) filter with $\int_{-\infty}^{\infty} p_T(t)p^*(t)dt = 1$. The spreading code \mathbf{c}_m satisfies $\mathbf{c}_m^H \mathbf{c}_m = N$, with $(\cdot)^H$ representing the Hermitian transpose. In a system with pilot symbol assisted modulation (PSAM), the transmit symbols $b_m(i)$ of each user are divided into slots, with the pilot symbols being distributed within each slot.

Let $g_m(t, \tau)$ be the time-varying fading channel impulse response for the m th user, then at the base station, the received signal $r(t)$ is the superposition of the fading distorted signals from all the M users plus the additive noise. $r(t)$ can be expressed as follows

$$r(t) = \sum_{m=1}^M s_m(t - \Delta_m) \otimes g_m(t, \tau) + v(t), \quad (3.2)$$

where \otimes denotes the convolution operation, Δ_m is the differential transmission delay experienced by the m th user, and $v(t)$ is the additive white Gaussian noise (AWGN) with variance N_0 . For a quasi-synchronous system, the relative delay Δ_m is assumed to be uniformly distributed within $[-DT_c, +DT_c]$ with $D \ll N$ [57]. The received signal $r(t)$ is passed through the receive filter $p_R(t) = p_T^*(-t)$, which is matched to the transmit

²The normalized signature waveform of the m th user is given by $w_m(t) = \frac{1}{\sqrt{N}} \sum_{k=0}^{N-1} c_m(k) p_T(t - kT_c)$.

filter $p_T(t)$, and the output $y(t) = r(t) \otimes p_T^*(-t)$ can be expressed by

$$y(t) = \sqrt{\frac{P_m}{N}} \sum_{m=1}^M \sum_{i=-\infty}^{+\infty} \sum_{k=0}^{N-1} b_m(i) c_m(k) \times \int_{-\infty}^{\infty} R_{pp}(t - iT_s - kT_c - \Delta_m - \alpha) g_m(t, \alpha) d\alpha + z(t), \quad (3.3)$$

where

$$\begin{aligned} R_{pp}(t) &= \int_{-\infty}^{\infty} p_T(t + \tau) p_T^*(\tau) d\tau, \\ z(t) &= v(t) \otimes p_T^*(-t). \end{aligned}$$

If we define the m th user's composite channel impulse response (CIR) $h_m(t, \tau)$ as

$$h_m(t, \tau) = \int_{-\infty}^{+\infty} R_{pp}(\tau - \Delta_m - \alpha) g_m(t, \alpha) d\alpha, \quad (3.4)$$

then the chip-rate sampled output of the matched filter can be written by

$$\begin{aligned} y_j(n) &= \sqrt{\frac{P_m}{N}} \sum_{m=1}^M \sum_{i=-\infty}^{+\infty} \sum_{k=0}^{N-1} b_m(i) \cdot c_m(k) \cdot h_m[jN + n, (j - i)N + (n - k)] + z_j(n), \\ &= \sqrt{\frac{P_m}{N}} \sum_{m=1}^M \sum_{i=-\infty}^{+\infty} \sum_{l=-\infty}^{+\infty} b_m(i) \cdot c_m[(j - i)N + (n - l)] \cdot h_m(jN + n, l) + z_j(n), \end{aligned}$$

for $n = 0, 1, \dots, N - 1$; $j = 1, 2, 3, \dots$ (3.5)

where $y_j(n)$ is the n th chip-rate sample of j th data symbol of $y(t)$ with $t = jT_s + nT_c$, and $z_j(n)$ is the chip-rate sample of $z(t)$ at the time instant $t = jT_s + nT_c$. Likewise, $h_m(jN + n, l) = h_m(jT_s + nT_c, lT_c)$ is the discrete-time version of the CIR $h_m(t, \tau)$, and we set $l = (j - i)N + (n - k)$ in the second equality. The noise component $z_j(n)$ is still AWGN with variance N_0 because the chip matched filter $p_T^*(-t)$ is normalized RRC filter.

To simplify the representation of (3.5), we note that the chip index k of $c_m(k)$ satisfies $0 \leq k < N$. Combining this inequality with $k = (j - i)N + (n - l)$, we can immediately get

$$j + \frac{n - l}{N} - 1 < i \leq j + \frac{n - l}{N}, \quad (3.6)$$

where i is the symbol index of the transmitted symbol $b_m(i)$, and it can only take integer values. In the range of i described in (3.6), there exists one and only one integer value, which must be $i = j + \lfloor \frac{n-l}{N} \rfloor$, where $\lfloor \cdot \rfloor$ denotes rounding to the nearest smaller integer. Substituting the value of i to $k = (j - i)N + (n - l)$, we can get

$$k = -\lfloor \frac{n-l}{N} \rfloor N + (n-l) = (n-l)_N, \quad (3.7)$$

where $(x)_N$ can be viewed as the residue of x/N with $0 \leq (x)_N \leq N - 1$. The above analysis leads to a simplified representation of (3.5)

$$\begin{aligned} y_j(n) &= \sqrt{\frac{P_m}{N}} \sum_{m=1}^M \sum_{l=-\infty}^{+\infty} b_m \left(j + \lfloor \frac{n-l}{N} \rfloor \right) \cdot c_m [(n-l)_N] \cdot h_m(jN + n, l) + z_j(n), \\ &= \sqrt{\frac{P_m}{N}} \sum_{m=1}^M \sum_{l=-\infty}^{+\infty} d_m(j, l, n) \cdot h_m(jN + n, l) + z_j(n), \end{aligned} \quad (3.8)$$

where $d_m(j, l, n) = b_m \left(j + \lfloor \frac{n-l}{N} \rfloor \right) \cdot c_m [(n-l)_N]$. The relationship of j , n and l is illustrated in Fig. 3.1, where the l th delayed version of the transmitted symbols is given as an example, and the corresponding sampling time is $t = jT_s + (n-l)T_c$.

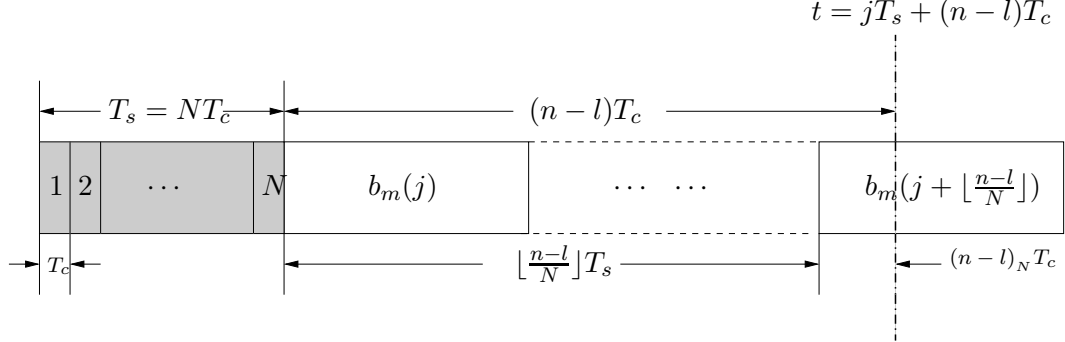


Figure 3.1: The l th delayed version of the transmitted symbols.

In the discrete-time system (3.8), the chip-wise time-varying and frequency selective fading channel coefficients are represented by $h_m(jN + n, l)$, where l is the channel tap index, j is the symbol index, n is the chip index within a symbol. Utilizing the same procedure described in Chapter 2, we can prove that the channel tap coefficients $h_m(j_1N + n_1, l_1)$ and $h_m(j_2N + n_2, l_2)$ are both temporally correlated and inter-tap correlated in a Rayleigh fading channel. If the physical channel $g_m(t, \tau)$ experiences

WSSUS Rayleigh fading in which $g_m(t, \tau)$ is a zero mean complex Gaussian random variable with autocorrelation given by $E[g_m(t_1, \tau) \cdot g_m^*(t_2, \tau')] = J_0[2\pi f_d \cdot (t_1 - t_2)] \cdot G_m(\tau) \cdot \delta(\tau - \tau')$, where $J_0(\cdot)$ is the zero-order Bessel function of the first kind, f_d is the maximum Doppler frequency, $G_m(\mu)$ is normalized power delay profile of the channel with $\int_{-\infty}^{+\infty} G_m(\mu) d\mu = 1$, then the cross-correlation between $h_m(j_1N + n_1, l_1)$ and $h_m(j_2N + n_2, l_2)$ contains the temporal correlation and inter-tap correlation as follows

$$\mathbb{E}[h_m(j_1N + n_1, l_1)h_m^*(j_2N + n_2, l_2)] = J_0[2\pi f_d(j_1N - j_2N + n_1 - n_2)T_c] \rho_m(l_1, l_2), \quad (3.9)$$

where $\rho_m(l_1, l_2)$ is the inter-tap correlation coefficient given by (c.f. eqn. (2.17))

$$\rho_m(l_1, l_2) = \int_{-\infty}^{+\infty} R_{pp}(l_1T_c - \Delta_m - \mu)R_{pp}^*(l_2T_c - \Delta_m - \mu)G_m(\mu)d\mu. \quad (3.10)$$

We will show in this chapter that the inter-tap correlations can be exploited to enhance channel estimation accuracy. To achieve our objective, we would like to simplify the discrete-time system (3.8) with taking some practical issues into considerations.

In (3.8), we assumed that the discrete-time channel $h_m(jN + n, l)$ is a non-causal infinite impulse response (IIR) filter, where the tap index $l \in (-\infty, +\infty)$ for all j and m . The validity of this assumption lies in the fact that the time duration of the RRC filter $p(t)$ is infinite in theory to have a limited frequency bandwidth. In practice, the time-domain tails of RRC filter $p(t)$ falls off rapidly, and the physical channel impulse response $g_m(t, \tau)$ has finite support in the τ domain. Thus, the amplitude of $h_m(k, l)$ will decrease quickly with the increase of $|l|$. When a channel tap coefficient's average power (or squared amplitude) is smaller than a certain threshold, this tap has very little impact on the output signals, and thus it can be discarded. Therefore, the time-varying non-causal IIR channel can be truncated to a finite impulse response (FIR) channel. Without loss of generality, we use $\mathbf{l}_m = [-L_{m1}, \dots, L_{m2}]^T \in \mathbb{I}^{\lambda_m \times 1}$ to represent the tap index vector of the m th user ³, where L_{m1} and L_{m2} are non-negative integers, and λ_m is the length of the vector. Furthermore, it is pointed out that the chip-wise time-varying

³It should be noted that the non-causality of the discrete-time channel model is due to the effects of transmit filter and receive filter, and the physical fading channel is always causal. Moreover, the non-causal effects of the discrete-time channel model can be removed by introducing proper delays at the receiver.

frequency selective Rayleigh fading coefficient $h_m(jN+n, l)$ in (3.8) can be approximated by symbol-wise time-varying frequency selective Rayleigh fading coefficient $h_m(jN, l)$ if $f_d T_s \ll 1$, because in this case the symbol duration T_s is much shorter than the channel coherence time $\frac{1}{f_d}$. It is noted that the condition $f_d T_s \ll 1$ is generally valid for the current third generation (3G) CDMA systems. For example, in a worst scenario, a UMTS mobile handset with 2GHz carrier frequency travels at a high speed of 120 km/h, the maximum Doppler frequency $f_d = 222$ Hz. For a high spreading gain $N = 512$, the symbol duration $T_s = 512T_c = 13.33$ ms, and therefore $f_d T_s = 0.0296 \ll 1$. Based on these two aforementioned arguments, we can now simplify (3.8) as follows

$$y_j(n) = \sqrt{\frac{P_m}{N}} \sum_{m=1}^M \sum_{l=-L_{m1}}^{L_{m2}} d_m(j, l, n) \cdot h_m(jN, l) + z_j(n). \quad (3.11)$$

We define the multiuser channel tap coefficient vector $\mathbf{h}(j)$ as follows

$$\mathbf{h}(j) = [\mathbf{h}_1(j)^T, \mathbf{h}_2(j)^T, \dots, \mathbf{h}_M(j)^T]^T, \quad (3.12)$$

where $\mathbf{h}_m(j) = [h_m(jN, -L_{m1}), \dots, h_m(jN, L_{m2})]^T$ is the channel tap coefficient vector of the m th user. Then (3.11) can be written into a matrix format as follows

$$\mathbf{y}(j) = \mathbf{D}(j) \cdot \mathbf{h}(j) + \mathbf{z}(j), \quad (3.13)$$

where $\mathbf{y}(j) = [y_j(0), y_j(1), \dots, y_j(N-1)]^T$ and $\mathbf{z}(j) = [z_j(0), z_j(1), \dots, z_j(N-1)]^T$ are the received sample vector and the additive noise vector of the j th symbol, respectively, and the matrix $\mathbf{D}(j) = \begin{bmatrix} \mathbf{D}_1(j) & \mathbf{D}_2(j) & \dots & \mathbf{D}_M(j) \end{bmatrix} \in \mathbb{C}^{N \times \lambda}$ is made up of the data and spreading codes of all the users. The sub-matrix $\mathbf{D}_m(j)$ related to the m th user is defined by

$$\mathbf{D}_m(j) = \sqrt{\frac{P_m}{N}} \cdot [\mathbf{d}_m(j, -L_{m1}), \mathbf{d}_m(j, -L_{m1} + 1), \dots, \mathbf{d}_m(j, L_{m2})], \quad (3.14)$$

with the n th element of the vector $\mathbf{d}_m(j, l) \in \mathbb{C}^{N \times 1}$ being $d_m(j, l, n)$, for $n = 1, 2, \dots, N$. Eqn. (3.13) is a discrete-time representation of the multiuser CDMA system, and the time-varying and frequency selective fading channel is represented as a T_c -spaced tapped delay line filter. With this representation, the necessary knowledge of the multiuser

channel is the set of symbol-wise time-varying coefficients characterizing each path of the channel, and the problem of multiuser channel estimation is converted to the estimation of the time-varying channel coefficients $h_m(jN, l)$ and the T_c -spaced delay index vector \mathbf{l}_m . It should be noted from (3.4) that the relative delay Δ_m of each user is incorporated into the representation of the discrete-time CIR $h_m(jN, l)$. With the estimation of $\mathbf{h}(j)$ and \mathbf{l}_m , there is no need to explicitly recover the relative transmission delay Δ_m of all the users.

3.3 Multiuser Channel Estimation

In this section, we focus on the estimation of the channel coefficients at pilot positions, which will be interpolated to obtain the time-varying channel coefficients over one entire slot. In order to exploit the channel inter-tap correlation information, the proposed algorithm is based on the MMSE criterion, which is capable of utilizing and preserving the inter-tap correlation information of the fading channel.

We assume that the physical fading channels of different users are uncorrelated to each other, then the multiuser channel inter-tap correlation matrix $\mathbf{R}_h = \mathbb{E}[\mathbf{h}(j)\mathbf{h}^H(j)]$ can be written as

$$\mathbf{R}_h = \begin{bmatrix} \mathbf{R}_{h_1} & 0 & \cdots & 0 \\ 0 & \mathbf{R}_{h_2} & \cdots & 0 \\ \vdots & \vdots & \ddots & \vdots \\ 0 & 0 & \cdots & \mathbf{R}_{h_M} \end{bmatrix}, \quad (3.15)$$

where $\mathbf{R}_{h_m} = \mathbb{E}[\mathbf{h}_m(j)\mathbf{h}_m^H(j)] \in \mathbb{C}^{\lambda_m \times \lambda_m}$ is the inter-tap correlation matrix of the m th user. With the definition of $\mathbf{h}_m(j)$ and (3.9), \mathbf{R}_{h_m} can be written as

$$\mathbf{R}_{h_m} = \begin{bmatrix} \rho_m(-L_{m1}, -L_{m1}) & \cdots & \rho_m(-L_{m1}, L_{m2}) \\ \vdots & \ddots & \vdots \\ \rho_m(L_{m2}, -L_{m1}) & \cdots & \rho_m(L_{m2}, L_{m2}) \end{bmatrix}. \quad (3.16)$$

It can be seen from (3.10) and (3.16) that the multiuser channel inter-tap correlation matrix \mathbf{R}_h is a function of the power delay profile $G_m(\mu)$, the relative transmission delay

Δ_m , and the tap delay index vector \mathbf{l}_m . These parameters are usually unavailable at the receiver. Therefore, \mathbf{R}_h is generally not known to the receiver. In this section, we focus on the formulation of the MMSE-based channel estimation algorithm. The estimation of \mathbf{R}_h will be discussed in the next section.

For a QS-CDMA system, it is assumed that all the users are slot synchronized, and the received signals at pilot positions are the superposition of the faded pilot symbols of all the users. For convenience of representation, the symbol ‘1’ is used as pilot symbols. According to (3.11), the received samples contributed exclusively by pilot symbols can be written as

$$\mathbf{y}(j_p) = \mathbf{C}\mathbf{h}(j_p) + \mathbf{z}(j_p), \quad (3.17)$$

where j_p is the index of the p th pilot symbol for a slot with P pilot symbols, $\mathbf{y}(j_p) = [y_{j_p}(0), y_{j_p}(1), \dots, y_{j_p}(N-1)]^T$, $\mathbf{z}(j_p) = [z_{j_p}(0), z_{j_p}(1), \dots, z_{j_p}(N-1)]^T$, and the multiuser code matrix \mathbf{C} is defined by

$$\mathbf{C} = [\mathbf{C}_1 \vdots \mathbf{C}_2 \vdots \dots \vdots \mathbf{C}_M] \quad (3.18)$$

with

$$\mathbf{C}_m = [\mathbf{c}_m(-L_{m1}), \dots, \mathbf{c}_m(L_{m2})], \quad (3.19)$$

where $\mathbf{c}_m(i) = [c_m(N-i), \dots, c_m(N-1), c_m(0), \dots, c_m(N-i-1)]^T$ is obtained from circularly shifting i symbols of the original code vector \mathbf{c}_m . It is important to note that the multiuser code matrix \mathbf{C} is determined by both the spreading codes and the tap delay index vector \mathbf{l}_m . For a multiuser detector, the spreading code of each user is known to the base station, while \mathbf{l}_m needs to be estimated. We will show in the next section that \mathbf{l}_m can be jointly estimated with \mathbf{R}_h based on a novel iterative method.

Based on (3.17), we can immediately obtain the multiuser channel estimation at pilot symbol locations by utilizing least-squares (LS) method [69],

$$\hat{\mathbf{h}}_{LS}(j_p) = \mathbf{C}^\dagger \mathbf{y}(j_p), \quad \text{for } p = 1, 2, \dots, P, \quad (3.20)$$

where \mathbf{C}^\dagger is the pseudo-inverse of the multiuser code matrix \mathbf{C} , j_p is the position index of the p th pilot symbol in a slot with P pilot symbols.

It's apparent from (3.20) that the multiuser channel tap correlation matrix \mathbf{R}_h is not utilized in the LS estimation of the channel. To increase the channel estimation accuracy, we resort to the MMSE estimate of the multiuser channel tap $\mathbf{h}(j_p)$ from the corresponding received vector $\mathbf{y}(j_p)$ and the multiuser code matrix \mathbf{C} , and the corresponding cost function is defined as

$$\phi = \mathbb{E} \left\{ [\mathbf{h}(j_p) - \hat{\mathbf{h}}(j_p)]^H [\mathbf{h}(j_p) - \hat{\mathbf{h}}(j_p)] | \mathbf{y}(j_p), \mathbf{C} \right\}. \quad (3.21)$$

The solution that minimize ϕ is

$$\hat{\mathbf{h}}(j_p) = \mathbb{E}[\mathbf{h}(j_p) | \mathbf{y}(j_p), \mathbf{C}]. \quad (3.22)$$

For Rayleigh fading channel, it can be seen from (3.17) that $\mathbf{h}(j_p)$ and $\mathbf{y}(j_p)$ conditioned on \mathbf{C} are jointly zero-mean Gaussian distributed, therefore the conditional mean in (3.22) is a linear function of $\mathbf{y}(j_p)$, then $\hat{\mathbf{h}}(j_p)$ can be written as

$$\hat{\mathbf{h}}(j_p) = \mathbf{\Lambda}(j_p) \mathbf{y}(j_p), \quad (3.23)$$

where $\mathbf{\Lambda}(j_p)$ is the MMSE estimation matrix. Substitute (3.23) in (3.21), the MMSE solution of $\mathbf{\Lambda}(j_p)$ can be derived as

$$\mathbf{\Lambda}(j_p) = \mathbb{E} [\mathbf{h}(j_p) \mathbf{y}^H(j_p)] \cdot \left\{ \mathbb{E} [\mathbf{y}(j_p) \mathbf{y}^H(j_p)] \right\}^{-1} \quad (3.24)$$

From (3.17) and the fact that $z_j(n)$ is AWGN with variance N_0 , we can get

$$\mathbb{E}[\mathbf{y}(j_p) \mathbf{y}^H(j_p)] = \mathbf{C} \mathbf{R}_h \mathbf{C}^H + N_0 \mathbf{I}_N, \quad (3.25)$$

$$\mathbb{E}[\mathbf{h}(j_p) \mathbf{y}^H(j_p)] = \mathbf{R}_h \mathbf{C}^H, \quad (3.26)$$

where \mathbf{I}_N is an $N \times N$ identity matrix, and \mathbf{R}_h is the multiuser channel inter-tap correlation matrix defined in (3.15). Combining (3.24) - (3.26), the MMSE estimation matrix $\mathbf{\Lambda}(j_p)$ can be written as

$$\mathbf{\Lambda}(j_p) = \mathbf{R}_h \mathbf{C}^H \cdot [\mathbf{C} \mathbf{R}_h \mathbf{C}^H + N_0 \mathbf{I}_N]^{-1}. \quad (3.27)$$

It can be seen from (3.27) that $\mathbf{\Lambda}(j_p)$ is independent of the variable j_p , hence we denote it as $\mathbf{\Lambda}$.

With (3.23) and (3.27), we can get the MMSE-based estimation of the multiuser channel tap coefficients $\mathbf{h}(j_p)$ at pilot symbol positions,

$$\hat{\mathbf{h}}_{MMSE}(j_p) = \mathbf{R}_h \mathbf{C}^H \cdot [\mathbf{C} \mathbf{R}_h \mathbf{C}^H + N_0 \mathbf{I}_N]^{-1} \cdot \mathbf{y}(j_p), \quad \text{for } p = 1, 2, \dots, P. \quad (3.28)$$

To fulfill the MMSE-based channel estimation, we need to know the multiuser channel inter-tap correlation matrix \mathbf{R}_h , the delay index vector \mathbf{l}_m , and the additive noise variance N_0 . The estimation of these parameters are discussed in the next section.

For comparison purpose, a pilot assisted subspace-based estimation of $\mathbf{h}(j_p)$ for quasi-static multiuser fading channels is derived in Appendix A.

3.4 MMSE-parameter Estimation

In this section, we consider the estimation of the multiuser channel inter-tap correlation matrix \mathbf{R}_h , the tap delay index vector \mathbf{l}_m , and the additive noise variance N_0 . The noise variance N_0 is estimated by exploiting the eigen structure of the received signals. Likewise, the matrix \mathbf{R}_h and the vector \mathbf{l}_m are jointly estimated by a novel iterative method.

3.4.1 Estimation of the Additive Noise Variance N_0

The variance N_0 of the additive noise component $\mathbf{z}(j)$ can be extracted by exploiting the eigen structure of the channel correlation matrix with the help of the temporal correlation of the fading channel.

According to the input-output relationship of the pilot symbols described in (3.17), the correlation matrix of the received pilot symbols $\mathbf{R}_{y_p} = \mathbb{E}[\mathbf{y}(j_p) \mathbf{y}^H(j_p)]$ can be written by

$$\mathbf{R}_{y_p} = \mathbf{C} \mathbf{R}_h \mathbf{C}^H + N_0 \mathbf{I}_N. \quad (3.29)$$

Within one slot duration, the correlation matrix \mathbf{R}_{y_p} and \mathbf{R}_h can be approximated by

their sample means

$$\widehat{\mathbf{R}}_{y_p} = \frac{1}{P} \sum_{p=1}^P \mathbf{y}(j_p) \mathbf{y}^H(j_p), \quad (3.30a)$$

$$\widehat{\mathbf{R}}_h = \frac{1}{P} \sum_{p=1}^P \mathbf{h}(j_p) \mathbf{h}^H(j_p). \quad (3.30b)$$

Correspondingly, the correlation matrix of the received pilot symbols can be approximated by (c.f. eqn. (3.29))

$$\widehat{\mathbf{R}}_{y_p} = \mathbf{C} \widehat{\mathbf{R}}_h \mathbf{C}^H + N_0 \mathbf{I}_N. \quad (3.31)$$

In order to estimate the noise variance N_0 from (3.31), we need to exploit the eigen structure of $\widehat{\mathbf{R}}_h$, which is the sum of P correlated random matrices as described in (3.30a). According to the physical properties of the doubly-selective fading channel, we have the following theorem about the rank of the random matrix $\widehat{\mathbf{R}}_h$.

Theorem 3.1: If we define the temporal correlation matrix $\mathbf{R}_t \in \mathbb{C}^{P \times P}$ as

$$\mathbf{R}_t = \begin{bmatrix} 1 & J_0[2\pi f_d(j_1 - j_2)T_s] & \cdots & J_0[2\pi f_d(j_1 - j_P)T_s] \\ J_0[2\pi f_d(j_2 - j_1)T_s] & 1 & \cdots & J_0[2\pi f_d(j_2 - j_P)T_s] \\ \vdots & \vdots & \ddots & \vdots \\ J_0[2\pi f_d(j_P - j_1)T_s] & J_0[2\pi f_d(j_P - j_2)T_s] & \cdots & 1 \end{bmatrix}, \quad (3.32)$$

where $J_0(\cdot)$ is the zero-order Bessel function of the first kind, f_d is the maximum Doppler frequency of the time-varying fading channel, T_s is the symbol period, and j_p is the index of the p th pilot symbol of a slot with P pilot symbols, then we have the following rank inequality between the random matrix $\widehat{\mathbf{R}}_h = \frac{1}{P} \sum_{p=1}^P \mathbf{h}(j_p) \mathbf{h}^H(j_p)$ and the deterministic matrix \mathbf{R}_t

$$\text{rank}(\widehat{\mathbf{R}}_h) \leq \text{rank}(\mathbf{R}_t). \quad (3.33)$$

Proof: For each of the time-varying tap coefficient $h_m(jN, l)$ of the discrete-time channel impulse response, define the branch CIR vector $\mathbf{h}_{m,l} \in \mathbb{C}^{P \times 1}$ as

$$\mathbf{h}_{m,l} = \left[h_m(j_1 N, l) \quad h_m(j_2 N, l) \quad \cdots \quad h_m(j_P N, l) \right]^T, \quad (3.34)$$

for $l \in \mathbf{l}_m$, $m = 1, 2, \dots, M$,

where P is the number of pilot symbols of one slot. For WSSUS Rayleigh fading channel, the vectors $\mathbf{h}_{m,l}$ and $\mathbf{h}_{n,k}$ are zero-mean Gaussian distributed, and their cross-correlation matrix can be obtained from (3.9) as

$$\mathbf{R}_{ml,nk} = \mathbb{E}[\mathbf{h}_{m,l}\mathbf{h}_{n,k}^H] = \delta(m, n) \cdot \rho_m(l, k) \cdot \mathbf{R}_t, \quad (3.35)$$

where $\delta(m, l)$ is the Kronecker delta function, $\rho_m(l, k)$ is the tap correlation given in (3.10), and \mathbf{R}_t is defined in (3.32).

With (3.35), $\mathbf{h}_{m,l}$ can be equivalently represented as the linear transformation of Gaussian vector with independent and identically distributed (i.i.d.) elements

$$\mathbf{h}_{m,l} \sim \mathbf{R}_t^{1/2} \cdot \mathbf{w}_{m,l}, \quad (3.36)$$

where the symbol \sim defines an equivalence relation between two random variables if they have the same statistical distributions, the vector $\mathbf{w}_{m,l} = [w_m(1, l), w_m(2, l), \dots, w_m(P, l)]^T \sim \mathcal{N}(0, \rho_m(l, l)\mathbf{I}_P)$ is Gaussian distributed with zero-mean and covariance matrix $\rho_m(l, l) \cdot \mathbf{I}_P$, and the cross correlation matrix between $\mathbf{w}_{m,l}$ and $\mathbf{w}_{n,k}$ is $\mathbb{E}[\mathbf{w}_{m,l}\mathbf{w}_{n,k}^H] = \delta(m, n) \cdot \rho_m(l, k) \cdot \mathbf{I}_P$. The matrix $\mathbf{R}_t^{1/2}$ is the square root of \mathbf{R}_t defined as

$$\mathbf{R}_t^{1/2} = \mathcal{U}_t \cdot \Lambda_t^{1/2}, \quad (3.37)$$

where $\Lambda_t = \text{diag}\{\lambda_{t1}, \dots, \lambda_{tP}\}$ is a diagonal matrix with λ_{tp} , for $p = 1, 2, \dots, P$, being the eigen values of \mathbf{R}_t in decreasing order, and $\mathcal{U}_t = [\mathbf{u}_{t1}, \dots, \mathbf{u}_{tP}] \in \mathbb{C}^{P \times P}$ are the corresponding orthonormal eigen vectors.

From the analysis above, we can see that the family of vectors $\{\mathbf{h}_{m,l} | l \in \mathbf{l}_m, m = 1, \dots, M\}$ has exactly the same distribution as $\{\mathbf{R}_t^{1/2} \cdot \mathbf{w}_{m,l} | l \in \mathbf{l}_m, m = 1, \dots, M\}$. Therefore we have the following equivalent relation about the inner product of two branch CIR vectors

$$\mathbf{h}_{m,l}^H \cdot \mathbf{h}_{n,k} \sim \mathbf{w}_{m,l}^H (\mathbf{R}_t^{1/2})^H \cdot \mathbf{R}_t^{1/2} \mathbf{w}_{n,k}, \quad (3.38a)$$

$$\sim \sum_{p=1}^R \lambda_p w_m(p, l) w_n^*(p, k), \quad (3.38b)$$

where $R = \text{rank}(\mathbf{R}_t)$, and the equality $(\mathbf{R}_t^{1/2})^H \mathbf{R}_t^{1/2} = \Lambda_t$ from (3.37) is used in (3.38b).

Noting the fact that each element of the matrix $\widehat{\mathbf{R}}_h$ defined in (3.30b) can be written as the normalized inner product of two branch CIRs as

$$\frac{1}{P} \mathbf{h}_{m,l}^H \cdot \mathbf{h}_{n,k} = \frac{1}{P} \sum_{p=1}^P h_m(j_p, l) h_n^*(j_p, k), \quad (3.39)$$

we can replace the elements of $\widehat{\mathbf{R}}_h$ with $\frac{1}{P} \sum_{p=1}^P \lambda_p w_m(p, l) w_n^*(p, k)$ corresponding to each value of m, n, l and k without altering the statistical property of $\widehat{\mathbf{R}}_h$, and the obtained matrix is

$$\widehat{\mathbf{R}}_h \sim \mathbf{S}_h = \sum_{p=1}^R \lambda_p \mathbf{w}(p) \mathbf{w}^H(p), \quad (3.40)$$

where $\mathbf{w}(p) = [\mathbf{w}_1^T(p) \ \mathbf{w}_2^T(p) \ \cdots \ \mathbf{w}_M^T(p)]^T$, and $\mathbf{w}_m(p) = [w_m(p, -L_{m1}), \dots, w_m(p, L_{m2})]^T \in \mathbb{C}^{(L_{m1}+L_{m2}+1) \times 1}$ is the branch channel impulse response vector of the m th user. Therefore the random matrix $\widehat{\mathbf{R}}_h$ is statistically equivalent to the sum of R rank 1 matrices. According to the inequality $\text{rank}(\mathbf{A} + \mathbf{B}) \leq \text{rank}(\mathbf{A}) + \text{rank}(\mathbf{B})$ [71, p.13], we have

$$\text{rank}(\mathbf{S}_h) \leq \sum_{p=1}^R \text{rank} [\lambda_p \mathbf{w}(p) \mathbf{w}^H(p)] \leq R, \quad (3.41)$$

where $R = \text{rank}(\mathbf{R}_t)$. Since $\widehat{\mathbf{R}}_h$ and \mathbf{S}_h have the same stochastic property, the supremum of their ranks should be the same, and this completes the proof. \blacksquare

It should be noted that the value of the actual multiuser correlation matrix \mathbf{R}_h is determined by the frequency-selective property of the fading channel, while the matrix \mathbf{R}_t reflects the time-varying property of the channel. According to (3.9), there should be no interaction between \mathbf{R}_h and \mathbf{R}_t . However, the approximation matrix $\widehat{\mathbf{R}}_h$ is the average of P time-domain samples, which are correlated with each other due to the temporal correlation of the fading channel. Therefore the properties of $\widehat{\mathbf{R}}_h$ depend on both \mathbf{R}_h and \mathbf{R}_t , and the interactions between $\widehat{\mathbf{R}}_h$ and \mathbf{R}_t are deployed here for the estimation of the noise variance.

With the rank inequality given in (3.33) and the fact that $\text{rank}(\mathbf{A} \cdot \mathbf{B}) \leq \min[\text{rank}(\mathbf{A}), \text{rank}(\mathbf{B})]$ [71, p.13], we will have

$$\text{rank}(\mathbf{C} \widehat{\mathbf{R}}_h \mathbf{C}^H) \leq \text{rank}(\mathbf{R}_t). \quad (3.42)$$

Combining (3.31) and (3.42), we can see that the noise variance N_0 is equal to the smallest $N - \text{rank}(\mathbf{R}_t)$ eigen values of the correlation matrix $\widehat{\mathbf{R}}_{yp}$. It is shown in [70] that $\text{rank}(\mathbf{R}_t) \approx \lfloor 2Nf_dT_s \rfloor + 1$. For CDMA systems, we always have $f_dT_s \ll 1$, which means $\lfloor 2Nf_dT_s \rfloor + 1 \ll N$. Therefore, an estimation of N_0 can be obtained by averaging over the smallest $N - \lfloor 2Nf_dT_s \rfloor - 1$ eigen values of $\widehat{\mathbf{R}}_{yp}$. Since the maximum Doppler frequency f_d is not available at the receiver, we can replace f_d by its maximum possible value for practical CDMA systems, *e.g.*, 200 Hz, without losing the estimation accuracy. It should be noted that the value of $\widehat{\mathbf{R}}_h$ and \mathbf{R}_t are not required during the estimation of the noise variance, although the estimation method is derived based on the properties of these two matrices.

3.4.2 Joint Estimation of \mathbf{R}_h and \mathbf{l}_m

In this subsection, an iterative method is proposed for the joint estimation of the multiuser channel inter-tap correlation matrix \mathbf{R}_h and tap delay index vector \mathbf{l}_m , for $m = 1, 2, \dots, M$. The elements of the inter-tap correlation matrix \mathbf{R}_h are mainly determined by the relative transmission delay Δ_m and the fading channel power delay profile $G_m(\mu)$ of each user. In the tapped delay line representation of the fading channel, the effects of Δ_m and the delay spread of $G_m(\mu)$ are incorporated into the T_c -spaced tap delay index vector $\mathbf{l}_m = [-L_{m1}, \dots, L_{m2}]^T$. Both \mathbf{R}_h and \mathbf{l}_m are interacted to each other, and this interaction can be utilized for the joint estimation of \mathbf{R}_h and \mathbf{l}_m . It is pointed out here that our algorithm does not need to estimate either $G_m(\mu)$ or Δ_m .

The interactions between \mathbf{R}_h and \mathbf{l}_m can be explored via the help of the statistical properties of the received pilot samples. According to (3.17), the correlation matrix $\mathbf{R}_{yp} = \mathbb{E}[\mathbf{y}(j_p)\mathbf{y}(j_p)^H]$ of the received pilot symbols can be written by

$$\mathbf{R}_{yp} = \mathbf{C}\mathbf{R}_h\mathbf{C}^H + N_0\mathbf{I}_N. \quad (3.43)$$

In the equation above, the noise variance N_0 can be obtained from the method described in Section 3.4.1, \mathbf{R}_{yp} can be estimated from the received pilot symbols as

$\widehat{\mathbf{R}}_{y_p} = \frac{1}{P} \sum_{p=1}^P \mathbf{y}(j_p) \mathbf{y}^H(j_p)$, while \mathbf{R}_h and the multiuser code matrix \mathbf{C} are two unknown matrices to be determined. From the definition of \mathbf{C} in (3.19), we can see that \mathbf{C} is determined by both the spreading codes and the tap delay index vector $\mathbf{l}_m = [-L_{m1}, \dots, L_{m2}]^T$. As discussed in Section 3.2, the vector \mathbf{l}_m is obtained by discarding the channel taps with power smaller than a certain threshold, and the channel tap power $\mathbb{E}[h_m(jN, l) \cdot h_m^*(jN, l)] = \rho_m(l, l)$ can be found from the diagonal of \mathbf{R}_h . If we know the power of all the possible channel taps, then we can obtain \mathbf{l}_m by discarding the negligible taps. Furthermore, when \mathbf{l}_m is known, we can form the code matrix \mathbf{C} , with which \mathbf{R}_h can be computed from (3.43).

Based on the reciprocal relationship between \mathbf{R}_h and \mathbf{l}_m , an iterative method is proposed for the joint estimation of these two parameters.

Algorithm: Joint estimation of the multiuser channel inter-tap correlation matrix \mathbf{R}_h and the tap delay index vector \mathbf{l}_m .

Step I: Set the initial value of the tap delay index vector as $\mathbf{l}_m = [-D - 1, L_{m0} + D]^4$, where D is the maximum relative transmission delay factor, and $L_{m0} \approx \tau_{max}^{(m)} / T_c$ with $\tau_{max}^{(m)}$ being the maximum possible delay spread of the m th user's physical channel.

Step II: Based on the current value of \mathbf{l}_m , construct the multiuser code matrix \mathbf{C} according to (3.19). With the estimated value of \mathbf{R}_{y_p} , N_0 , and the current value of \mathbf{C} , compute \mathbf{R}_h as follows

$$\mathbf{R}_h = \mathbf{C}^\dagger (\mathbf{R}_{y_p} - N_0 \mathbf{I}_N) (\mathbf{C}^H)^\dagger. \quad (3.44)$$

Step III: With the diagonal elements of \mathbf{R}_h obtained from Step II, find the maximum power taps for each user, and represent the maximum tap power of the m th user as \mathcal{P}_m . For all the taps of the m th user, discard the taps that are smaller than $\epsilon \cdot \mathcal{P}_m$, with $0 < \epsilon < 1$ being a pre-defined threshold value.

⁴The reason we choose $-D - 1$ as the smallest possible tap delay index lies in the fact that the absolute amplitude of the raised cosine filter is very small for samples one chip period away from the peak value and the physical fading channel is always causal.

Step IV: After discarding the negligible taps for each user, a new tap delay index vector \mathbf{l}_m for each user can be formed, and go back to Step II. If there are no more taps to discard, or the maximum number of iterations is reached, then the current values of \mathbf{R}_h and \mathbf{l}_m are the desired values.

With the proposed iterative method, the value of \mathbf{R}_h and \mathbf{l}_m can be jointly estimated from the received pilot samples for each slot. When we set $\epsilon = 1\%$, simulations show that the iterative method usually converges within 2 iterations, and it leads to accurate estimations of \mathbf{R}_h and \mathbf{l}_m . The estimated values of \mathbf{R}_h , \mathbf{l}_m and N_0 are utilized to form the MMSE solution of the multiuser channel tap coefficients $\mathbf{h}_m(j_p)$ at pilot positions as stated in (3.28).

The time-varying channel coefficients of one entire slot can be obtained by interpolating the MMSE-estimated CIR at pilot positions. The topic of channel interpolation for systems with PSAM has been researched extensively in the literature [65]- [67]. Among these methods, Weiner filter interpolation [65] is an optimum solution in the sense of mean square error, provided that the temporal correlation of each time-varying channel tap is accurately known to the receiver, which is unlikely in practice. Therefore, we adopt a sub-optimum constant matrix interpolation method [67], which was proposed for TDMA-based systems. The extension of this method to CDMA system is straightforward, and details are omitted here for brevity.

3.5 Simulation Results

Simulations are carried out in this section to evaluate the performance of the proposed multiuser channel estimation algorithm for QS-CDMA systems undergo time-varying and frequency selective channel fading.

3.5.1 System Configurations

The slot structure used in our simulations is shown in Fig. 3.2. Each slot has 4 head pilot symbols and 2 tail pilot symbols with 56 data symbols in the middle. The time duration of each slot is 2ms, and every 2 slots are combined as a hyper-slot in the estimation process. Gold sequences with processing gain of $N = 127$ are used as the spreading codes. The chip rate of the system is chosen to be 3.84 Mcps. The transmitted data are QPSK modulated. Root raised cosine (RRC) filter with rolloff factor of 0.22 is used as both the transmit filter and the chip matched filter. Vehicular A propagation profile [13] [23], shown in Fig. 3.3, is chosen to be the power delay profile $G_m(\tau)$ for simulations with the normalized Doppler frequency set to $f_d T_{slot} = 0.1$. The time varying channel fading is generated with the method described in Section 2.3.3. The relative transmission delay Δ_m of each user is uniformly distributed in $[-DT_c, DT_c]$. Unless otherwise stated, we set $D = 3$ in the simulations. In the iterative estimation of \mathbf{R}_h and \mathbf{l}_m , the maximum number of iterations are set to 2, and the discarding threshold ϵ is set to 1%.

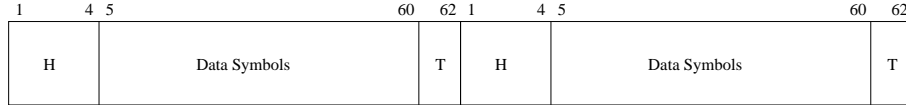


Figure 3.2: The slot structure to be utilized for simulations.

A successive interference canceller [42] is employed for coherent multiuser detection. The users are sorted according to their received power, which can be obtained from the diagonal elements of \mathbf{R}_h . The users are then detected and canceled from the strongest to the weakest. In the detection of each of the users, coherent Rake combining is used, with the number of Rake fingers equal to the number of channel taps of the corresponding user being detected, which is λ_m for the m th user.

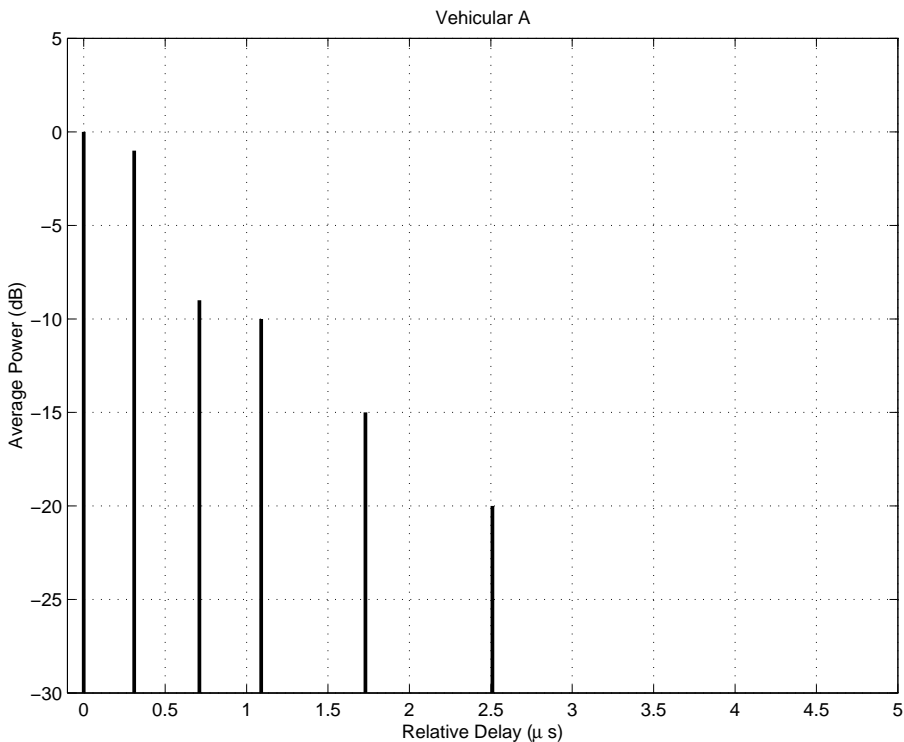


Figure 3.3: Vehicular A propagation profile. The differential delays between multiple paths are non-integer of the chip period T_c .

3.5.2 Performance Evaluation

The proposed multiuser channel estimation algorithm requires knowledge of the additive noise variance N_0 , the multiuser channel inter-tap correlation matrix \mathbf{R}_h , and the tap delay index vector \mathbf{l}_m . These parameters can be obtained from the received data samples with the methods described in Section 3.4. The validity of these methods is evaluated in the sequel.

Consider a QS-CDMA system with 5 users. The additive noise variance N_0 is estimated by utilizing the method described in Section 3.4.1. For comparison purpose, Fig. 3.4 shows the estimated noise variances along with the actual noise variances for various values of E_b/N_0 . The estimation results are based on averaging 1000 estimated values. As we can see from Fig. 3.4, the estimation of the noise variances is very accurate.

The effectiveness of the estimation for \mathbf{R}_h and \mathbf{l}_m can be demonstrated by the bit error

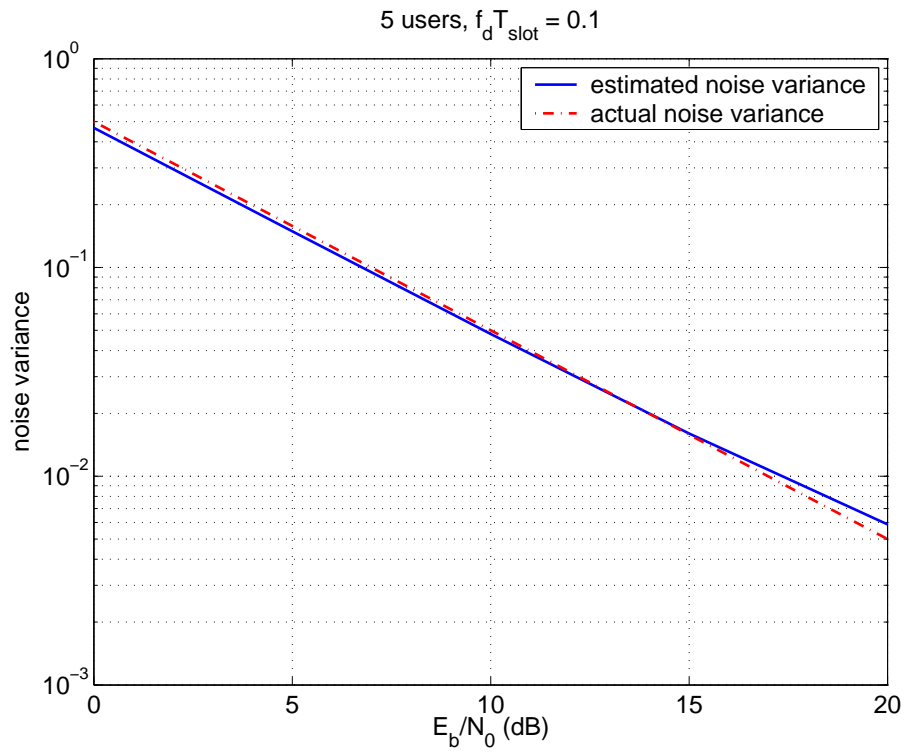


Figure 3.4: Comparison of the estimated noise variance and its corresponding actual noise variance at different level of E_b/N_0 .

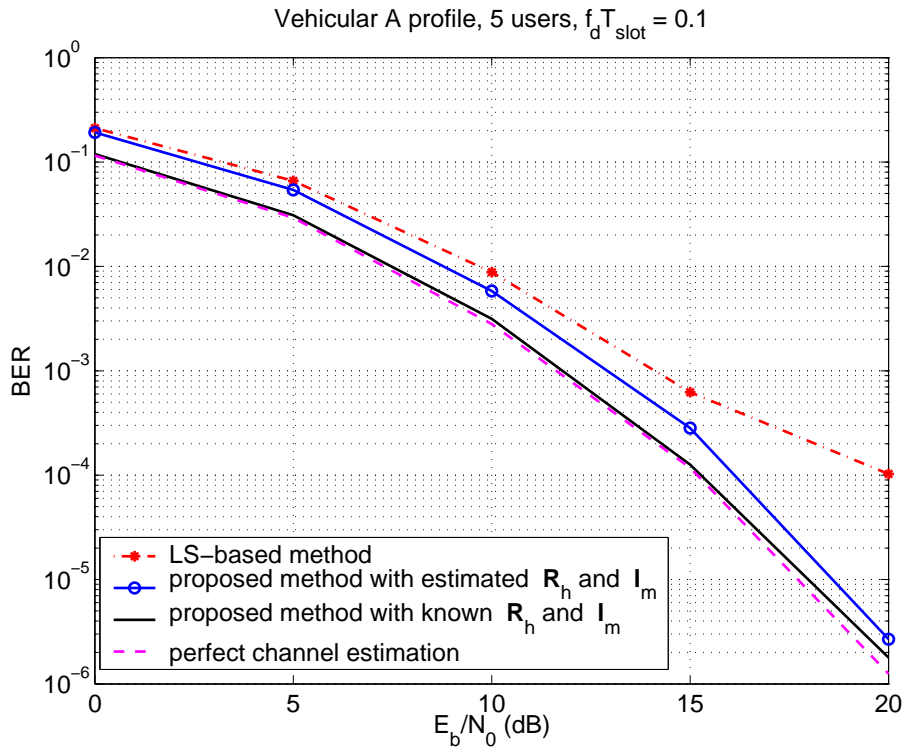


Figure 3.5: BER performance comparison of the system which employs our multiuser channel estimation algorithm and the ideally perfect channel estimation.

rate (BER) performance of a 5-user CDMA system which employs the proposed channel estimation algorithm. In Fig. 3.5, four cases are depicted for BER comparison. The first case is the BER performance of the system that has perfect knowledge of the multiuser fading channels. This BER shall serve as a benchmark for our channel estimation performance. The second case is the BER of the system with knowledge of the multiuser channel inter-tap correlation matrix \mathbf{R}_h and the tap index vector \mathbf{l}_m , which are utilized to estimate (and interpolate) the multiuser fading channels. The third case is the BER of the system that has estimated both \mathbf{R}_h and \mathbf{l}_m , then utilize them to estimate (and interpolate) the multiuser fading channels. The fourth case is the BER of the system that employs the LS-based method to estimate the channel coefficients at pilot locations, where the LS-based algorithm only utilizes the first order statistics of the fading channel, and the results are labeled as “LS-based method”. As can be seen from Fig. 3.5, when the receiver knows the channel inter-tap correlation matrix \mathbf{R}_h and the tap index vector \mathbf{l}_m , our multiuser channel estimation algorithm has nearly the same BER performance as the ideally perfect channel estimation case. However, as expected, when the receiver has to estimate both the channel correlation matrix and the tap index vector, our multiuser channel estimation algorithm will have a little degradation on the BER performance from the perfect channel estimation case, but the degradation is within an acceptable range. For example, it is about 0.8dB when the BER is at the level of 10^{-4} .

Comparing the four curves discussed above, we can see that the multiuser channel inter-tap correlation matrix \mathbf{R}_h plays a very important role in the performance of the estimation algorithm. If we do not take advantage from this correlation information for multiuser channel estimation, we will get BER performance penalty which can be significant compared to our proposed MMSE-based algorithm.

In Fig. 3.6, we compare the BER performance of the system with our proposed MMSE-based channel estimation algorithm to that of the pilot assisted subspace-based algorithm shown in the appendix. The subspace-based estimation algorithm is derived for quasi-static fading channels, where the channels can be viewed as *deterministic* during the entire estimation process, therefore the correlation information does not play

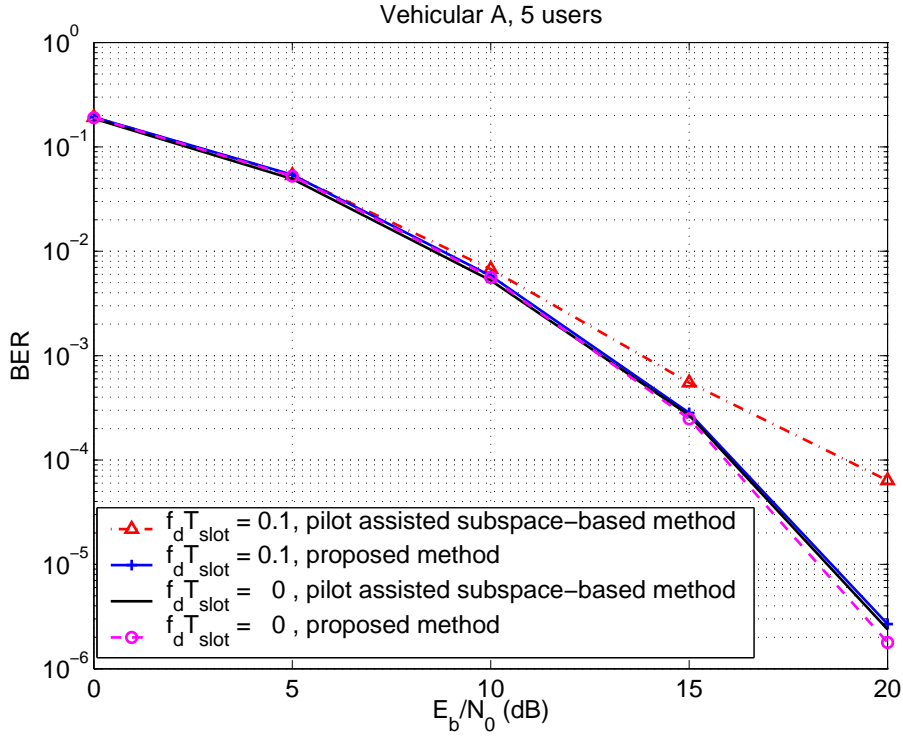


Figure 3.6: BER performance comparison of the system which employs our multiuser channel estimation algorithm and the pilot assisted subspace-based channel estimation.

an important role in the estimation. For quasi-static fading channels ($f_d T_{slot} = 0$), we can see from the figure that the subspace-based algorithm can achieve nearly the same performance as the proposed MMSE algorithm. However, when we increase $f_d T_{slot}$ to 0.1, performance degradation can be clearly observed for the subspace-based method for $E_b/N_0 \geq 10$ dB, while the performance of the proposed algorithm is not apparently affected.

To further show our proposed algorithm’s ability of estimating the tap index vector \mathbf{l}_m , we consider two cases that the maximum transmission delay factor D is set to 3 and 6. This means that the relative transmission delay Δ_m of each user is uniformly distributed in $[-3T_c, 3T_c]$ and $[-6T_c, 6T_c]$, respectively. In the simulation, we consider two scenarios for both $D = 3$ and $D = 6$ cases. First, we assume that the tap index vector \mathbf{l}_m is known to the receiver, and the obtained BER curves are labeled “known \mathbf{l}_m ” as shown in Fig. 3.7. Second, when the vector \mathbf{l}_m is estimated with our proposed iterative method, the

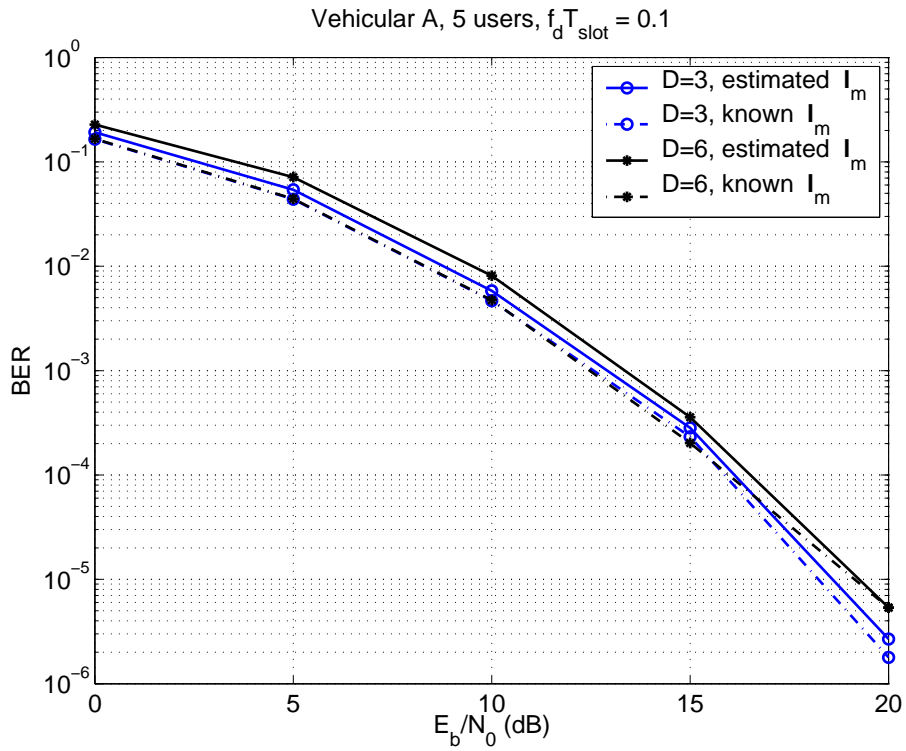


Figure 3.7: BER comparison for the effect of the estimated tap delay index vector \mathbf{l}_m and ideally known tap delay index vector on system performance. Note: all the curves are based on estimated \mathbf{R}_h using the proposed algorithm.

obtained BER curves are labeled “estimated \mathbf{l}_m ”. It is noted that all the four curves in Fig. 3.7 are based on the estimated \mathbf{R}_h by using our iterative algorithm. From Fig. 3.7, we have three observations. First, when the receiver has knowledge of \mathbf{l}_m , changing the maximum transmission delay range has no apparent effect on the system performance. Second, whereas for a system with \mathbf{l}_m being estimated, a slight BER degradation will occur if the maximum transmission delay range is increased. Third, the BER performance of a system with estimated \mathbf{l}_m are close to that of a system with perfect information of \mathbf{l}_m . These results indicate that the proposed algorithm provides accurate estimation of \mathbf{l}_m in a wide range of E_b/N_0 .

We are now in a position to take a look at the normalized mean square error (MSE). Let $\hat{\mathbf{h}}(j)$ be the estimation of the multiuser channel tap coefficient vector $\mathbf{h}(j)$. We define the normalized MSE as $\mathbb{E} \left\{ \left[\mathbf{h}(j) - \hat{\mathbf{h}}(j) \right]^H \left[\mathbf{h}(j) - \hat{\mathbf{h}}(j) \right] \right\} / \mathbb{E} \left[\mathbf{h}(j)^H \mathbf{h}(j) \right]$, and present the channel estimation errors of the LS-based method, the pilot assisted subspace-based method and the proposed MMSE algorithm in Fig. 3.8. It is observed that given a value of E_b/N_0 , the normalized MSE of the proposed MMSE method with known \mathbf{R}_h and \mathbf{l}_m is always smaller than that of the proposed MMSE method with estimated \mathbf{R}_h and \mathbf{l}_m , and the MSE of the LS-based and subspace-based method is always larger than that of the proposed MMSE method with estimated \mathbf{R}_h and \mathbf{l}_m . The MSE’s of these four cases are well reflected in the BER performances listed in Fig. 3.5 and Fig. 3.6.

So far, all the simulation results are focused on the Vehicular A propagation profile, which has discrete-time power delay profile (or discrete-time delayed multiple paths). We would like to point out that our algorithm can be directly applied to fading channels which have continuous-time power delay profile. For example, we replace Vehicular A power delay profile by an exponentially decaying profile, whose power delay profile is defined as $G_m^c(\tau) = A \cdot \exp\left(-\frac{\tau}{1\mu s}\right)$ with $0 \leq \tau \leq 1.5\mu s$. If we keep the rest of the simulation configurations of Fig. 3.5 unchanged, then we get the corresponding BER comparison for $G_m^c(\tau)$ as shown in Fig. 3.9, which indicates that our multiuser channel estimation algorithm is still very effective under continuous-time power delay profile fading environment. However, it should be pointed out that most existing channel

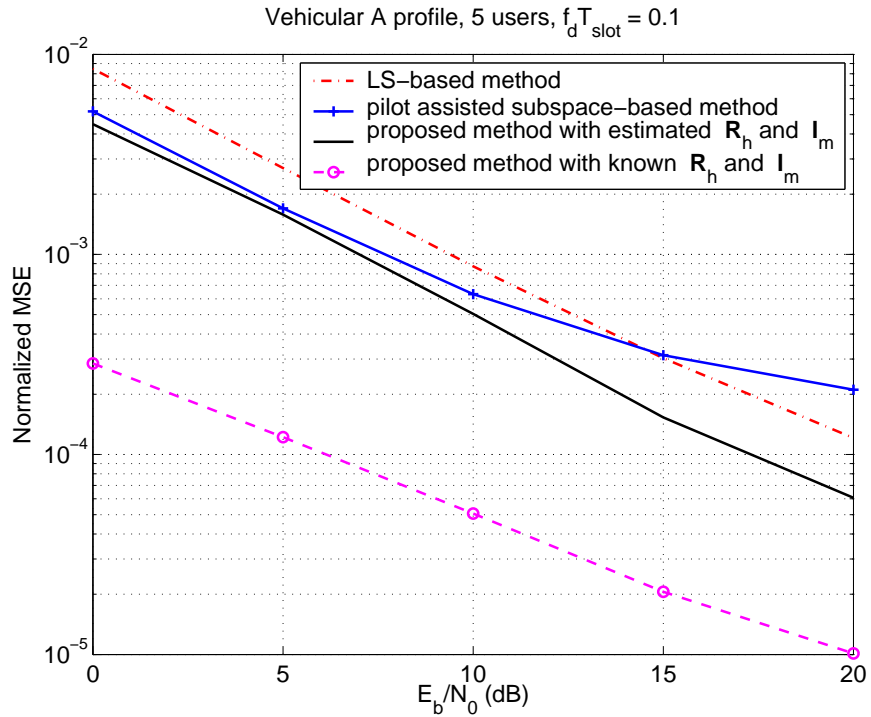


Figure 3.8: The normalized MSE performance of the system which uses the proposed algorithm, the LS-based method, and the pilot assisted subspace-based method.

estimation algorithms will fail under this fading condition.

3.6 Conclusions

In this chapter, a pilot assisted minimum mean square error (MMSE) multiuser channel estimation algorithm was proposed for quasi-synchronous CDMA systems undergoing time-varying and frequency selective channel fading. The algorithm was developed based on the only assumption that the base station receiver knows the spreading codes and pilot symbols of all the mobile users, which is very reasonable in practice. The combined effects of the frequency selective physical fading channel, the transmit filter and receive filter were represented as a symbol-wise time-varying chip-spaced tapped delay line filter with *correlated* filter taps. A novel iterative method was then proposed for the joint estimation of the multiuser channel inter-tap correlations and tap delays, which were further utilized to form the MMSE-based multiuser channel tap coefficient estimation.

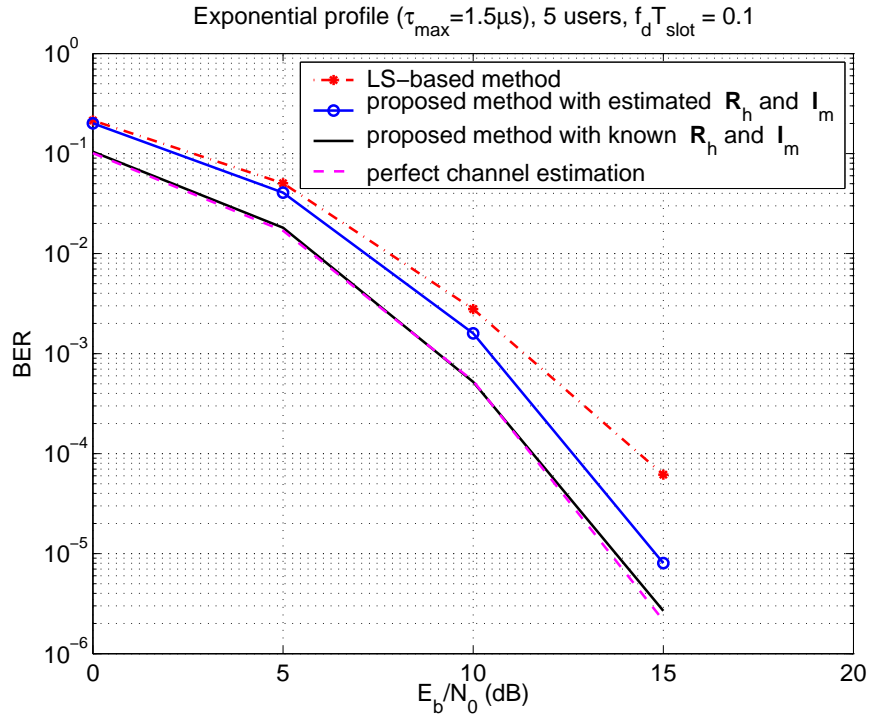


Figure 3.9: BER performance comparison of the system which employs our multiuser channel estimation algorithm and the ideally perfect channel estimation, where the power delay profile is a continuous-time exponentially decaying function.

The multiuser channel estimation algorithm can be used to estimate fading channels which have either discrete-time or continuous-time power delay profiles. Simulation results showed that the information of the channel inter-tap correlations is critical to the performance of the multiuser channel estimation, and the discrete-time composite channel taps at different delays may not be assumed uncorrelated for CDMA systems which experience physical WSSUS fading. Furthermore, when the channel inter-tap correlation is known to the receiver, the BER performance of the proposed MMSE algorithm is nearly the same as that of the perfect channel estimation case; when the channel inter-tap correlation is estimated from the received signals, the proposed algorithm's BER performance is close to that of the perfect channel estimation case.

Chapter 4

Optimal Diversity Combining based on Noisy Channel Estimation

4.1 Introduction

Diversity reception is a classical method used in wireless communication systems for combating the hostile nature of fading channels, and the error performance analysis of diversity receivers in fading channels has been a field of long-time interest, see [72]- [79] and the references therein. A commonly used method for analyzing error probability of digital communication systems is to obtain the conditional error probability (CEP) $P(E|\gamma)$, where γ is the signal to noise ratio (SNR) at the output of the receiver, and then average $P(E|\gamma)$ over γ using the probability density function (pdf) $p(\gamma)$. For example, this method is applied in [73] for the performance analysis of maximum ratio combining (MRC) receivers in uncorrelated Rayleigh fading channels, the SNR of which is χ^2 -distributed with $2N$ degrees of freedom, with N being the diversity order [73]. However, in some cases, such as the equal gain combining (EGC) receivers with diversity order higher than two [74], it is notoriously difficult or even impossible to obtain a closed-form solution for the pdf of the output SNR γ . This problem can be eluded by resorting to the characteristic function (CHF) $\mathbb{E}(e^{j\omega\gamma})$ [74], [75] or moment generating function (MGF) $\mathbb{E}(e^{s\gamma})$ [76], [77] of γ , which are usually more readily found in closed-form. To implement the CHF or MGF method, the CEP $P(E|\gamma)$ must be in the form of

an exponential function of γ . However, the CEP for most systems with coherent, differentially coherent, and non-coherent detections are in the form of Gaussian or Marcum Q-functions. This problem is elegantly tackled by Simon and Alouini *et. al.* in [78] using alternative exponential representations of the Gaussian and Marcum-Q functions. A unified approach for error performance evaluation of systems with various modulation and detection methods in general fading channels is given in [78].

Most previous works about performance analyses of coherent diversity systems assume that the receiver has perfect knowledge (noiseless estimation) of the fading channels. In order to facilitate the design of practical diversity systems, it is highly desirable to have analytical performance expressions for systems operating with noisy channel estimation. In the literature, only few works are devoted to the performance analyses of non-ideal systems. In [80], the effect of Gaussian error in maximal ratio combining is studied. However, the mathematical models assumed preclude using the analysis for independent additive noise and the analysis is valid only for Gaussian error originating from temporal decorrelation [81]. Further, digital modulations and error probability are not considered in [80]. The error probabilities of systems with non-ideal channel information for *non-diversity* systems are obtained in [82] and [83] by seeking the pdf of the equivalent output noise at the receiver, which is usually non-Gaussian distributed and extremely complicated for analyses.

In this chapter, error performances of optimal coherent diversity receivers operating on independent and identically distributed (i.i.d.) fading channels with noisy channel estimation are analyzed. It is shown that the conventional MRC receiver is no longer optimal when there is channel estimation error in the system. A new optimal decision rule for coherent diversity receivers with noisy channel estimation is proposed to minimize the error probability of the system, and this decision rule is different from the conventional MRC receiver in that it takes into account the effects of the channel estimation error. Based on this decision rule, the error probabilities for optimal coherent diversity receivers are derived for MPSK systems in both Rayleigh and Ricean fading channels. The symbol error probability conditioned on the estimated fading channel is

first evaluated using the polar coordinate method proposed by Craig in [84] for additive white Gaussian noise (AWGN) channels and extended here for systems using noisy estimated fading channel information. The CEPs generated with the modified polar coordinate method have the desired exponential forms, and the symbol error rate of the corresponding systems can be obtained by averaging these CEPs over the estimated fading channels. For Rayleigh fading channels, the averaging operation is performed with the MGF method, and closed-form expressions are obtained for some special cases. For Ricean fading channels, the non-central distribution of the estimated channel prohibits the use of the MGF or CHF method, therefore a complex Gaussian distribution based functional equivalence is employed for the evaluation of the system error performance. Simulation results are in excellent agreement with the theoretical results.

The rest of this chapter is organized as follows. The system models are given in Section 4.2. Section 4.3 derives a new optimal decision rule for diversity receivers operating with noisy estimates of i.i.d. fading channels. The error probabilities of the corresponding receivers in Rayleigh and Ricean fading channels are derived in Section 4.4. Numerical examples are given in Section 4.5, and Section 4.6 concludes the paper.

4.2 System and Channel Models

We consider a communication system with flat fading channels and N diversity receivers. After sampling at the receiver, the discrete-time representation of the equivalent base-band system can be written in matrix form as

$$\mathbf{y}_k = \mathbf{h}_k \cdot x_k + \mathbf{z}_k, \quad (4.1)$$

where $\mathbf{y}_k = [y_1(k), y_2(k), \dots, y_N(k)]^T \in \mathbb{C}^{N \times 1}$ is the sampled output of the receivers with \mathbf{A}^T representing the transpose of matrix \mathbf{A} , $\mathbf{h}_k = [h_1(k), h_2(k), \dots, h_N(k)]^T \in \mathbb{C}^{N \times 1}$ is the equivalent discrete-time channel gain (CG) vector of the physical time-varying fading channels, x_k is the MPSK modulated symbol transmitted at time instant k , and $\mathbf{z}_k = [z_1(k), z_2(k), \dots, z_N(k)]^T \in \mathbb{C}^{N \times 1}$ is a zero-mean additive white Gaussian noise vector with covariance matrix $N_0 \mathbf{I}_N$, and \mathbf{I}_N is the $N \times N$ identity matrix.

For Rayleigh and Ricean fading channels, the discrete-time CG vector \mathbf{h}_k is made up of complex Gaussian random variables (CGRVs) with mean vector \mathbf{u} and covariance matrix \mathbf{R}_{hh} , *i.e.*, $\mathbf{h}_k \sim \mathcal{N}(\mathbf{u}, \mathbf{R}_{hh})$, and the probability density function of \mathbf{h}_k is [85, eqn. (7-62)]

$$p(\mathbf{h}_k) = \frac{1}{\det(\pi \mathbf{R}_{hh})} \exp [-(\mathbf{h}_k - \mathbf{u})^H \mathbf{R}_{hh}^{-1} (\mathbf{h}_k - \mathbf{u})], \quad (4.2)$$

where \mathbf{A}^H is the Hermitian of matrix \mathbf{A} . The variance $\sigma_{h_n}^2$, power Ω_n , and mean value u_n of $h_n(k)$ have the following relationships,

$$|u_n| = \sqrt{\frac{K\Omega_n}{K+1}} = \sqrt{K\sigma_{h_n}^2}, \quad (4.3)$$

where K is the Ricean factor defined as the ratio of the powers of the specular component and the scattering components of the fading channel. For Rayleigh fading channel, we have $K = 0$, and, thus, $\mathbf{u} = \mathbf{0}$.

The receiver performs coherent detection of the received samples based on the estimated CG vector $\hat{\mathbf{h}}_k = [\hat{h}_1(k), \hat{h}_2(k), \dots, \hat{h}_N(k)]^T \in \mathbb{C}^{N \times 1}$. The estimated CG vector $\hat{\mathbf{h}}_k$ is modeled as the sum of the true CG vector \mathbf{h}_k and the estimation error vector $\mathbf{e}_k = [e_1(k), e_2(k), \dots, e_N(k)]^T$ as

$$\hat{\mathbf{h}}_k = \mathbf{h}_k + \mathbf{e}_k, \quad (4.4)$$

where the elements of the error vector \mathbf{e}_k are assumed to be independent zero-mean CGRVs, and they are independent of the elements of \mathbf{h}_k . Then the covariance matrices $\mathbf{R}_{h\hat{h}} = \mathbb{E}(\mathbf{h}_k^H \hat{\mathbf{h}}_k)$ and $\mathbf{R}_{\hat{h}\hat{h}} = \mathbb{E}(\hat{\mathbf{h}}_k^H \hat{\mathbf{h}}_k)$ can be computed as

$$\mathbf{R}_{h\hat{h}} = \mathbb{E}[\mathbf{h}_k (\mathbf{h}_k + \mathbf{e}_k)^H] = \mathbf{R}_{hh}, \quad (4.5a)$$

$$\mathbf{R}_{\hat{h}\hat{h}} = \mathbb{E}[(\mathbf{h}_k + \mathbf{e}_k)(\mathbf{h}_k + \mathbf{e}_k)^H] = \mathbf{R}_{hh} + \mathbf{R}_{ee}, \quad (4.5b)$$

where $\mathbf{R}_{ee} = \text{diag}(\sigma_{e_1}^2, \sigma_{e_2}^2, \dots, \sigma_{e_N}^2)$ is an $N \times N$ diagonal matrix with $\sigma_{e_n}^2 = \mathbb{E}[|e_n(k)|^2]$ being the power (variance) of the channel estimation error $e_n(k)$. Based on these definitions, we have the following proposition.

Proposition 4.1: The estimated CG vector $\hat{\mathbf{h}}_k$ and the true CG vector \mathbf{h}_k are jointly Gaussian distributed, and the conditional pdf $p(\mathbf{h}_k|\hat{\mathbf{h}}_k)$ can be written as

$$p(\mathbf{h}_k|\hat{\mathbf{h}}_k) = \frac{1}{\det(\pi\mathbf{R}_{h|\hat{h}})} \exp \left[-(\mathbf{h}_k - \mathbf{u}_{h|\hat{h}})^H \mathbf{R}_{h|\hat{h}}^{-1} (\mathbf{h}_k - \mathbf{u}_{h|\hat{h}}) \right], \quad (4.6)$$

where

$$\mathbf{u}_{h|\hat{h}} = \mathbf{u} + \mathbf{R}_{hh}(\mathbf{R}_{hh} + \mathbf{R}_{ee})^{-1}(\hat{\mathbf{h}}_k - \mathbf{u}), \quad (4.7a)$$

$$\mathbf{R}_{h|\hat{h}} = \mathbf{R}_{hh} - \mathbf{R}_{hh}(\mathbf{R}_{hh} + \mathbf{R}_{ee})^{-1}\mathbf{R}_{hh} \quad (4.7b)$$

are the conditional mean vector and conditional covariance matrix, respectively.

Proof: The proof of Proposition 4.1 is given in Appendix B. ■

To facilitate analysis, we define the covariance coefficient between the estimated CG $\hat{h}_n(k)$ and the true CG $h_n(k)$ of the n th sub-channel as

$$\rho_n = \frac{\mathbb{E}\{[h_n(k) - u][\hat{h}_n(k) - u]^*\}}{\sqrt{\sigma_{h_n}^2 \sigma_{\hat{h}_n}^2}} = \sqrt{\frac{\sigma_{h_n}^2}{\sigma_{h_n}^2 + \sigma_{e_n}^2}}, \quad (4.8)$$

where a^* denotes the complex conjugate of the complex number a , $\sigma_{h_n}^2 = \mathbb{E}[|h_n(k) - u|^2]$ and $\sigma_{\hat{h}_n}^2 = \mathbb{E}[|\hat{h}_n(k) - u|^2] = \sigma_{h_n}^2 + \sigma_{e_n}^2$ is the variance of $h_n(k)$ and $\hat{h}_n(k)$, respectively. The value of ρ_n is in the interval $(0, 1]$ with $\rho_n = 1$ corresponding to noiseless (perfect) channel information at the receiver. Since diversity receivers usually use the same channel estimation algorithm for all the branches, we assume that $\rho = \rho_1 = \rho_2 = \dots = \rho_N$ for systems with i.i.d. fading channels, and the coefficient ρ is assumed to be known to the receiver once the channel estimation algorithm is chosen.

4.3 Optimal Diversity Receiver with Noisy Channel Estimation

In this section, an optimal decision rule for coherent diversity reception is proposed to minimize the error probability of systems with noisy channel estimation.

In order to design the optimal coherent diversity receiver, we need to know the statistical properties of the received sample vector \mathbf{y}_k . From Proposition 4.1, we know that \mathbf{h}_k conditioned on $\hat{\mathbf{h}}_k$ is Gaussian distributed; it follows from (4.1) that \mathbf{y}_k conditioned on $\hat{\mathbf{h}}_k$ and x_k is also Gaussian distributed. If we assume that the symbol $s_m \in \mathcal{S}$ is transmitted, where \mathcal{S} is the modulation alphabet set, then we have $\mathbf{y}_k | (\hat{\mathbf{h}}_k, s_m) \sim \mathcal{N}(\mathbf{u}_{y|\hat{h},s_m}, \mathbf{R}_{y|\hat{h},s_m})$. Combining (4.1), (4.7), (4.8) and the fact that $\mathbf{R}_{hh} = \sigma_h^2 \mathbf{I}_N$ for i.i.d. fading channels, we can write the conditional pdf $p(\mathbf{y}_k | \hat{\mathbf{h}}_k, s_m)$ as

$$p(\mathbf{y}_k | \hat{\mathbf{h}}_k, s_m) = \frac{1}{\det(\pi \mathbf{R}_{y|\hat{h},s_m})} \exp \left[-(\mathbf{y}_k - \mathbf{u}_{y|\hat{h},s_m})^H \mathbf{R}_{y|\hat{h},s_m}^{-1} (\mathbf{y}_k - \mathbf{u}_{y|\hat{h},s_m}) \right], \quad (4.9)$$

where the conditional mean vector $\mathbf{u}_{y|\hat{h},s_m}$ and covariance matrix $\mathbf{R}_{y|\hat{h},s_m}$ are

$$\mathbf{u}_{y|\hat{h},s_m} = [\rho^2 \hat{\mathbf{h}}_k + (1 - \rho^2) \mathbf{u}] s_m, \quad (4.10a)$$

$$\mathbf{R}_{y|\hat{h},s_m} = (\rho^2 \sigma_e^2 E_s + N_0) \mathbf{I}_N. \quad (4.10b)$$

With the conditional pdf given in (4.9), we can get the following optimal decision rule for coherent diversity receivers with noisy channel estimation stated as Theorem 4.1.

Theorem 4.1: For diversity receivers with noisy estimation of i.i.d. fading channels, if the transmitted symbols are equiprobable, then the detection rule that minimizes the system error probability is

$$\hat{x}_k = \underset{s_m \in \mathcal{S}}{\operatorname{argmin}} \{ |\alpha_k - s_m|^2 \}, \quad (4.11)$$

where $\mathcal{S} = \{s_m = \sqrt{E_s} e^{-j2\pi \frac{m}{M}} | m = 1, 2, \dots, M\}$ is the modulation alphabet set, and $\alpha_k = [\rho^2 \hat{\mathbf{h}}_k + (1 - \rho^2) \mathbf{u}]^H \mathbf{y}_k$ is the decision variable.

Proof: The system error probability P_e can be expressed as

$$P_e = \sum_{m=1}^M P(s_m) \cdot \left\{ 1 - \int_{\{\hat{\mathbf{h}}_k\}} \left[\int_{\mathcal{R}_m} p(\mathbf{y}_k | \hat{\mathbf{h}}_k, s_m) d\mathbf{y}_k \right] d\hat{\mathbf{h}}_k \right\}, \quad (4.12)$$

where $P(s_m) = \frac{1}{M}$ for equiprobable transmitted symbols, and the N dimensional complex plane \mathcal{R}_m is the decision region for the symbol s_m , *i.e.*, $\mathbf{y}_k \in \mathcal{R}_m$ implies $\hat{x}_k = s_m$.

The error probability given in (4.12) can be minimized by the maximum *a posteriori* (MAP) rule, which selects the decision region \mathcal{R}_m so that the conditional pdf $p(\mathbf{y}_k|\hat{\mathbf{h}}_k, s_m)$ is maximized,

$$\mathcal{R}_m = \left\{ \mathbf{y}_k \mid p(\mathbf{y}_k|\hat{\mathbf{h}}_k, s_m) \geq p(\mathbf{y}_k|\hat{\mathbf{h}}_k, s_n), \quad \forall n \neq m \right\}. \quad (4.13)$$

Combining the decision region given in (4.13) with the conditional pdf of (4.9), we can get the decision rule as

$$\hat{x}_k = \underset{s_m \in \mathcal{S}}{\operatorname{argmin}} \{ \|\mathbf{y}_k - [\rho^2 \hat{\mathbf{h}}_k + (1 - \rho^2) \mathbf{u}] s_m\|^2 \}, \quad (4.14)$$

where $\|\mathbf{a}\| = \sqrt{\mathbf{a}^H \mathbf{a}}$ is the l_2 -norm of vector \mathbf{a} .

To simplify the representation of the decision rule given in (4.14), we let $\mathbf{d}_k = \rho^2 \hat{\mathbf{h}}_k + (1 - \rho^2) \mathbf{u}$, and expand the term in (4.14) to be minimized as

$$\|\mathbf{y}_k - \mathbf{d}_k s_m\|^2 = \mathbf{y}_k^H \mathbf{y}_k + \mathbf{d}_k^H \mathbf{d}_k E_s - 2\Re(\mathbf{d}_k^H \mathbf{y}_k s_m), \quad (4.15)$$

where the operation $\Re(a)$ returns the real part of a . Noting that \mathbf{y}_k and \mathbf{d}_k are independent of s_m , we can get the following equivalent decision rule

$$\hat{x}_k = \underset{s_m \in \mathcal{S}}{\operatorname{argmin}} \{ -2\Re(\mathbf{d}_k^H \mathbf{y}_k s_m) \}. \quad (4.16)$$

After some algebraic manipulations, we can show that (4.16) is equivalent to (4.11), and this completes the proof. ■

If the receiver has perfect knowledge of the fading channel, *i.e.*, $\rho = 1$, then the decision variable becomes $\alpha_k = \hat{\mathbf{h}}_k^H \mathbf{y}_k$, and the decision rule specializes to the conventional MRC diversity receiver. However, when $\rho < 1$, it can be seen from the decision rule given in (4.11) that the conventional MRC receiver is not optimal in the presence of channel estimation error.

4.4 Error Performance Analyses

Based on the optimal decision rule presented in Theorem 4.1, we evaluate the error performance of diversity receivers with non-perfect channel information, in both Rayleigh and Ricean fading channels.

4.4.1 Conditional Error Probability

We first evaluate the conditional error probability (CEP) $P(E|\hat{\mathbf{h}}_k)$, which will be used to obtain the error probability of the diversity system in Rayleigh and Ricean fading channels.

It can be seen from the decision rule of (4.11) that the detected symbol \hat{x}_k should have the smallest Euclidean distance from the decision variable α_k . Based on this decision rule, the detection region for α_k of the MPSK symbol s_m should be a $\frac{2\pi}{M}$ angle sector centered around s_m as shown in Fig. 4.1, and the conditional error probability $P(E|\hat{\mathbf{h}}_k, s_m)$ equals to the probability that α_k is outside of the detection region of s_m when s_m is transmitted.

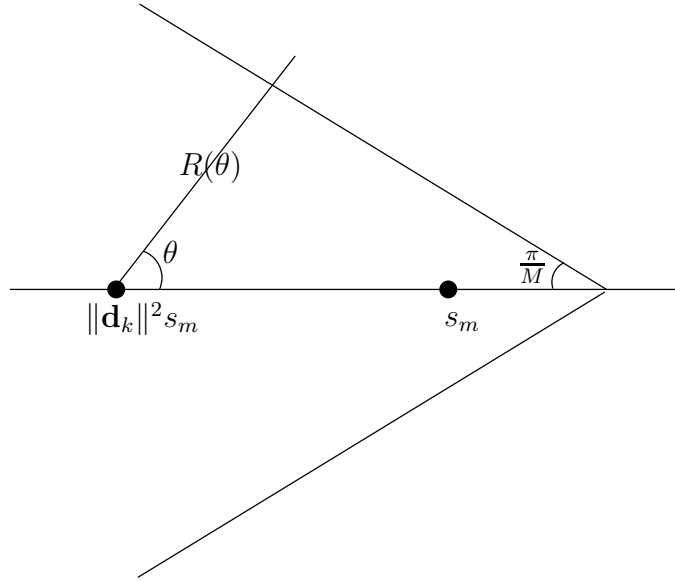


Figure 4.1: The decision region for MPSK modulation.

Since the received sample vector \mathbf{y}_k conditioned on $\hat{\mathbf{h}}_k$ is Gaussian distributed, the decision variable $\alpha_k = [\rho^2 \hat{\mathbf{h}}_k + (1 - \rho^2) \mathbf{u}]^H \mathbf{y}_k$ conditioned on $\hat{\mathbf{h}}_k$ is also Gaussian distributed with the conditional pdf given by

$$p(\alpha_k | \hat{\mathbf{h}}_k, s_m) = \frac{r}{\pi u_{\alpha | \hat{h}, s_m}} \exp \left[-\frac{|\alpha_k - u_{\alpha | \hat{h}, s_m}|^2}{\sigma_{\alpha | \hat{h}, s_m}^2} \right]. \quad (4.17)$$

where

$$u_{\alpha | \hat{h}, s_m} = \|\mathbf{d}_k\|^2 s_m \quad (4.18a)$$

$$\sigma_{\alpha | \hat{h}, s_m}^2 = \|\mathbf{d}_k\|^2 (\rho^2 \sigma_e^2 E_s + N_0) \quad (4.18b)$$

with $\mathbf{d}_k = \rho^2 \hat{\mathbf{h}}_k + (1 - \rho^2) \mathbf{u}$.

To simplify the derivations of the CEP, we represent the conditional pdf $p(\alpha_k | \hat{\mathbf{h}}_k, s_m)$ in a polar coordinate system with origin at $u_{\alpha | \hat{h}, s_m} = \|\mathbf{d}_k\|^2 s_m$, and the corresponding pdf written in the polar coordinate system is

$$p(r, \theta | \hat{\mathbf{h}}_k, s_m) = \frac{r}{\pi \sigma_{\alpha | \hat{h}, s_m}^2} \exp\left(-\frac{r^2}{\sigma_{\alpha | \hat{h}, s_m}^2}\right). \quad (4.19)$$

With (4.19) and the decision region shown in Fig. 4.1, the CEP $P(E | \hat{\mathbf{h}}_k)$ can be computed as

$$\begin{aligned} P(E | \hat{\mathbf{h}}_k) &= 2 \sum_{m=1}^M P(s_m) \int_0^{\pi - \frac{\pi}{M}} \int_{R(\theta)}^{+\infty} p(r, \theta | \hat{\mathbf{h}}_k, s_m) dr d\theta, \\ &= \frac{1}{\pi} \int_0^{\pi - \frac{\pi}{M}} \exp\left\{-\frac{\|\mathbf{d}_k\|^4 E_s \sin^2(\frac{\pi}{M})}{\sigma_{\alpha | \hat{h}, s_m}^2 \sin^2(\phi)}\right\} d\phi, \end{aligned} \quad (4.20)$$

where $R(\theta) = \frac{\|\mathbf{d}_k\|^2 |s_m| \sin(\pi/M)}{\sin(\theta + \pi/M)}$, $P(s_m) = \frac{1}{M}$ for equiprobable transmitted symbols, and we have changed the integration variable to $\phi = \pi - (\theta + \frac{\pi}{M})$ in the second equality. If we define the average SNR γ_n as

$$\gamma_n = \frac{\Omega_n E_s}{N_0} = \frac{(K+1)\sigma_{h_n}^2 E_s}{N_0} \quad (4.21)$$

where Ω_n is the power of the n th fading channel, then the CEP can be written in the following form

$$P(E | \hat{\mathbf{h}}_k) = \frac{1}{\pi} \int_0^{\pi - \frac{\pi}{M}} \prod_{n=1}^N \exp\left\{-\frac{\rho^2 \gamma_n |\hat{h}_n(k) - u_n(1 - \frac{1}{\rho^2})|^2 \sin^2(\frac{\pi}{M})}{\sigma_{\hat{h}_n}^2 [\gamma_n(1 - \rho^2) + K + 1] \sin^2(\phi)}\right\} d\phi, \quad (4.22)$$

where $\sigma_{\hat{h}_n}^2$ is the variance of the estimated CG $\hat{h}_n(k)$, and the identity $\rho^2 = \sigma_{h_n}^2 / \sigma_{\hat{h}_n}^2$ from (4.8) has been used.

The polar coordinate method was used by Craig in [84] for the evaluation of error probability of communication systems with 2-dimensional modulation constellations in AWGN channels. It is extended here for diversity systems with noisy estimated fading channels. The CEP obtained with this method only involves one integration with finite integration limits, and the integrand is the product of exponential functions. We will show next that expressing the CEP in this form can lead to relatively simple evaluations of the unconditional error performance in fading channels.

4.4.2 Error Probability in Rayleigh Fading Channels

The unconditional error probability $P(E)$ of the optimal diversity receiver in Rayleigh fading channels is derived in this subsection based on the CEP presented in (4.22).

For Rayleigh fading channels, the Ricean factor $K = 0$, and both the true CG \mathbf{h}_k and the estimated CG $\hat{\mathbf{h}}_k$ are zero-mean CGRVs, *i.e.*, $\mathbf{u} = 0$. The CEP described in (4.22) for Rayleigh fading channels can be simplified to

$$P(E|\hat{\mathbf{h}}_k) = \frac{1}{\pi} \int_0^{\pi - \frac{\pi}{M}} \prod_{n=1}^N \exp \left\{ -\tilde{\gamma}_{ray} \frac{|\hat{h}_n(k)|^2 \sin^2(\frac{\pi}{M})}{\sigma_{\hat{h}_n}^2 \sin^2(\phi)} \right\} d\phi \quad (4.23)$$

where

$$\tilde{\gamma}_{ray} = \frac{\rho^2}{\gamma_n(1 - \rho^2) + 1} \gamma_n \quad (4.24)$$

is the equivalent SNR for systems with channel estimation error, and is obtained from scaling the average SNR γ_n by a factor $\beta = \frac{\rho^2}{\gamma_n(1 - \rho^2) + 1}$. Based on the fact that $0 < \rho \leq 1$, it can be easily shown that $\tilde{\gamma}_{ray} \leq \gamma_n$, and equality holds when $\rho = 1$.

If we let $g_n = |\hat{h}_n(k)|^2$, then the random variable g_n is χ^2 -distributed with 2-degree of freedom and the unconditional error probability can be directly evaluated with the MGF method. The MGF of the χ^2 -distributed random variable g_n is [76, p. 19]

$$\Phi_g(s) = \mathbb{E}(e^{sg_n}) = (1 - s\sigma_{\hat{h}_n}^2)^{-1} \quad (4.25)$$

where $\sigma_{\hat{h}_n}^2 = \mathbb{E}(|\hat{h}_n(k)|^2) = \mathbb{E}(g_n)$ is the variance of the estimated Rayleigh fading channel. Using the identity presented in (4.25), the unconditional error probability $P(E) = \mathbb{E}[P(E|\hat{\mathbf{h}}_k)]$ for i.i.d. Rayleigh fading channels can be computed as

$$P(E) = \frac{1}{\pi} \int_0^{\pi - \frac{\pi}{M}} \prod_{n=1}^N \left[1 + \tilde{\gamma}_{ray} \frac{\sin^2(\frac{\pi}{M})}{\sin^2(\phi)} \right]^{-1} d\phi. \quad (4.26)$$

Note that the result in (4.26) agrees with [78, eqn. (24)] for the special case of $\rho = 1$, corresponding to the case when the receiver has perfect knowledge of the fading channel. For communication systems with BPSK modulation, we have $M = 2$, and (4.26) can be written as

$$P(E) = \frac{1}{\pi} \int_0^{\frac{\pi}{2}} \left[1 + \frac{\tilde{\gamma}_{ray}}{\sin^2(\phi)} \right]^{-N} d\phi \quad (4.27)$$

Putting the substitution $z = \cot(\phi)$ in (4.27) yields

$$P(E) = \frac{1}{\pi(\tilde{\gamma}_{ray} + 1)^N} \int_0^{+\infty} \frac{1}{(1+z^2)(1 + \frac{\tilde{\gamma}_{ray}}{\tilde{\gamma}_{ray}+1}z^2)^N} dz \quad (4.28)$$

which can then be written in closed-form [87, eqn. (3.259.3)] as

$$P(E) = \frac{1}{2\pi(\tilde{\gamma}_{ray} + 1)^N} B\left(\frac{1}{2}, N + \frac{1}{2}\right) {}_2F_1\left(N, \frac{1}{2}; N + 1; \frac{1}{\tilde{\gamma}_{ray} + 1}\right) \quad (4.29)$$

where $B(\cdot)$ is the Beta function, and ${}_2F_1(\cdot)$ is the Gauss hypergeometric function. With the alternative representation of $B(x, y) = \frac{\Gamma(x)\Gamma(y)}{\Gamma(xy)}$ [87, eqn. (8.384.1)] and noting that $\Gamma(\frac{1}{2}) = \sqrt{\pi}$ [87, eqn. (8.338.2)], we get the closed-form representation of the error probability for BPSK systems as,

$$P(E) = \frac{\Gamma(N + \frac{1}{2})}{2\sqrt{\pi}N!(\tilde{\gamma}_{ray} + 1)^N} {}_2F_1\left(N, \frac{1}{2}; N + 1; \frac{1}{\tilde{\gamma}_{ray} + 1}\right) \quad (4.30)$$

where $\Gamma(x)$ is the Gamma function.

When there is no diversity in the system, *i.e.* $N = 1$, the error probability (4.26) for the MPSK system can be expressed in closed-form by changing the variable of integration to $z = \cot(\phi)$. Substituting $N = 1$ and $z = \cot(\phi)$ in (4.26), we will have

$$P(E) = \frac{1}{\pi} \int_{\alpha}^{+\infty} \left(\frac{1}{z^2 + 1} - \frac{1}{z^2 + b + 1} \right) dz, \quad (4.31)$$

where $\alpha = \pi - \frac{\pi}{M}$, and $b = (\gamma_{ray} \sin^2(\frac{\pi}{M}))^{-1}$. According to the indefinite integral $\int (a^2 + z^2)^{-1} dz = \frac{1}{a} \arctan \frac{z}{a} + C$, where C is a constant, we can write (4.31) into closed-form,

$$P(E) = \frac{1}{\pi} \left[\frac{\pi}{2} - \arctan(\cot(\phi)) \right] - \frac{1}{\pi\sqrt{b+1}} \left[\frac{\pi}{2} - \arctan\left(\frac{1}{a+1} \cot(\phi)\right) \right]. \quad (4.32)$$

Noting that $\phi = \pi - \frac{\pi}{M}$ is in the range of $[0, \pi]$, and put $b = (\gamma_{ray} \sin^2(\frac{\pi}{M}))^{-1}$ in the above equation, we can obtain the closed-form error probability expression for non-diversity MPSK system as

$$P(E) = \frac{M-1}{M} - \sqrt{\frac{\tilde{\gamma}_{ray} \sin^2(\frac{\pi}{M})}{1 + \tilde{\gamma}_{ray} \sin^2(\frac{\pi}{M})}} \left[\frac{1}{2} + \frac{1}{\pi} \arctan \left(\sqrt{\frac{\tilde{\gamma}_{ray} \sin^2(\frac{\pi}{M})}{1 + \tilde{\gamma}_{ray} \sin^2(\frac{\pi}{M})}} \cot\left(\frac{\pi}{M}\right) \right) \right]. \quad (4.33)$$

For the special case of perfect channel information, we have $\tilde{\gamma}_{ray} = \gamma_n$, and (4.33) agrees with the result previously obtained in [83, eqn. (36)] through a different approach.

For diversity systems with $M > 2$, the symbol error rate given in (4.26) must be evaluated numerically. The expression for the SER in (4.26) contains one integration with finite limits, and the integrand is constituted of only elementary functions. Thus, it can be easily evaluated with simple numerical methods. In this thesis, all the numerical integrals are performed with the composite Simpson's method.

4.4.3 Error Probability in Ricean Fading Channels

The unconditional error probability in Ricean fading channels is derived in this subsection.

For i.i.d. fading channels, the pdf of the estimated CG $\hat{\mathbf{h}}_k$ is

$$p(\hat{\mathbf{h}}_k) = \prod_{n=1}^N \frac{1}{\pi \sigma_{\hat{h}_n}^2} \exp \left[-\frac{|\hat{h}_n(k) - u_n|^2}{\sigma_{\hat{h}_n}^2} \right], \quad (4.34)$$

Combining (4.22) with (4.34), we obtain the unconditional error probability $P(E) = \int_{\{\hat{\mathbf{h}}_k\}} P(E|\hat{\mathbf{h}}_k) p(\hat{\mathbf{h}}_k) d\hat{\mathbf{h}}_k$ in a Ricean fading channel as

$$P(E) = \frac{1}{\pi} \int_0^{\pi - \frac{\pi}{M}} \prod_{n=1}^N \lambda_n(\phi) d\phi, \quad (4.35)$$

where

$$\lambda_n(\phi) = \frac{1}{\pi \sigma_{\hat{h}_n}^2} \int_{\{\hat{h}_n\}} \exp \left\{ -\frac{\tilde{\gamma}_{\text{rice}} |\hat{h}_n - u_n(1 - \frac{1}{\rho^2})|^2 \sin^2(\frac{\pi}{M})}{\sigma_{\hat{h}_n}^2 \sin^2(\phi)} - \frac{|\hat{h}_n - u_n|^2}{\sigma_{\hat{h}_n}^2} \right\} d\hat{h}_n, \quad (4.36)$$

with the equivalent SNR $\tilde{\gamma}_{\text{rice}}$ for the Ricean fading channel being defined as

$$\tilde{\gamma}_{\text{rice}} = \frac{\rho^2}{\gamma_n(1 - \rho^2) + K + 1} \gamma_n, \quad (4.37)$$

and the dependence on k has been suppressed by replacing $\hat{h}_n(k)$ by \hat{h}_n in going from (4.34) to (4.36) because the integral does not depend on k . Since the integrand of (4.36) is an exponential function of the square of the integration variable \hat{h}_n , we can write it as the product of a Gaussian pdf and a constant term.

If we let

$$g = \frac{\tilde{\gamma}_{\text{rice}} \sin^2(\frac{\pi}{M})}{\sin^2(\phi)}, \quad (4.38a)$$

$$a = \left(1 - \frac{1}{\rho^2}\right), \quad (4.38b)$$

then (4.36) can be simplified to

$$\lambda_n(\phi) = \frac{1}{\pi\sigma_{\hat{h}_n}^2} \int_{\{\hat{h}_n\}} \exp \left[-\frac{g|\hat{h}_n - au_n|^2 + |\hat{h}_n - u_n|^2}{\sigma_{\hat{h}_n}^2} \right] d\hat{h}_n. \quad (4.39)$$

In order to rewrite the integrand of (4.39) in the functional form of a Gaussian pdf, we need to expand the exponential term $\zeta = g|\hat{h}_n(k) - au_n|^2 - |\hat{h}_n(k) - u_n|^2$,

$$\begin{aligned} \zeta &= g|\hat{h}_n - au_n|^2 + |\hat{h}_n - u_n|^2, \\ &= (g+1)|\hat{h}_n|^2 - 2(ga+1)u_n\hat{h}_n + (ga^2+1)|u_n|^2, \\ &= (g+1) \left| \hat{h}_n - \frac{ga+1}{g+1}u_n \right|^2 + \frac{g(a-1)^2}{g+1}|u_n|^2. \end{aligned} \quad (4.40)$$

Using (4.40), the integrand of (4.39) can be written as the product of a Gaussian pdf and a constant, and $\lambda_n(\phi)$ can be written as

$$\begin{aligned} \lambda_n(\phi) &= \frac{1}{g+1} \exp \left[-\frac{g(a-1)^2}{(g+1)\sigma_{\hat{h}_n}^2}|u_n|^2 \right] \int_{\{\hat{h}_n\}} \frac{1}{\pi\sigma_{\hat{h}_n}^2/(g+1)} \exp \left[-\frac{|\hat{h}_n - \frac{ga+1}{g+1}u_n|^2}{\sigma_{\hat{h}_n}^2/(g+1)} \right] d\hat{h}_n, \\ &= \frac{1}{g+1} \exp \left[-\frac{g(a-1)^2}{(g+1)\sigma_{\hat{h}_n}^2}|u_n|^2 \right]. \end{aligned} \quad (4.41)$$

Substituting g and a from (4.38) into (4.41) yields

$$\lambda_n(\phi) = \exp\left(-\frac{|u_n|^2}{\rho^4\sigma_{\hat{h}_n}^2}\right) \left[1 + \frac{\tilde{\gamma}_{rice} \sin^2(\frac{\pi}{M})}{\sin^2(\phi)} \right]^{-1} \exp \left\{ \frac{|u_n|^2}{\rho^4\sigma_{\hat{h}_n}^2} \left[1 + \frac{\tilde{\gamma}_{rice} \sin^2(\frac{\pi}{M})}{\sin^2(\phi)} \right]^{-1} \right\}. \quad (4.42)$$

From (4.3) and (4.8), we have

$$|u_n|^2 = K \cdot \sigma_{\hat{h}_n}^2 = K \cdot \rho^2 \sigma_{\hat{h}_n}^2. \quad (4.43)$$

Combining (4.42) with (4.43), we get the closed-form representation of $\lambda_n(\phi)$, which is expressed as

$$\lambda_n(\phi) = e^{-\frac{K}{\rho^2}} \left[1 + \tilde{\gamma}_{Ricean} \frac{\sin^2(\frac{\pi}{M})}{\sin^2(\phi)} \right]^{-1} \exp \left\{ \frac{K}{\rho^2} \left[1 + \tilde{\gamma}_{Ricean} \frac{\sin^2(\frac{\pi}{M})}{\sin^2(\phi)} \right]^{-1} \right\}. \quad (4.44)$$

Replacing $\lambda_n(\phi)$ in (4.35) with (4.44), we have the symbol error probability for diversity receivers in estimated Ricean fading channels

$$P(E) = e^{-N\frac{K}{\rho^2}} \int_0^{\pi-\frac{\pi}{M}} \prod_{n=1}^N \left[1 + \tilde{\gamma}_{rice} \frac{\sin^2(\frac{\pi}{M})}{\sin^2(\phi)} \right]^{-1} \exp \left\{ \frac{K}{\rho^2} \left[1 + \tilde{\gamma}_{rice} \frac{\sin^2(\frac{\pi}{M})}{\sin^2(\phi)} \right]^{-1} \right\} d\phi, \quad (4.45)$$

where K is the Ricean factor, ρ is the covariance coefficient between the true CG and the estimated CG, and $\tilde{\gamma}_{rice}$ is defined in (4.37). When $K = 0$, which corresponds to a Rayleigh fading channel, it can be seen that $\tilde{\gamma}_{rice} = \tilde{\gamma}_{ray}$ and (4.45) will specialize to the error probability for a Rayleigh fading channel given in (4.26).

4.5 Numerical Examples

Numerical examples are given in this section to illustrate the influences of noisy channel estimation on the error performances of diversity receivers in fading channels. Some simulation results are also shown to validate our analytical results.

We are using the signal to channel estimation error ratio (SCER) λ as the measure of the quality of the estimated channel since it is independent of the Ricean factor K for a certain channel estimation algorithm. The SCER λ is defined as

$$\lambda = \frac{E_s \Omega}{\sigma_e^2}, \quad (4.46)$$

where E_s is the energy of the transmitted symbol, Ω is the power gain of the fading channel, and σ_e^2 is the power (variance) of the corresponding channel estimation error. Combining this definition with (4.8), we can get a relationship between λ and the covariance coefficient ρ given by

$$\lambda = E_s(K + 1) \frac{\rho^2}{1 - \rho^2}. \quad (4.47)$$

The values of λ and ρ are computed for the pilot assisted polynomial interpolation channel estimation algorithm with off-line training [67] for channels with different Ricean factors, and the results are shown in Fig. 4.2. We can see that for a given signal to noise ratio, the SCER remains almost constant for different values of K , while the covariance coefficient ρ decreases with the increase of K .

The first example is used to validate the analytical error probability expressions derived for a system with a practical channel estimation algorithm. The channel estimation algorithm used in this example is the pilot assisted polynomial interpolation method with off-line training of [67], and the results are shown in Fig. 4.3 and 4.4 for BPSK

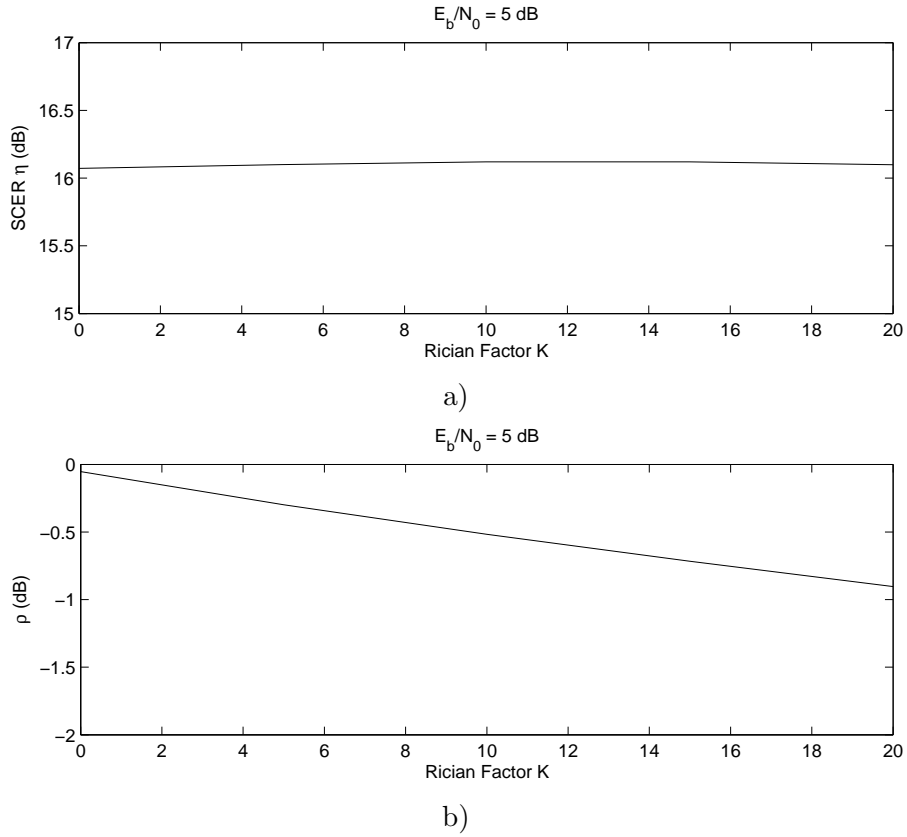


Figure 4.2: The a) SCER λ and b) covariance coefficient ρ vs. the Rician factor K .

and 8PSK systems, respectively. We observe excellent agreement between the results obtained from Monte-Carlo simulation and analysis for various values of the Rician factor K and the diversity order N in both of these two figures.

Next we evaluate the influence of channel estimation error on system performances. The system error probabilities for different values of SCER are shown in Fig. 4.5 and 4.6 for Rayleigh and Rician fading channels, respectively. From the figures, we can see that the symbol error rates of all the systems decrease monotonically with the increase of SCER, as expected, but at different rates for different values of constellation size M and diversity order N . The larger the value of M or N , the larger the rate of decrease. Observe from these figures that systems with higher diversity order and larger constellation size are more sensitive to channel estimation error, as expected. Therefore,

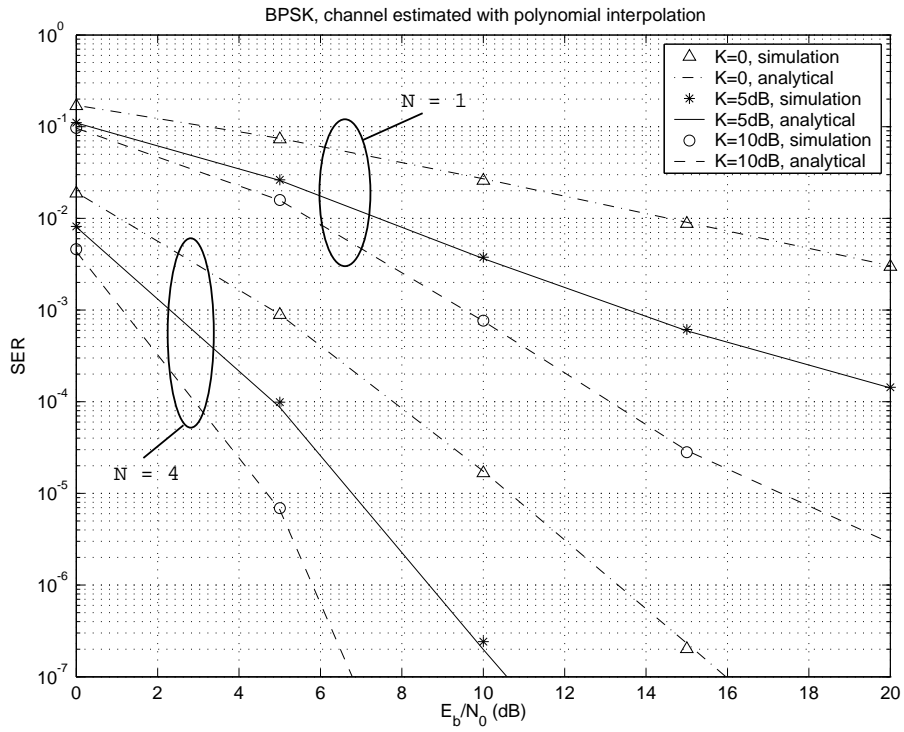


Figure 4.3: The SER of BPSK systems with polynomial interpolation channel estimation.

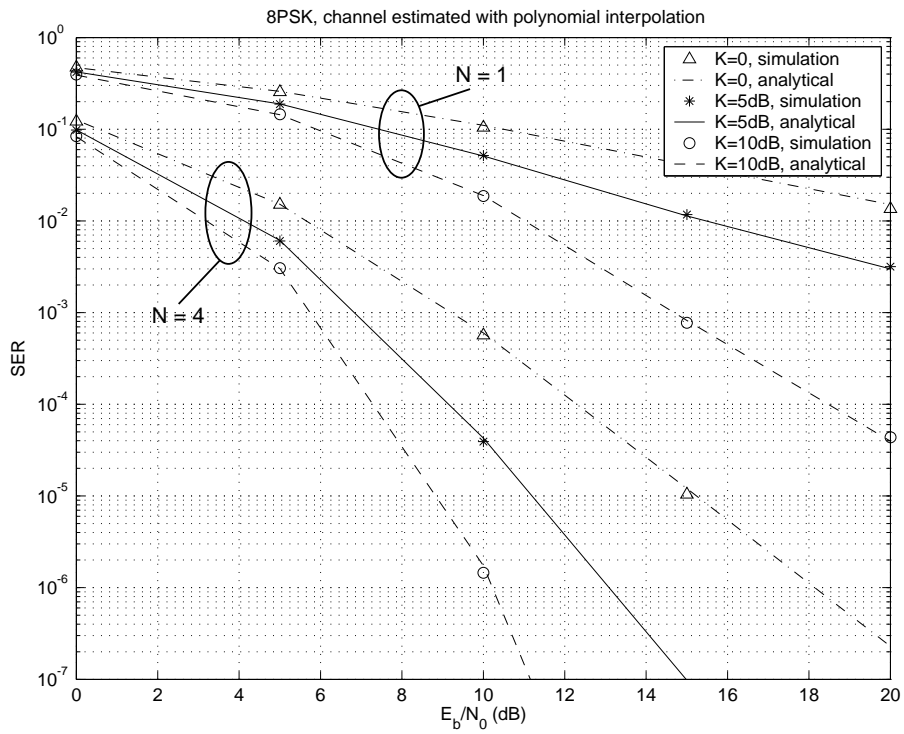


Figure 4.4: The SER of 8PSK systems with polynomial interpolation channel estimation.

more accurate channel estimation algorithms should be employed for systems with larger M or N .

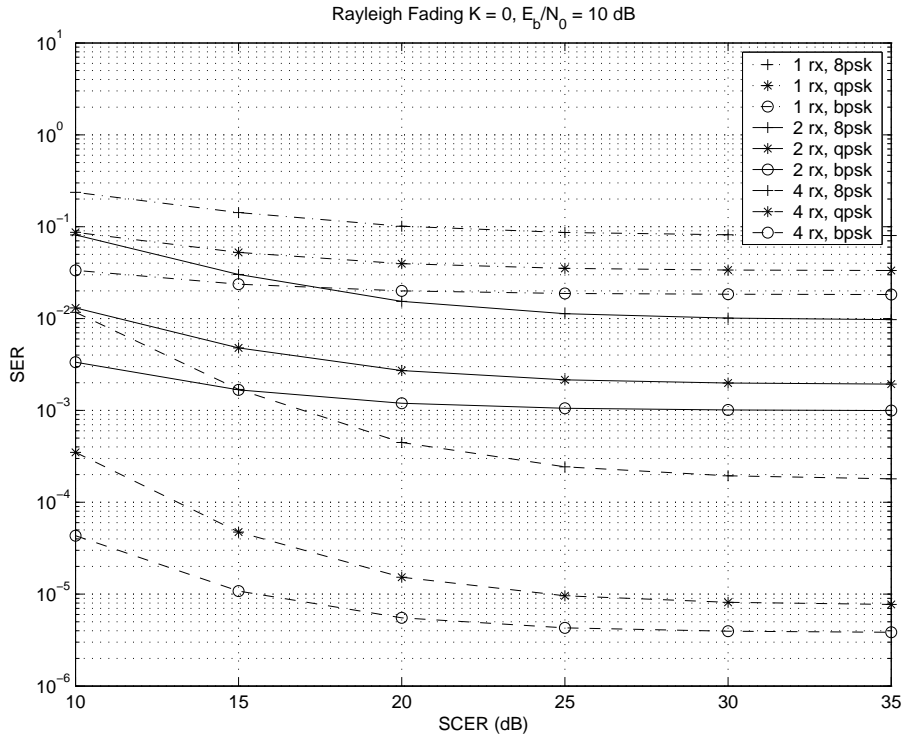


Figure 4.5: The effect of SCER on system performance for Rayleigh fading channels.

The last example is used to study the relationship between channel estimation error and constellation size. Fig. 4.7 shows the SERs of systems with different constellation sizes versus the corresponding diversity orders. The absolute values of the curves' slopes are proportional to the value of SCER, and inversely proportional to the constellation size M . An interesting observation from Fig. 4.7 is that the SER performance of the system with $\text{SCER} = +\infty$ dB, $M = 8$ is close to the performance of the system with $\text{SCER} = 10$ dB and $M = 4$. The same observation holds for the curve with $\text{SCER} = +\infty$ dB, $M = 16$ relative to the curve with $\text{SCER} = 10$ dB and $M = 8$. This observation highlights the importance of having good channel estimation for MPSK systems operating in fading environments. Fig. 4.6 shows that $\text{SCER} = 25$ dB gives essentially the same SER performance as $\text{SCER} = +\infty$ dB. Thus increasing the SCER from 10 dB to 25 dB allows doubling M while maintaining approximately the same SER.

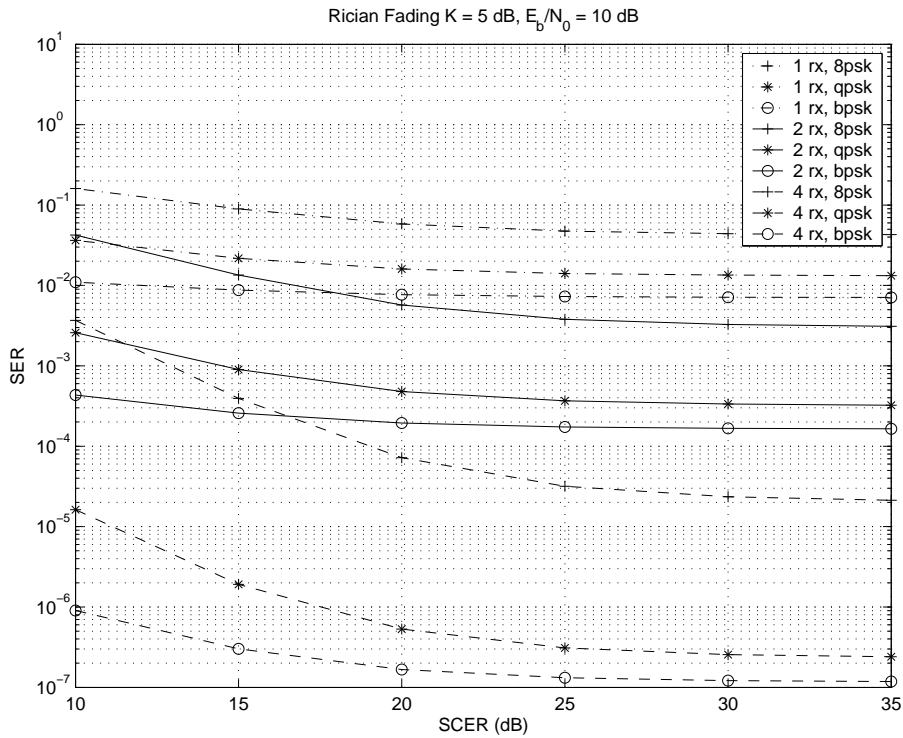


Figure 4.6: The effect of SCER on system performance for Ricean fading channels.

4.6 Conclusion

It has been shown that the conventional MRC diversity receiver structure which is optimal when perfect channel state information is available is not optimal when the channel estimation is corrupted by additive noise. A novel diversity receiver structure which is optimal for noisy channel state information has been derived. Exact, closed-form expressions for the average error probability of the optimal diversity receiver operating with noisy channel state information have been derived for MPSK modulation in both Rayleigh and Ricean channels. The new results for systems with noisy channel state information include systems with perfect channel state information as special cases. Simulation results are in excellent agreement with the theoretical results. Numerical examples considered showed the expected sensitivity of higher-order modulation formats to channel estimation error. A useful observation of significant practical design value was that improving the channel estimation SNR beyond 25 dB does not achieve worthwhile decrease in the SER. A second, interesting and useful observation was that improving

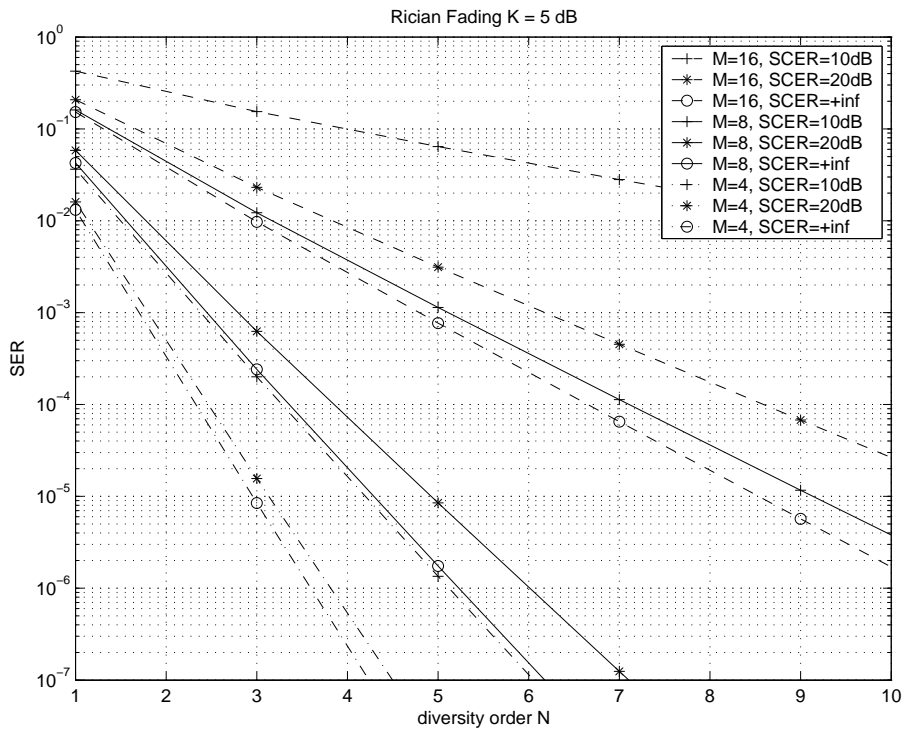


Figure 4.7: The system performance for different constellation sizes and diversity orders.

the channel estimation SNR about 15 dB, from 10 dB to 25 dB allows doubling the constellation size while maintaining approximately the same SER. These observations, and others that can be obtained using the new receiver structures and analytical results given in this chapter, provide useful insights into the design of practical diversity systems.

Chapter 5

On the Performance of Wireless Systems with Doubly Selective Rayleigh Fadings

5.1 Introduction

Error performance analysis of wireless communication systems experiencing frequency-selective fading has been a field of long time interests [14], [89]- [98]. One of the most popular analytical methods used for performance analysis of systems with frequency-selective fading channels (or other trellis structured systems) is the union bound technique [14], [76], [89]- [92], with which system performance upper bounds are evaluated by summing over pairwise error probabilities (PEP) of mutually overlapped error events. Based on the methods used for the computation of the error events PEP, the union bounds are classified as union Chernoff bound and true union bound (TUB) in [76].

Most of the union bound results are for systems with symbol spaced equalizers, *i.e.*, the sampling period T_s at the receiver is equal to the system symbol period T_{sym} . It is well known that the performance of symbol spaced systems depends critically on the sampler timing phase [99], [100]. The timing phase sensitivity of symbol spaced equalizers is induced by the effects of spectrum aliasing of the sampled signals, and it can be avoided by the implementation of fractionally spaced equalizers with $T_s < T_{sym}$ [100]. The

design and union bounds of fractionally spaced receiver with MLSE equalizers are briefly discussed in [73]. The union bound technique provides an effective way to evaluate the upper bounds of system performances. However, the results obtained with union bound are very loose, and the bounds usually diverge at low signal to noise ratio (SNR).

More efficient matched filter bounds are derived in [93]- [97] by assuming that ideal equalization are available at the receiver and the receive filter is perfectly matched to the combined impulse response of the transmit filter and the channel fading. The matched filter bound for a simple two ray fading channel is analyzed in [93], and systems with general power delay profiles are discussed in [94] and [97] with the help of frequency domain analysis and Karhunen-Loève expansion. With the ideal receiver assumption, the matched filter bounds defines the best performance that may be achieved under certain system configuration, whereas it is usually far below the actual error performances of systems with practical receivers.

In this chapter, error performance analysis is carried out for systems with doubly selective Rayleigh fading channels and practical system configurations, and new, tight, closed-form error performance lower bounds are derived for linearly modulated systems with both symbol spaced equalizers and fractionally spaced equalizers. The combined effects of the transmit filter, receive filter, and the physical doubly selective fading channel are represented as a T_s -spaced discrete-time tapped-delay-line filter with *correlated* tap coefficients, with the correlation information being determined by the sampler timing phase, maximum Doppler spread, and power delay profile of the physical channel fading. Instead of resorting to the complex trellis structure analysis utilized in union bound technique, the new performance bound is evaluated on a sample by sample basis with an equivalent single-input multiple-output (SIMO) system method, where the single-input single-output (SISO) communication systems with doubly selective fading channels and additive white Gaussian noise (AWGN) are equivalently represented as SIMO systems with mutually correlated frequency flat fading channels and colored Gaussian noise, with the noise correlation introduced by the time span of the receive filter and receiver oversampling [101]. Compared to the frequency domain analysis utilized by

the matched filter bound [94], much simpler time domain analysis is employed in the derivation of the new bounds. It is shown by simulations that our new analytical results can accurately predicate the error performances of maximum *a posteriori* (MAP) and maximum likelihood sequence estimation (MLSE) equalizers at both low SNR and high SNR. Moreover, it is observed from the analytical results that for systems with practical power delay profiles, fractionally spaced equalizer can not only overcome the problem of timing phase sensitivity, but also achieve significant performance gain over systems with symbol spaced receivers.

The rest of this chapter is organized as follows. Section 5.2 presents a discrete-time representation of the communication systems with doubly selective fading channels, and the statistical properties of the discrete-time system model are analyzed. In Section 5.3, an equivalent SIMO system representation is presented to facilitate the error performance analysis. Based on an optimum decision rule proposed for the equivalent SIMO system, closed-form expressions of the new error probability bounds for doubly selective fading channels are derived in Section 5.4. Numerical examples and simulation results are given in Section 5.5, and Section 5.6 concludes this chapter.

5.2 Discrete-time System Model

An equivalent discrete-time system model is derived in this section for systems experiencing time-varying and frequency-selective channel fadings.

Let $p_T(t)$ and $p_R(t)$ be the time-invariant impulse response of the transmit filter and the receive filter, respectively, and both are normalized with energy of unity. Let $g(t, \tau)$ be the time-varying impulse response of the doubly selective fading channel, and it can be viewed as the response of the fading channel at time t to an impulse input applied at time $t - \tau$. We define the composite impulse response (CIR) of the channel as follows

$$h(t, \tau) = p_R(\tau) \odot g(t, \tau) \odot p_T(\tau), \quad (5.1)$$

where $a(t, \tau) \odot b(t, \tau) = \int_{-\infty}^{+\infty} b(t, \mu) a(t - \mu, \tau - \mu) d\mu$ represents the convolution operation

of time-varying systems. Therefore, the received signal $y(t)$ can be represented by

$$y(t) = \sum_{n=-\infty}^{+\infty} s(n)h(t, t - nT_{sym}) + z(t), \quad (5.2)$$

where $s(n)$ is the modulated information symbol with symbol period T_{sym} , $z(t) = p_R(t) \odot v(t)$ is the noise component at the output of the receive filter, and $v(t)$ is the zero-mean complex-valued white Gaussian noise with variance N_0 . The sampled output of the receive filter at the sampling instant $kT_s + \tau_0$ can be expressed by

$$y(k) = \sum_{l=0}^{L-1} x(k-l)h(k, l) + z(k), \quad (5.3)$$

where the sampling period T_s satisfies $T_s = T_{sym}/\nu$ with the integer ν being the over-sampling factor, $\tau_0 \in [-\frac{T_s}{2}, \frac{T_s}{2}]$ is the sampler timing offset, $y(k) = y(kT_s + \tau_0)$ and $z(k) = z(kT_s + \tau_0)$ are the time-shifted T_s -spaced samples of the received signals and noise components, respectively, $h(k, n) = h(kT_s + \tau_0, nT_s + \tau_0)$ is the sampled version of the continuous-time composite impulse response $h(t, \tau)$, and $x(k)$ is the over-sampled version of the transmitted signals $s(k)$ defined as

$$x(k) = \begin{cases} s(k/\nu), & k/\nu \text{ is integer,} \\ 0, & \text{otherwise.} \end{cases}$$

In the representation of (5.3), the CIR $h(k, l)$ is represented as a causal finite impulse response (FIR) filter in the delay domain l by discarding negligible channel taps. This FIR representation can be verified by the facts that the power delay profile (PDP) $G(\mu)$ of the physical fading channel has finite time domain support, and the tails of the transmit filter and receive filter fall off rapidly in the time domain. Moreover, systems with non-causal CIR can always be made causal by appropriate delays at the receiver. Equation (5.3) is a discrete-time representation of the communication system, and the doubly selective fading channel is represented as a T_s -spaced tapped-delay-line filter. It has been shown in Chapter 2 that the tap coefficients of $h(k, l)$ are mutually correlated in both the temporal domain k and the delay domain l . If the channel experiences wide sense stationary uncorrelated scattering (WSSUS) Rayleigh fadings, then the correlation

function $\rho(k_1 - k_2; l_1, l_2) = E[h(k_1, l_1)h^*(k_2, l_2)]$ can be expressed as (Proposition 2.2)

$$\rho(k_1 - k_2; l_1, l_2) = J_0[2\pi f_d(k_1 - k_2)T_s] \cdot c(l_1, l_2), \quad (5.4)$$

$$\text{with } c(l_1, l_2) = \int_{-\infty}^{+\infty} R_{p_T p_R}(l_1 T_s + \tau_0 - \mu) R_{p_T p_R}^*(l_2 T_s + \tau_0 - \mu) G(\mu) d\mu, \quad (5.5)$$

where $R_{p_T p_R}(t) = p_T(t) \odot p_R(t)$ is the convolution of the transmit filter and receive filter, $J_0(x)$ is the zero-order Bessel function of the first kind, f_d is the maximum Doppler spread of the channel fading, and $G(\mu)$ is the normalized channel power delay profile with $\int_{-\infty}^{+\infty} G(\mu) d\mu = 1$. It needs to point out that (5.5) holds for the condition that $f_d T_s \ll 1$, which is satisfied for most practical conditions. The delay domain correlation $c(l_1, l_2)$ of the discrete-time CIR is introduced by the effects of the time span of the filters $p_T(t)$ and $p_R(t)$, and the underlying WSSUS physical fading channels are white in the delay domain τ . As defined in (5.4) and (5.5), the values of the temporal-delay two-dimensional correlation $\rho(k; l_1, l_2)$ are jointly determined by the maximum Doppler spread f_d , the power delay profile $G(\mu)$ of the physical channel fading, the sampler timing offset τ_0 , and the effects of the transmit filter $p_T(t)$ and receive filter $p_R(t)$. The noise component $z(k)$ of the discrete-time system is a linear transformation of the AWGN $v(t)$, thus it is still Gaussian distributed with zero-mean, and the auto-correlation function is given by (Proposition 2.1)

$$E[z(m+n)z^*(m)] = N_0 \cdot R_{p_R p_R}(nT_s), \quad (5.6)$$

where $R_{p_R p_R}(nT_s) = \int_{-\infty}^{+\infty} p_R(nT_s + \tau) p_R(\tau) d\tau$ is the autocorrelation function of the receive filter. It should be noted that the statistical properties of the noise component are not affected by the timing offset τ_0 . If $R_{p_R p_R}(nT_s) = 0$ for $n \neq 0$, then the discrete-time noise component $z(k)$ is still white, and this is valid for T_{sym} spaced receivers with Nyquist filter. For fractionally spaced receivers, $z(k)$ becomes a colored Gaussian noise process, and the correlation among noise samples is introduced by the effects of oversampling and the time span of the receive filter. It will show in this chapter that the temporal-delay correlation information of $h(k, l)$ along with the noise correlation are critical to the performances of the communication systems.

5.3 Equivalent System Representation

An equivalent SIMO representation of system with doubly selective channel fading is presented in this section to facilitate the system error performance analysis.

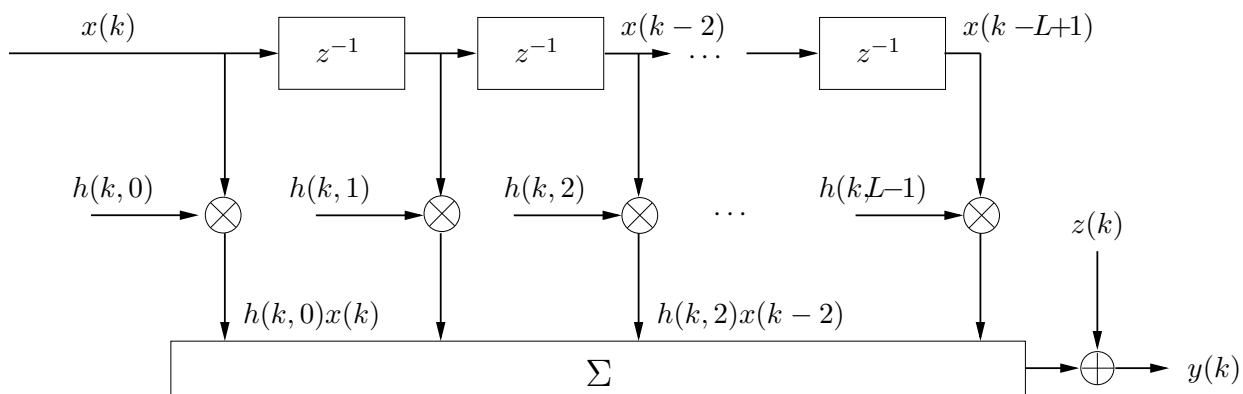
Based on the discrete-time representation of the system given in (5.3), the input-output relationship of the system can be written in matrix format as

$$\mathbf{y}_k = \mathbf{h}_k \cdot x(k) + \tilde{\mathbf{H}}_k \cdot \tilde{\mathbf{x}}_k + \mathbf{z}_k, \quad (5.7)$$

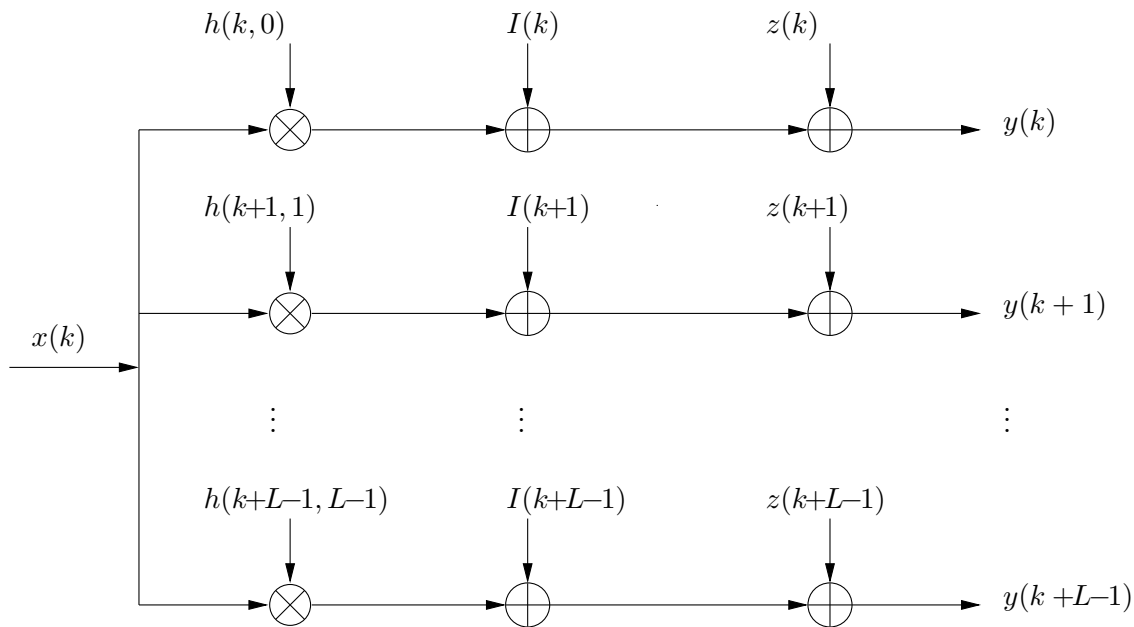
where the vectors $\mathbf{y}_k = [y(k), y(k+1), \dots, y(k+L-1)]^T \in \mathbb{C}^{L \times 1}$, $\mathbf{z}(k) = [z(k), z(k+1), \dots, z(k+L-1)]^T \in \mathbb{C}^{L \times 1}$ comprises all the received samples and noise samples related to the transmitted symbol $x(k)$, with \mathbf{A}^T representing the operation of matrix transpose, $\mathbf{h}_k = [h(k, 0), h(k+1, 1), \dots, h(k+L-1, L-1)]^T \in \mathbb{C}^{L \times 1}$ is the CIR vector related to $x(k)$, $\tilde{\mathbf{x}}_k = [x(k-L+1), \dots, x(k-1), x(k+1), \dots, x(k+L-1)]^T \in \mathbb{C}^{2(L-1) \times 1}$ is the interference vector relative to $x(k)$, and $\tilde{\mathbf{H}}_k \in \mathbb{C}^{L \times 2(L-1)}$ is the corresponding interference CIR matrix defined as

$$\tilde{\mathbf{H}}_k = \begin{bmatrix} h_k(L-1) & \cdots & h_k(1) & 0 & \cdots & 0 \\ 0 & h_{k+1}(L-1) & \cdots & h_{k+1}(2) & h_{k+1}(0) & 0 \\ \vdots & \vdots & \vdots & \vdots & \vdots & \vdots \\ 0 & \cdots & 0 & h_{k+L-1}(L-2) & \cdots & h_{k+L-1}(0) \end{bmatrix}. \quad (5.8)$$

In the representation of (5.7), $x(k)$ is treated as the desired information symbol being transmitted in L parallel frequency-flat fading channels, and the SISO systems with doubly selective fading channels are equivalently represented as an SIMO system with mutually correlated flat fading channels \mathbf{h}_k and colored additive noise \mathbf{z}_k . The ISI components $\mathbf{I}_k = \tilde{\mathbf{H}}_k \tilde{\mathbf{x}}_k = [I(k), I(k+1), \dots, I(k+L-1)]^T$ are represented as cross-channel interference in this equivalent system. The block diagrams of the original SISO system along with its SIMO counterpart are depicted in Fig. 5.1. With such system configurations, the system error performances can be analyzed on a sample-wise basis without resorting to the trellis structure utilized by union bound techniques. Moreover, we are going to show by simulations that the results obtained by this method is more accurate than those obtained from union bounds and matched filter bound.



(a) The discrete-time SISO system with doubly selective fading channel.



(b) The equivalent SIMO system representation.

Figure 5.1: The block diagrams of the SISO system and its equivalent SIMO system representation.

If the interference components $\mathbf{I}_k = \tilde{\mathbf{H}}_k \tilde{\mathbf{x}}_k$ are fully canceled by the receiver, then the error probability of the SIMO system can be minimized. It is well known that MLSE equalizers and MAP equalizers are optimum in the sense of maximizing the likelihood functions or *a posteriori* probabilities of the transmitted symbols. In this chapter, we are going to show by simulations that the MLSE equalizers and MAP equalizers are also asymptotic optimum for the equivalent SIMO systems in the sense of interference cancellation, *i.e.*, the interference components \mathbf{I}_k will tend to 0 if MAP or MLSE equalization algorithms are employed to systems with long enough decoding length. Therefore, tight error probability lower bounds of MLSE and MAP equalizers can be obtained by assuming $\mathbf{I}_k = 0$.

It's worth pointing out that the interference free assumption is also employed in the derivation of the matched filter bounds [93]- [97], where ideal lower bounds are obtained by assuming that the receive filter is perfectly matched to the combined response of the transmit filter and channel fadings. The ideal receiver assumption makes the matched filter bounds unachievable for most practical systems. On the other hand, by considering the effects of practical receive filter and sampler timing phase, the error performance bounds obtained by the equivalent SIMO system method can accurately predicate the performance of systems with practical equalizers.

From (5.7), the interference free SIMO system can be represented as

$$\mathbf{y}_k = \mathbf{h}_k \cdot x_k + \mathbf{z}_k, \quad (5.9)$$

where \mathbf{z}_k is a zero-mean colored Gaussian noise vector. The correlation among the noise samples is introduced by the time span of the receive filter as expressed in (5.6), and the covariance matrix of \mathbf{z}_k is $\mathbf{R}_z = E [\mathbf{z}_k \mathbf{z}_k^H] = N_0 \cdot \mathbf{R}_p$, where \mathbf{A}^H denoting the matrix Hermitian operation, and \mathbf{R}_p is the receive filter correlation matrix defined as

$$\mathbf{R}_p = \begin{bmatrix} R_{p_R p_R}(0) & R_{p_R p_R}(T_s) & \cdots & R_{p_R p_R}[(L-1)T_s] \\ R_{p_R p_R}(T_s) & R_{p_R p_R}(0) & \cdots & R_{p_R p_R}[(L-2)T_s] \\ \vdots & \vdots & \vdots & \vdots \\ R_{p_R p_R}[(L-1)T_s] & R_{p_R p_R}[(L-2)T_s] & \cdots & R_{p_R p_R}(0) \end{bmatrix}. \quad (5.10)$$

The Rayleigh fading channel vector \mathbf{h}_k contains zero-mean complex Gaussian random variables (CGRVs) with covariance matrix $\mathbf{R}_h = E[\mathbf{h}_k \mathbf{h}_k^H]$ given by

$$\mathbf{R}_h = \begin{bmatrix} \rho(0; 0, 0) & \rho(1; 0, 1) & \cdots & \rho(L-1; 0, L-1) \\ \rho(1; 1, 0) & \rho(0; 1, 1) & \cdots & \rho(L-2; 1, L-1) \\ \vdots & \vdots & \vdots & \vdots \\ \rho(L-1; L-1, 0) & \rho(L-2; L-1, 1) & \cdots & \rho(0; L-1, L-1) \end{bmatrix}. \quad (5.11)$$

The correlation coefficient $\rho(k; l_1, l_2)$ is defined in (5.4), and it contains the information of both the temporal correlation $J_0(2\pi f_d k T_s)$ and the delay domain correlation $c(l_1, l_2)$, which are in turn determined by the maximum Doppler spread f_d , the timing phase offset τ_0 , and the power delay profile $G(\mu)$ of the channel fadings.

Based on the statistical properties of the noise vector \mathbf{z}_k and the CIR vector \mathbf{h}_k , the error probabilities of the communication system are analyzed in the next section.

5.4 Error Performance Analysis

Closed-form expressions of symbol error rate (SER) of linearly modulated systems are derived based on an optimum decision rule of the interference free SIMO system, and SERs obtained by this methods are tight lower performance bounds of the corresponding SISO system.

5.4.1 Optimum Combining

An optimum decision rule is presented in this subsection for the interference free SIMO system based on the statistical properties of the colored noise vector \mathbf{z}_k .

The eigenvalue decomposition (EVD) of the receive filter correlation matrix \mathbf{R}_p is

$$\mathbf{R}_p = \mathbf{V} \mathbf{\Omega}_p \mathbf{V}^H, \quad (5.12)$$

where $\mathbf{\Omega}_p = \text{diag}[\omega_1, \cdots, \omega_L] \in \mathbb{R}^{L \times L}$ is a diagonal matrix with the decreasing sequence ω_l , for $l = 1, \cdots, L$ being the eigenvalues of \mathbf{R}_p , and the matrix $\mathbf{V} = [\mathbf{v}_1, \cdots, \mathbf{v}_L]$ are formed by the corresponding eigenvectors. Since the eigenvectors form an orthonormal

basis of the dimension L vector space, \mathbf{V} is an unitary matrix satisfying $\mathbf{V}^H\mathbf{V} = \mathbf{V}\mathbf{V}^H = \mathbf{I}_L$. For systems with rank deficient receive filter correlation matrix \mathbf{R}_p , the statistical properties of the SIMO system cannot be directly evaluated due to the fact that the probability density function (pdf) of the CGRV vector \mathbf{z}_k involves the inverse of the covariance matrix $\mathbf{R}_z = N_0\mathbf{R}_p$ [85, eqn. (7-62)]. To avoid the inverse operation of a rank deficient matrix, we define a new matrix $\mathbf{\Psi}_p$ based on the non-zero eigenvalues of \mathbf{R}_p ,

$$\mathbf{\Psi}_p = \bar{\mathbf{V}}\bar{\mathbf{\Omega}}_p^{-1}\bar{\mathbf{V}}^H \in \mathbb{C}^{L \times L}, \quad (5.13)$$

$$\text{with } \bar{\mathbf{V}} = \begin{bmatrix} \mathbf{v}_1 & \mathbf{v}_2 & \cdots & \mathbf{v}_{L_p} \end{bmatrix} \in \mathbb{C}^{L \times L_p}, \quad (5.14a)$$

$$\bar{\mathbf{\Omega}}_p = \text{diag} \left[\omega_1 \quad \omega_2 \quad \cdots \quad \omega_{L_p} \right] \in \mathbb{R}^{L_p \times L_p}, \quad (5.14b)$$

where L_p is the number of non-zero eigenvalues of \mathbf{R}_p , $\bar{\mathbf{\Omega}}_p$ is a diagonal matrix with its diagonal elements being the non-zero eigenvalues of \mathbf{R}_p , and the corresponding orthonormal eigenvectors \mathbf{v}_l , for $l = 1, 2, \dots, L_p$ form the reduced eigenvector matrix $\bar{\mathbf{V}}$. With these definitions, the error probability minimizing decision rule of the interference free SIMO systems can be stated as follows.

Theorem 5.1: For SIMO systems with colored Gaussian noise, if the transmitted symbols are equiprobable and the fading vector \mathbf{h}_k are known perfectly to the receiver, then the decision rule that minimizes the system error probability is

$$\hat{x}(k) = \underset{s_m \in \mathcal{S}}{\text{argmin}} |\eta_k - q_k \cdot s_m|^2, \quad \frac{k}{\nu} \text{ is integer.} \quad (5.15)$$

where $\hat{x}(k)$ is the detected symbol at time instant k , \mathcal{S} is the modulation alphabet set with Cardinality M , $\eta_k = \mathbf{h}_k^H \mathbf{\Psi}_p \mathbf{y}_k$ is the decision variable, the real-valued scalar $q_k = \mathbf{h}_k^H \mathbf{\Psi}_p \mathbf{h}_k$ is a quadratic form of the CGRV vector \mathbf{h}_k , and the Hermitian matrix $\mathbf{\Psi}_p$ is defined in (5.13) based on the non-zero eigenvalues of the colored noise covariance matrix $\mathbf{R}_z = N_0\mathbf{R}_p$.

Proof: Multiplying both sides of the SIMO system described by equation (5.9) with the reduced eigenvector matrix $\bar{\mathbf{V}}^H$, we will have an equivalent system

$$\bar{\mathbf{y}}_k = \bar{\mathbf{V}}^H \mathbf{h}_k \cdot x(k) + \bar{\mathbf{z}}_k, \quad (5.16)$$

where $\bar{\mathbf{y}}_k = \bar{\mathbf{V}}^H \mathbf{y}_k \in \mathbb{C}^{L_p \times 1}$, $\bar{\mathbf{z}}_k = \bar{\mathbf{V}}^H \mathbf{z}_k \in \mathbb{C}^{L_p \times 1}$ are the sample vector and noise vector of the system, respectively. The noise vector $\bar{\mathbf{z}}_k$ is obtained from linear transformation of the colored Gaussian vector $\mathbf{z}_k \sim \mathcal{N}(\mathbf{0}, N_0 \mathbf{R}_p)$, thus $\bar{\mathbf{z}}_k$ is still Gaussian distributed with zero-mean. The covariance matrix $\mathbf{R}_{\bar{\mathbf{z}}} = E[\bar{\mathbf{z}}_k \bar{\mathbf{z}}_k^H]$ of $\bar{\mathbf{z}}_k$ is

$$\mathbf{R}_{\bar{\mathbf{z}}} = \bar{\mathbf{V}}^H \mathbf{R}_z \bar{\mathbf{V}}_z = N_0 \bar{\mathbf{\Omega}}_p, \quad (5.17)$$

where $\mathbf{R}_z = N_0 \mathbf{R}_p$ is the covariance matrix of the colored noise vector \mathbf{z}_k , $\bar{\mathbf{\Omega}}_p$ is a diagonal matrix containing the non-zero eigenvalues of \mathbf{R}_p , and the second equality of (5.17) is based on the orthonormality of the eigenvectors of \mathbf{R}_p . Since the covariance matrix $\mathbf{R}_{\bar{\mathbf{z}}}$ is diagonal, the elements of $\bar{\mathbf{z}}_k$ are uncorrelated, and the system with colored Gaussian noise \mathbf{z}_k is equivalently converted to a system with white Gaussian noise $\bar{\mathbf{z}}_k$ as described in (5.16).

From (5.16), the sample vector $\bar{\mathbf{y}}_k$ conditioned on the fading vector \mathbf{h}_k and the transmitted symbol $x(k) = s_m$ is Gaussian distributed with mean $\bar{\mathbf{V}}^H \mathbf{h}_k s_m$ and covariance matrix $N_0 \bar{\mathbf{\Omega}}_p$, *i.e.*, $\bar{\mathbf{y}}_k | (\mathbf{h}_k, s_m) \sim \mathcal{N}(\bar{\mathbf{V}}^H \mathbf{h}_k s_m, N_0 \bar{\mathbf{\Omega}}_p)$, and the conditional pdf $p(\bar{\mathbf{y}}_k | \mathbf{h}_k, s_m)$ is

$$p(\bar{\mathbf{y}}_k | \mathbf{h}_k, s_m) = \frac{1}{\det(\pi \bar{\mathbf{\Omega}}_p N_0)} \exp \left[-\frac{1}{N_0} (\bar{\mathbf{y}}_k - \bar{\mathbf{V}}^H \mathbf{h}_k s_m)^H \bar{\mathbf{\Omega}}_p^{-1} (\bar{\mathbf{y}}_k - \bar{\mathbf{V}}^H \mathbf{h}_k s_m) \right]. \quad (5.18)$$

If the transmitted symbol are equiprobable, then the error probability of the system described in (5.16) can be minimized by the maximum *a posteriori* (MAP) rule as

$$\hat{x}_k = \underset{s_m \in \mathcal{S}}{\operatorname{argmin}} \left[(\bar{\mathbf{y}}_k - \bar{\mathbf{V}}^H \mathbf{h}_k s_m)^H \bar{\mathbf{\Omega}}_p^{-1} (\bar{\mathbf{y}}_k - \bar{\mathbf{V}}^H \mathbf{h}_k s_m) \right]. \quad (5.19)$$

Expanding the cost function of (5.19), and noting that the term $\bar{\mathbf{y}}_k^H \bar{\mathbf{\Omega}}_p^{-1} \bar{\mathbf{y}}_k$ is independent of the selection of s_m , the decision rule can be equivalently represented as

$$\begin{aligned} \hat{x}_k &= \underset{s_m \in \mathcal{S}}{\operatorname{argmin}} \left[\mathbf{h}_k^H \mathbf{\Psi}_p \mathbf{h}_k \cdot |s_m|^2 - 2\Re(\mathbf{h}_k^H \mathbf{\Psi}_p \mathbf{y}_k \cdot s_m^*) \right], \\ &= \underset{s_m \in \mathcal{S}}{\operatorname{argmin}} \left[q_k \cdot |s_m|^2 - 2\Re(\eta_k \cdot s_m^*) \right], \end{aligned} \quad (5.20)$$

where $\mathbf{\Psi}_p$ is defined in (5.13), $\eta_k = \mathbf{h}_k^H \mathbf{\Psi}_p \mathbf{y}_k$ is the decision variable, $\Re(a)$ is the real part operator, and $q_k = \mathbf{h}_k^H \mathbf{\Psi}_p \mathbf{h}_k$. Based on the fact that q_k is a real-valued scalar, it's straightforward that (5.20) is equivalent to (5.15), and this completes the proof. \blacksquare

The decision rule given in (5.15) states that the detected symbol multiplied by $q_k = \mathbf{h}_k^H \mathbf{\Psi}_p \mathbf{h}_k$ should have the smallest Euclidean distance with the decision variable η_k . Based on this decision rule, symbol error probabilities are derived for linearly modulated systems with correlated channel fadings and colored Gaussian noise.

5.4.2 Conditional Error Probabilities

The conditional error probabilities (CEP) are derived in this subsection based on the optimum decision rule given in Theorem 5.1.

From (5.9), the decision variable $\eta_k = \mathbf{h}_k^H \mathbf{\Psi}_p \mathbf{y}_k$ can be expressed as

$$\eta_k = \mathbf{h}_k^H \mathbf{\Psi}_p \mathbf{h}_k \cdot x(k) + \mathbf{h}_k^H \mathbf{\Psi}_p \mathbf{z}_k. \quad (5.21)$$

If the modulated symbol $s_m \in \mathcal{S}$ is transmitted, then the decision variable η_k conditioned on the fading vector \mathbf{h}_k and s_m is Gaussian distributed with the conditional pdf $p(\eta_k | \mathbf{h}_k, s_m)$ given by

$$p(\eta_k | \mathbf{h}_k, s_m) = \frac{1}{\pi \sigma_{\eta|h,s_m}^2} \exp\left(-\frac{|\eta_k - \mu_{\eta|h,s_m}|^2}{\sigma_{\eta|h,s_m}^2}\right), \quad (5.22)$$

with the conditional mean $\mu_{\eta|h,s_m}$ and conditional variance $\sigma_{\eta|h,s_m}^2$ defined as

$$\mu_{\eta|h,s_m} = q_k s_m, \quad (5.23a)$$

$$\sigma_{\eta|h,s_m}^2 = q_k N_0, \quad (5.23b)$$

where $q_k = \mathbf{h}_k^H \mathbf{\Psi}_p \mathbf{h}_k$ is a quadratic form of the CGRV vector \mathbf{h}_k , and the identity $\bar{\mathbf{V}}^H \mathbf{R}_p \bar{\mathbf{V}} = \bar{\mathbf{\Omega}}_p$ is used in the derivation of (5.23b). Since the conditional mean $\mu_{\eta|h,s_m}$ and the conditional variance $\sigma_{\eta|h,s_m}^2$ are explicit functions of the quadratic form q_k , the conditional pdf $p(\eta_k | \mathbf{h}_k, s_m)$ can also be equivalently represented as $p(\eta_k | q_k, s_m)$, and $\eta_k | (q_k, s_m) \sim \mathcal{N}(q_k s_m, q_k N_0)$.

To simplify the derivation of the CEP, we represent the conditional pdf $p(\eta_k | q_k, s_m)$ in a polar coordinate system with origin at $\mu_{\eta|h,s_m} = q_k s_m$, and the corresponding pdf written in the polar coordinate system is

$$p(r, \theta | q_k, s_m) = \frac{r}{\pi q_k N_0} \exp\left(-\frac{r^2}{q_k N_0}\right). \quad (5.24)$$

Based on the conditional pdf of the decision variable η_k , the CEPs for M-ary phase-shift-keying (MPSK), M-ary amplitude-shift-keying (MASK) and square M-ary quadrature-amplitude-modulation (MQAM) systems are derived as follows.

■ **MPSK:**

Based on the decision rule given in (5.15), the decision region for η_k of the MPSK symbol s_m should be a $\frac{2\pi}{M}$ angle sector centered around $q_k s_m$, and the CEP $P_{\text{MPSK}}(E|q_k, s_m)$ equals to the probability that η_k is outside of the decision region.

With (5.24) and the analysis in Section 4.4.1, the CEP $P(E|q_k)$ can be computed as

$$\begin{aligned} P_{\text{MPSK}}(E|q_k) &= 2 \sum_{m=1}^M P(s_m) \int_0^{\pi - \frac{\pi}{M}} \int_{R(\theta)}^{+\infty} p(r, \theta|q_k, s_m) dr d\theta, \\ &= \frac{1}{\pi} \int_0^{\pi - \frac{\pi}{M}} \exp \left\{ -\frac{\gamma \cdot q_k \sin^2 \left(\frac{\pi}{M} \right)}{\sin^2 \phi} \right\} d\phi, \end{aligned} \quad (5.25)$$

where $R(\theta) = \frac{q_k |s_m| \sin(\pi/M)}{\sin(\theta + \pi/M)}$, $P(s_m) = \frac{1}{M}$ for equiprobable transmitted symbols, $\gamma = \frac{E_s}{N_0}$ is the average signal to noise ratio without fading, and we have changed the integration variable to $\phi = \pi - (\theta + \frac{\pi}{M})$ in the second equality.

■ **MASK:**

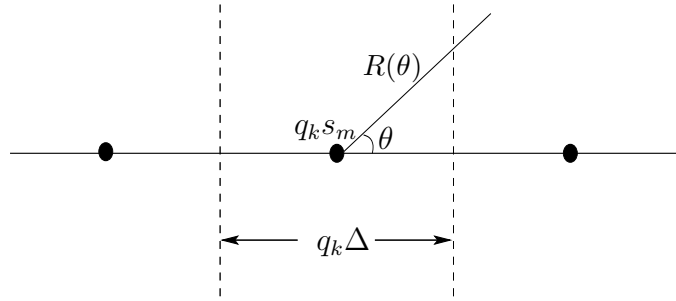
The decision regions for the MASK signal s_m is shown in Fig. 5.2, where Δ is the minimum Euclidean distance between two adjacent MASK symbols. Consider the error probability of both the $M - 2$ inner symbols and 2 marginal symbols of the MASK constellation, the CEP $P_{\text{MASK}}(E|q_k)$ can be computed as

$$\begin{aligned} P_{\text{MASK}}(E|q_k) &= \frac{1}{M} [(M - 2) \times 4 + 2 \times 2] \int_0^{\frac{\pi}{2}} \int_{R(\theta)}^{+\infty} p(r, \theta|\mathbf{h}_k, s_m) dr d\theta, \\ &= 2 \left(1 - \frac{1}{M} \right) \cdot \frac{1}{\pi} \int_0^{\frac{\pi}{2}} \exp \left\{ -\frac{3\gamma \cdot q_k}{(M^2 - 1) \sin^2 \phi} \right\} d\phi, \end{aligned} \quad (5.26)$$

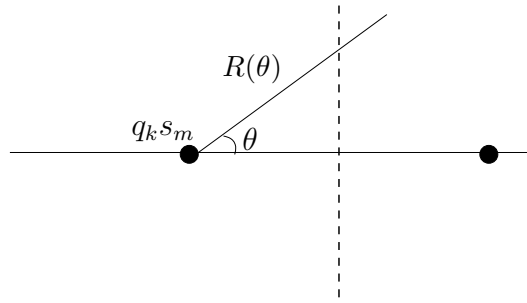
where $R(\theta) = q_k \cdot \sqrt{\frac{3E_s}{(M^2 - 1) \cos^2 \theta}}$, with $E_s = \frac{\Delta^2(M^2 - 1)}{12}$ being the average symbol energy of the MASK constellation, $\gamma = \frac{E_s}{N_0}$ is the average SNR, and the integration variable is changed to $\phi = \frac{\pi}{2} - \theta$ in the second equality. With the alternative representation of the Gaussian-Q function [76, eqn. (4.2)], the CEP can also be written as

$$P_{\text{MASK}}(E|q_k) = 2 \left(1 - \frac{1}{M} \right) \cdot Q \left(\sqrt{\frac{6\gamma \cdot q_k}{M^2 - 1}} \right), \quad (5.27)$$

where $Q(x) = \int_x^{+\infty} \frac{1}{\sqrt{2\pi}} \exp\left(-\frac{y^2}{2}\right) dy$ is the Gaussian Q-function.



(a) The decision region for the inner symbol s_m of the MASK constellation is a strip area defined by the dashed-lines.



(b) The decision region for the marginal symbol s_m of the MASK constellation is a half-plane to the left of the dashed-line.

Figure 5.2: the decision region for MASK symbol

■ **MQAM:**

The square MQAM can be viewed as the orthogonal combination of two independent \sqrt{M} -ASK signals, each with average symbol energy $\frac{E_s}{2}$. The event of correct decision of the MQAM system is equivalent to the event that correct decisions are made on both of the two independent \sqrt{M} -ASK systems. Based on (5.27), the CEP $P_{\text{MQAM}}(E|q_k)$ can

Table 5.1: Parameters of the Unified Error Probability Expressions for Linearly Modulated Systems

Parameters	ζ	β_1	β_2	ψ_1	ψ_2
MPSK	$\sin^2 \frac{\pi}{M}$	1	0	$\pi \left(1 - \frac{1}{M}\right)$	0
MASK	$\frac{3}{M^2-1}$	$2\left(1 - \frac{1}{M}\right)$	0	$\frac{\pi}{2}$	0
MQAM	$\frac{3}{2(M-1)}$	$4\left(1 - \frac{1}{\sqrt{M}}\right)$	$4\left(1 - \frac{1}{\sqrt{M}}\right)^2$	$\frac{\pi}{2}$	$\frac{\pi}{4}$

be expressed by

$$\begin{aligned}
 P_{\text{MQAM}}(E|q_k) &= 1 - \left[1 - P_{\sqrt{M}\text{-ASK}, \frac{E_s}{2}}(E|q_k)\right]^2, \\
 &= 4\left(1 - \frac{1}{\sqrt{M}}\right) \cdot Q\left(\sqrt{\frac{3\gamma q_k}{M-1}}\right) - \\
 &\quad 4\left(1 - \frac{1}{\sqrt{M}}\right)^2 \cdot Q^2\left(\sqrt{\frac{3\gamma q_k}{M-1}}\right). \tag{5.28}
 \end{aligned}$$

With the alternative expressions of the two-dimensional Gaussian Q-function [76, eqn. (4.2), (4.9)], the CEP $P_{\text{MQAM}}(E|q_k)$ can be written in the desired exponential form,

$$\begin{aligned}
 P_{\text{MQAM}}(E|q_k) &= \frac{4}{\pi} \left(1 - \frac{1}{\sqrt{M}}\right) \int_0^{\frac{\pi}{2}} \exp\left\{-\frac{3\gamma \cdot q_k}{2(M-1) \sin^2 \phi}\right\} d\phi - \\
 &\quad \frac{4}{\pi} \left(1 - \frac{1}{\sqrt{M}}\right)^2 \int_0^{\frac{\pi}{4}} \exp\left\{-\frac{3\gamma \cdot q_k}{2(M-1) \sin^2 \phi}\right\} d\phi. \tag{5.29}
 \end{aligned}$$

Eqns. (5.25), (5.26) and (5.29) are the conditional error probabilities for MPSK, MASK, and MQAM systems, respectively. Since all of the CEPs contain integrations with integrand in the form of an exponential function of $q_k = \mathbf{h}_k^H \mathbf{\Psi}_p \mathbf{h}_k$, the CEPs for the three modulated systems can be written in a unified form as follows,

$$P(E|q_k) = \sum_{i=1}^2 \frac{\beta_i}{\pi} \int_0^{\psi_i} \exp\left\{-\zeta \cdot \frac{\gamma \cdot q_k}{\sin^2 \theta}\right\} d\theta, \tag{5.30}$$

where γ is the average SNR without fading, and the values of ζ , β_i and ψ_i for the various modulation schemes are listed in Table 5.1.

5.4.3 Symbol Error Rate

The unconditional error probabilities $P(E)$ of the linearly modulated systems with colored noise and correlated Rayleigh fading channels are derived in this subsection with

the help of the characteristic function (CHF) of quadratic form of CGRV vector.

For Rayleigh fading channels, the fading vector \mathbf{h}_k is zero-mean Gaussian distributed with covariance matrix \mathbf{R}_h given in (5.11), *i.e.*, $\mathbf{h}_k \sim \mathcal{N}(\mathbf{0}, \mathbf{R}_h)$. In the unified representation of the CEPs in (5.30), the integrands have the form of an exponential function of the real-valued random variable $q_k = \mathbf{h}_k^H \mathbf{\Psi}_p \mathbf{h}_k$. Since $\mathbf{\Psi}_p$ is a Hermitian matrix, q_k is a quadratic form of the zero-mean CGRV vector \mathbf{h}_k , and the CHF of q_k is [102]

$$\Phi_q(w) = \mathbb{E} \left(e^{jwq_k} \right) = [\det (\mathbf{I}_L - jw\mathbf{R}_h\mathbf{\Psi}_p)]^{-1}, \quad (5.31)$$

where w is a dumb variable, and \mathbf{I}_L is an $L \times L$ identity matrix.

With the CHF defined in (5.31) and the unified CEP $P(E|q_k)$ given in (5.30), the unconditional error probability $P(E) = \mathbb{E} [P(E|q_k)]$ in Rayleigh fading channels can be computed as

$$\begin{aligned} P(E) &= \sum_{i=1}^2 \frac{\beta_i}{\pi} \int_0^{\psi_i} \left[\det \left(\mathbf{I}_L + \frac{\zeta\gamma}{\sin^2\theta} \mathbf{R}_h \mathbf{\Psi}_p \right) \right]^{-1} d\theta, \\ &= \sum_{i=1}^2 \frac{\beta_i}{\pi} \int_0^{\psi_i} \left\{ \det \left[\mathbf{I}_L + \frac{\zeta\gamma}{\sin^2\theta} \mathbf{\Psi}_p^{\frac{1}{2}} \mathbf{R}_h \left(\mathbf{\Psi}_p^{\frac{1}{2}} \right)^H \right] \right\}^{-1} d\theta, \end{aligned} \quad (5.32)$$

where $\mathbf{\Psi}_p^{\frac{1}{2}}$ is the square root of the matrix $\mathbf{\Psi}_p$ satisfying $\left(\mathbf{\Psi}_p^{\frac{1}{2}} \right)^H \mathbf{\Psi}_p^{\frac{1}{2}} = \mathbf{\Psi}_p$, and the identity $\det(\mathbf{I} + \mathbf{A}\mathbf{B}) = \det(\mathbf{I} + \mathbf{B}\mathbf{A})$ is used in (5.32).

Performing eigenvalue decomposition of the product matrix $\mathcal{R} = \mathbf{\Psi}_p^{\frac{1}{2}} \mathbf{R}_h \left(\mathbf{\Psi}_p^{\frac{1}{2}} \right)^H$, we will have

$$\mathcal{R} = \mathbf{U}\mathbf{\Lambda}\mathbf{U}^H, \quad (5.33)$$

where $\mathbf{\Lambda} = \text{diag}[\lambda_1, \dots, \lambda_{\tilde{L}}, 0, \dots, 0] \in \mathbb{R}^{L \times L}$ is a diagonal matrix with the diagonal elements being the eigenvalues of \mathcal{R} , \tilde{L} is the number of non-zero eigenvalues of \mathcal{R} , and the columns of the unitary matrix \mathbf{U} are the corresponding orthonormal eigenvectors with $\mathbf{U}\mathbf{U}^H = \mathbf{I}_L$. The values of \tilde{L} and λ_l , for $l = 1, 2, \dots, \tilde{L}$ are determined by both $\mathbf{\Psi}_p$ and the temporal-delay correlation matrix \mathbf{R}_h , which are in turn related to the sampler timing offset, and the statistical properties of the colored Gaussian noise and the doubly selective channel fadings.

Substituting (5.32) with (5.33), we can write the symbol error probability as

$$\begin{aligned}
P(E) &= \sum_{i=1}^2 \frac{\beta_i}{\pi} \int_0^{\psi_i} \left\{ \det \left[\mathbf{U} \left(\mathbf{I}_L + \frac{\zeta \gamma}{\sin^2 \theta} \mathbf{\Lambda} \right) \mathbf{U}^H \right] \right\}^{-1} d\theta \\
&= \sum_{i=1}^2 \frac{\beta_i}{\pi} \int_0^{\psi_i} \prod_{l=1}^{\tilde{L}} \left[1 + \gamma \cdot \frac{\zeta \lambda_l}{\sin^2 \theta} \right]^{-1} d\theta.
\end{aligned} \tag{5.34}$$

The closed-form expressions of the SER given in (5.34) can be obtained by partial fraction expansion. For all systems with practical PDPs, *e.g.*, the exponential profile [94], the Typical Urban profile [22], the non-zero eigenvalues λ_l , for $l = 1, \dots, \tilde{L}$ are different from each other, and the SER can be expressed as

$$P(E) = \sum_{i=1}^2 \sum_{l=1}^{\tilde{L}} \frac{\beta_i d_l}{\pi} \int_0^{\psi_i} \left[1 + \gamma \cdot \frac{\zeta \lambda_l}{\sin^2 \theta} \right]^{-1} d\theta \tag{5.35}$$

where the value of d_l can be computed by

$$\begin{aligned}
d_l &= \prod_{\substack{j=1 \\ j \neq l}}^{\tilde{L}} \left[1 + \gamma \cdot \frac{\zeta \lambda_j}{\sin^2 \theta} \right]_{\sin^2 \theta = -\gamma \zeta \lambda_l}^{-1} \\
&= \prod_{\substack{j=1 \\ j \neq l}}^{\tilde{L}} \frac{\lambda_l}{\lambda_j - \lambda_l}, \quad \text{for } l = 1, 2, \dots, \tilde{L}.
\end{aligned} \tag{5.36}$$

The integral in (5.35) can be expressed in closed-form as,

$$\begin{aligned}
\frac{1}{\pi} \int_0^{\psi} \left[1 + \frac{\gamma \zeta \lambda_l}{\sin^2 \theta} \right]^{-1} d\theta &= \frac{\psi}{\pi} - \sqrt{\frac{\gamma \zeta \lambda_l}{1 + \gamma \zeta \lambda_l}} \times \\
&\quad \left[\frac{1}{2} - \frac{1}{\pi} \arctan \left(\sqrt{\frac{\gamma \zeta \lambda_l}{1 + \gamma \zeta \lambda_l}} \cot \psi \right) \right], \forall \psi \in [0, 2\pi],
\end{aligned} \tag{5.37}$$

and the derivation of (5.37) is outlined in Appendix C.

From (5.35)-(5.37), the unified closed-form SER solutions of the linearly modulated systems can be expressed by

$$\begin{aligned}
P(E) &= \sum_{i=1}^2 \sum_{l=1}^{\tilde{L}} \prod_{\substack{j=1 \\ j \neq l}}^{\tilde{L}} \frac{\beta_i \lambda_l}{\lambda_j - \lambda_l} \left\{ \frac{1}{\pi} - \sqrt{\frac{\gamma \alpha \lambda_l}{1 + \gamma \alpha \lambda_l}} \times \right. \\
&\quad \left. \left[\frac{1}{2} - \frac{1}{\pi} \arctan \left(\sqrt{\frac{\gamma \alpha \lambda_l}{1 + \gamma \alpha \lambda_l}} \cot \psi_i \right) \right] \right\}.
\end{aligned} \tag{5.38}$$

With the variables of ζ , β_i , and ψ_i in (5.38) substituted by the values given in Table 5.1, the closed-form expressions of the SER lower bounds for MPSK, MASK, and MQAM systems with doubly selective channel fadings can be written as follows.

■ **MPSK:**

$$P_{\text{MPSK}}(E) = \sum_{l=1}^{\tilde{L}} \prod_{\substack{j=1 \\ j \neq l}}^{\tilde{L}} \frac{\lambda_l}{\lambda_j - \lambda_l} \left\{ \frac{M-1}{M} - \sqrt{\frac{\gamma \lambda_l \sin^2(\frac{\pi}{M})}{1 + \gamma \lambda_l \sin^2(\frac{\pi}{M})}} \times \left[\frac{1}{2} + \frac{1}{\pi} \arctan \left(\sqrt{\frac{\gamma \lambda_l \sin^2(\frac{\pi}{M})}{1 + \gamma \lambda_l \sin^2(\frac{\pi}{M})}} \cot \left(\frac{\pi}{M} \right) \right) \right] \right\}. \quad (5.39)$$

■ **MASK:**

$$P_{\text{MASK}}(E) = \sum_{l=1}^{\tilde{L}} \prod_{\substack{j=1 \\ j \neq l}}^{\tilde{L}} \frac{\lambda_l}{\lambda_j - \lambda_l} \left[\frac{M-1}{M} \left(1 - \sqrt{\frac{3\gamma \lambda_l}{M^2 - 1 + 3\gamma \lambda_l}} \right) \right]. \quad (5.40)$$

■ **MQAM:**

$$P_{\text{MQAM}}(E) = \sum_{l=1}^{\tilde{L}} \prod_{\substack{j=1 \\ j \neq l}}^{\tilde{L}} \frac{\lambda_l}{\lambda_j - \lambda_l} \left\{ 2 \left(1 - \frac{1}{\sqrt{M}} \right) \left(1 - \sqrt{\frac{3\gamma \lambda_l}{3\gamma \lambda_l + 2M - 2}} \right) + \left(1 - \frac{1}{\sqrt{M}} \right)^2 \times \left[\frac{4}{\pi} \sqrt{\frac{3\gamma \lambda_l}{3\gamma \lambda_l + 2M - 2}} \left(\frac{\pi}{2} - \arctan \sqrt{\frac{3\gamma \lambda_l}{3\gamma \lambda_l + 2M - 2}} \right) - 1 \right] \right\}. \quad (5.41)$$

For the special case of frequency-flat fading channel, we have $\tilde{L} = 1$, and (5.39) and (5.41) agree with the exact error probability expressions previously obtained in [83, eqn. (36), (43)] for systems with flat fading channels.

In some special cases, such as the equal gain T_{sym} -spaced PDP with T_{sym} -spaced receiver, some of the eigen values of \mathcal{R} may have identical values. To avoid the complexity of partial fraction expansion of expressions with roots multiplicity, an approximation method is presented in [102], where identical eigenvalues are slightly modified without apparently affecting the system performance. By subtracting different small positive random numbers from identical eigenvalues, a valid error probability lower bound can still be obtained from (5.38). Moreover, exact values of $P(E)$ can still be computed

from numerical integration of (5.34), which can be easily evaluated since it has finite integration limits and the integrand contains only elementary functions.

In the SER expressions given in (5.34) and (5.39)-(5.41), the effects of receiver over-sampling, sampler timing offset τ_0 , Doppler spread f_d and power delay profile $G(\mu)$ of the physical channel fadings are quantified as the eigenvalues of the matrix \mathcal{R} , which is a function of the temporal-delay correlation matrix \mathbf{R}_h and the matrix $\mathbf{\Psi}_p$. It should be noted that the dependence of $P(E)$ on f_d is introduced by the relative time delay among the elements of the fading vector \mathbf{h}_k . For conventional SIMO systems in flat fading channels, *i.e.*, a system with one transmit antenna and L receive antennas, the uncoded performances are usually not affected by the Doppler spread of the channel.

5.5 Numerical Examples

Numerical examples are given in this section to illustrate the error performances of wireless communication systems with doubly selective fading channels, and simulation results are also provided to validate our analytical expressions.

In the examples, the symbol period is set to $T_{sym} = 3.69\mu s$, and the maximum Doppler spread f_d is assumed to be 200Hz, which corresponds to a mobile speed of 120 km/hr at the carrier frequency of 1.8 GHz. Unless otherwise specified, root raised cosine (RRC) filter with roll-off factor $\alpha = 0.3$ is used as both the transmit filter and receive filter.

In the first example, we are going to compare our new analytical results with the well-known union Chernoff bounds and TUB [76]. Since the inter-tap correlation information will lead to “considerable analytical difficulty” [73] to obtain the union bounds, a simple two ray equal-gain T_{sym} -spaced power delay profile with uncorrelated channel gains are used in this example. The analytical results along with the corresponding simulation results obtained with MLSE and MAP equalizers are shown in Fig. 5.3. In the computation of the union bounds, the trellis structure of the system is analyzed based on the error state transition matrix method [90]. It is clearly from the figure that our new performance results are superior than both of the two union bounds. The new SER

lower bound can accurately predict the performances of MLSE and MAP equalizers at both low SNR and high SNR. On the other hand, the union Chernoff bound and TUB converges only when E_b/N_0 is higher than 20dB. Even at high SNR, the union Chernoff bound is still 1dB away from the actual error performances. Moreover, Since the error probabilities of the newly proposed methods are analyzed on a symbol by symbol basis, considerable computation efforts can be saved compared to the trellis structure analysis used by the union bounds.

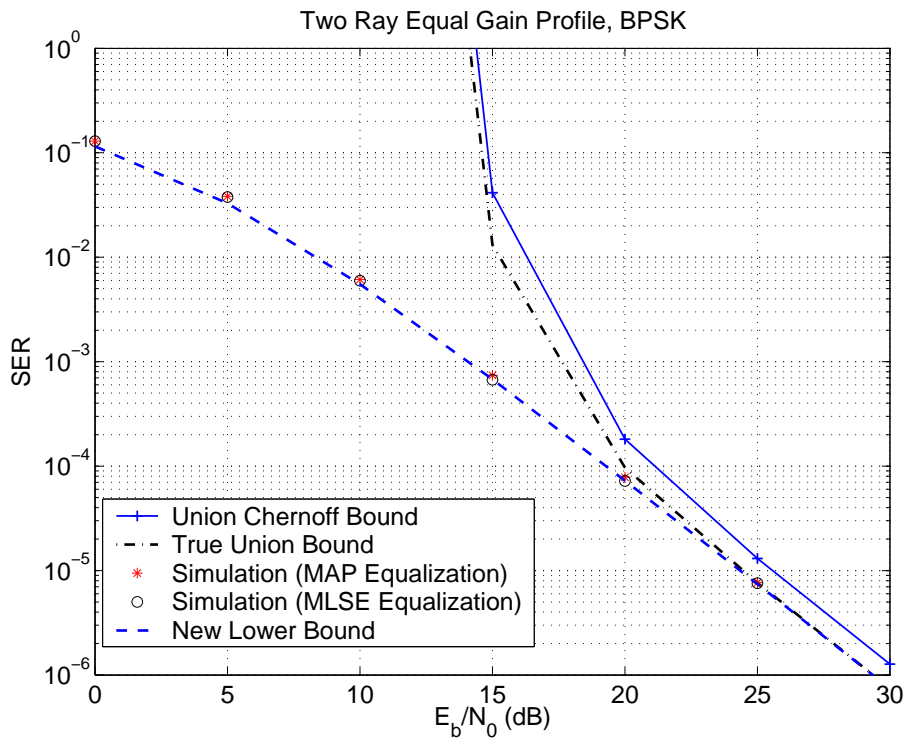


Figure 5.3: Comparison of performance bounds of systems with two ray equal gain channel profile. Decoding length for the equalizers: 1024 symbols.

The performances of systems with practical power delay profiles are illustrated in the next example, and the Typical Urban (TU) profile [22] is used to model the frequency-selective channel fading. Root raised cosine filters with 100% excessive bandwidth ($\alpha = 1$) are used as the transmit filter and receive filter. Fig. 5.4 shows the theoretical error performances as well as the simulation results obtained with the MAP equalizer, and the matched filter bound is also listed in the figure for comparison. From the figure, it

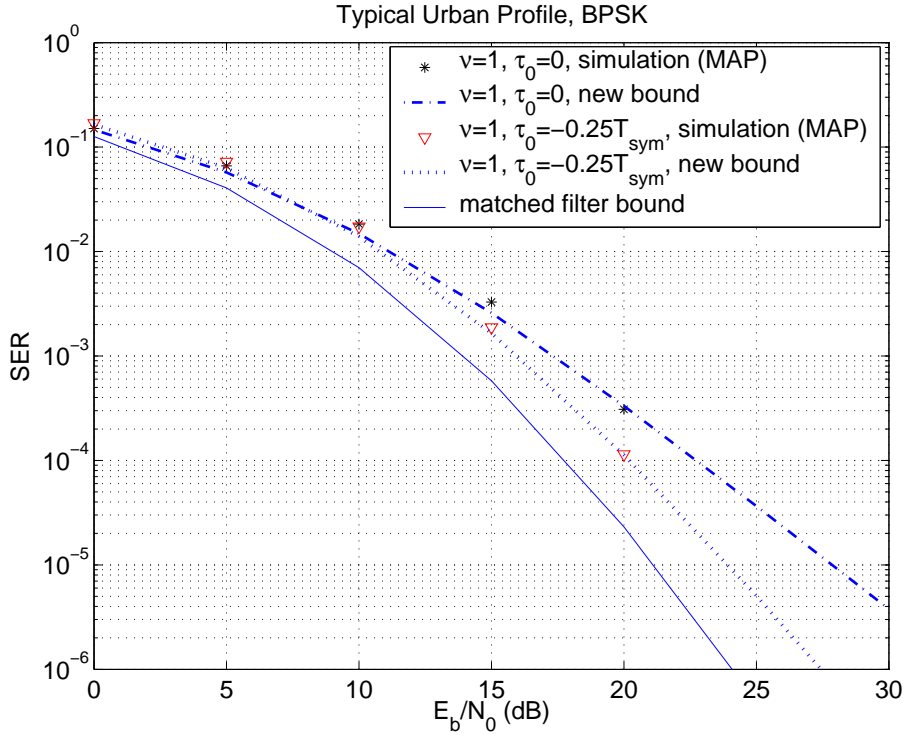
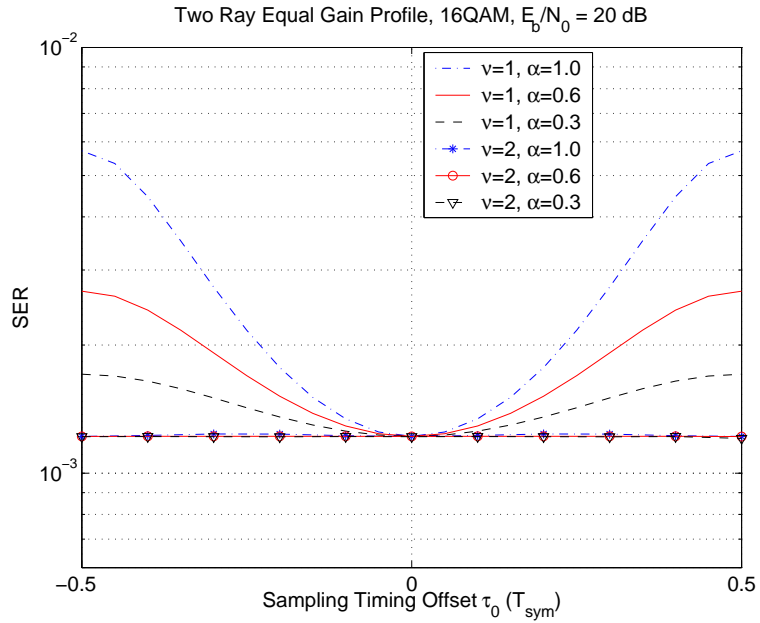


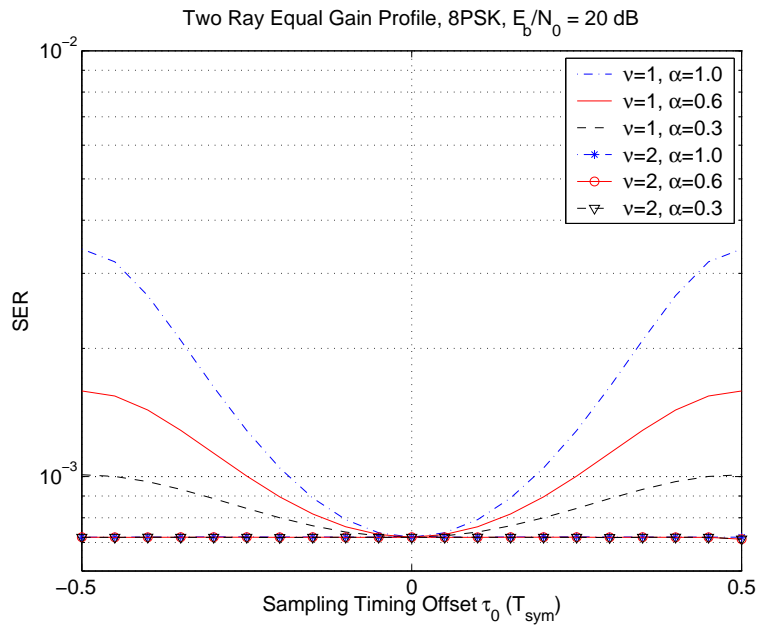
Figure 5.4: Performances of systems with Typical Urban profile. ν : oversampling factor. τ_0 : sampling timing offset. Decoding length of the equalizers: 1024 symbols.

is interesting to note that for systems without oversampling ($\nu = 1$), the performance of the system with sampler timing offset $\tau_0 = -0.25T_{sym}$ is superior than that of the system with $\tau_0 = 0$. This phenomenon is due to the fact that the power of the TU profile is dominated by the delayed scattering rays of the physical channel fadings, and the power of the first ray (or the zero-delay scattering ray) of the channel accounts for only 19.0% of the total channel power.

Moreover, excellent agreements between the simulation results and our new performance bounds can be observed from the figure for $E_b/N_0 \geq 10$ dB. The results in Fig. 5.3 and 5.4 shows that the performances of MLSE and MAP equalizers coincide with the performance of interference free systems at high SNR, which means the MLSE and MAP equalizers are asymptotic optimum in the sense of interference cancellation. Even at low SNR, the lower bounds are still very tight compared to the simulation results. It can also be observed from Fig. 5.4 that the matched filter bound is a loose lower bound for such



(a) 16QAM



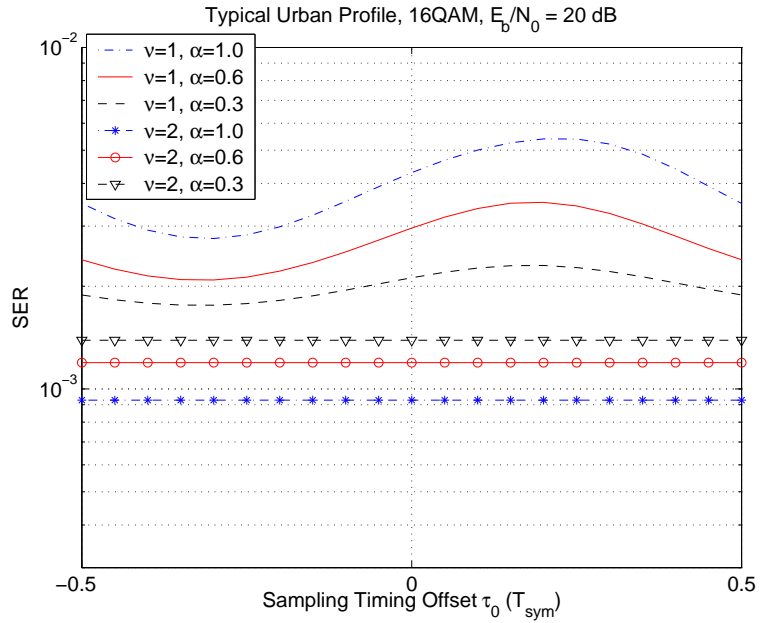
(b) 8PSK

Figure 5.5: The effects of sampler timing offset on system performance for two ray equal gain profile. ν : oversampling factor. τ_0 : sampler timing offset. α : roll-off factor of the root raised cosine filter.

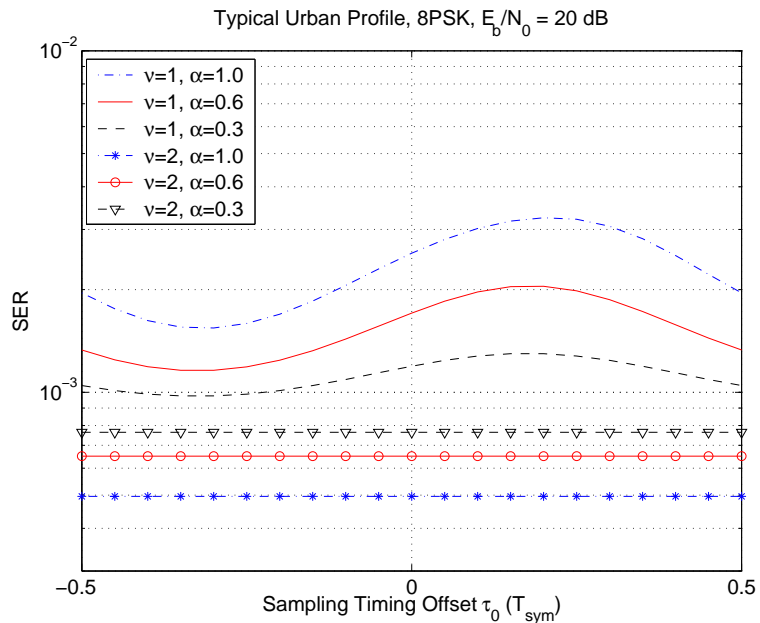
system configuration. At the SER level of 10^{-5} , there is a 7dB difference between the matched filter bound and the simulation results of systems with $\tau_0 = 0$. This difference is mainly induced by the ideal matched filter assumptions adopted in the derivation of the matched filter bound, and the effects of timing phase offset can not be represented by the matched filter bound either.

The effects of sampler timing phase and oversampling on system performance are further analyzed in the third example, where the SER lower bounds are plotted against the sampler timing offset τ_0 for systems with and without oversampling. Fig. 5.5 shows the performances of systems with the two ray equal-gain uncorrelated T_{sym} -spaced power delay profile, and the performances of systems with TU profile are displayed in Fig. 5.6. For systems without oversampling, *i.e.*, $\nu = 1$, the system performances vary dramatically with the timing phase offset τ_0 . This variation is induced by the effects of spectrum aliasing [100] of the received signals, since the sampling rate $1/T_{sym}$ is smaller than the Nyquist rate $(1 + \alpha)/T_{sym}$ of the received signals, where α is the roll-off factor of the RRC filter. For different values of sampler timing phase, the amplitude of the overlapped spectrum could add up constructively or destructively, which will lead to performance improvement or degradation. The effects of spectrum aliasing becomes more serious for systems with larger excessive bandwidth (or larger value of α), thus the performances of systems with larger α are more sensitive to the sampler phase offset. From Fig. 5.5, we can see that for systems with the equal gain two ray profile, the optimum sampler timing offset is $\tau_0 = 0$. However, for systems with TU profile, $\tau_0 = -0.3T_{sym}$ is the optimum timing offset due to the power dominance of the delayed scattering rays of the channel fadings.

As pointed out in [100], the timing phase sensitivity of the receiver can be avoided by oversampling. For systems with at most 100% excessive bandwidth, spectrum aliasing at the receiver can be completely removed by setting the oversampling factor $\nu = 2$. This statement is supported by our new performance bounds illustrated in Fig. 5.5 and Fig. 5.6, where the SERs for oversampled systems keep constant regardless of the values of the sampler timing offset τ_0 . For systems with TU profile, the performance

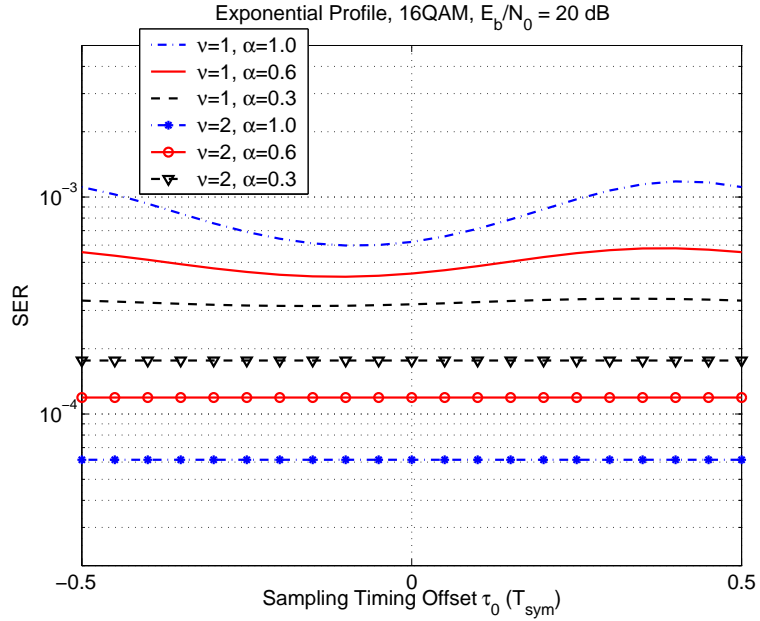


(a) 16QAM

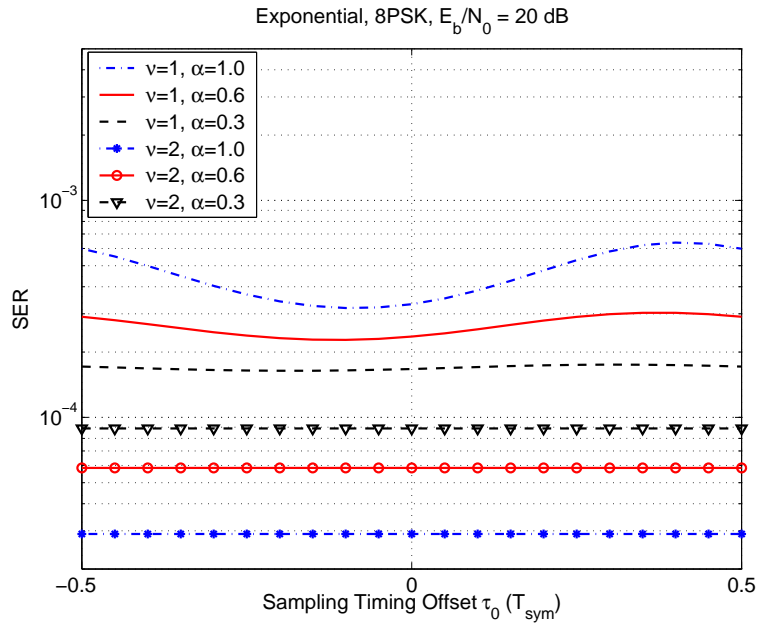


(b) 8PSK

Figure 5.6: The effects of sampler timing offset on system performance for Typical Urban profile. ν : oversampling factor. τ_0 : sampling timing offset. α : roll-off factor of the root raised cosine filter.



(a) 16QAM



(b) 8PSK

Figure 5.7: The effects of sampler timing offset on system performance for Exponential Decaying profile. ν : oversampling factor. τ_0 : sampling timing offset. α : roll-off factor of the root raised cosine filter.

of the oversampled system improves with the increase of the roll-off factor, since more bandwidth are consumed by the signal and there is no aliasing in the receiver.

So far, all of the examples are focused on systems with discrete-time power delay profiles, where the frequency-selective fading has discrete-time delayed multipaths. The analytical results proposed in this chapter can also be directly applied to systems with continuous-time power delay profiles, such as the exponentially decaying power delay profile defined as $G(\mu) = A \exp(-\tau/T_{sym})$, for $0 \leq \tau \leq 2T_{sym}$, with A being a normalization factor. The timing phase sensitivity of systems with exponentially decaying profile are shown in Fig. 5.7. From this figure, we can see that systems with exponentially decaying profile has similar performances with the TU profile, and the optimum sampling timing offset for the exponentially decaying profile is $\tau_0 = -0.1T_{sym}$.

5.6 Conclusions

New, tight theoretical performance bounds were derived for wireless communication systems with time-varying and frequency-selective channel fading and sampler timing offset. The SISO systems with doubly selective Rayleigh fading channels and fractionally spaced receivers were equivalently represented as an SIMO system with mutually *correlated* frequency-flat fading channels and colored Gaussian noise. Closed-form error probability expressions were derived as lower bounds of symbol error probabilities for systems suffering both doubly selective channel fading and sampler timing offset. The information of timing phase offset, the statistical properties of the channel fading, as well as the effects of fractionally spaced receiver are quantified in the error probability expressions.

Compared to the loose union bound and matched filter bound, our new analytical results can accurately predict the error performances of MLSE and MAP equalizers in practical system configurations at a wide range of SNR, and the results are obtained with a simple time domain equivalent SIMO system method. Moreover, with the help of the theoretical expressions, the effects of receiver oversampling and timing phase sensitivity

of communication systems are analyzed, and we have the following observations. 1) For systems with symbol spaced receiver and practical power delay profiles, zero sampler timing offset ($\tau = 0$) is not always optimum. 2) For systems with at most 100% excessive bandwidth, two times oversampling at the receiver can completely remove the phenomenon of timing phase sensitivity, which agrees with the theoretical analysis presented in [100]. 3) The timing phase sensitivity of systems with symbol spaced receivers becomes more serious with the increase of the bandwidth of the received signals.

Chapter 6

Receiver Timing Phase Sensitivity of Systems with Frequency Selective Rayleigh Fading Channels

6.1 Introduction

The results presented in Chapter 5 show that the performance of communication system with symbol spaced sampler suffers from extreme sensitivity to receiver timing phase offset, which is introduced by the phase difference between the transmitter clock and receiver clock. It is pointed out in [99] and [100] that the dependence of system performance on timing phase offset is introduced by the effects of spectrum aliasing of the sampled signals at the receiver. For different system configurations, the overlapped spectral components of the signal samples at the receiver could add up either constructively or destructively based on their phase differences, and this leads to performance enhancement or degradation, accordingly. The phase differences among the overlapped spectral components is a direct result of timing phase offset at the receiver, and the relationship between receiver timing phase and system performance fluctuation is heuristically discussed in [99] and [100]. However, no analytical result is available in the literature to quantify the effects of timing phase offset on system error performance. In this chapter, with the help of the matched filter bound technique, we are going to derive a tight

theoretical performance bound that is able to quantitatively identify the effects of both timing phase offset and receiver oversampling.

The matched filter bound is a well known technique used to predict the performance for systems experiencing frequency selective fading [93]- [96]. By assuming there is no intersymbol interference (ISI) present at the receiver, matched filter bound defines the best possible error performance for certain system configurations. The matched filter bounds for system with discrete-time power delay profiles are discussed in [93] and [95], and the performance of systems with arbitrary power delay profiles is derived in [94] and [97] with the help of frequency domain analysis. The assumption of quasi static (or slowly time varying) fading is adopted by [93]- [97], and matched filter bound results for systems with time varying channel is reported in [96].

The matched filter bounds presented in most previous works are loose performance low bounds, and they are usually far below the actual error performance of practical communication systems. At the first glance, it seems that the performance difference is a result of the ISI free assumption. However, it is shown in [107] that both maximum likelihood sequence estimation (MLSE) and maximum *a posteriori* (MAP) equalizers are asymptotic optimum in the sense of interference cancellation, *i.e.*, the ISI components at the output of MLSE equalizer or MAP equalizer tend to zero provided that the decoding length is long enough. Indeed, conventional matched filter bounds fail to capture the effects of timing phase offset and receiver oversampling, both of which have significant impact on communication system performance. We are going to show in this chapter that the performance difference between matched filter bound and actual system performance is mainly contributed by the overlook of sampler timing phase and spectrum aliasing at the receiver.

To remove the effects of spectrum aliasing at the receiver, fractionally spaced equalizers are discussed in [99], [104]- [105]. In [104], the performances of systems with various fractionally spaced receivers are investigated with simulations. The theoretical performance of fractionally spaced equalizer is analyzed in [105] with the union bound technique, where the pair wise error probabilities of mutually overlapped error events are added

up as an upper bound of system error probability. It is well known that union bound is rather loose compared to the actual system performance, especially at low signal to noise ratio. Moreover, union bound technique cannot quantify the effects of timing phase offset and spectrum aliasing.

In this chapter, a tight performance low bound for systems with frequency selective fading channels is derived by considering the effects of both receiver oversampling and timing phase offset. The ISI free assumption used in the conventional matched filter bound is adopted in the development of this new bound. With the help of Karhunen-Loève expansion, a unified error probability expression is derived as a tight low bound for the performance of various linearly modulated communication systems. The effects of timing phase offset, receiver oversampling, as well as the power delay profile of the frequency selective fading are explicitly expressed in the statistical representations of the instantaneous SNR observed by the receiver, and they are further quantified in the analytical error probability expressions. The conventional matched filter bound can be treated as a special case of the new performance bound. With the help of the analytical results, it is proved in this chapter that when there is no spectrum aliasing present at the receiver, system with receive filter matched to the time-invariant transmit filter have the same performance as system with statistical receive filter matched to the joint response of transmit filter and frequency selective fading. Hence time varying matched filter in oversampled systems can be replaced by simple time-invariant receive filter without sacrificing system performance.

Simulation results show that the performance bound derived in this chapter can accurately predict the performance of communication systems with practical receivers in a wide range of SNR. Moreover, It is observed that perfect synchronization between transmitter and receiver (timing phase offset is 0) doesn't guarantee optimum system performance. Rather, the choice of optimum timing phase offset at the receiver depends on specific channel realizations. The optimum sampling time for various system configurations are investigated with the help of numerical examples.

The rest of the chapter is organized as follows. Section 6.2 presents the system model

used for analysis. In Section 6.3, a tight error performance bound for systems experiencing timing phase offset is derived by analyzing the statistical properties of the instantaneous SNR at the receiver. Based on the new performance bound, case studies of several exemplary communication systems are carried out in Section 6.4 to investigate the effects of timing phase offset, receiver oversampling, as well as receiver filter on system performances. Numerical examples are provided in Section 6.5, and Section 6.6 concludes the chapter.

6.2 System Model

To adopt the ISI free assumption employed by matched filter bound, it is assumed that the information symbol is transmitted in isolation, *i.e.*, at each transmission epoch, only one symbol is being sent out by the transmitter. The baseband representation of the transmitted waveform can be expressed as

$$s(t) = x_0 \cdot p_T(t), \quad (6.1)$$

where x_0 is the M -ary modulated information symbol with symbol period T_{sym} and symbol energy E_s , and $p_T(t)$ is the time-invariant impulse response of the transmit filter with unit energy, *i.e.*, $\int_{-\infty}^{+\infty} p_T(t - \mu) p_T^*(\mu) d\mu = 1$, with a^* denoting complex conjugate of a .

In the channel, the transmitted signal is corrupted by both frequency selective fading and additive noise. Let $g(t)$ be the impulse response of the frequency selective channel. The channel is assumed to be quasi static, meaning that the impulse response $g(t)$ remains invariant per transmission burst but may change from burst to burst. Thus the signal at the receiver can be represented by

$$y(t) = x_0 \cdot p_T(t) \otimes g(t) + n(t), \quad (6.2)$$

where \otimes denotes the operation of convolution, and $n(t)$ is the additive white Gaussian noise (AWGN) with variance N_0 .

The received signal $y(t)$ is passed through the receive filter $p_R(t)$. The signal at the output of $p_R(t)$ is

$$z(t) = x_0 \cdot p_T(t) \otimes g(t) \otimes p_R(t) + v(t), \quad (6.3)$$

where $v(t) = n(t) \otimes p_R(t)$ is the noise component at the output of the receive filter.

If we define the composite impulse response (CIR) of the system as

$$h(t) = p_T(t) \otimes g(t) \otimes p_R(t), \quad (6.4)$$

then the sampled output of the receive filter at sampling instant $t = kT_s + \tau_0$ can be expressed as

$$z(k) = x_0 \cdot h(k) + v(k), \quad (6.5)$$

where $z(k) = z(kT_s + \tau_0)$, $v(k) = v(kT_s + \tau_0)$ are the received signal and noise samples, respectively, $T_s = T_{sym}/\mu$ is the sampling period, with the integer μ being the oversampling factor, $\tau_0 \in [-\frac{T_s}{2}, \frac{T_s}{2}]$ is the phase difference between the sampler clock and the transmitter clock, and $h(k) = h(kT_s + \tau_0)$ is the discrete-time version of the CIR $h(t)$.

The noise sample $v(k)$ is a linear transformation of AWGN $n(t)$, hence it is zero-mean Gaussian distributed with the auto-correlation function $r_{vv}(m-n) = \mathbb{E}[v(m)v^*(n)]$ given by [101]

$$r_{vv}(m-n) = N_0 \cdot r_{p_R p_R} [(m-n)T_s], \quad (6.6)$$

where $\mathbb{E}(x)$ is the operation of mathematical expectation, and $r_{p_R p_R}(t) = \int_{-\infty}^{+\infty} p_R(t+\tau)p_R^*(\tau)d\tau$ is the auto-correlation function of the receive filter $p_R(t)$. Due to the time span of the receive filter and the effects of oversampling, the noise component $z(k)$ becomes a colored Gaussian process with auto-correlation function defined in (6.6), even though the original additive noise $n(t)$ is white in the time domain. The power spectral density (PSD) $\widehat{R}_{vv}(f)$ of $v(k)$ is

$$\widehat{R}_{vv}(f) = N_0 \widehat{R}_{p_R p_R}(f), \quad -f_0 \leq f \leq f_0, \quad (6.7)$$

where $f \in [-1/2, 1/2]$ is the digital frequency of discrete-time signals, $f_0 \in (0, 1/2]$ is the digital bandwidth of the receive filter, $\widehat{R}_{vv}(f)$ and $\widehat{R}_{p_R p_R}(f)$ are the discrete-time

Fourier transform (DTFT) of $r_{vv}(k)$ and $r_{p_R p_R}(k)$, respectively. Let $R_{p_R p_R}(F)$ be the Fourier transform (FT) of the continuous-time auto-correlation function $r_{p_R p_R}(t)$, where $F = f/T_s$ is the analog frequency. According to the sampling theorem, the PSD $\widehat{R}_{zz}(f)$ can also be written as

$$\widehat{R}_{vv}(f) = \frac{N_0}{T_s} \sum_{n=-\infty}^{+\infty} R_{p_R p_R} \left[\frac{f-n}{T_s} \right], \quad -f_0 \leq f \leq f_0. \quad (6.8)$$

It should be noted from (6.8) that the statistical property of the sampled noise component $z(k)$ is independent of the timing phase offset τ_0 .

With the PSD of the noise component given in (6.8), the instantaneous signal to noise ratio (SNR) of the ISI free system is

$$\gamma = \gamma_0 T_s \cdot \int_{-f_0}^{f_0} \frac{|\widehat{H}(f)|^2}{\sum_{n=-\infty}^{+\infty} R_{p_R p_R} \left[\frac{f-n}{T_s} \right]} df, \quad (6.9)$$

where $\gamma_0 = E_s/N_0$ is the SNR without fading, and $\widehat{H}(f)$ is the DTFT of the discrete-time CIR $h(k)$. Based on (6.4) and the sampling theorem, $\widehat{H}(f)$ can be written by

$$\widehat{H}(f) = \frac{e^{j2\pi f \frac{\tau_0}{T_s}}}{T_s} \sum_{n=-\infty}^{+\infty} P_T \left(\frac{f-n}{T_s} \right) G \left(\frac{f-n}{T_s} \right) P_R \left(\frac{f-n}{T_s} \right) e^{-j2\pi n \frac{\tau_0}{T_s}}, \quad (6.10)$$

where $j^2 = -1$ is the imaginary part symbol, $P_T(F)$, $P_R(F)$ and $G(F)$ are the Fourier transforms of $p_T(t)$, $p_R(t)$ and $g(t)$, respectively. It should be noted that the frequency domain support of $\widehat{H}(f)$ is smaller than or equal to that of $\widehat{R}_{p_R p_R}(f)$ because the effect of receive filter $p_R(t)$ is included in the CIR $h(k)$.

Combining (6.9) and (6.10), the instantaneous SNR at the output of the sampler can be expressed as

$$\gamma = \gamma_0 \cdot \int_{-F_0}^{F_0} \frac{\left| \sum_{n=-\infty}^{+\infty} R_{P_T P_R}(F - nF_s) G(F - nF_s) e^{-j2\pi n \frac{\tau_0}{T_s}} \right|^2}{\sum_{n=-\infty}^{+\infty} R_{p_R p_R}(F - nF_s)} dF \quad (6.11)$$

where $F_s = 1/T_s$ is the sampling rate, $F_0 = f_0/T_s \in (0, \frac{1}{2T_s}]$ is the analog bandwidth, $R_{P_T P_R}(F) = P_T(F)P_R(F)$, and the integration variable has been changed to the analog frequency $F = f/T_s$ in (6.11).

It is interesting to note that the SNR γ is a periodic function of the timing phase offset τ_0 with the fundamental period equal to the sampling period T_s , and this result justifies our assumption that τ_0 is in the range of $[-T_s/2, T_s/2]$. The statistical properties of the instantaneous SNR γ are analyzed in the next section, and the results are used to derive the theoretical system performance.

6.3 Error Performance of System with Timing Phase Offset

The error performance of linearly modulated system with timing phase offset is investigated in this section by analyzing the statistical properties of the instantaneous SNR at the receiver.

6.3.1 Statistical Properties of SNR

If we define

$$\Psi(F) = \frac{\sum_{n=-\infty}^{+\infty} R_{P_T P_R}(F - nF_s) G(F - nF_s) e^{-j2\pi n \frac{\tau_0}{T_s}}}{\sqrt{\sum_{n=-\infty}^{+\infty} R_{P_R P_R}(F - nF_s)}}, \quad (6.12)$$

then the SNR γ given in (6.11) can be alternatively written as

$$\gamma = \gamma_0 \cdot \int_{-F_0}^{F_0} |\Psi(F)|^2 dF. \quad (6.13)$$

For Rayleigh fading channel, the Fourier transform $G(F)$ of the channel impulse response is zero-mean complex Gaussian distributed, thus the function $\Psi(F)$, which is a linear combination of $G(F)$, is also a zero-mean Gaussian process in the frequency domain F . To facilitate the analysis of the statistical properties of the instantaneous SNR γ , Karhunen-Loève expansion is applied to the Gaussian process $\Psi(F)$ in the frequency domain, and the result is

$$\Psi(F) = \sum_{l=1}^L \sqrt{\lambda_l} \sum_{k=1}^{K_l} w_{l,k} \phi_{l,k}(F), \quad (6.14)$$

where $\{w_{l,k}\}$ are a set of independent identically distributed (i.i.d.) zero-mean Gaussian random variables with unit variance, $\{\lambda_l\}$ are a set of distinct eigenvalues of the function $\Psi(F)$, $\{\phi_{l,k}(f)\}$ the corresponding orthonormal eigenfunctions with frequency domain support $[-F_0, F_0]$, and they satisfy $\int_{-F_0}^{F_0} \phi_{l,k}(f)\phi_{m,i}^*(f)df = \delta_{l,m}\delta_{k,i}$, with $\delta_{l,m}$ being the Kronecker delta function.

Given the fact that the set of eigenfunctions $\{\phi_{l,k}(f)\}$ are orthonormal, we can get an alternative representation of the instantaneous SNR by substituting (6.14) into (6.13),

$$\gamma = \gamma_0 \cdot \sum_{l=1}^L \lambda_l \sum_{k=1}^{K_l} |w_{l,k}|^2, \quad (6.15)$$

In (6.15), the instantaneous SNR γ is expressed as the summation of L independent χ^2 -distributed random variables $\sum_{k=1}^{K_l} |w_{l,k}|^2$. Thus the characteristic function (CHF) of γ can be expressed as [76]

$$\begin{aligned} \Phi_\gamma(\omega) &= \mathbb{E}(e^{j\omega\gamma}) \\ &= \prod_{l=1}^L (1 - j\omega\lambda_l\gamma_0)^{-K_l}. \end{aligned} \quad (6.16)$$

It's apparent from (6.15) and (6.16) that the statistical properties of γ is uniquely determined by the eigenvalues λ_l of the random function $\Psi(F)$ as defined in (6.14).

The analysis of the statistical properties of γ requires the knowledge of the eigenvalues λ_l . To solve the eigenvalues, we formulate the following eigensystem representation from (6.14) by utilizing the orthonormal properties of the eigenfunctions $\phi_{l,k}(f)$,

$$\int_{-F_0}^{F_0} R_\Psi(F_1, F_2)\phi_{l,k}(F_2)dF_2 = \lambda_l\phi_{l,k}(F_1), \quad (6.17)$$

where $R_\Psi(F_1, F_2) = \mathbb{E}[\Psi(f_1)\Psi^*(f_2)]$ is the frequency domain auto-correlation function of the random function $\Psi(F)$, and the mathematical expectation operation is performed over the statistical channel response $G(F)$.

The eigenvalues λ_l and the corresponding eigenfunctions $\phi_{l,k}(f)$ can be obtained by solving the eigensystem described in (6.17) given the knowledge of $R_\Psi(F_1, F_2)$. For systems with fixed receive filter, the frequency domain auto-correlation function $R_\Psi(F_1, F_2)$ can be expressed by [c.f. (6.12)]

$$R_\Psi(F_1, F_2) = \frac{\sum_{m=-\infty}^{+\infty} \sum_{n=-\infty}^{+\infty} R_{p_T p_R}(F_1 - mF_s) R_{p_T p_R}^*(F_2 - nF_s) R_G[(F_1 - F_2) - (m - n)F_s] e^{-j2\pi \frac{(m-n)\tau_0}{T_s}}}{\sqrt{\sum_{m=-\infty}^{+\infty} \sum_{n=-\infty}^{+\infty} R_{p_R p_R}(F_1 - mF_s) R_{p_R p_R}^*(F_2 - nF_s)}} \quad (6.18)$$

where $R_G(F_1, F_2) = \mathbb{E}[G(F_1)G^*(F_2)]$ is the frequency domain auto-correlation function of the impulse response of the physical channel. For system with uncorrelated scattering (US) [19] fading, the function $R_G(F_1, F_2)$ can be calculated from

$$\begin{aligned} R_G(F_1, F_2) &= \int_0^{+\infty} \int_0^{+\infty} \mathbb{E}[g(t_1)g^*(t_2)] e^{-j2\pi(F_1t_1 - F_2t_2)} dt_1 dt_2, \\ &= \int_0^{+\infty} \varphi(t) e^{-j2\pi(F_1 - F_2)t} dt, \end{aligned} \quad (6.19)$$

where $\varphi(t)$ is the power delay profile (PDP) of the frequency selective channel. From (6.19), the function $R_G(F_1, F_2)$ is wide sense stationary (WSS) in the frequency domain F , *i.e.*, $R_G(F_1, F_2) = R_G(F_1 - F_2)$; in addition, $R_G(F)$ can be interpreted as the FT of the PDP $\varphi(t)$.

For most wireless communication systems, the PDP can be represented in the form of a discrete-time function

$$\varphi(t) = \sum_{i=1}^I \varphi_i \delta(t - t_i), \quad (6.20)$$

where I is the number of resolvable multipaths of the frequency selective channel, φ_i and t_i are the average power and relative delay of the i th multipath, respectively, and $\sum_{i=1}^I \varphi_i = 1$ for normalized PDP. The function $R_G(F)$ of such system configuration can be calculated from the Fourier transform of (6.20), and the result is

$$R_G(F) = \sum_{i=1}^I \varphi_i e^{-j2\pi F t_i}. \quad (6.21)$$

Another commonly used PDP is the exponentially decaying profile. The exponential PDP along with its FT $R_G(F)$ can be expressed as

$$\varphi(t) = \frac{1}{T_{sym} \left[\exp\left(\frac{\tau_{\max}}{T_{sym}}\right) - 1 \right]} \exp\left(-\frac{t - \tau_{\max}}{T_{sym}}\right), \quad 0 \leq t \leq \tau_{\max}, \quad (6.22a)$$

$$R_G(F) = \frac{1}{\left[\exp\left(\frac{\tau_{\max}}{T_{sym}}\right) - 1 \right] [1 + j2\pi T_{sym} F]} \left[e^{\frac{\tau_{\max}}{T_{sym}}} - e^{-j2\pi F \tau_{\max}} \right], \quad (6.22b)$$

where τ_{\max} is the maximum delay spread of the frequency selective channel.

Given transmit filter $p_T(t)$, receive filter $p_R(t)$, and the PDP $\varphi(t)$, we can formulate the frequency domain auto-correlation function $R_\Psi(F_1, F_2)$ by using (6.18), (6.21) or

(6.22b). Substituting the resultant function $R_{\Psi}(F_1, F_2)$ into the eigensystem of (6.17) leads to the solution of the eigenvalues λ_l , which are then used in (6.15) and (6.16) to represent the statistical properties of the SNR γ .

From (6.15), (6.17) and (6.18), we conclude that the statistical properties of the instantaneous SNR γ are jointly determined by the transmit filter $p_T(t)$, the receive filter $p_R(t)$, the channel power delay profile $g(t)$, the sampling frequency F_s , and the sampler timing phase offset τ_0 . Moreover, it's apparent that the frequency domain autocorrelation function $R_{\Psi}(F_1, F_2)$, the form of which depends on individual receiver implementations, plays a critical role in determining the properties of γ .

6.3.2 Error Performance Bound

Based on the statistical properties of the instantaneous SNR γ , theoretical performance low bounds of systems with M -ary phase-shift-keying (MPSK), M -ary amplitude-shift-keying (MASK), and M -ary quadrature-amplitude-modulation (MQAM) are derived in this subsection.

The derivation of the theoretical performance bounds is based on the assumption that the information symbol x_0 is transmitted in isolation, *i.e.*, there is no intersymbol interference present at the receiver. Based on the ISI free assumption, the conditional error probability (CEP) $P(E|\gamma)$ for MPSK, MASK, and MQAM systems can be written in a unified form as [107]

$$P(E|\gamma) = \sum_{i=1}^2 \frac{\beta_i}{\pi} \int_0^{\psi_i} \exp \left\{ -\zeta \cdot \frac{\gamma}{\sin^2 \theta} \right\} d\theta, \quad (6.23)$$

where the parameters ζ , β_i and ψ_i for various modulation schemes are listed in Table 5.1.

The unconditional error probability can be evaluated by averaging over the statistical distribution of the instantaneous SNR as $P(E) = \mathbb{E}[P(E|\gamma)]$. Since the CEP given in (6.23) is in the form of an exponential function of the instantaneous SNR γ , the expectation operation can be performed with the help of the CHF of γ as defined in (6.16). Combining (6.16) and (6.23), we have the unconditional error probability $P(E)$

as

$$\begin{aligned} P(E) &= \mathbb{E}[P(E|\gamma)], \\ &= \sum_{i=1}^2 \frac{\beta_i}{\pi} \int_0^{\psi_i} \prod_{l=1}^L \left(1 + \frac{\zeta \gamma_0 \lambda_l}{\sin^2 \theta}\right)^{-K_l} d\theta. \end{aligned} \quad (6.24)$$

The closed-form expression of the unconditional error probability $P(E)$ can be obtained by partial fraction expansion of the integrand in (6.24), which is

$$\prod_{l=1}^L \left(1 + \frac{\zeta \gamma_0 \lambda_l}{\sin^2 \theta}\right)^{-K_l} = \sum_{l=1}^L \sum_{k=1}^{K_l} c_{l,k} \left(1 + \frac{\zeta \gamma_0 \lambda_l}{\sin^2 \theta}\right)^{-k}, \quad (6.25)$$

with the partial fraction coefficient $c_{l,k}$ defined as

$$c_{l,k} = \left(\frac{\sin^2 \theta}{\zeta \gamma_0}\right)^{K_l-k} \frac{\partial^{K_l-k}}{\partial \lambda_l^{K_l-k}} \left[\prod_{i \neq l}^L \left(1 + \frac{\zeta \gamma_0 \lambda_i}{\sin^2 \theta}\right)^{-K_i} \right] \Bigg|_{\lambda_l = -\sin^2 \theta / (\zeta \gamma_0)}. \quad (6.26)$$

Substituting (6.25) into (6.24), we have the unconditional error probability $P(E)$ represented by

$$P(E) = \sum_{i=1}^2 \frac{\beta_i}{\pi} \sum_{l=1}^L \sum_{k=1}^{K_l} c_{l,k} \int_0^{\psi_i} \prod_{l=1}^L \left(1 + \frac{\zeta \gamma_0 \lambda_l}{\sin^2 \theta}\right)^{-k} d\theta. \quad (6.27)$$

The integral in (6.27) can be solved by employing the definition of the Appell Hypergeometric function $F_1(\alpha; \beta, \beta'; \gamma; x, y)$ [106], and the results is

$$P(E) = \sum_{i=1}^2 \frac{\beta_i}{\pi} \sum_{l=1}^L \sum_{k=1}^{K_l} c_{l,k} (\zeta \gamma_0 \lambda_l)^{-k} F_1 \left[\frac{1}{2} + k, k, 1, \frac{3}{2} + k, - \left(1 + \frac{1}{\zeta \gamma_0 \lambda_l}\right) \tan^2 \psi, - \tan^2 \psi \right] \quad (6.28)$$

Eqn. (6.28) gives a unified closed-form expression of the performance low bound for MPSK, MASK, and MQAM systems with frequency selective fading, and the values of the parameters ζ , β_i , ψ_i are given in Table 5.1. For the special case that $K_l = 1$, for $l = 1, 2, \dots, L$, which is true for most practical PDPs, the closed-form solutions of the error probability low bound can be solved without resorting to hypergeometric functions, and the results are given in [107]. Moreover, the integral in (6.24) only involves elementary functions and finite integration limits, thus it can be easily evaluated with numerical methods.

In (6.24) and (6.28), the effects of frequency selective fading, timing phase offset τ_0 , and receiver oversampling are quantified in the error probability expressions via the eigenvalues λ_l of the eigensystem defined in (6.17). Since the eigensystem is fully characterized by the frequency domain auto-correlation function $R_\Psi(F_1, F_2)$, the error performance of linearly modulated systems with frequency selective fading is uniquely determined by $R_\Psi(F_1, F_2)$, where the effects of receiver oversampling and timing phase offset are explicitly expressed.

Before concluding this section, we summarize the process of performance bounds evaluation for systems with frequency selective fading and timing phase offset.

- Step 1:** Given transmit filter $p_T(t)$, receive filter $p_R(t)$, and channel PDP $\varphi(t)$, evaluate their respective Fourier transforms $P_R(F)$, $P_T(F)$, and $G(F)$.
- Step 2:** With the FTs obtained in step 1, formulate the frequency domain auto-correlation $R_\Psi(F_1, F_2)$ as defined in (6.18) for certain timing phase offset τ_0 and oversampling factor μ .
- Step 3:** Substitute $R_\Psi(F_1, F_2)$ into (6.17), and solve the eigenvalues λ_l . One of the methods for solving the eigensystem is presented in [94].
- Step 4:** With the eigenvalues λ_l from step 3 and the parameters defined in Table 5.1, evaluate the system error probability low bounds by using either (6.24) or (6.28).

6.4 Case Studies

In this section, we perform case studies of various representative communication systems to further investigate the effects of timing phase offset and receiver oversampling on system performance. In the analysis, we only consider system with at most 100% excessive bandwidth, *i.e.*, the frequency domain support of the composite impulse response $h(t)$ is in the range of $[-2/T_{sym}, 2/T_{sym}]$, and the analysis can be directly extended to systems with arbitrary amount of excessive bandwidth.

As highlighted in Section 6.3, system error performance is uniquely determined by the eigensystem defined (6.17), which is in turn fully characterized by the frequency domain auto-correlation function $R_\Psi(F_1, F_2)$ as given in (6.18). In addition, the timing phase offset τ_0 is explicitly expressed in the representation of $R_\Psi(F_1, F_2)$. For this reason, to investigate the effects of τ_0 on system performance, it suffices to examine the statistical properties of $R_\Psi(F_1, F_2)$ for the various representative system configurations.

6.4.1 Case 1: T_{sym} -spaced Receiver ($\mu = 1$), Arbitrary PDP

$\varphi(t)$.

For system with symbol spaced ($T_{sym} = T_s$) receiver and at most 100% excessive bandwidth, there are at most three frequency components overlapped in the frequency range of $[-\frac{1}{2T_s}, \frac{1}{2T_s}]$. If the receive filter $p_R(t)$ is matched to the time-invariant transmit filter $p_T(t)$, or $P_R(F) = P_T^*(F)$, then the instantaneous SNR γ can be written by [c.f. (6.11)]

$$\gamma = \gamma_0 \cdot \int_{-\frac{1}{2T_s}}^{\frac{1}{2T_s}} |\Psi(F)|^2 dF, \quad (6.29a)$$

$$\Psi(F) = \frac{|P_T(F)|^2 G(F) + \sum_{n=\pm 1} |P_T(F - nF_s)|^2 G(F - nF_s) e^{-j2n\pi\frac{\tau_0}{T_s}}}{\sqrt{|P_T(F)|^2 + \sum_{n=\pm 1} |P_T(F - nF_s)|^2}}. \quad (6.29b)$$

The statistical distribution of γ can be evaluated with the help of the eigensystem defined in (6.17), which is in turn characterized by the frequency domain auto correlation function $R_\Psi(F_1, F_2) = \mathbb{E}[\Psi(F_1)\Psi^*(F_2)]$. Based on the definition of $\Psi(f)$ given in (6.29b), the frequency domain auto correlation function $R_\Psi(F_1, F_2)$ is

$$R_\Psi(F_1, F_2) = \frac{\sum_{m=-1}^{+1} \sum_{n=-1}^{+1} |P_T(F_1 - mF_s) P_T(F_2 - nF_s)|^2 R_G[(F_1 - F_2) - (m - n)F_s] e^{-j2\pi\frac{(m-n)\tau_0}{T_s}}}{\sqrt{\sum_{m=-1}^{+1} \sum_{n=-1}^{+1} |P_T(F_1 - mF_s) P_T(F_2 - nF_s)|^2}} \quad (6.30)$$

where $R_G(F_1 - F_2) = \mathbb{E}[G(F_1)G^*(F_2)]$ is the FT of the channel PDP $\varphi(t)$.

In the representation of (6.29) and (6.30), the values and statistical properties of the instantaneous SNR γ is explicitly expressed as periodic functions of the timing phase

offset τ_0 , and the function period is equal to the sampling period T_s . Moreover, it's apparent from (6.29) that the dependence of γ on τ_0 is introduced by the effect of spectrum aliasing. Since the eigenvalues λ_l and error probability $P(E)$ are uniquely determined by the eigensystem characterized by the periodic function $R_\Psi(F_1, F_2)$ as described in (6.17), we can conclude that both λ_l and $P(E)$ are periodic with respect to τ_0 . As an example, the eigenvalues and the corresponding error performance bounds of a system with two path equal gain channel profile $\varphi(t) = \sum_{i=0}^1 0.5\delta(t - iT_{sym})$ is plotted in Fig. 6.1. Root raised cosine (RRC) filters are used as both transmit filter and receive filter. It's apparent from these two figures that the values of both λ_l and $P(E)$ fluctuates periodically with respect to τ_0 with period T_s .

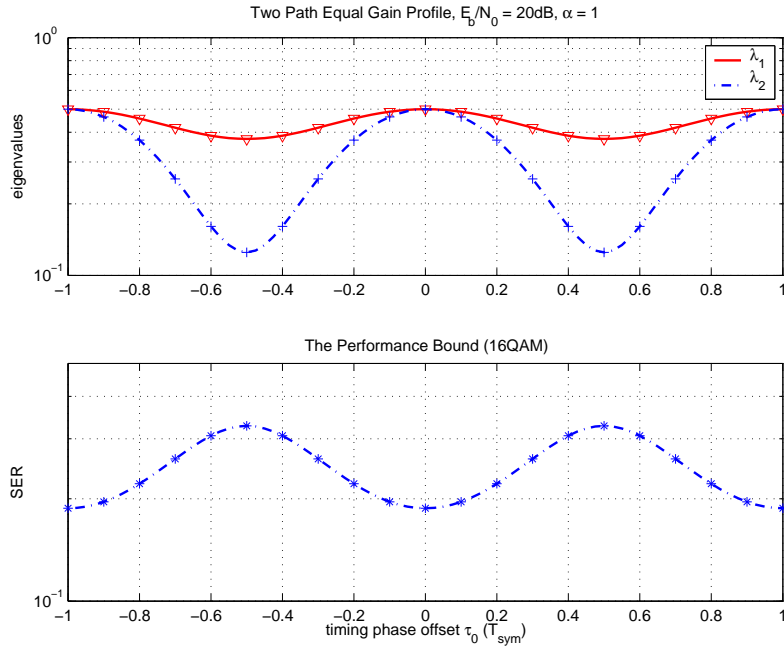


Figure 6.1: The variations of eigenvalues and performance bound with respect to timing phase offset for systems with two path equal gain profile. α : roll-off factor of the RRC filter.

The performance fluctuation is a result of the τ_0 dependent phase difference among the overlapped spectral components of the receiver signal samples. For different values of timing phase offset τ_0 , the overlapped spectrum could add up either constructively or destructively due to the phase difference between the overlapped spectral components,

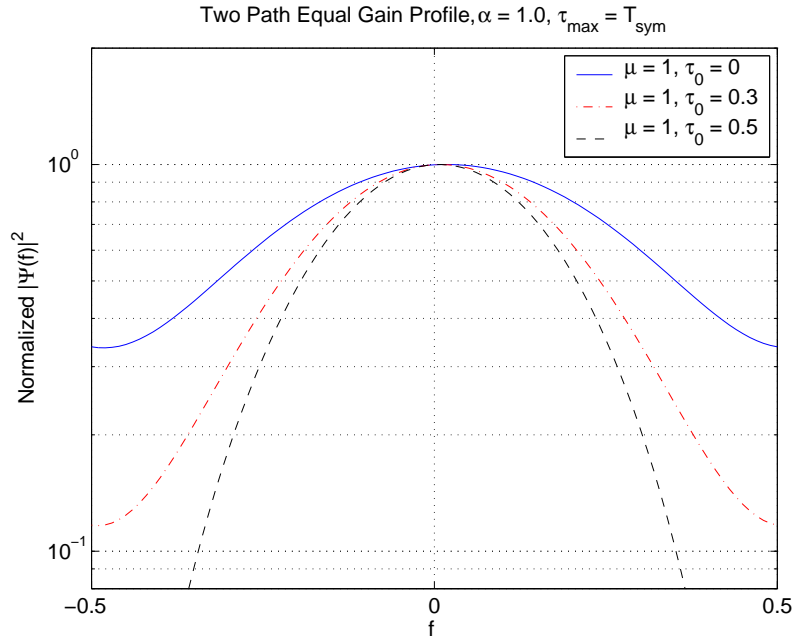


Figure 6.2: The overlapped power spectrum of the received signal samples for systems with two path equal gain profile. μ : oversampling factor. τ_0 : receiver timing phase offset. α : roll-off factor of the RRC filter.

and this will lead to performance improvement or degradation, correspondingly. To illustrate the effects of spectrum aliasing, one example of the overlapped power spectrum $|\Psi(F)|^2$ of the received signal samples is plotted in Fig. 6.2 for various values of τ_0 . It's clear from this figure that the shape of the overlapped power spectrum varies dramatically with respect to the timing phase offset τ_0 . The corresponding analytical error performance bounds are shown in Fig. 6.3. As expected, system with $\tau_0 = 0.5T_s$ has the worst performance of all the three curves, and the best performance is achieved by system with zero timing phase offset. The symbol error rate (SER) presented in Fig. 6.3 agrees with the power spectrum results shown in Fig. 6.2.

It's worth pointing out that the timing phase sensitivity was qualitatively discussed in [100]. However, no analytical result was available in the literature to quantitatively describe the relationship between the timing phase offset and system performance. In this chapter, the timing phase offset τ_0 is explicitly expressed in the representation of the instantaneous SNR γ as described in (6.29), and the effects of τ_0 and oversampling factor μ are quantified in the unified error performance bound expression via the eigenvalues

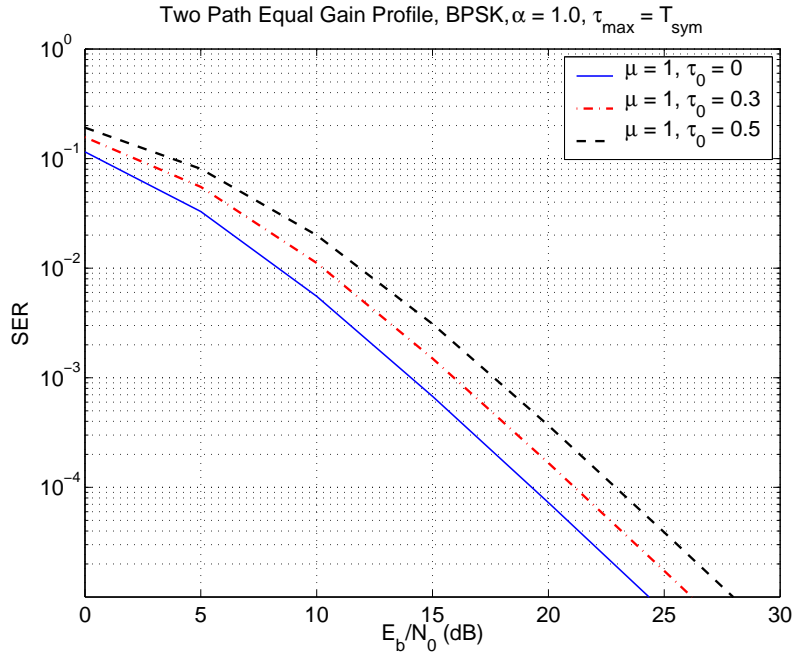


Figure 6.3: The SER performance bounds for two path equal gain channels with different values of timing phase offset. μ : oversampling factor. τ_0 : receiver timing phase offset. α : roll-off factor of the RRC filter.

λ_l , which clearly describes the dependence of system performance on receiver timing phase.

6.4.2 Case 2: T_{sym} -spaced Receiver ($\mu = 1$), PDP $\varphi(t) = \sum_{l=0}^{L-1} \varphi_l \delta(t - lT_s)$

The functions $\Psi(F)$ and $R_\Psi(F_1, F_2)$ for system with symbol spaced receiver can be further simplified if the impulse response of the frequency selective fading can be represented as a T_s -spaced tapped delay line filter, *i.e.*, $\varphi(t) = \sum_{l=0}^{L-1} \varphi_l \delta(t - lT_s)$. It can be easily shown that for such system configuration, both the frequency impulse response $G(F)$ and the Fourier transform of the channel PDP $R_G(F)$ are periodic functions in the frequency domain with period F_s . Thus the SNR given in (6.29) can be simplified

to

$$\gamma = \gamma_0 \cdot \int_{-\frac{1}{2T_s}}^{\frac{1}{2T_s}} |\Psi(F)|^2 dF. \quad (6.31a)$$

$$\Psi(F) = G(F) \frac{\sum_{n=-1}^{+1} |P_T(F - nF_s)|^2 e^{-j2n\pi\frac{\tau_0}{T_s}}}{\sqrt{\sum_{n=-1}^{+1} |P_T(F - nF_s)|^2}}, \quad (6.31b)$$

and the corresponding frequency domain auto-correlation function $R_\Psi(F_1, F_2)$ is

$$R_\Psi(F_1, F_2) = R_G(F_1 - F_2) \frac{\sum_{m=-1}^{+1} \sum_{n=-1}^{+1} |P_T(F_1 - mF_s) P_T(F_2 - nF_s)|^2 e^{-j2\pi\frac{(m-n)\tau_0}{T_s}}}{\sqrt{\sum_{m=-1}^{+1} \sum_{n=-1}^{+1} |P_T(F_1 - mF_s) P_T(F_2 - nF_s)|^2}}. \quad (6.32)$$

So far, all the analyses are carried out by assuming that the receive filter $p_R(t)$ is matched to the time-invariant transmit filter $p_T(t)$. However, in the development of conventional matched filter bound, a statistical receive filter matched to the joint response of the transmit filter and the frequency selective fading is assumed to be available at the receiver [94]. We have the following proposition about the relationship between the performances of systems with fixed receive filter and statistical receive filter.

Proposition 6.1: If the channel impulse response of the frequency selective channel can be represented as a sample spaced tapped delay line filter, then system with receive filter matched to the joint response of the transmit filter and fading has the same error performance as that of system with receive filter matched to the transmit filter only.

Proof: The frequency response of the receive filter matched to the joint response of frequency selective fading and transmit filter can be written as

$$P_R(F) = P_T^*(F)G^*(F), \quad (6.33)$$

and the receive filter becomes a statistical filter due to its dependence on the frequency domain channel impulse response $G(F)$.

Substituting (6.33) into (6.12) leads to

$$\Psi(F) = \frac{\sum_{n=-1}^{+1} |P_T(F - nF_s) G(F - nF_s)|^2 e^{-j2n\pi\frac{\tau_0}{T_s}}}{\sqrt{\sum_{n=-1}^{+1} |P_T(F - nF_s) G(F - nF_s)|^2}}. \quad (6.34)$$

For system with $g(t)$ in the form of T_s -spaced tapped delay line filter, $G(F)$ is a periodic function with period F_s , thus the function $\Psi(F)$ of (6.34) can be alternatively written as

$$\Psi(F) = |G(F)| \frac{\sum_{n=-1}^{+1} |P_T(F - nF_s)|^2 e^{-j2n\pi\frac{\tau_0}{T_s}}}{\sqrt{\sum_{n=-1}^{+1} |P_T(F - nF_s)|^2}}, \quad (6.35)$$

and the corresponding SNR for system with statistical receive filter is

$$\gamma = \gamma_0 \cdot \int_{-\frac{1}{2T_s}}^{\frac{1}{2T_s}} \frac{|G(F)|^2 \sum_{n=-1}^{+1} |P_T(F - nF_s)|^2 e^{-j2n\pi\frac{\tau_0}{T_s}}}{\sum_{n=-1}^{+1} |P_T(F - nF_s)|^2} dF. \quad (6.36)$$

It's apparent that this SNR expression is exactly the same as the one given in (6.31), which is obtained for system with fixed receive filter. Since the statistical properties of the SNR γ fully determine the system error probability as expressed by (6.15) and (6.24), we conclude that fixed receive filter and statistical receive filter will yield the same system error performance, given the condition that the channel impulse response can be represented as a T_s -spaced tapped delay line filter, and this completes the proof. ■

Proposition 6.1 states that for system with channel impulse response in the form of a sample spaced tapped delay line filter, system error performance is independent of the choice of fixed filter or statistical filter at the receiver.

A special case of the tapped delay line channel is flat fading, where there is only one channel tap with zero delay. For system with flat fading, the error probability expressions given in (6.24) or (6.28) are exact because there is no ISI present at the system.

6.4.3 Case 3: $T_{sym}/2$ -spaced Receiver ($\mu = 2$).

For systems with at most 100% excessive bandwidth, two times oversampling ($\mu = 2$) is enough to remove the phenomenon of spectrum aliasing at the receiver. We first consider the performance of system with receive filter matched to the transmit filter, *i.e.*, $P_M(f) = P_T^*(F)$, and the instantaneous SNR γ can be simplified to

$$\gamma = \gamma_0 \cdot \int_{-\frac{1}{2T_s}}^{\frac{1}{2T_s}} |\Psi(F)|^2 dF. \quad (6.37a)$$

$$\Psi(F) = P_T(F) G(F). \quad (6.37b)$$

With the definition of $\Psi(F)$ given in (6.37b), the frequency auto-correlation function $R_\Psi(F_1, F_2)$ is

$$R_\Psi(F_1, F_2) = P_T(F_1) P_T^*(F_2) R_G(F_1 - F_2), \quad (6.38)$$

Substituting (6.38) into (6.17) will lead to the solution of the eigenvalues λ_l , for $l = 1, \dots, L$, which are used in the error performance bound evaluation as described in (6.24) and (6.28).

It can be seen from (6.37) and (6.38) that the statistical properties of SNR γ are independent of the timing phase offset τ_0 thanks to the the removal of spectrum aliasing at the receiver. Since the system performance is uniquely determined by the statistical properties of SNR γ , it can be concluded that the system performance for systems without spectrum aliasing is independent of the receiver timing phase.

For system with statistical receive filter matched to the joint response of the frequency-selective channel and the transmit filter, we have the following proposition about the performance of the oversampled system.

Proposition 6.2: For system without spectrum aliasing at the receiver, the system error performance is independent of the sampler timing offset. Moreover, system with receive filter matched to the transmit filter has the same performance as that of system with statistical receive filter matched to the joint impulse response of the transmit filter and the frequency selective fading.

Proof: The frequency response of the statistical matched filter is $P_R(F) = P_T^*(F)G^*(F)$. Substituting $P_R(F)$ into (6.11) yields the SNR expression for oversampled systems with statistical matched filters

$$\gamma = \gamma_0 \cdot \int_{-\frac{1}{2T_s}}^{\frac{1}{2T_s}} |P_T(F)G(F)|^2 dF. \quad (6.39)$$

The SNR expression given in (6.39) is exactly the same as the SNR defined in (6.37), which is the instantaneous SNR for oversampled systems with fixed transmit filter.

Given the fact that the system error performance is uniquely determined by the statistical properties of the instantaneous SNR γ , it's apparent that the choice of fixed matched filter or statistical matched filter doesn't affect the performance of system without spectrum aliasing. ■

Since it is much simpler to implement a filter matched to the fixed impulse response of the transmit filter, we can always use simple time-invariant matched filter at the receiver of oversampled system without sacrificing the system performance. It worth pointing out that similar observation was made in [73]. In this chapter, we not only provide rigorous proof of the receive filter independence observation for systems without spectrum aliasing, but also obtained tight performance low bounds for such system.

It should be noted that even both Proposition 6.1 and Proposition 6.2 are about the independence of system performance on the choice of fixed filter or statistical filter at the receiver, these two propositions are built on different conditions. Proposition 6.1 holds for system with channel impulse response in the form of a tapped delay line filter, while Proposition 6.2 is true for arbitrary channel profile as long as there is no spectrum aliasing at the receiver.

To further verify this receive filter Independence statement for oversampled systems, we perform simulations to compare the symbol error rates of two oversampled systems equipped with fixed receive filter and statistical receive filter, respectively. In the simulation, one information symbol is sent out at each transmission epoch such that no ISI is present at the receiver. RRC filter with rolloff factor $\alpha = 0.5$ (50% excessive bandwidth) is used as the transmit filter. The oversampling factor is $\mu = 2$. The channel power delay profile used in the simulation is the Typical Urban profile [22]. Figure 6.4

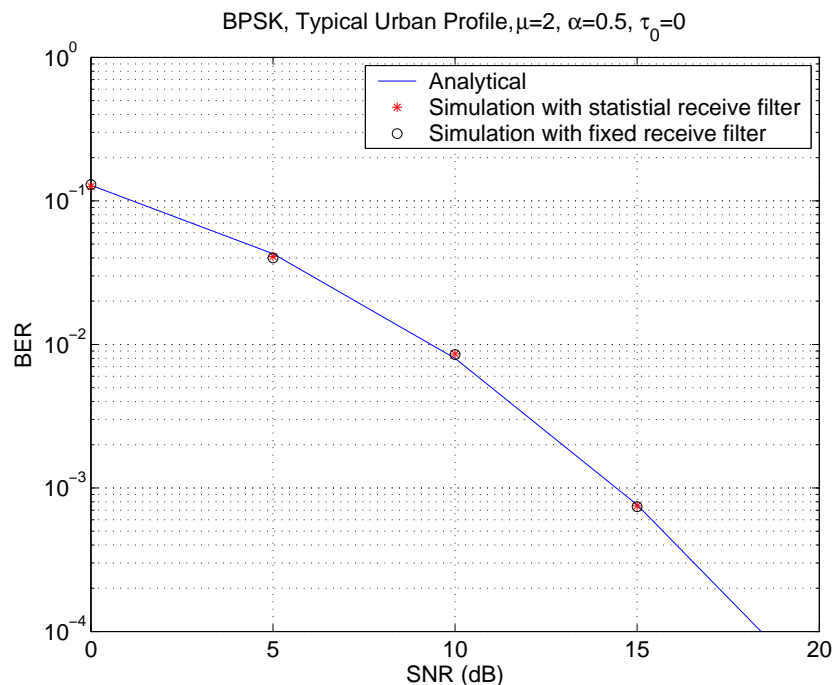


Figure 6.4: Comparison of the performances of ISI-free systems with fixed receive filter and statistical receive filter. $\mu = 2$: oversampling factor. $\alpha = 0.5$: roll-off factor of the RRC filter.

shows the simulation results along with the corresponding theoretical error probability under such system configuration. As predicted by the theoretical analysis, perfect match are observed between the symbol error rates of the two oversampled systems with fixed filter and statistical filter.

After studying the statistical properties of the three representative communication systems, we conclude this section by the following remarks about the performance of systems with frequency selective fading and sampler timing offset.

Remark 1: If there is spectrum aliasing present at the receiver, then the system error performance is a periodic function of the timing phase offset τ_0 , with the period equal to sampling period T_s . On the other hand, for system without spectrum aliasing, the timing phase offset has no effect on system performance.

Remark 2: If the channel impulse response can be represented as a T_s -spaced tapped delay line filter, then the performance of system with fixed receive filter matched to the

transmit filter is the same as that of system with statistical receive filter matched to the combined impulse response of the transmit filter and the frequency selective channel.

Remark 3: When there is no spectrum aliasing at the receiver, the choice between fixed receive filter or statistical receive filter has no effect on system performance. Thus simple time-invariant receive filter can always be used in oversampled systems without sacrificing performance.

Remark 4: For systems without spectrum aliasing at the receiver, the performance bounds derived in this chapter coincide with the conventional matched filter bound previously obtained in [93]- [97]. Therefore the conventional matched filter bounds can be viewed as special cases of the performance low bounds derived in this chapter.

6.5 Numerical Examples

In this section, the analytical error performance expressions derived in this chapter are verified with Monte-Carlo simulations, and some numerical examples are provided to reveal the effects of receiver timing phase offset on system performances.

The analytical SER performance low bounds along with the corresponding simulation results for system with symbol spaced receiver and Typical Urban PDP are shown in Fig. 6.5. In the simulation, MAP equalizers are employed at the receiver to fight against ISI. For comparison purpose, the conventional matched filter bound [94] is also plotted in the figure. RRC filters with roll-off factor $\alpha = 1$ (100% excessive bandwidth) are used as both transmit filter and receive filter. The symbol error rate results presented in Fig. 6.5 show that the performance bound derived in this chapter is very tight compared to the empirical simulation results obtained from system with ISI present at the receiver. Moreover, for $E_b/N_0 > 10\text{dB}$, excellent agreement are observed between the theoretical expressions and simulation results. This verifies the claim that MAP equalizer is asymptotic optimum in the sense of ISI cancellation. On the other hand, the conventional matched filter bound is significantly lower than the actual system performance. For example, at the SER level of 10^{-5} , there is a 5dB performance difference

between the conventional matched filter bound and the simulation results for system with $\tau_0 = 0$. This performance difference is mainly contributed by the overlook of the effects of spectrum aliasing and receiver timing phase by conventional matched filter bound. An interesting observation from Fig. 6.5 is that systems with zero timing phase offset ($\tau_0 = 0$) doesn't yield the best error performance. This phenomenon can be explained by the fact that the power of the Typical Urban profile is dominated by the delayed paths.

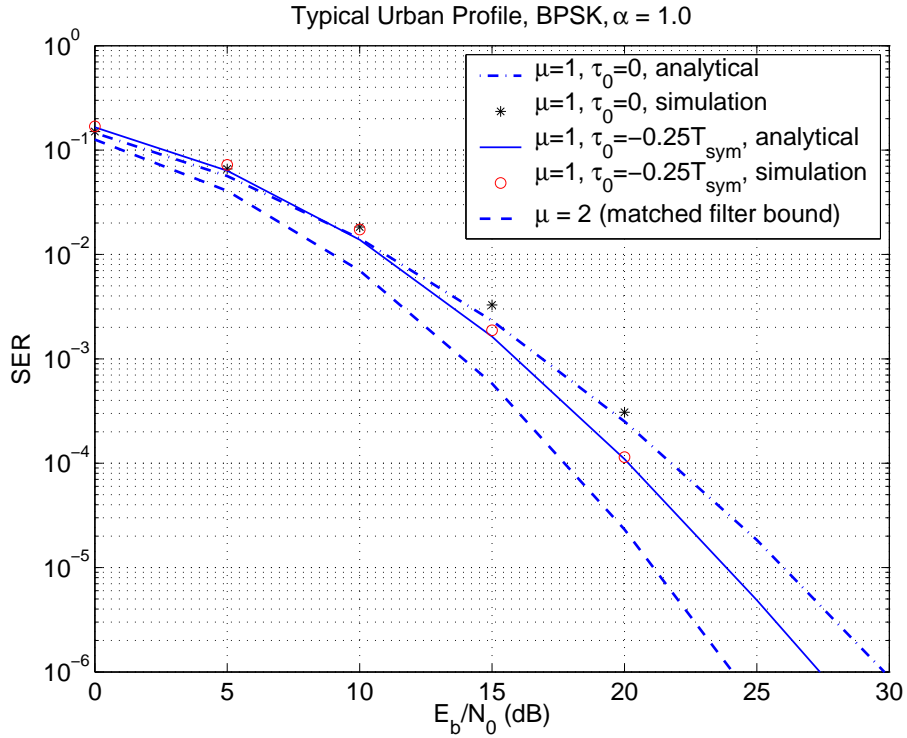


Figure 6.5: Comparison of performance bounds with simulation results of systems with Typical Urban channel profile. Decoding length for the MAP equalizers: 1024 symbols. μ : oversampling factor. τ_0 : receiver timing phase offset. α : roll-off factor of the RRC filter.

The effects of timing phase offset on system performance are further illustrated in Fig. 6.6 and Fig. 6.7, where the results are plotted against τ_0 for systems with exponentially decaying power profile. Fig. 6.6 shows the variations of the non-zero eigenvalues λ_i of the eigensystem defined in (6.17) with respect to the timing phase offset τ_0 . As analyzed in Section 6.4, the non-zero eigenvalues and performance bounds of system with symbol

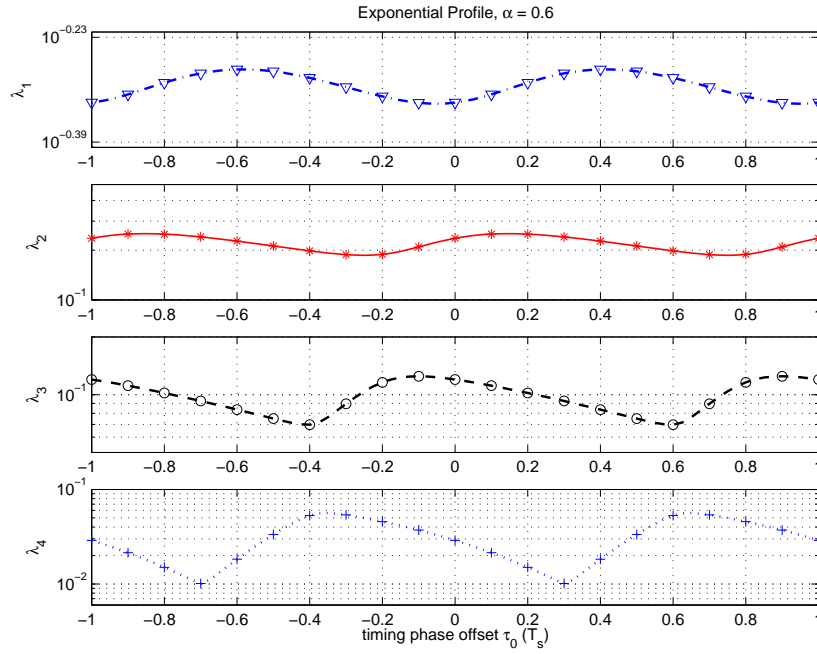


Figure 6.6: The variations of non-zero eigenvalues λ_l of the eigensystem (6.17) with respect to the timing phase offset. Exponentially decaying profile with $\tau_{\max} = 3T_{\text{sym}}$. α : roll-off factor of the RRC filter.

spaced receiver are both periodic functions of τ_0 . It can be seen from Fig. 6.7 that the optimum sampling time for Typical Urban profile is $\hat{\tau}_0 = -0.12T_{\text{sym}}$. For systems with at most 100% excessive bandwidth, two-times oversampling ($\mu = 2$) will completely avoid spectrum aliasing in the received signals. Fig. 6.7 shows that the performance of systems with $\mu = 2$ and α up to 1 keeps unchanged regardless of the values of τ_0 .

Moreover, the results displayed in Fig. 6.7 also reveals the effects of signal bandwidth (as represented by the roll-off factor α) on the timing sensitivity of the system performance. For systems with symbol spaced receivers, the numerical results show that the performances of systems with larger signal bandwidth (or larger value of α) is more sensitive to the timing phase offset τ_0 . This phenomenon can be explained by the fact that larger excessive bandwidth will result in more spectral components being aliased. On the contrary, for systems without spectrum aliasing, the system performance improves with the increase of α , because more bandwidth is consumed in transmission.

The results presented in the previous examples show that the optimum sampling time

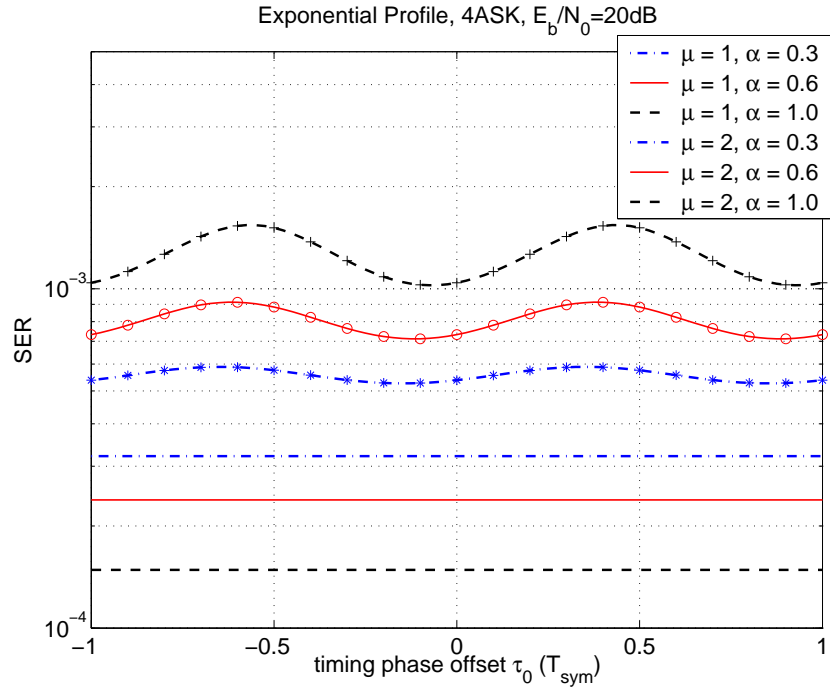


Figure 6.7: The effects of receiver timing phase and excessive bandwidth on the error performance of system with Exponentially Decaying profile with $\tau_{\max} = 3T_{sym}$. μ : oversampling factor. α : roll-off factor of the RRC filter.

$\hat{\tau}_0$ is a function of the power distribution of the channel profile. To investigate the relationship between the PDP and optimum receiver sampling time, we use a simple two path equal gain channel profile $\varphi(t) = 0.5\delta(t) + 0.5\delta(t - \tau_{\max})$ in this example. The SER performance of systems with various values of τ_{\max} are shown in Fig. 6.8. It's clear from this figure that the optimum sampling time $\hat{\tau}_0$ varies with the change of τ_{\max} . In this example, the optimum sampling time for systems with $\tau_{\max} = T_{sym}$ is 0 as expected, and $\hat{\tau}_0 = -0.2T_{sym}, 0.2T_{sym}$ for systems with $\tau_{\max} = 0.6T_{sym}, 1.4T_{sym}$, respectively.

The relationship between optimum sampling time and power delay profile is illustrated from a different perspective in Fig. 6.9, where the SER performance low bounds of systems with various values of τ_0 are plotted against the maximum delay spread τ_{\max} for two path equal gain channel profiles. From this figure, we have the following observations. 1) For systems without spectrum aliasing ($\mu = 2$), the SER decreases monotonically with the increase of τ_{\max} when $\tau_{\max} \leq T_{sym}$, and it keeps constant after $\tau_{\max} > T_{sym}$ since no extra diversity gain can be achieved. 2) For systems with symbol spaced sampling,

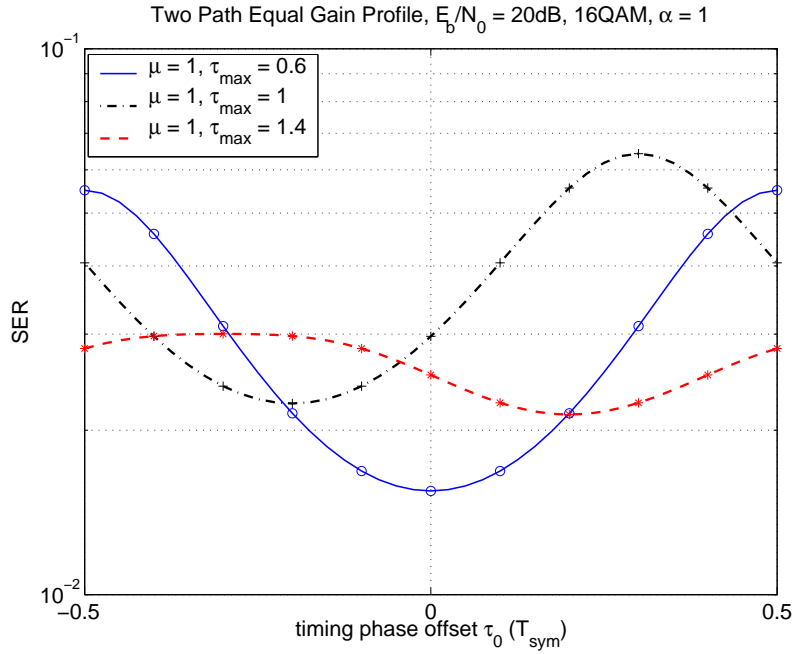


Figure 6.8: The effects of timing phase offset and maximum delay spread on the error performance of system with two path equal gain channel profile. τ_{\max} : the relative delay between the two channel paths. μ : oversampling factor. τ_0 : receiver timing phase offset. α : roll-off factor of the RRC filter.

the SER performances fluctuate with respect to the max delay spread τ_{\max} . 3) System without spectrum aliasing always outperforms systems with symbol spaced receivers, this conforms to the fact that the conventional matched filter bound is a theoretical low bound for systems with frequency selective fading. 4) For systems with $\tau_0 = 0$ and $\tau_{\max} = T_{sym}$, the performance of symbol spaced receiver is the same as that of system without spectrum aliasing. For this special case, all the overlapped spectral components have the same phase and are added up constructively, therefore no information is lost due to spectrum aliasing.

6.6 Conclusions

The effects of timing phase offset and receiver oversampling on the performance of systems with frequency selective fading was investigated based on a tight error performance

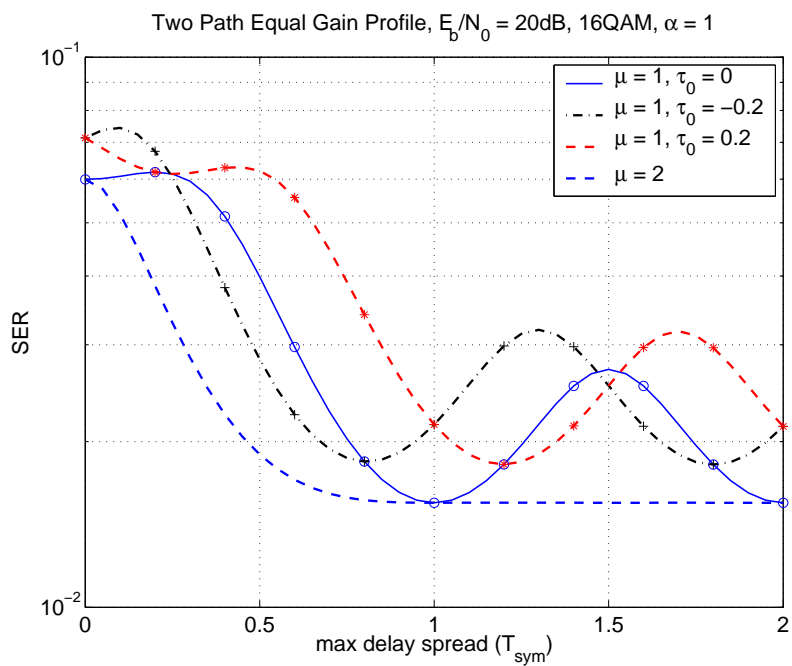


Figure 6.9: The SER performance of systems with two path equal gain profile with respect to the maximum delay spread of the channel (or the relative delay between the two channel paths). μ : oversampling factor. τ_0 : receiver timing phase offset. α : roll-off factor of the RRC filter.

low bound derived in this chapter. The effects of timing phase offset and receiver oversampling were explicitly expressed in the statistical representation of the receiver SNR, which was further quantified in the error probability bound expressions. The conventional matched filter bound can be viewed as a special case of the performance bound derived in this chapter. Simulation results showed that the new error probability bound can accurately predict the performance of practical communication systems by taking into account the effects of sampler timing phase offset and receiver oversampling.

Both theoretical analysis and numerical examples showed that for system with spectrum aliasing, the system error performance is a periodic function of the receiver timing phase offset, with the period equal to the sampling period; for system without spectrum aliasing, the system error performance is independent of the timing phase offset. Moreover, if the effect of spectrum aliasing is completely removed at the receiver, then the choice between fixed receive filter or statistical receive filter doesn't affect system error performance. Therefore, simple time-invariant receive filter can always be employed by

oversampled systems without sacrificing system performance. An interesting observation from numerical examples is that the optimum sampling time of communication systems depends on the power distribution of channel profiles, and zero timing offset doesn't always yield the best system performance.

Chapter 7

Flexible Lognormal Sum Approximation based on Gauss-Hermite Expansion of Moment Generating Function

7.1 Introduction

The lognormal distribution models the attenuation due to shadowing in wireless channels. Therefore, in the analysis of wireless systems, one often encounters the sum of lognormal random variables (RV). It arises, for example, in cellular systems when modeling the co-channel interference (CCI) power from transmissions in neighboring cells. It also occurs in outage probability analysis [73, Chp. 3] and in ultra wide band systems [108]. Given the importance of the lognormal sum distribution, considerable efforts have been devoted in wireless communications as well as in other fields to analyze its statistical properties. While exact closed-form expressions for the lognormal sum probability distribution functions (pdf) are unknown, several analytical approximation methods exist in the literature [109–114].

The methods proposed in the literature can be classified into two broad categories. The methods by Fenton-Wilkinson [109], Schwartz-Yeh [110], and Beaulieu-Xie [112]

approximate the lognormal sum by a single lognormal RV. The proven permanence of the lognormal pdf when the number of summands approaches infinity lends credence to these methods [111, 115]. The methods by Farley [73, 110], Ben Slimane [113], and Schleher [114] instead compute a compound distribution. Of these, the first two specify the approximating distribution in terms of strict lower bounds of the cumulative distribution function (cdf), while the last one partitions the lognormal sum range into three segments, with each segment being approximated by a distinct lognormal RV.

Beaulieu *et al.* [112, 116] have studied in detail the accuracy of several of the above methods, and shown that each method has its own advantages and disadvantages; none is unquestionably better than the others. Farley's method and, more generally, the formulae derived in [113] are strict bounds that can be loose approximations for certain typical parameters. The methods also differ considerably in their complexity. Only the Fenton-Wilkinson method offers closed-form solution for the underlying parameters of the approximating lognormal pdf.

In this chapter, we present a flexible lognormal sum approximation method motivated by the fact the MGF of an RV can be interpreted as the weighted integral of the pdf. As elaborated later, the weight function can be adjusted to emphasize the accuracy in approximating different portions of the lognormal sum pdf. Moreover, the MGF of a sum of independent RVs can be easily calculated from the MGFs of the individual RVs. By using an approximate Gauss-Hermite expansion of the lognormal MGF, the proposed method circumvents the requirement for very precise numerical computations; it is not recursive; it is numerically stable and accurate; and offers considerable flexibility compared to previous approaches.

As mentioned, the moment generating function (MGF) and the characteristic function (CHF) possess the desirable property that the MGF (CHF) of a sum of independent RVs is the product of the MGFs (CHF) of the individual RVs [117].¹ This property of the CHF has been exploited by Barakat [111] and Beaulieu-Xie [112] to numerically evaluate

¹While the CHF can be considered a special case of the MGF, we choose to treat the two as separate to keep the discussion clear.

the exact distribution function of lognormal sum. However, their methods require very accurate numerical computation of the characteristic function and are quite involved. Barakat numerically computed the CHF of the lognormal distribution using Taylor series expansion, and inverse Fourier transform was then applied to the product of lognormal CHFs to determine the pdf of lognormal sum. However, the oscillatory property of the Fourier integrand as well as the slow decay rate of the lognormal pdf tail make the numerical evaluation difficult [112]. Also, no effort was made to find the analytical expressions of the approximate distribution. A similar approach was also suggested by Anderson [118]. Beaulieu-Xie's elegant and conceptually simple method first numerically evaluates the lognormal sum cdf, to a high degree of accuracy, at several points. Given the stringent precision requirements, a modified Clenshaw-Curtis method had to be used. The composite cdf is obtained by numerically calculating the inverse Fourier transform, and is plotted on 'lognormal chapter'. The parameters of the approximating lognormal distribution, which is a straight line on lognormal chapter, are determined by minimizing the maximum error in a given interval. While the method is optimal in the minimax sense on lognormal chapter, this does not imply optimality in directly matching the probability distribution.

The chapter is organized as follows: Section 7.2 reviews the lognormal sum approximation methods in the literature and investigates the reasons behind their observed behaviors. Section 7.3 motivates and defines the Gauss-Hermite integration-based MGF method proposed in this chapter. Numerical examples based on an actual cellular layout are used to demonstrate the accuracy of the proposed method and compare it with other methods in Section 7.4. The conclusions follow in Section 7.5.

7.2 Comparison of Various Lognormal Sum Approximation Methods

Let X_1, \dots, X_K be K independent, but not necessarily identical, lognormal RVs with pdfs, $p_{X_i}(x)$, for $1 \leq i \leq K$. Then each X_i can be written as $10^{0.1Y_i}$ such that Y_i is

a Gaussian random variable with mean, μ_{Y_i} dB, and standard deviation, σ_{Y_i} dB, *i.e.*, $Y_i \sim \mathcal{N}(\mu_{Y_i}, \sigma_{Y_i}^2)$.

General closed-form expressions for the pdf or cdf of the lognormal sum $\sum_{i=1}^K X_i$ are not available. However, the lognormal sum can be well approximated by a new lognormal RV $X = 10^{0.1Y}$, where Y is a Gaussian RV with mean μ_Y and variance σ_Y^2 . Thus, the problem is now equivalent to estimating the lognormal moments μ_Y and σ_Y^2 given the statistics of the lognormal RVs X_i , for $i = 1, \dots, K$.

The Fenton-Wilkinson (F-W) method computes μ_Y and σ_Y^2 by exactly matching the first and second central moments of X with that of $\sum_{i=1}^K X_i$:

$$\int_0^\infty x p_X(x) dx = \sum_{i=1}^K \int_0^\infty x p_{X_i}(x) dx, \quad (7.1a)$$

$$\int_0^\infty (x - \mu_X)^2 p_X(x) dx = \sum_{i=1}^K \int_0^\infty (x - \mu_{X_i})^2 p_{X_i}(x) dx, \quad (7.1b)$$

where μ_X and μ_{X_i} are the means of X and X_i , respectively. If the K lognormal RVs are identically distributed, then the approximating lognormal moments μ_Y and σ_Y can even be expressed in closed-form. While the F-W method accurately models the *tail portion* (large values of X) of the lognormal sum pdf, it is quite inaccurate near the *head portion* (small values of X) of the sum pdf, especially for large values of σ_{Y_i} [116]. The mean square error in μ_Y and σ_Y increases with a decrease in the spread of the mean values or an increase in the spread of the standard deviations of the summands [119]. Also, in modeling the behavior of $10 \log_{10} \left(\sum_{i=1}^K X_i \right)$ the method breaks down when $\sigma_{Y_i} > 4$ dB [73].

The Schwartz-Yeh (S-Y) method instead matches the moments in the log-domain, *i.e.*, it equates the first and second central moments of $\log_{10} X$ with those of $\log_{10}(\sum_{i=1}^K X_i)$:

$$\int_0^\infty (\log_{10} x) p_X(x) dx = \int_0^\infty (\log_{10} x) p_{(\sum_{i=1}^K X_i)}(x) dx, \quad (7.2a)$$

$$\int_0^\infty (\log_{10} x - \mu_Y)^2 p_X(x) dx = \int_0^\infty (\log_{10} x - \mu_{Y_i})^2 p_{(\sum_{i=1}^K X_i)}(x) dx, \quad (7.2b)$$

where μ_Y and μ_{Y_i} are the mean values of $Y = 10 \log_{10} X$ and $Y_i = 10 \log_{10} X_i$, respectively. While the match is exact for $K = 2$, an iterative technique needs to be used

for $K > 2$. The parameters μ_Y and σ_Y are evaluated numerically. The S-Y method is more involved than the F-W method because the expectation of the logarithm sum cannot be directly written in terms of the expectations of the individual random variables. It is inaccurate near the tail portion of the distribution function and can significantly underestimate small values of the cdf [116].

Interpreting the moments as weighted integrals of the pdf, both the F-W method and the S-Y method can be generalized by the following system of equations for $m = 1, 2$:

$$\int_0^{\infty} w_m(x) p_X(x) dx = \int_0^{\infty} w_m(x) p_{(\sum_{i=1}^K x_i)}(x) dx. \quad (7.3)$$

The F-W method uses the weight functions $w_1(x) = x$ and $w_2(x) = (x - \mu_X)^2$, both of which monotonically increase with x . Thus, errors in the tail portion of the sum pdf are penalized more. This explains why the F-W method tracks the tail portion well. On the other hand, the S-Y method employs the weight function $w_1(x) = \log_{10} x$ and $w_2(x) = (\log_{10} x - \mu_Y)^2$. Due to the singularity of $\log_{10} x$ at $x = 0$, mismatches near the origin are severely penalized by both these weight functions. Compared to the F-W method, the S-Y method gives less weight to the pdf tail. For these reasons, it does a better job tracking the head portion of the distribution function. However, both the F-W and the S-Y methods use fixed weight functions and offer no way of overcoming their respective shortcomings.

Similarly, Schleher's cumulants matching method [114] accords a polynomially increasing penalty to the approximation error in the tail portion of the pdf. This is because the first three cumulants are, in effect, the first three central moments of an RV [120]. By plotting the x-axis in dB scale on lognormal chapter, the Beaulieu-Xie method also accords a higher priority to the tail portion.

Motivated by the weighted integral interpretations of these approximation methods, a simple method is proposed in the next section that exploits the desirable properties of the MGF.

7.3 Lognormal Sum Approximation Using Gauss-Hermite Expansion of MGF

7.3.1 Motivation

The simplicity of the F-W method arises from the fact that the mean and variance of a sum of independent RVs can be written directly as the sum of the mean and variance of the individual RVs. The MGF of the sum of independent RVs also possesses this desirable property, in that it can be written directly in terms of the MGFs of the individual RVs. The MGF of an RV X is defined as

$$\Psi_X(s) = \int_0^{\infty} \exp(-sx)p_X(x)dx, \quad (s \geq 0). \quad (7.4)$$

From (7.4), the MGF can also be interpreted as a weighted integral of the pdf $p_X(x)$, with the weight function being a monotonically decreasing exponential function $\exp(-sx)$ for real and positive values of s . Varying s from 0 to ∞ adjusts, as required, the weights allocated to the head and tail portions of the sum pdf. Figure 7.1 compares in log scale the absolute values of the various weight functions discussed above. Moreover, since the lognormal RVs X_i , ($1 \leq i \leq K$), are independently distributed, the MGF of $\sum_{i=1}^K X_i$ is given by

$$\Psi_{(\sum_{i=1}^K X_i)}(s) = \prod_{i=1}^K \Psi_{X_i}(s). \quad (7.5)$$

Based on the discussion above, we can see that the MGF possesses two desirable properties. First, the MGF is a weighted integral of the pdf with a weight function that is adjustable. Second, the MGF of the sum pdf can be easily expressed as the product of the MGFs of the individual RVs. These two properties make the MGF a preferable candidate for the lognormal sum approximation problem.

7.3.2 MGF-based Lognormal Sum Approximation

The development of the MGF-based lognormal sum approximation method requires a closed-form expression for the MGF of lognormal RV. While no general closed-form

expression for the lognormal MGF is available, it can be readily expressed by a series expansion based on Gauss-Hermite integration.² The MGF of a lognormal RV X can be written as

$$\Psi_X(s) = \int_0^\infty \frac{\xi \exp(-sx)}{x\sigma_Y\sqrt{2\pi}} \exp\left[-\frac{(\xi \log_e x - \mu_Y)^2}{2\sigma_Y^2}\right] dx, \quad (7.6a)$$

$$= \sum_{n=1}^N \frac{w_n}{\sqrt{\pi}} \exp\left[-s \exp\left(\frac{\sqrt{2}\sigma_Y a_n + \mu_Y}{\xi}\right)\right] + R_N, \quad (7.6b)$$

where μ_Y and σ_Y are the mean and standard deviation of the Gaussian RV $Y = 10 \log_{10} X$. Eqn. (7.6b) is the Gauss-Hermite series expansion of the MGF function, N is the Hermite integration order, $\xi = 10/\log_e 10$ is a scaling constant, and R_N is a remainder term. The weights, w_i , and the abscissas, a_i , are tabulated in [120, Table. 25.10] for $N \leq 20$. From (7.6b), we can define the Gauss-Hermite representation of the MGF, $\widehat{\Psi}_X$, by removing R_N as follows:

$$\widehat{\Psi}_X(s; \mu, \sigma) = \sum_{n=1}^N \frac{w_n}{\sqrt{\pi}} \exp\left[-s \exp\left(\frac{\sqrt{2}\sigma a_n + \mu}{\xi}\right)\right]. \quad (7.7)$$

The lognormal sum $\sum_{i=1}^K X_i$ can now be approximated by a lognormal RV $X = 10^{0.1Y}$, where $Y \sim \mathcal{N}(\mu_Y, \sigma_Y^2)$, by matching the MGF of X with the MGF of $\sum_{i=1}^K X_i$ at two different, real and positive values of s : s_1 and s_2 . This sets up a system of two independent equations to calculate μ_Y and σ_Y^2 , as follows:

$$\sum_{n=1}^N \frac{w_n}{\sqrt{\pi}} \exp\left[-s_m \exp\left(\frac{\sqrt{2}\sigma_Y a_n + \mu_Y}{\xi}\right)\right] = \prod_{i=1}^K \widehat{\Psi}_X(s_m; \mu_{Y_i}, \sigma_{Y_i}), \quad (7.8)$$

for $m = 1$ and 2 .

Note that the right hand side of the above two equations is a constant number. These non-linear equations in μ_Y and σ_Y can be readily solved numerically using standard functions such as `fsolve` in Matlab and `NSolve` in Mathematica.

Better estimates of μ_Y and σ_Y are obtained by increasing the Hermite integration order N at the expense of additional computational complexity. Figure 7.2 shows the impact

²Naus [121] has derived a formula for the MGF of the sum of two lognormal RVs, which can be extended to handle the sum of any even number of lognormal RVs. However, formula applies only to i. i. d. RVs and is in the form an infinite series.

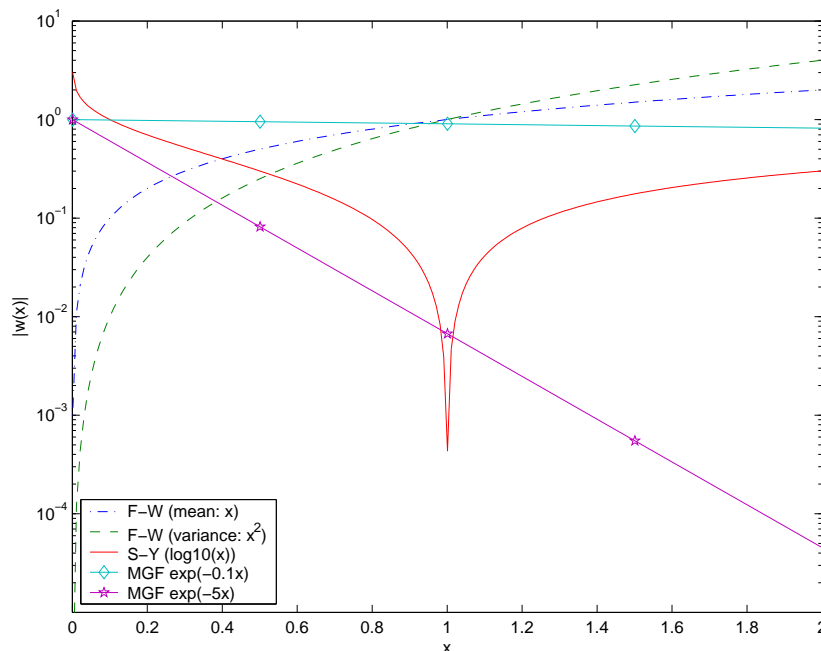


Figure 7.1: Weight functions employed by F-W, S-Y, and MGF methods

of N on the accuracy of the Gauss-Hermite representation of the MGF. We have found $N = 6$ to be sufficient to accurately determine μ_Y and σ_Y . This is small compared to the 20 to 40 terms required to achieve numerical accuracy in the S-Y method [122]. Furthermore, unlike the S-Y method, no iteration in K is required – the right hand side of eqn. (7.8) can be computed for any K at the very beginning at $s = s_1$ and s_2 . Most importantly, as highlighted before, the penalty for pdf mismatch can be adjusted by choosing s appropriately. Increasing s penalizes more the errors in approximating head portion of the sum pdf, while reducing s penalizes errors in the tail portion, as well. For example, when the lognormal sum arises because various signal components add up [108], the main performance metric is the outage probability. For this, the tail of the cdf needs to be computed accurately. On the other hand, head portion of the sum pdf that needs to be calculated accurately when the lognormal sum appears as a denominator term, for example, when the co-channel interference powers are added up in the signal to noise plus interference ratio calculation. The proposed method can handle both of these applications by using different pairs (s_1, s_2) . Guidelines for choosing (s_1, s_2) are developed in the following section.

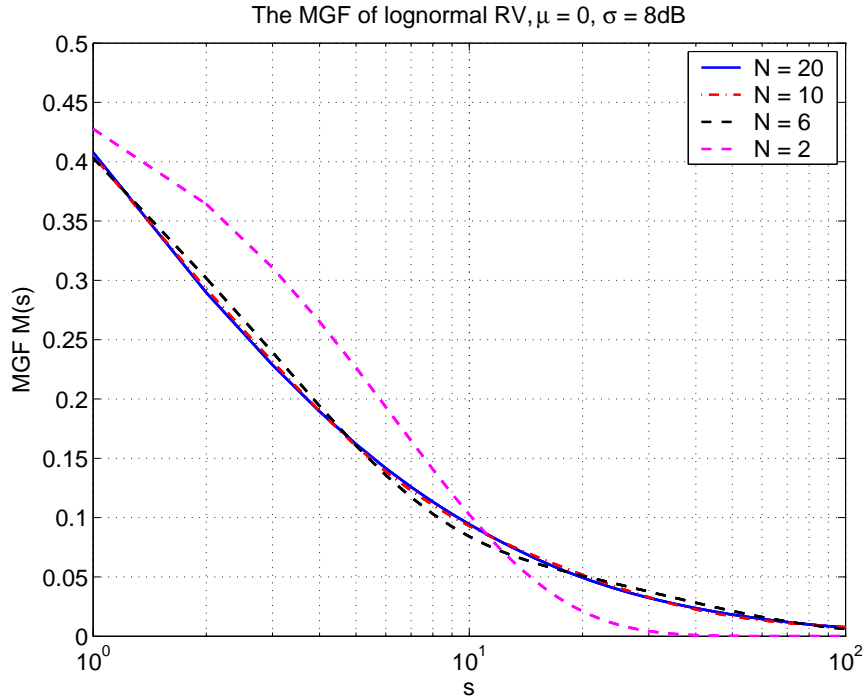


Figure 7.2: $\widehat{\Psi}_X(s; \mu, \sigma)$ as a function of s for different Hermite integration orders, N ($\mu = 0$ and $\sigma = 8$ dB)

7.4 Numerical Examples

Given the importance of CCI in cellular systems, we use a representative hexagonal cellular layout with one and two rings of interfering base stations (BS) to compare the performance of the Hermite-MGF method with other methods. The lognormal RVs in the examples below arise in the downlinks of cellular systems. Due to pathloss, the mean values of the CCI from the second-tier interferers differ considerably from those of the first-tier interferers.

Figure 7.3 shows the cell layout with 6 first-tier interferers and 12 second-tier interferers as well as the location of the desired mobile station (MS). In this system, the i^{th} lognormal RV X_i observed by the MS is given by $X_i = \gamma_0 \left(\frac{d_i}{R}\right)^{-\eta} 10^{0.1Y_i}$, where γ_0 is the signal to noise ratio (SNR) at the corner of the center cell, R is the cell radius, η is the pathloss exponent, d_i is the distance between the k^{th} BS and the MS, and Y_i is a zero-mean Gaussian RV with variance, σ , which varies from 4 to 12 dB. The examples

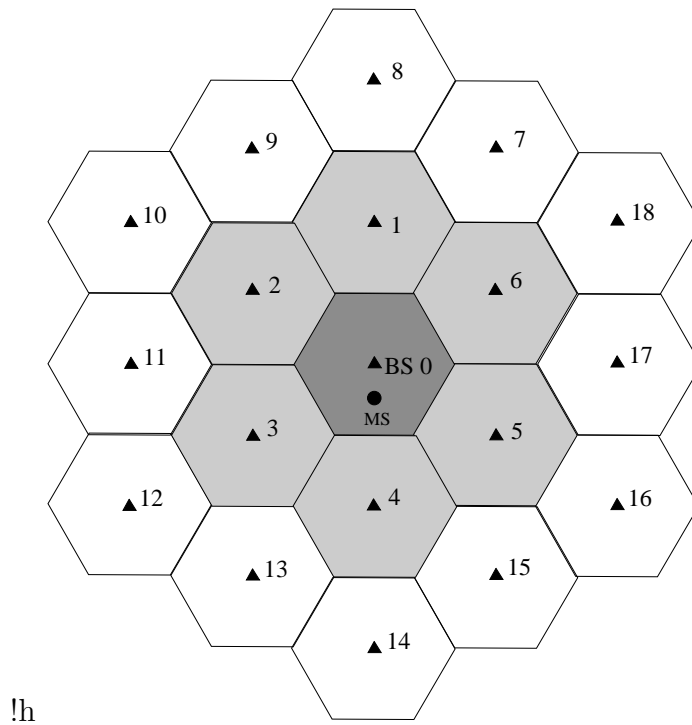


Figure 7.3: Cellular layout with up to two rings of downlink co-channel interferers

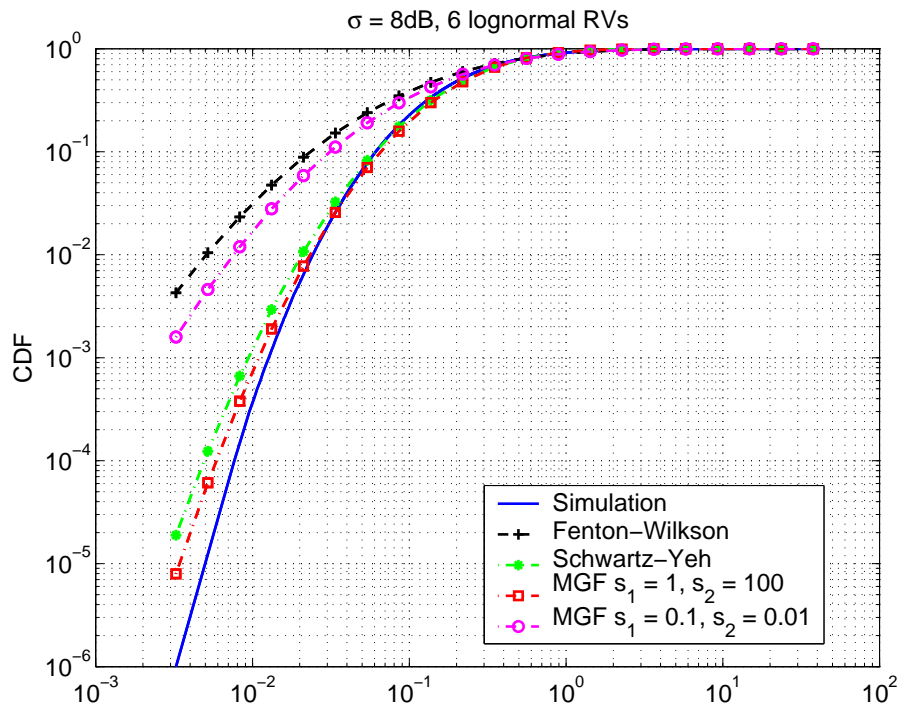


Figure 7.4: cdf of co-channel interference from first-tier interferers ($K = 6$) for $\sigma = 8$ dB

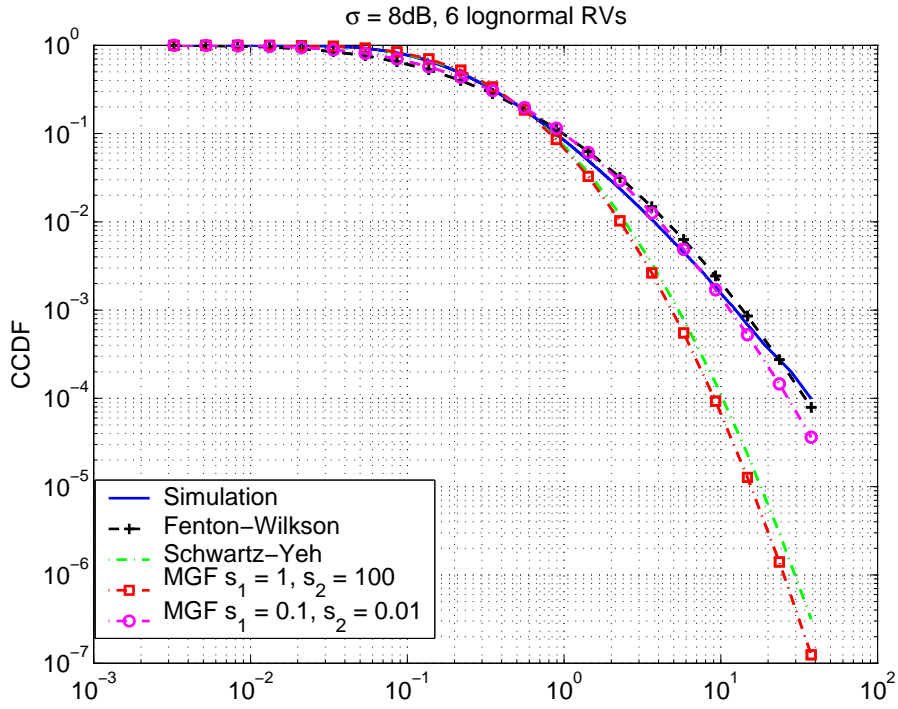


Figure 7.5: ccdf of co-channel interference from first-tier interferers ($N = 6$) for $\sigma = 8$ dB

that follow use $\gamma_0 = 10$ dB, $\eta = 3.7$, and assume that the MS is at a distance of $R/2$ from the serving (central) BS.³

In the examples, we plot the cdf and complementary cdf (ccdf) and use these results to provide guidelines on choosing generic values for s_1 and s_2 . Small values of the cdf reveal the accuracy in tracking the head portion of the pdf, while small values of the ccdf reveal the accuracy in tracking the tail portion of the pdf.

Figure 7.4 plots the cdf of the CCI from the first-tier interferers, which corresponds to the sum of $K = 6$ non-identical lognormal RVs, for $\sigma = 8$ dB. It can be seen that the Hermite-MGF method matches the head portion of the distribution function very well when $(s_1, s_2) = (1, 100)$, and is more accurate than both the F-W and the S-Y methods. The ccdf for the same parameters is plotted in Figure 7.5. While the S-Y method diverges from the actual ccdf in this scenario, the proposed method matches the simulation results well for $(s_1, s_2) = (0.01, 0.1)$, and is as accurate as the F-W method.

³The pathloss factor $(\frac{d_k}{R})^{-\eta}$ affects only the mean of X_k , but not its variance.

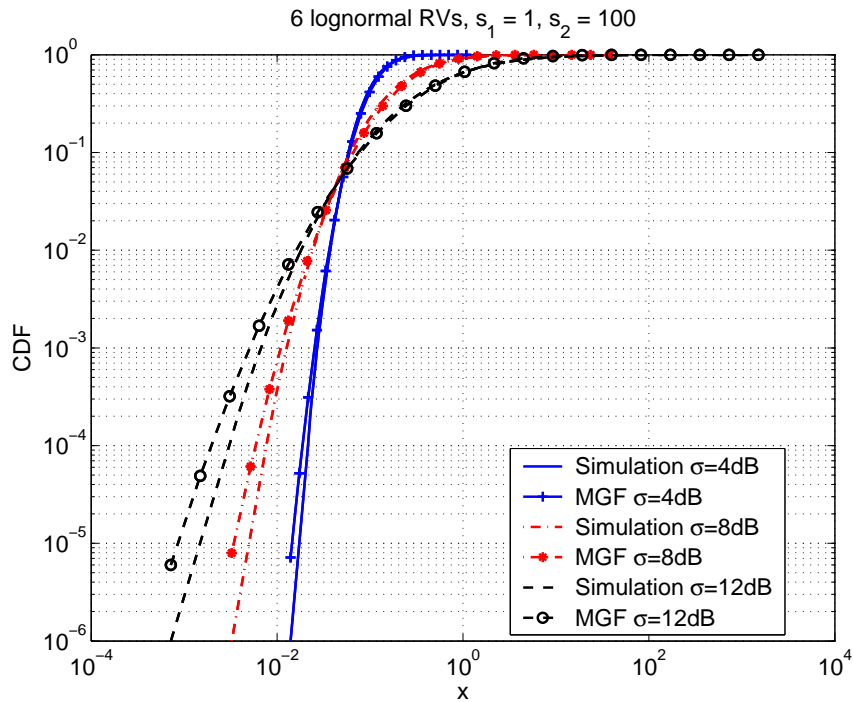


Figure 7.6: cdf as a function of σ ($K = 6, s_1 = 1, s_2 = 100$)

The above two figures (Figures 7.4 and 7.5) also plot the cdf for $(s_1, s_2) = (0.01, 0.1)$ and cdf for $(s_1, s_2) = (1, 100)$, respectively, and show the inevitable trade-off that needs to be made in approximating both the head and tail portions of the pdf.

Figure 7.6 shows the cdf of CCI from the first-tier interferers for different values of the lognormal variance and shows that the MGF method remains accurate. The effect of increasing the number of interferers is shown in Figure 7.7, which plots the cdf of the CCI from both first-tier and second-tier interferers, *i.e.*, $K = 18$. It can be seen from these two figures that $(s_1, s_2) = (1, 100)$ provides a good fit for various values of σ and K for approximating the head portion of the pdf. Similarly, $(s_1, s_2) = (0.01, 0.1)$ is suitable for approximating the tail of the pdf. Variance-specific optimization of s_1 and s_2 (not shown here) can further improve the accuracy of the method.

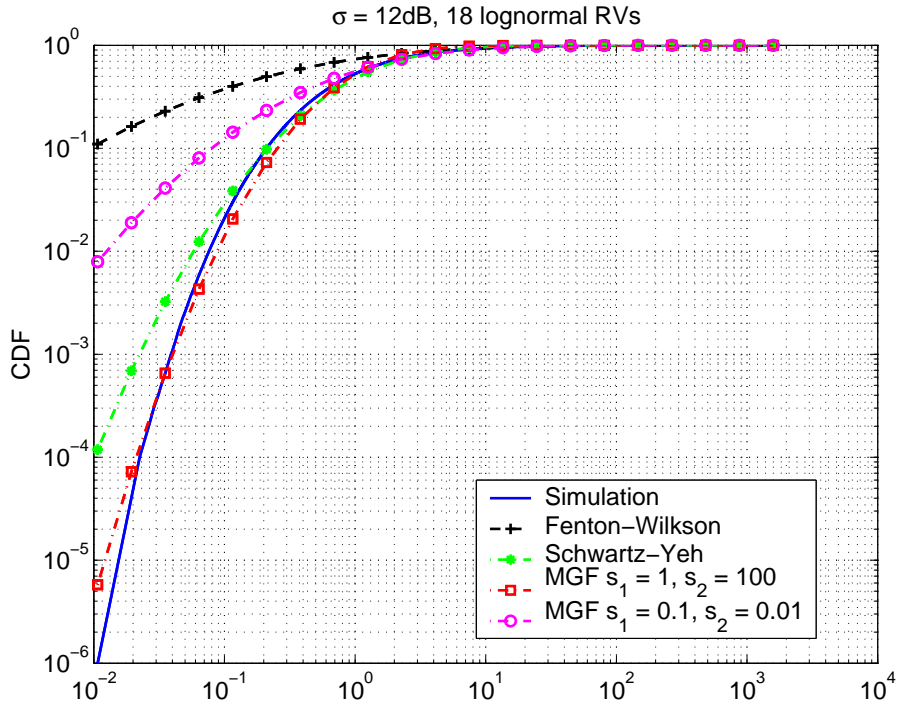


Figure 7.7: cdf of co-channel interference from both first and second-tier interferers ($K = 18$) for $\sigma = 12$ dB

7.5 Conclusions

We proposed a simple and novel method to approximate the sum of several independent, but not necessarily identical, lognormal random variables with a single lognormal random variable. The method was motivated by an interpretation of MGF as a weighted integral of the pdf. The weighted integral interpretation also explains the observed shortcomings of some of the methods currently available in the literature. Matching the Gauss-Hermite representation of the MGFs of the approximating lognormal RV and the lognormal sum at a sufficient number of points leads to a system of independent equations to compute the parameters of the approximating lognormal distribution. The computational complexity is similar to that of the Schwartz-Yeh method. A cellular layout with multiple rings of interferers was used to verify its accuracy. It also provides the flexibility required to handle the inevitable trade-off required in accurately approximating both the head and tail portions of the pdf.

Chapter 8

Spectral Efficiency Analysis of Multiuser Cellular System with Channel Aware Schedulers

8.1 Introduction

In a multiuser multi-cell mobile radio system, cochannel interference (CCI) from neighboring cells and the radio resource competition among the same cell users are two primary performance limiting factors. Therefore, the proper identifications of the effects of both CCI and multiuser resource competition on system performance are critical for cellular system planning.

Theoretical performance analysis of systems with CCI has received considerable attentions recently [123] - [127]. In [123], Alouini and Goldsmith formulated an analytical framework to quantify the spectral efficiency of an interference-limited systems, where CCI is the dominant channel impairment such that the effect of additive noise is negligible. The average spectral efficiencies under various system configurations are expressed as functions of reuse distance of the cellular system. The outage probability and spectral efficiency of interference-limited systems with successive interferences cancellation receivers is analyzed in [124], and the theoretical performances of systems with smart receiver antenna array are discussed in [125].

The works mentioned above share the same critical assumption: all the interferences are identically distributed. This assumption fails to capture the actual behaviors of practical cellular systems. For example, for a cellular layout with a center cell surrounded by two tiers of interfering cells, the CCI from the first tier interferers and second tier interferers cannot be modeled as identically distributed due to the effects of pathloss. The spectral efficiency of interference-limited systems with non-identical interferers and multiple-input multiple-output (MIMO) antennas are studied in [126] with Monte-Carlo simulation, and asymptotic spectral efficiency of MIMO interference-limited systems with non-identical CCI is obtained in [127] by assuming that the number of receive antennas tends to infinity.

In a multiuser cellular system, the users in the same cell (or sector) are competing with each other for the limited radio resource. Therefore, resource scheduling algorithms, or schedulers, are employed in the mobile radio system to manage the radio resource allocation among users. Various schedulers are proposed and analyzed in [129]- [135]. Among them, Round Robin (RR) scheduler [129], [130] provides a fair resource sharing environment for all the users by sacrificing the overall system throughput; maximum signal to interference plus noise ratio (Max-SINR) [131] scheduler maximize the system throughput at the expense of fairness among users. All the other algorithms are classified as proportional fair (PF) schedulers since they are designed based on the trade-off between the user fairness and the overall system throughput. The spectral efficiency or system throughput of various schedulers are evaluated in [129], [131]- [133] with Monte-Carlo simulations. In [134], the analytical throughput were obtained via numerical integration for a noise-limited system, *i.e.*, no CCI is present at the system. To the best of the authors' knowledge, no analytical spectral efficiency results for systems with both CCI and multiuser scheduling are available in the literature.

In this chapter, theoretical spectral efficiencies are investigated for multiuser cellular mobile radio systems operating in a Rayleigh fading and lognormal shadowing environment and with both cochannel interference and resource competition among users. Based on the geometric layout of the cellular system, the cochannel interferences from

neighboring cells are modeled as independent but *non-identically* distributed random processes, with the power of interferers being determined by the distance between the desired user and the corresponding interferer. By analyzing the statistical properties of post detection signal to interference plus noise ratio (SINR) at the receiver, spectral efficiency expressions are derived for multiuser multi-cell systems with RR schedulers and Max-SINR schedulers, and some results are expressed in closed-form. The spectral efficiency of all the other schedulers should fall within the performance range defined by these two schedulers due to the fairness and throughput trade off.

In addition, most of the previous works on theoretical spectral efficiency analysis assume that systems with adaptive modulation can employ modulation schemes with unlimited constellation size given the SINR is good enough [123], [126]- [128], [134]. However, in practical system configuration, there is an upper limit on the modulation constellation size. The effects of constellation limit on system spectral efficiency are analyzed in this chapter as well.

The rest of this chapter is organized as follows. The model of the cellular mobile radio network to be analyzed is introduced in Section 8.2. In Section 8.3, the theoretical spectral efficiency systems with RR scheduler is derived based on the statistical properties of SINR of each individual users. The multiuser spectral efficiency of systems with Max-SINR scheduler is investigated in Section 8.4. Numerical examples and simulation results are provided in Section 8.6, and Section 8.7 concludes the letter.

8.2 System Model

In this section, we present the system model representing the downlink of a multiuser cellular environment, The corresponding analysis and the results obtained therein can be directly applied to the cellular uplink. In the downlink of a mobile radio system with N active users, the received signal at the n th mobile station can be modeled as

$$r_n = \sqrt{\alpha_{n0}}h_{n0} \cdot x_{n0} + \sum_{m=1}^M \sqrt{\alpha_{nm}}h_{nm} \cdot x_{nm} + z_n, \quad (8.1)$$

where M is the number of cochannel interferers, x_{n0} is the normalized desired signal with unit symbol power, x_{nm} , for $m = 1, \dots, M$, are mutually independent, normalized interfering signals as observed by the n th mobile station, and z_n is additive white Gaussian noise with variance N_0 . In the system representation given in (8.1), the fading channel between the n th mobile station (MS) and the m th base station (BS) is represented as $\sqrt{\alpha_{nm}}h_{nm}$, where h_{nm} , for $n = 1, \dots, N$, and $m = 1, \dots, M$, are independent complex Gaussian random variables (CGRV) with zero-mean and unit variance. The coefficient α_{nm} denotes the power of the signals received by the n th mobile station from the m th base station. The power coefficient α_{nm} is determined by both the transmission power of the m th BS and the corresponding BS-MS distance d_{nm} following the exponential path-loss rule.

The number of interferers M depends on the geometric layout and configurations of the cellular system. For example, if we only consider the cochannel interferences from the first tier neighboring cells in a hexagonal cellular system with frequency reuse factor of 1, then $M = 6$ for non-sectored system, and the value of M is reduced to 2 and 1 for 3-sector and 6-sector systems, respectively [73].

From the system defined in (8.1), the instantaneous SINR γ_n at the receiver of the n th MS can be expressed by

$$\gamma_n = \frac{\alpha_{n0}|h_0|^2}{\sum_{m=1}^M \alpha_{nm}|h_{nm}|^2 + 1/\gamma_0}, \quad (8.2)$$

where $\gamma_0 = 1/N_0$ is the normalized signal to noise ratio (SNR) for system with unit transmission power.

With the definition of the instantaneous post detection SINR γ_n , we can find the spectral efficiency of each individual user in the cellular system. Spectral efficiency identifies the highest data throughput per unit bandwidth that can be achieved by a mobile user or the entire cellular system. If we assume that the mobile user is being able to continuously adapt their transmission rates according to the condition of the channel such that the bit error rate (BER) tends to 0, then the instantaneous spectral efficiency $C(\gamma_n)$ of the

n th user is defined by the Shannon capacity as

$$C(\gamma_n) = \begin{cases} \log_2(1 + \gamma_n), & \gamma_n \leq \gamma_T, \\ \log_2(T), & \gamma_n > \gamma_T, \end{cases} \quad (8.3)$$

where T is the maximum constellation size allowed in the system, and γ_T is the corresponding maximum capacity achieving SINR, *i.e.*, $\log_2(T) = \log_2(1 + \gamma_T)$, or $\gamma_T = T - 1$. For system with unlimited constellation size, we have $T = +\infty$.

The instantaneous spectral efficiency $C(\gamma_n)$ varies with time due to the time-varying nature of the fading channel, and the average spectral efficiency of the n th user can be obtained by averaging the instantaneous spectral efficiency over the SINR γ_n as

$$C_n = \int_0^{+\infty} C(\gamma) f_{\gamma_n}(\gamma) d\gamma, \quad (8.4)$$

where $f_{\gamma_n}(\gamma)$ is the probability density function (pdf) of the n th user's SINR γ_n . The average spectral efficiency for multiuser cellular systems with both limited and unlimited constellation size are discussed in the next section by analyzing the statistical properties of the post detection SINR as well as the properties of the RR and Max-SINR scheduler.

8.3 Spectral Efficiency of Round Robin Scheduler

In this section, the spectral efficiency of a multiuser cellular system with Round Robin Schedulers are analyzed based on the average spectral efficiency analysis of individual users in the system.

In a system with Round Robin scheduler, mobile users are being served on a rotating basis, *i.e.*, after a particular user is served by the base station, it will not be served again until all the other users in the system have been served for exactly once. By providing equal opportunities to all the users in the system regardless of their channel condition, Round Robin scheduler guarantees the fairness among users. It can be easily shown that Round Robin scheduler has the same spectral efficiency as random scheduler, which randomly schedule a user from all the users with equal probabilities. Based on the analysis above, we have the following theorem about the multiuser spectral efficiency of cellular systems with Round Robin scheduler.

Lemma 8.1: For a multiuser cellular system with Round Robin scheduler, the average spectral efficiency \bar{C}_{RR} of the system is

$$\bar{C}_{\text{RR}} = \frac{1}{N} \sum_{n=1}^N C_n, \quad (8.5)$$

where N is the number of active users in the system, C_n is the average spectral efficiency of the n th user as defined in (8.4).

Proof: For systems with Round Robin scheduler, all the users have equal probability of being served at any time instant regardless of the specific channel condition. If there are N active users in the system, then the probability that the n th user is going to be served at the current time instant is $1/N$. With the analysis above, the instantaneous spectral efficiency of the N -user system can be expressed by

$$C_{\text{RR}} = \frac{1}{N} \sum_{n=1}^N C(\gamma_n), \quad (8.6)$$

where $C(\gamma_n)$ is the instantaneous spectral efficiency of the n th user, $\mathbf{r} = [\gamma_1, \gamma_2, \dots, \gamma_N]$ is the time-varying SINR vector, and the mathematical expectation is operated over all the N users. The average multiuser spectral efficiency can be obtained by averaging $C_{\text{RR}}(\mathbf{r})$ over the time-varying SINR vector \mathbf{r} as

$$\bar{C}_{\text{RR}} = \mathbb{E}_{\mathbf{r}} [C_{\text{RR}}(\mathbf{r})], \quad (8.7)$$

and this immediately leads to (8.5). ■

Lemma 8.1 states that the multiuser spectral efficiency of a cellular system with Round Robin scheduler can be computed by averaging over all the user's individual spectral efficiencies. This is in consistence with the fact that all the users in such system have equal opportunities of being served, *i.e.*, the Round Robin scheduler is a fair scheduler. On the other hand, since the post detection SINR of each user is not considered in the scheduling process, the fairness among users is achieved by sacrificing the system throughput. Thus the spectral efficiency obtained from Round Robin scheduler can be used as a lower bound to the spectral efficiency of systems with practical scheduling algorithms.

In order to evaluate the average spectral efficiency of Round Robin system in a Rayleigh fading environment, we need to know the average spectral efficiency C_n of each individual users as defined in (8.4), which is in turn determined by the statistical properties of the post detection SINR γ_n . Next we analyze the statistical properties of γ_n , which is further utilized in the derivation of the single user average spectral efficiency C_n .

8.3.1 Statistical Properties of Post Detection SINR

The statistical properties of the post detection SINR at the receiver of the individual users are analyzed in this subsection to facilitate the spectral efficiency analysis.

Lemma 8.2: For a user inside a cellular system experiencing Rayleigh fading and cochannel interference, the probability density function of the post detection SINR of the n th user can be expressed by

$$f_{\gamma_n}(\gamma) = -\frac{\partial}{\partial \gamma} \left[\prod_{m=1}^M \left(1 + \frac{\alpha_{nm}}{\alpha_{n0}} \gamma \right)^{-1} \times \exp \left(-\frac{\gamma}{\gamma_0} \cdot \frac{1}{\alpha_{n0}} \right) \right], \quad (8.8)$$

where α_{n0} is the average power from the signal channel as observed by the n th user, α_{nm} , for $m = 1, 2, \dots, M$, are the power coefficients of the interfering channels, and $\gamma_0 = 1/N_0$ is the normalized signal to noise ratio.

Proof: If we define

$$\eta = \sum_{m=1}^M \alpha_{nm} |h_{nm}|^2 + \frac{1}{\gamma_0}, \quad (8.9)$$

then the instantaneous SINR γ_n given in (8.2) conditioned on η is χ^2 -distributed with 2-degree of freedom, and the conditional pdf can be written as

$$f_{\gamma_n}(\gamma|\eta) = \frac{1}{\alpha_0/\eta} \exp \left(-\frac{\gamma}{\alpha_0/\eta} \right). \quad (8.10)$$

With the conditional pdf $f_{\gamma_n}(\gamma|\eta)$ defined in (8.10), the pdf $f_{\gamma_n}(\gamma)$ can be written as

$$\begin{aligned} f_{\gamma_n}(\gamma) &= \int_0^{+\infty} f_{\gamma_n}(\gamma|\eta) f(\eta) d\eta, \\ &= \int_0^{+\infty} \frac{\eta}{\alpha_0} \exp \left(-\frac{\gamma}{\alpha_0} \eta \right) f(\eta) d\eta, \end{aligned} \quad (8.11)$$

where $f(\eta)$ is the pdf of the random variable (RV) η as defined in (8.9).

It can be seen from (8.9) that η is the sum of M independent χ^2 -distributed random variables $\alpha_{nm}|h_{nm}|^2$ plus a constant $1/\gamma_0$. The power coefficient α_{nm} depends on the distance between the MS and the BSs, thus the χ^2 -distributed random variables $\alpha_{nm}|h_{nm}|^2$ could be either identically or non-identically distributed for different locations inside the cell. Since it's extremely complicated to find the pdf of the sum of non-identically distributed χ^2 -distributed random variables, we resort to the moment generating function (MGF) of η , which can be written as

$$M_\eta(s) = \int_0^{+\infty} e^{\eta s} f(\eta) d\eta, \quad (8.12a)$$

$$= \prod_{m=1}^M (1 - \alpha_{nm}s)^{-1} \times e^{s/\gamma_0}. \quad (8.12b)$$

Comparing (8.11) with (8.12a), we note that the pdf $f_{\gamma_n}(\gamma)$ can be alternatively written as

$$f_{\gamma_n}(\gamma) = \frac{1}{\alpha_0} \frac{\partial}{\partial s} M_\eta(s) \Big|_{s=-\gamma/\alpha_0}. \quad (8.13)$$

Combining (8.12b) and (8.13) will lead to (8.8), and this completes the proof. \blacksquare

In Lemma 8.2, the pdf of the post detection SINR is expressed in a form involving function differentiation, even though more direct form is readily to be expressed. We opt for the differentiation form because it can simplify the derivation of the cumulative distribution function (cdf) and average spectral efficiency.

Corollary 8.1: For the n th user inside the multiuser cellular system defined by (8.1), the cumulative distribution function of the post detection SINR γ_n can be expressed by

$$F_{\gamma_n}(\gamma) = 1 - \prod_{m=1}^M \left(1 + \frac{\alpha_{nm}}{\alpha_{n0}} \gamma \right)^{-1} \times \exp \left(-\frac{\gamma}{\gamma_0} \cdot \frac{1}{\alpha_{n0}} \right). \quad (8.14)$$

Proof: According to the definition of cdf, $F_{\gamma_n}(\gamma)$ can be written as

$$F_{\gamma_n}(\gamma) = P(\gamma_n < \gamma) = \int_0^\gamma f_{\gamma_n}(x) dx. \quad (8.15)$$

Substituting (8.8) into (8.15) will lead to (8.14). \blacksquare

It's worth pointing out that the cdf of the post detection SINR can be directly used to evaluate the user's outage probability, which is defined as the probability of failing to achieve a specified SINR γ_{th} sufficient to provide satisfactory link qualities [125]. Based on this definition, we have

$$P_{\text{out}} = P(\gamma_n < \gamma_{\text{th}}) = F_{\gamma_n}(\gamma_{\text{th}}). \quad (8.16)$$

The outage probability P_{out} defines a measure for assessing the quality of services provided by the cellular system. The smaller the outage probability, the better the quality of service of the system. It can be seen from Corollary 8.1 that for a certain γ_{th} , the outage probability can be reduced by increasing either the individual signal to interference ratio γ_{n0}/γ_{nm} or the receiver single to noise ratio $\gamma_0\alpha_{n0}$.

8.3.2 Average Spectral Efficiency for Single User

To facilitate the derivation of the n th user's spectral efficiency, the $(M + 1)$ power coefficients α_{nm} , for $m = 0, \dots, M$, are grouped into L_n subsets, such that the elements belonging to the same subset sharing the same value of α_{nm} , and the values of α_{nm} of different subsets are distinct. Without loss of generality, it is assumed that the cardinality of the l th subset is m_{nl} , and $M = \sum_{l=1}^{L_n} m_{nl}$. Based on this partitioning scheme of channel power coefficients, we have the following theorem about the average spectral efficiency for a single user in the cellular system.

Theorem 8.1: For a given user inside the cellular system operating in Rayleigh fading environment with both CCI and additive noise, the average spectral efficiency of the n th user can be expressed by

$$C_n = \log_2 e \cdot \sum_{l=1}^{L_n} \sum_{i=1}^{m_{nl}} \beta_{l_i} \cdot \left(\frac{\alpha_{n0}}{\alpha_{nl}} \right)^{m_{nl}} \cdot \bar{\gamma}_{n0}^{i-m_{nl}} \cdot e^{\frac{1}{\bar{\gamma}_{nl}}} \times \left[\Gamma \left(i - m_{nl}, \frac{1}{\bar{\gamma}_{nl}} \right) - \Gamma \left(i - m_{nl}, \frac{1}{\bar{\gamma}_{nl}} + \frac{T-1}{\bar{\gamma}_{n0}} \right) \right], \quad (8.17)$$

where $\Gamma(k, x)$ is the incomplete Gamma function, L_n is the number of distinct values of the $(M + 1)$ power coefficients α_{nm} , T is the maximum modulation constellation size

allowed in the system, $\bar{\gamma}_{nl} = \gamma_0 \alpha_{nl}$, and β_{l_i} is defined as

$$\beta_{l_i} = \frac{1}{(i-1)!} \frac{\partial^{i-1}}{\partial \gamma^{i-1}} \left[\left(1 + \frac{\alpha_{nl} \gamma}{\alpha_{n0}}\right)^{m_{nl}} \prod_{m=0}^M \left(1 + \frac{\alpha_{nk} \gamma}{\alpha_{n0}}\right)^{-1} \right] \Bigg|_{\gamma = -\alpha_{n0}/\alpha_{nl}}, \quad (8.18)$$

for $l = 1, \dots, L_n, \quad i = 1, \dots, m_{nl}$.

Proof: Combining (8.3) and (8.4), we can write the average spectral efficiency for the n th user as

$$C_n = - \int_0^{\gamma_T} \log_2(1 + \gamma) d[1 - F_{\gamma_n}(\gamma)] + \int_{\gamma_T}^{+\infty} \log_2(T) f_{\gamma_n}(\gamma) d\gamma \quad (8.19a)$$

$$= \log_2 e \int_0^{\gamma_T} \frac{1}{1 + \gamma} [1 - F_{\gamma_n}(\gamma)] d\gamma \quad (8.19b)$$

where integral by part is applied to the first integral in (8.19a), and the identity $\log_2(\gamma_T) = \log_2(T)$ is used in the derivation of (8.19b).

Substituting the cdf $F_{\gamma_n}(\gamma)$ in (8.19) with that given in Corollary 8.1, we have the spectral efficiency as

$$C_n = \log_2 e \int_0^{\gamma_T} \exp\left(-\frac{\gamma}{\gamma_0 \alpha_{n0}}\right) \prod_{m=0}^M \left(1 + \frac{\alpha_{nm} \gamma}{\alpha_{n0}}\right)^{-1} d\gamma, \quad (8.20a)$$

$$= \log_2 e \int_0^{\gamma_T} \exp\left(-\frac{\gamma}{\gamma_0 \alpha_{n0}}\right) \prod_{l=1}^{L_n} \left(1 + \frac{\alpha_{nl} \gamma}{\alpha_{n0}}\right)^{-m_{nl}} d\gamma, \quad (8.20b)$$

where the identity $\alpha_0/\alpha_0 = 1$ is used in the expression of (8.20a), and the second equality is based on the subset partition of the power coefficients set $\{\alpha_{nm}\}_{m=0}^M$, with L_n being the number of distinct values of α_{nm} , and m_{nl} is the cardinality of the l th subset.

Performing partial fraction expansion of the product term in the integrand of (8.20b), we will have

$$C_n = \log_2 e \sum_{l=1}^{L_n} \sum_{i=1}^{m_{nl}} \bar{\beta}_{l_i} \int_0^{\gamma_T} \left(1 + \frac{\alpha_{nl} \gamma}{\alpha_{n0}}\right)^{-(m_{nl}-i+1)} \exp\left(-\frac{\gamma}{\gamma_0 \alpha_{n0}}\right) d\gamma, \quad (8.21)$$

where $\bar{\beta}_{l_i}$ is the partial fraction coefficient expressed by

$$\bar{\beta}_{l_i} = \frac{\alpha_{n0}^{i-1}}{\alpha_{nl}^{i-1} (i-1)!} \frac{\partial^{i-1}}{\partial \gamma^{i-1}} \left[\left(1 + \frac{\alpha_{nl} \gamma}{\alpha_{n0}}\right)^{m_{nl}} \prod_{m=0}^M \left(1 + \frac{\alpha_{nm} \gamma}{\alpha_{n0}}\right)^{-1} \right] \Bigg|_{\gamma = -\alpha_{n0}/\alpha_{nl}}. \quad (8.22)$$

Combining (8.21), (8.22) and the definition of the incomplete Gamma function [87],

$$\Gamma(k, x) = \int_x^{+\infty} t^{k-1} e^{-t} dt, \quad (8.23)$$

we will have (8.17) and (8.18), and this completes the proof. \blacksquare

Theorem 8.1 gives the closed-form representation of the average spectral efficiency of a specified user inside a cellular system with maximum constellation size of T . The spectral efficiency is expressed as a function of the signal power α_{n0} and interfering power $\{\alpha_{nm}\}_{m=1}^M$ observed by the user, which are in turn determined by the relative position between the mobile user and the serving or interfering base stations. The single user spectral efficiency of system with no modulation limit can be obtained by setting $T = +\infty$ in (8.17).

If all the channel power coefficients α_{nm} are distinct, which is true for most practical system configurations due to the effect of path-loss and shadowing, then the spectral efficiency can be simplified from (8.17) to

$$C = \log_2 e \cdot \sum_{m=0}^M \frac{\alpha_{n0}}{\alpha_{nm}} \cdot \prod_{\substack{i=0 \\ i \neq m}}^M \frac{\alpha_{nm}}{\alpha_{nm} - \alpha_{ni}} \cdot e^{\frac{1}{\bar{\gamma}_{nm}}} \cdot \left[\Gamma\left(0, \frac{1}{\bar{\gamma}_{nm}}\right) - \Gamma\left(0, \frac{1}{\bar{\gamma}_{nl}} + \frac{T-1}{\bar{\gamma}_{n0}}\right) \right] \quad (8.24)$$

A direct consequence of Theorem 8.1 is the spectral efficiency of noise-limited system, where the cochannel interference is so small compared with additive noise that the effects of CCI can be ignored. By setting $M = 0$ in (8.17) or (8.24), we have the spectral efficiency of noise-limited system summarized in the following Corollary.

Corollary 8.2: The average spectral efficiency of a given user in a noise-limited environment (or single cell system) can be expressed by

$$C_n = \log_2 e \cdot e^{\frac{1}{\bar{\gamma}_{n0}}} \cdot \left[\Gamma\left(0, \frac{1}{\bar{\gamma}_{n0}}\right) - \Gamma\left(0, \frac{T}{\bar{\gamma}_{n0}}\right) \right], \quad (8.25)$$

where $\bar{\gamma}_{n0} = \gamma_0 \alpha_{n0}$ is the average SNR at the receiver. \blacksquare

By recognizing the identity $\Gamma(0, x) = \text{expint}(x)$, where $\text{expint}(x) = \int_x^{+\infty} e^{-t}/t dt$ is the exponential integral, we can easily find that the result presented in (8.25) with $T = +\infty$ agrees with the result previously obtained in [128, eqn. (12)] for noise-limited systems with unlimited modulations.

Combining the single user average spectral efficiency results with Theorem 8.1, we can get the multiuser spectral efficiency for Round Robin system operating in Rayleigh fading environments.

8.4 Spectral Efficiency of Max-SINR Scheduler

The average spectral efficiency of systems with Max-SINR scheduler is analyzed in this section. At any time instant, base station equipped with Max-SINR scheduler will always serve the mobile station with the highest SINR among all the mobile users. If we define

$$\gamma_{\max} = \max \{ \gamma_1, \gamma_2, \dots, \gamma_N \}, \quad (8.26)$$

then the average spectral efficiency of system with Max-SINR scheduler can be written by [c.f. (8.3) and (8.4)]

$$\bar{C}_{\text{MSINR}} = \int_0^{\gamma_T} \log_2(1 + \gamma) f_{\gamma_{\max}}(\gamma) d\gamma + \log_2(T) [1 - F_{\gamma_{\max}}(\gamma_T)]. \quad (8.27)$$

where $f_{\gamma_{\max}}(\gamma)$ and $F_{\gamma_{\max}}(\gamma)$ are the pdf and cdf of the Max-SINR γ_{\max} , respectively, T is the maximum modulation constellation size allowed in the system, and γ_T is the corresponding SINR threshold.

8.4.1 Statistical Properties of Post Detection SINR

Before moving on to the average spectral efficiency analysis, we have the following lemma about the cdf of γ_{\max} .

Lemma 8.3: In a cellular environment with Rayleigh fading and M cochannel interferers, the cdf of the Max-SINR $\gamma_{\max} = \max \{ \gamma_1, \gamma_2, \dots, \gamma_N \}$ is

$$F_{\gamma_{\max}}(\gamma) = 1 + \sum_{n=1}^N (-1)^n \sum_{k=1}^{\binom{N}{n}} \exp(-\sigma_{nk}\gamma) \prod_{i \in \mathcal{C}_k(N,n)} \prod_{m=1}^M (1 + \lambda_{im}\gamma)^{-1}, \quad (8.28)$$

where $\lambda_{im} = \alpha_{im}/\alpha_{i0}$ is the ratio between the power coefficients α_{im} of the m th interfering channel and α_{i0} of the signal channel observed by the i th user, the binomial coefficient

$\binom{N}{n}$ is the number of ways choosing n elements from a set with N distinct members, $\mathcal{C}_k(N, n)$ is an n -element set with its members corresponding to the k th combination of choosing n elements from the index set $\{1, 2, \dots, N\}$, for $k = 1, 2, \dots, \binom{N}{n}$, and σ_{nk} is defined as

$$\sigma_{nk} = \sum_{i \in \mathcal{C}_k(N, n)} \frac{1}{\gamma_{i0} \alpha_{i0}}. \quad (8.29)$$

Proof: The cdf of γ_{\max} is defined as

$$F_{\gamma_{\max}}(\gamma) = P(\gamma_1 < \gamma, \dots, \gamma_N < \gamma). \quad (8.30)$$

Since γ_n , for $n = 1, 2, \dots, N$, are mutually independent, (8.30) can be rewritten as

$$F_{\gamma_{\max}}(\gamma) = \prod_{n=1}^N F_{\gamma_n}(\gamma), \quad (8.31)$$

where $F_{\gamma_n}(\gamma)$ is the cdf of the post detection SINR of the n th user. Substituting the results of Corollary 8.1 into (8.31), we can write the cdf $F_{\gamma_{\max}}(\gamma)$ as

$$F_{\gamma_{\max}}(\gamma) = \prod_{n=1}^N \left[1 - \prod_{m=1}^M \left(1 + \frac{\alpha_{nm} \gamma}{\alpha_{n0}} \right)^{-1} \times \exp \left(-\frac{\gamma}{\gamma_0} \cdot \frac{1}{\alpha_{n0}} \right) \right], \quad (8.32)$$

which can be further expanded to

$$F_{\gamma_{\max}}(\gamma) = 1 + \sum_{n=1}^N (-1)^n \sum_{k=1}^{\binom{N}{n}} \prod_{i \in \mathcal{C}_k(N, n)} \exp \left(-\frac{\gamma}{\gamma_0} \cdot \frac{1}{\alpha_{i0}} \right) \prod_{m=1}^M \left(1 + \frac{\alpha_{im} \gamma}{\alpha_{i0}} \right)^{-1}. \quad (8.33)$$

Eqn. (8.28) immediately follows (8.33), and the proof is completed. \blacksquare

One byproduct of Lemma 8.3 is the outage probability P_{out} of the multiuser system with Max-SINR scheduler. As discussed in Section 8.3.1, P_{out} is directly related to the cdf of the post detection SINR, and it can be written as

$$P_{\text{out}} = F_{\gamma_{\max}}(\gamma_{\text{th}}), \quad (8.34)$$

where γ_{th} is the minimum SINR required by the system to provide satisfying services to the mobile users. Eqn. (8.34) states that the outage probability of a multiuser cellular system with Max-SINR scheduler is equal to the probability that the SINRs of all the users in the systems fail to achieve the minimum system requirement γ_{th} .

8.4.2 Spectral Efficiency Analysis

In Lemma 8.3, the cdf of the Max-SINR is expressed as the summation of a group of finite products $\exp(-\sigma_{nk}\gamma) \prod_{i \in \mathcal{C}_k(N,n)} \prod_{m=1}^M (1 + \lambda_{im}\gamma)^{-1}$. To facilitate the average spectral efficiency analysis of system with Max-SINR scheduler, we define the following function

$$\Phi_{n,k}(\gamma) = \frac{1}{1 + \gamma} \prod_{i \in \mathcal{C}_k(N,n)} \prod_{m=1}^M (1 + \lambda_{im}\gamma)^{-1},$$

for $n = 0, \dots, N$, and $k = 1, \dots, \binom{N}{n}$, (8.35)

with $\lambda_{im} = \alpha_{im}/\alpha_{i0}$. The $Mn + 1$ product terms $(1 + \lambda_{im}\gamma)^{-1}$ of $\Phi_{n,k}(x)$ can be grouped into $L(n, k)$ subsets, such that all members beckoning to the same subset are sharing the same value of $\lambda_{im} = \alpha_{im}/\alpha_{i0}$, and the values of λ_{im} are distinct from subset to subset. Without loss of generality, it is assumed that there are $m_l(n, k)$ elements in the l th subset. With such partitioning scheme, $\Phi_{n,k}(\gamma)$ can be rewritten as

$$\Phi_{n,k}(\gamma) = \prod_{l=1}^{L(n,k)} [1 + \lambda_l(n, k)\gamma]^{-m_l(n,k)},$$
(8.36)

where $\lambda_l(n, k)$ equals to the value of α_{im}/α_{i0} in the l th subset. With Lemma 8.3 and the definition given in (8.35) and (8.36), we have the following theorem about the average spectral efficiency of systems with Max-SINR scheduler.

Theorem 8.2: For a cellular mobile radio system with Max-SINR scheduler, if there are N active users experiencing Rayleigh fading and cochannel interference, then the average spectral efficiency of the multiuser system can be expressed by

$$\begin{aligned} \bar{C}_{\text{MSINR}} &= \log_2 e \sum_{n=0}^N (-1)^{n-1} \sum_{k=1}^{\binom{N}{n}} \sum_{l=1}^{L(n,k)} \lambda_l(n, k)^{-m_l(n,k)} \sum_{i=1}^{m_l(n,k)} \beta_{l_i}(n, k) \cdot \sigma_{nk}^{m_l(n,k)-i} \times \\ &\exp \left[\frac{\sigma_{nk}}{\lambda_l(n, k)} \right] \left\{ \Gamma \left[i - m_l(n, k), \frac{\sigma_{nk}}{\lambda_l(n, k)} \right] - \right. \\ &\left. \Gamma \left[i - m_l(n, k), \frac{\sigma_{nk}}{\lambda_l(n, k)} + \sigma_{nk}(T - 1) \right] \right\}, \end{aligned}$$
(8.37)

where σ_{nk} is given in (8.29), the coefficient $\beta_{l_i}(n, k)$ can be written as

$$\beta_{l_i}(n, k) = \frac{1}{(i-1)!} \frac{\partial^{i-1}}{\partial \gamma^{i-1}} \left[(1 + \lambda_l \gamma)^{m_l(n,k)} \times \Phi_{n,k}(\gamma) \right] \Bigg|_{\gamma=-1/\lambda_l(n,k)},$$

for $i = 1, \dots, m_l(n, j)$.

(8.38)

and the function $\Phi_{n,k}(\gamma)$ is defined in (8.35) and (8.36).

Proof: From (8.27) and integral by part, the average spectral efficiency can be written as

$$\bar{C}_{\text{MSINR}} = \log_2 e \int_0^{\gamma_T} \frac{1}{1+\gamma} [1 - F_{\gamma_{\max}}(\gamma)] d\gamma, \quad (8.39)$$

where $F_{\gamma_{\max}}(\gamma)$ is the cdf of γ_{\max} defined in Lemma 8.3.

From (8.28) and (8.35), the integrand in (8.39) can be written by

$$\frac{[1 - F_{\gamma_{\max}}(\gamma)]}{1 + \gamma} = \sum_{n=1}^N (-1)^{n-1} \sum_{k=1}^{\binom{N}{n}} e^{-\sigma_{nk}\gamma} \times \Phi_{n,k}(\gamma). \quad (8.40)$$

To obtain the closed-form expression of the average spectral efficiency, we perform partial fraction expansion expansion of $\Phi_{n,k}(\gamma)$ defined in (8.36), and the result is

$$\Phi_{n,k}(\gamma) = \sum_{l=1}^{L(n,k)} \sum_{i=1}^{m_l(n,k)} \bar{\beta}_{l_i}(n, k) [1 + \lambda_l(n, k)\gamma]^{-m_l(n,k)+i-1}, \quad (8.41)$$

with the partial fraction coefficients $\bar{\beta}_{l_i}(n, k)$ defined by

$$\bar{\beta}_{l_i}(n, k) = \frac{\lambda_l^{-(i-1)}}{(i-1)!} \frac{\partial^{i-1}}{\partial \gamma^{i-1}} \left\{ [1 + \lambda_l(n, k)\gamma]^{m_l(n,k)} \times \Phi_{n,k}(\gamma) \right\} \Bigg|_{\gamma=-1/\lambda_l(n,k)},$$

for $i = 1, \dots, m_l(n, k)$.

(8.42)

Substituting (8.40) - (8.42) into (8.39), we can rewrite the average spectral efficiency as

$$\bar{C}_{\text{MSINR}} = \log_2 e \sum_{n=0}^N (-1)^{n-1} \sum_{k=1}^{\binom{N}{n}} \sum_{l=1}^{L(n,k)} \sum_{i=1}^{m_l(n,k)} \bar{\beta}_{l_i}(n, k) \times \int_0^{\gamma_T} [1 + \lambda_l(n, k)\gamma]^{-m_l(n,k)+i-1} e^{-\sigma_{nk}\gamma} d\gamma. \quad (8.43)$$

Combining (8.43) with (8.23) will lead to (8.37), and this completes the proof. ■

The outage probability and average spectral efficiency of a noise-limited system with Max-SINR scheduler can be obtained by setting the number of interferers $M = 0$ in the derivation of (8.28) and (8.37), and the results are given by the following two corollaries.

Corollary 8.3: The cdf of the post detection SINR of a noise-limited system with Max-SINR scheduler is

$$F_{\gamma_{\max}}(\gamma) = 1 + \sum_{n=1}^N (-1)^n \sum_{k=1}^{\binom{N}{n}} \exp(-\sigma_{nk}\gamma), \quad (8.44)$$

where σ_{nk} is defined in (8.29). ■

Corollary 8.4: For a noise-limited system with Max-SINR scheduler, the average multiuser spectral efficiency is

$$C = \log_2 e \sum_{n=1}^N (-1)^{n+1} \sum_{k=1}^{\binom{N}{n}} \exp(\sigma_{nk}) [\Gamma(0, \sigma_{nk}) - \Gamma(0, \sigma_{nk}T - \sigma_{nk})], \quad (8.45)$$

where σ_{nk} is defined in (8.29), and T is the maximum modulation constellation size.

Proof: Combining the spectral efficiency expression in (8.27) with the cdf given in Corollary 8.4, we will have

$$C = -\log_2 e \sum_{n=1}^N (-1)^n \sum_{k=1}^{\binom{N}{n}} \int_0^{\gamma_T} \frac{1}{1+\gamma} \exp(-\sigma_{nk}\gamma) d\gamma, \quad (8.46)$$

and (8.45) immediately follows. ■

8.5 Spectral Efficiency in Composite Fading Shadowing Environment

So far, all the analyses are carried out for system with small scale fading only. In most cellular environments, due to large terrain features between transmitter and receiver, the propagation radio waveforms also undergo long term power variation, or, shadowing. In this section, we investigate the spectral efficiency of systems suffering from both short term fading and long term shadowing.

To simplify the spectral efficiency analysis, we follow the convention of most previous works [126], [123]- [127] and consider a system operating in an interference limited environment, where the additive noise power is negligible compared to CCI, . *i.e.*, the SNR $\gamma_0 \rightarrow \infty$. For interference limited environment, the post detection SINR γ_n of the n th user degrades to signal to interference ratio (SIR) $\tilde{\gamma}_n$, which can be written as [c.f. (8.2)]

$$\tilde{\gamma}_n = \frac{\alpha_{n0}|h_{n0}|^2}{\sum_{m=1}^M \alpha_{nm}|h_{nm}|^2}, \quad (8.47)$$

where the signal power or the interference power observed by the receiver are affected by both fading and shadowing.

8.5.1 Statistical Properties of Post Detection SIR

The statistical properties of shadowing can be well described by lognormal distribution. The pdf of a lognormal RV x is

$$f(x) = \frac{\xi}{\sqrt{2\pi}\sigma_x x} \exp\left[-\frac{(\xi \ln x - \mu_x)^2}{2\sigma_x^2}\right], \quad (x \geq 0), \quad (8.48)$$

where μ_x and σ_x^2 are the mean and variance of the Gaussian RV $10 \log_{10} x = \xi \ln x$, and $\xi = 10/\ln 10$ is a constant. Both μ_x and σ_x are in the unit of dB.

For a wireless environment with both Rayleigh fading and lognormal shadowing, the distribution of the received signal power can be modeled as a χ^2 -distributed RV (square of Rayleigh RV) superimposed by a lognormal RV, and the pdf of the resultant composite fading-shadowing distribution is [137]

$$f(v) = \int_0^{+\infty} \frac{1}{x} \exp\left(-\frac{v}{x}\right) \frac{\xi}{\sqrt{2\pi}\sigma_x x} \exp\left[-\frac{(\xi \ln x - \mu_x)^2}{2\sigma_x^2}\right] dx, \quad (v \geq 0). \quad (8.49)$$

where μ_x and σ_x^2 are the log-domain mean and variance of the underlying lognormal RV. This distribution is also called Suzuki distribution.

In (8.49), the pdf of the composite fading-shadowing distribution is expressed in an integral form, and it eludes closed-form solution. This integration representation of the pdf makes the SIR analysis extremely complicated. Fortunately, it is pointed out in [73] that the composite fading-shadowing distribution can be accurately approximated by a

new lognormal RV y , with the log-domain moments μ_y and σ_y^2 expressed as [73, eqn. (2.188)]

$$\mu_y = \xi[\psi(1) - \ln 1] + \mu_x, \quad (8.50a)$$

$$\sigma_y^2 = \xi^2 \zeta(2, 1) + \sigma_x^2, \quad (8.50b)$$

where μ_x and σ_x are the parameters of the composite distribution, $\psi(a)$ is the Euler psi function, and $\zeta(a, b)$ is Riemann's zeta function.

With the lognormal approximation of the composite fading-shadowing distribution, the post detection SIR of the n th user can be expressed by

$$\tilde{\gamma}_n = \frac{y_{n0}}{\sum_{m=1}^M y_{nm}}, \quad (8.51)$$

where y_{nm} , for $m = 0, 1, \dots, M$, are lognormal RVs used to approximate the composite fading-shadowing RV $\alpha_{nm}|h_{nm}|^2$, and their respective log-domain moments μ_{nm} and σ_{nm}^2 can be calculated from (8.50).

In the SIR representation of (8.51), the total interference power $\sum_{m=1}^M y_{nm}$ is the sum of M non-identically distributed lognormal RVs. Again, no closed-form expression is available in the literature for the sum of lognormal RVs. However, it is widely accepted that the lognormal sum distribution can be well approximated by another lognormal distribution [109]- [112], *i.e.*, $x_n \approx \sum_{m=1}^M y_{nm}$, where x_n is a new lognormal RV used to approximate the lognormal sum. lognormal distributed with the log-domain moments being μ_{x_n} and $\sigma_{x_n}^2$, which are the mean and variance of $\xi \ln x_n$.

The approximating lognormal RV x_n has two parameters μ_{x_n} and $\sigma_{x_n}^2$, which are the mean and variance of the underlying Gaussian RV $\xi \ln x$. Hence the problem of lognormal sum approximation is equivalent to find the values of μ_{x_n} and $\sigma_{x_n}^2$ of the approximating RV x_n based on the statistical properties of the original lognormal RVs y_{nm} , for $m = 1, \dots, M$. Several analytical methods exists in the literature for lognormal sum approximation. Among them, the method by Fenton-Wilkinson [109] provides closed-form expressions of the approximating log-domain moments μ_{x_n} and $\sigma_{x_n}^2$ by directly matching the first and second central moment of the approximating lognormal RV and

the lognormal sum. Schwartz and Yeh, instead, iteratively compute μ_{xn} and σ_{xn} by performing moment matching in the log-domain [110].

In the SIR analysis, we actually want to use a lognormal RV to approximate the sum of M independent but non-identically distributed Suzuki RVs. This approximation is justified by the facts that both Suzuki distribution and lognormal sum distribution can be well approximated by lognormal distribution. Therefore, to find the parameters μ_{xn} and σ_{xn}^2 of the approximating lognormal RV, two approximation steps needs to be performed according to conventional approximation methods.

Motivated by the fact that the moment generating function (MGF) of an RV can be interpreted as the weighted integral of the pdf, we presented in Chapter 7 a simple and flexible approximation method which is capable of directly matching the sum of independent Suzuki RVs into a new lognormal RV in one shot. Based on this method, we can directly solve the values of μ_{xn} and σ_{xn} based on the statistical properties of the composite fading-shadowing RVs $|h_{nm}|^2$ for the CCI component in the SIR representation.

With the lognormal approximation, the SIR $\tilde{\gamma}_n$ is expressed as the ratio of two lognormal RVs as $\tilde{\gamma}_n = y_{n0}/x_n$. Since the ratio of two lognormal RVs is still a lognormal RV, the SIR $\tilde{\gamma}_n$ is lognormal distributed with the lognormal mean and variance given by

$$\mu_{\tilde{\gamma}} = \mu_{y_n} - \mu_{x_n}, \quad (8.52a)$$

$$\sigma_{\tilde{\gamma}}^2 = \sigma_{y_n}^2 + \sigma_{x_n}^2, \quad (8.52b)$$

where $(\mu_{y_n}, \sigma_{y_n}^2)$ and $(\mu_{x_n}, \sigma_{x_n}^2)$ are the log-domain moments of the lognormal RV y_{n0} and x_n , respectively.

The CDF of the lognormal distributed instantaneous SIR $\tilde{\gamma}_n$ can be written as

$$F_{\tilde{\gamma}_n}(\gamma) = 1 - Q\left(\frac{\xi \ln \gamma - \mu_{\tilde{\gamma}_n}}{\sigma_{\tilde{\gamma}_n}}\right), \quad (8.53)$$

where $Q(x) = \frac{1}{\sqrt{2\pi}} \int_x^{+\infty} \exp(-\frac{y^2}{2}) dy$ is the Gaussian-Q function.

For systems with Max-SINR scheduler, the post detection SIR at the receiver is $\tilde{\gamma}_{\max} =$

$\max\{\tilde{\gamma}_1, \tilde{\gamma}_2, \dots, \tilde{\gamma}_N\}$. The CDF of $\tilde{\gamma}_{\max}$ can be written as

$$\begin{aligned} F_{\tilde{\gamma}_{\max}}(\gamma) &= \prod_{n=1}^N F_{\tilde{\gamma}_n}(\gamma), \\ &= \prod_{n=1}^N \left[1 - Q\left(\frac{\xi \ln \gamma - \mu_{\tilde{\gamma}_n}}{\sigma_{\tilde{\gamma}_n}}\right) \right]. \end{aligned} \quad (8.54)$$

With the statistical properties of the post detection SIR, we can move on to the spectral efficiency analysis for systems with both small scale fading and large scale shadowing.

8.5.2 Spectral Efficiency Analysis

The average spectral efficiency for the n th user in a system with lognormal shadowing can be computed by substituting (8.53) into (8.19b), and the result is

$$C_n = \log_2 e \int_0^{\gamma_T} \frac{1}{1+\gamma} Q\left(\frac{\xi \ln \gamma - \mu_{\tilde{\gamma}_n}}{\sigma_{\tilde{\gamma}_n}}\right) d\gamma. \quad (8.55)$$

where γ_T is the SIR cap imposed by modulation limit. Even though this spectral efficiency can not be expressed in closed-form, it can be easily evaluated with numerical methods.

Combining the result in (8.55) and Lemma 8.1 leads to the spectral efficiency expression for system with Round Robin scheduler and shadowing

$$C_{\text{RR}} = \frac{\log_2 e}{N} \int_0^{\gamma_T} \frac{1}{1+\gamma} \sum_{n=1}^N Q\left(\frac{\xi \ln \gamma - \mu_{\tilde{\gamma}_n}}{\sigma_{\tilde{\gamma}_n}}\right) d\gamma. \quad (8.56)$$

For system with Max-SINR scheduler, the spectral efficiency expression can be obtained by substituting (8.54) into (8.39), which yields

$$C_{\text{MSINR}} = \log_2 e \int_0^{\gamma_T} \frac{1}{1+\gamma} \left\{ 1 - \prod_{n=1}^N \left[1 - Q\left(\frac{\xi \ln \gamma - \mu_{\tilde{\gamma}_n}}{\sigma_{\tilde{\gamma}_n}}\right) \right] \right\} d\gamma. \quad (8.57)$$

The result presented in (8.57) can be evaluated with numerical integrations.

For systems operating in a environment with both short term fading and long term shadowing, Eqns. (8.56) and (8.57) give the spectral efficiency expressions of Round Robin scheduler and Max-SINR scheduler, respectively. It should be noted that these

spectral efficiency expressions are also applicable to system operating in a shadowing only environment, where the SIR can still be approximated by a lognormal RV, and the only adjustment required is the re-computation of lognormal parameters μ_n and σ_n^2 . Moreover, for noise limited environment, the SINR expression given in (8.2) degrades to SNR since the effects of CCI are negligible. For such system configuration, the SNR γ_n is composite fading-shadowing distributed, which can be approximated by a lognormal RV. Therefore, Eqns. (8.56) and (8.57) with appropriate γ_n and μ_n can also be applied to noise limited system operating in lognormal shadowing environment.

8.6 Numerical Examples

Numerical examples along with simulation results are provided in this section to investigate the multiuser spectral efficiency under various system configurations. A representative hexagonal cellular layout with one and two tiers of interfering BSs is used in the examples. Fig. 7.3 shows the system geometric layout with 6 first-tier interferers and 12 second-tier interferers. The spectral efficiency of the center cell is to be analyzed, and the frequency reuse factor of the system is assumed to be 1.

For a given position inside the center cell, the power coefficients α_{nm} observed by the users are affected by the BS transmission power, path-loss and lognormal shadowing. Since the effects of shadowing can be effectively averaged out at the receiver, it is assumed in the examples that α_{nm} is determined by transmission power and path-loss. The examples that follow use a pathloss exponent of 3.7.

8.6.1 Effects of CCI

Fig. 8.1 plots the Max-SINR spectral efficiencies of a 10-user system with different number of interferers. The distance between the MSs and the serving BS is $R/2$, with R being the cell radius. The results presented in the figure demonstrate that CCI has significant impact on system spectral efficiency. The spectral efficiency of a noise limited system (1-cell system) increases almost linearly with the increase of cell corner SNR μ ,

while the performance improvement of systems with CCI becomes negligible after $\mu > 12$ dB. This is because for system with CCI, both the signal power and interference power become larger with the increase of μ , thus there is no apparent improvement in the post detection SINR. The results also show that the spectral efficiency decreases as the increase of the number of interferers. For $\mu = 15$ dB, the spectral efficiency of system with only first-tier interferers (7-cell system) is 0.5 bps/Hz better than the system with 2 tiers interferers (19-cell system). Moreover, perfect agreements between the simulation results and analytical results can be observed in the results.

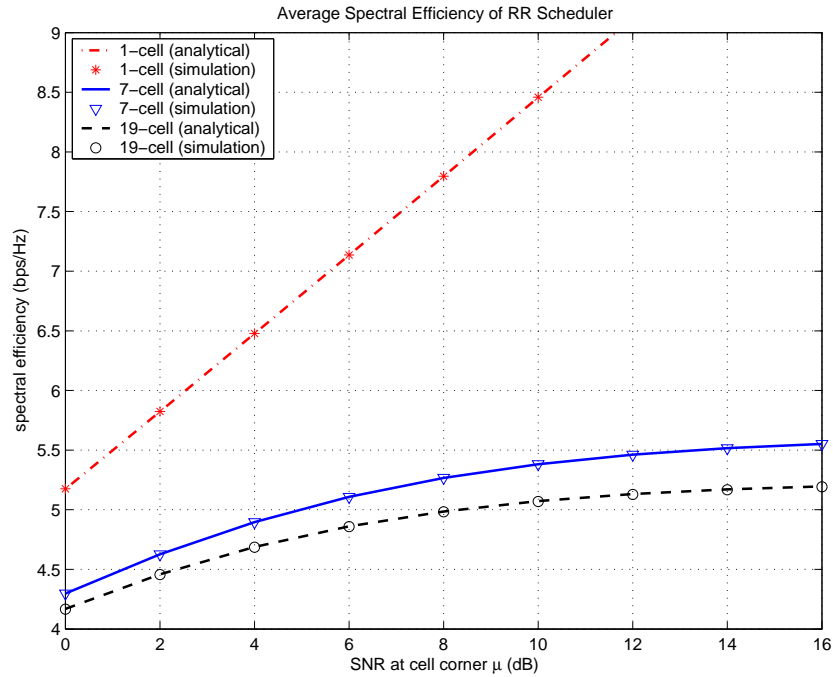


Figure 8.1: The spectral efficiencies of systems with Max-SINR scheduler with different number of cochannel interferers. Number of MS: $N = 10$. Number of sectors per cell: 1.

8.6.2 Effects of Schedulers

The spectral efficiencies of cellular systems with Max-SINR scheduler and RR scheduler are plotted in Fig. 8.2 as a function of the number of MS in the system. In this example, the distance between the serving BS and MS is half of the cell radius R , and the SNR at cell corner is assumed to be $mu = 10$ dB. It can be seen from Fig. 8.2 that the

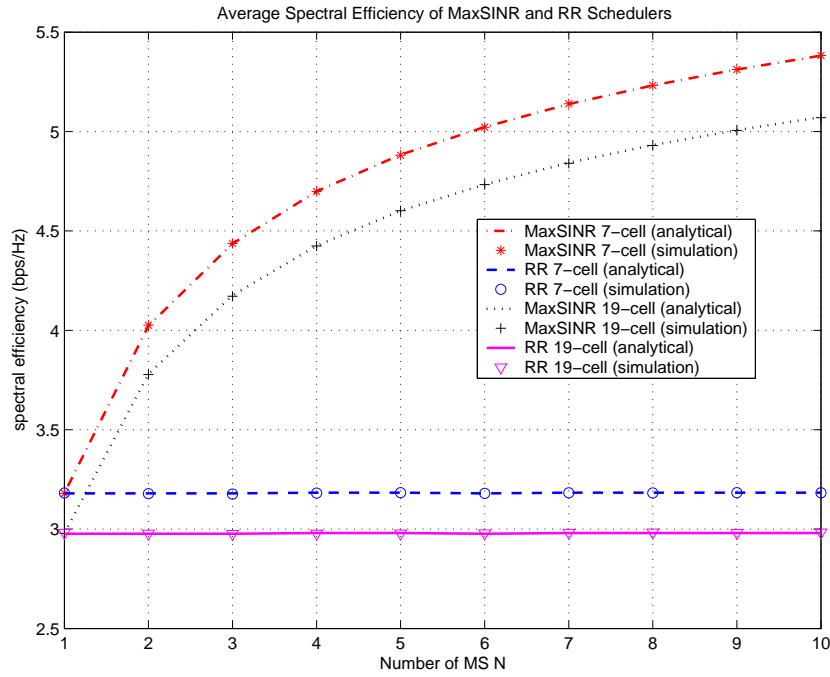


Figure 8.2: Spectral efficiencies of systems with Max-SINR scheduler and RR scheduler. SNR at cell corner: $\mu = 10\text{dB}$. Number of sectors per cell: 1.

average spectral efficiency of RR scheduler is independent of the number of users in the system. On the other hand, the Max-SINR spectral efficiency increases with the number of active users in the system thanks to the multiuser diversity inherent in the Max-SINR scheduler. The spectral efficiency of systems with proportional fair schedulers should fall between the performance range defined by the RR scheduler and Max-SINR scheduler. Moreover, as expected, the 7-cell system outperforms the 19-cell system for both RR scheduler and Max-SINR scheduler due to the decrease of CCIs.

8.6.3 Effects of Limit on Modulation Constellation Size

In all the previous examples, it is assumed that there is no limit for the modulation constellation size used in the system. However, in practical system, the modulation constellation size cannot be infinitely large. The spectral efficiencies of systems with different constellation size limits are shown in Fig. 8.3. It is assumed there are 5 users circling around the serving BS in the system, and the spectral efficiency is plotted as a

function of the distance between MS and serving BS. When the mobile users are close enough to the serving BS, the SINR of all the users are so good such that the system always choose the the modulation scheme with the largest constellation size. Under this situation, the RR scheduler and Max-SINR scheduler have the same spectral efficiency $\log_2(T)$, where T is the largest constellation size allowed by the system. When the MSs move away from the serving BS, the spectral efficiency decreases accordingly. It's interesting to note when the MSs are close to cell edge, the constellation limit has no apparent effect on system performance. This can be accounted by the fact that only modulation schemes with smaller constellation size are employed by the system due to the poor SINR quality at cell edge.

8.6.4 Effects of Cell Sectorization

The effects of cell sectorization on system performance are analyzed in this subsection. For sectorized cells, the base station antenna pattern is defined as follows [138]

$$A(\theta) = -\min \left[12 \left(\frac{\theta}{\theta_0} \right)^2, A_0 \right] \text{ dB}, \quad \text{for } -180^\circ \leq \theta \leq 180^\circ, \quad (8.58)$$

where θ is the angle between direction of interest and the boresight of the antenna. For 3-sector cell, $\theta_0 = 70^\circ$, $A_0 = 20$ dB; for 6-sector cell, $\theta_0 = 35^\circ$, and $A_0 = 23$ dB. Omni-directional antennas are assumed for non-sectorized cells.

To illustrate the effects of antenna pattern on spectral efficiency, Fig. 8.4 shows the single user spectral efficiency at different positions inside the center cell. Since the base station antenna is no longer omni-directional, the mobile spectral efficiency of a given user becomes a function of the line of sight direction between the desired user and the serving base station. As expected, for a given mobile-cell center distance d_0 , the mobiles positioned along the direction of antenna boresight has larger spectral efficiency than mobiles at other directions.

The multiuser spectral efficiency of the cellular system with RR scheduler are depicted in Fig. 8.5 for systems with different sectorization schemes. The users are assumed to be uniformly distributed in the center cell. It's apparent from this figure that sectorization

will benefit the overall system performance thanks to the decrease of cochannel interferers, and the largest performance improvement occurs at the transition from non-sector cell to 3-sector cell.

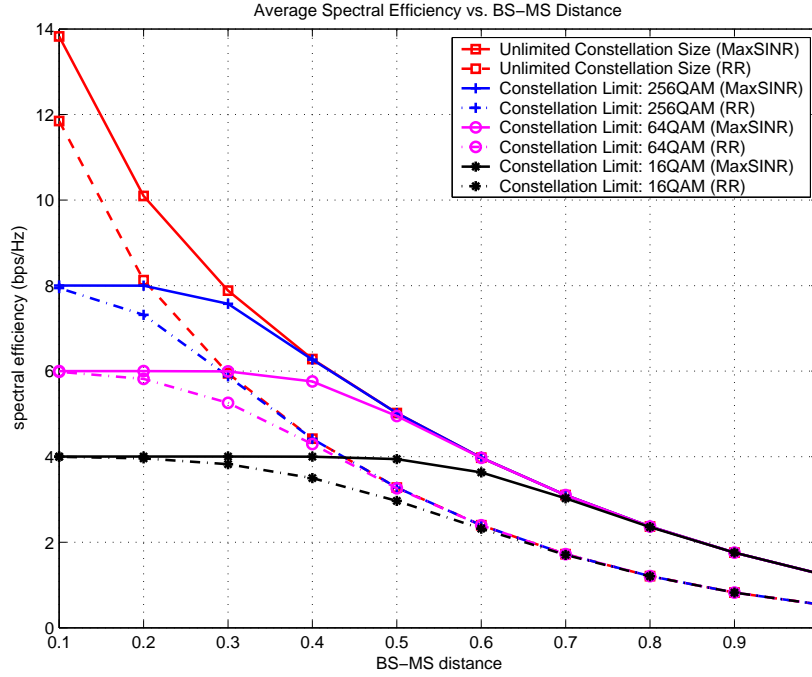


Figure 8.3: Spectral efficiencies of systems with different modulation constellation size limits. 7-cell system. SNR at cell corner: $\mu = 15\text{dB}$. Number of MS: $N = 5$. Number of sectors per cell: 1.

8.6.5 Effects of Shadowing

So far, all the examples are carried out for system with Rayleigh fading. In the last example, we evaluate the spectral efficiency for systems operating in a environment with both short term fading and long term shadowing. The analytical and simulation spectral efficiency results for systems with Round Robin scheduler and Max-SIR scheduler are presented in Fig. 8.6. The analytical results are evaluated with the help of the lognormal approximation of the sum of Suzuki RVs, while the simulation results are exact, *i.e.*, the power of the received signal or interference undergoes the fading-shadowing composite distribution. The results in Fig. 8.6 show that the approximation analytical results are very close to the actual spectral efficiency obtained by means of Monte-Carlo simulation.

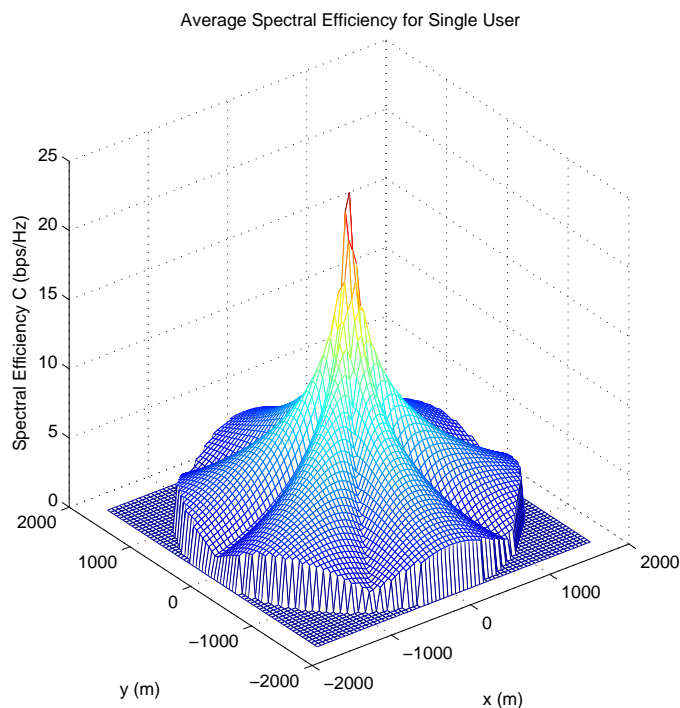


Figure 8.4: The single user spectral efficiency at various positions inside the center cell. 7-cell system. SNR at cell corner: $\mu = 15$ dB. Number of sectors per cell: 6.

This verifies that the new MGF based lognormal approximation method presented in this chapter is very accurate. Moreover, it's observed from Fig. 8.6 that larger shadowing sigma will benefit multiuser diversity. On the contrary, the performance of system with RR scheduler degrades with the increase of shadowing sigma.

8.7 Conclusions

In this chapter, theoretical spectral efficiency of multiuser multi-cell mobile radio systems with Round Robin scheduler and Max-SINR scheduler was analyzed. By identifying the statistical properties of the non-identically distributed cochannel interferers and the post detection SINR in a Rayleigh fading environment or composite fading-shadowing environment, we obtained spectral efficiency expressions for systems with RR scheduler and Max-SINR scheduler, and the effects of limited modulation constellation size was also

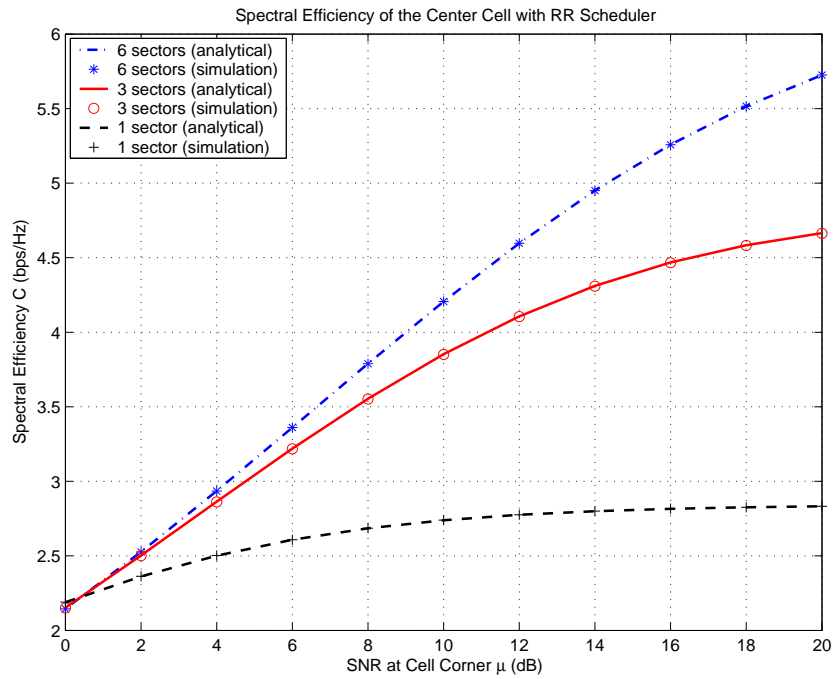


Figure 8.5: The spectral efficiency of the center cell with RR scheduler and various sectorization schemes. The MS are uniformly distributed inside the center cell

considered. The spectral efficiencies are expressed as functions of the signal and interfering channel power coefficients, which are in turn determined by the geometric layout of the cellular system. Numerical examples were used to illustrate the effects of CCI, scheduler, constellation limit and cell sectorization on system performance. Moreover, simulation results showed that the theoretical expressions obtained in this chapter can accurately predict the performance of cellular systems with practical system configurations.

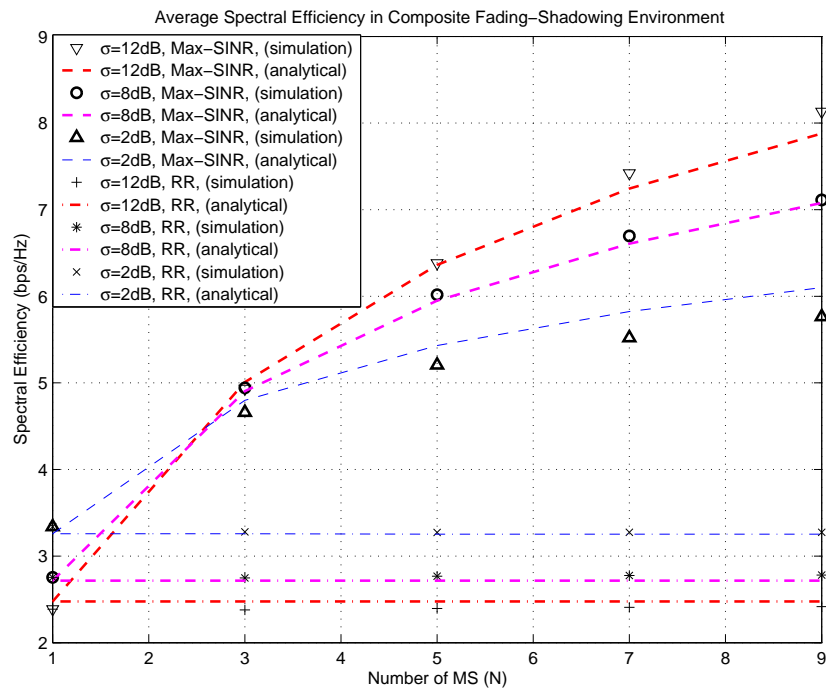


Figure 8.6: The spectral efficiency of the center cell undergoing fading and shadowing.

Chapter 9

Conclusions

This final chapter summarizes the main contributions of the dissertation, and directions for future research are outlined and discussed.

9.1 Contributions

The contents presented in this dissertation focused on the optimum receiver design as well as theoretical performance analysis of wireless communication systems operated in multipath fading environments, and the main contributions of this dissertation are summarized as follows.

First, a generic analytical discrete-time system model was presented for MIMO systems experiencing WSSUS Rayleigh fadings. It was discovered via this model that the discrete-time sample-spaced tapped delay line representation of frequency selective channel fadings has *correlated* tap coefficients due to the time span of the bandlimited pulse shaping filter, and this correlation information is essential to both system design and performance analysis. Moreover, based on the statistical properties of the analytical model, a new simulation model was also presented for efficient simulation of wireless communication systems. The statistical accuracy of the discrete-time MIMO channel model was rigorously verified through theoretical analysis and extensive simulations under various system configurations.

Second, based on the statistical properties of the discrete-time system model, an MMSE based multiuser channel estimation algorithm was proposed for quasi-synchronous CDMA

systems, and it can effectively compensate the impairments caused by doubly selective fading. The channel inter-tap correlation information of the discrete-time channel model was deemed as an essential factor in the development of the algorithm, and simulation results showed that this correlation information is critical to the accuracy of channel estimation.

Third, an optimum diversity receiver was developed for systems with practical channel estimation algorithms by analyzing the statistical properties of channel estimation error. Theoretical error probability expressions of systems employing this optimum receiver structure were derived for Rayleigh and Ricean fading environments. Simulation results validated the new theoretical results, and some interesting observations regarding practical diversity receiver design for higher-order modulation formats were drawn.

Fourth, the impacts of Doppler spread, delay spread, receiver oversampling, and receiver timing phase offset on system performance were identified via theoretical performance analysis of systems with doubly selective Rayleigh fading, and closed-form error probability expressions were derived as tight low performance bounds for linearly modulated systems. Specifically, with the help of frequency-domain analysis, the effects of receiver timing phase offset and receiver oversampling were explicitly expressed in the representations of post detection SINR, which was further quantified in the error probability expressions. Simulation results showed that the new analytical results can accurately predict the error performances of MLSE and MAP equalizers for practical wireless communication systems.

Finally, spectral efficiency and outage probability expressions were derived for multiuser cellular mobile radio systems with Round Robin scheduler and Max-SINR scheduler. The statistical properties of the receiver SINR are affected by small-scale fading, large-scale shadowing, and non-identically distributed CCI. With the help of the analytical results, the relationship between system performance and CCI was analyzed, which provides useful insights for the design of cellular mobile radio systems.

In summary, this dissertation covered algorithm design and performance analysis of a

broad range of wireless communication systems under various practical system configurations. The proposed algorithms can effectively combat the impairments caused by the harsh wireless environment by exploring the properties unique to wireless communication systems. In addition, the theoretical error performance derived in this dissertation can not only accurately predict the performance of practical communication systems, they also provide a set of analytical tools which can be applied for both communication system design and evaluation.

9.2 Future Works

Inspired by the contents presented in the earlier chapters of this dissertation, we now list some future research directions that might lead to promising and fruitful research discoveries.

First, the design of advanced transceiver technique which are capable of fully exploiting the diversity potential inherent in doubly selective fading channel. The theoretical error performance results presented in Chapter 5 for systems with doubly selective Rayleigh fadings are able to quantitatively identify the potential benefits offered by time-selectivity and frequency-selectivity wireless channel. However, the question of how to make use of these benefits so as to achieve full diversity order in both time-domain and frequency-domain remains unanswered. Therefore, the design of advanced channel coding along with efficient decoding technique with the capability of fully appreciating the potential offered by wireless channel will be of great values to the design of next generation wireless communication systems.

Second, error probability analysis of systems with interference is another promising topic worth studying. For example, spatial multiplexing of MIMO system will significantly improve system spectral efficiency. However, it will also introduces interferences among signals transmitted from different antennas. It's well known through simulation that successive interference canceller can asymptotically achieve the capacity advantages offered by the system. However, how to evaluate the performance of such systems analytically

is still an open question need to be answered.

Finally, the test bed development of wireless communication system will be another rewarding research topic in the future study. All the results presented in this dissertation are based on theoretical analysis or computer simulation. The practical values of the research results will be improved immensely if they can be implemented and evaluated in a practical wireless communication environment. Wireless communication system test bed provides a hardware based evaluation environment to satisfy this purpose, and it can serve as a pipeline between abstract theories and practical products. Moreover, the results obtained from test bed development might be in turn help the advancement of wireless communication system theories.

Bibliography

- [1] I.E. Telatar, "Capacity of multi-antenna Gaussian channels," *Eur. Trans. Telecom.*, vol.10, pp.585-595, Nov. 1999.
- [2] G.J. Foschini and M.J. Gans, "On limits of wireless communications in a fading environment when using multiple antennas," *Wireless Personal Communications*, vol.6, pp.311-335, 1998.
- [3] G.G. Raleigh and J.M. Cioffi, "Spatio-temporal coding for wireless communications," *IEEE Trans. Commun.*, vol.46, pp.357-366, Mar. 1998.
- [4] D.S. Shiu, G.J. Foschini, M.J. Gans, and J.M. Kahn, "Fading correlation and its effect on the capacity of multielement antenna systems," *IEEE Trans. Commun.*, vol.48, pp.502-513, Mar. 2000.
- [5] M. Stege, J. Jelitto, M. Bronzel, G. Fettweis, "A multiple input - multiple output channel model for simulation of TX- and RX- diversity wireless systems," in *Proc. IEEE VTC-2000 Fall*, pp.833-839, 2000.
- [6] K.I. Pedersen, J.B. Andersen, J.P. Kermoal and P. Mogensen, "A stochastic multiple-input-multiple-output radio channel model for evaluation of space-time coding algorithms," in *Proc. IEEE VTC-2000 Fall*, pp.893-897, 2000.
- [7] D. Gesbert, H. Bolcskei, D.A. Gore, and A.J. Paulraj, "MIMO wireless channels: capacity and performance prediction," in *Proc. IEEE Globecom*, pp.1083-1088, 2000.
- [8] T. Svantesson, "A physical MIMO radio channel model for multi-element multi-polarized antenna systems," in *Proc. IEEE VTC-2001 Fall*, pp.1083-1087, 2001.

- [9] M. Steinbauer, A.F. Molisch, and E. Bonek, "The double-directional radio channel," *IEEE Antennas and Propagation Magazine*, Vol. 43, pp.51-63, Aug. 2001.
- [10] G. German, Q. Spencer, L. Swindlehurst, and R. Valenzuela, "Wireless indoor channel modeling: statistical agreement of ray tracing simulations and channel sounding measurements," in *Proc. IEEE ICASSP*, pp.2501-2504, 2001.
- [11] A.M. Sayeed, "Modeling and capacity of realistic spatial MIMO channels," in *Proc. IEEE ICASSP*, pp.2489-2492, 2001.
- [12] J.P. Kermoal, L. Schumacher, K.I. Pedersen, P.E. Mogensen, and F. Frederiksen, "A stochastic MIMO radio channel model with experimental validation," *IEEE J. Select. Area Commun.*, vol.20, pp.1211-1226, Aug. 2002.
- [13] M.C. Jeruchim, P. Balaban, and K.S. Shanmugan, *Simulation of Communication Systems: modeling, methodology, and techniques*, 2nd Ed., Kluwer Academic Publisher, 2000.
- [14] G.D. Forney, "Maximum-likelihood sequence estimation of digital sequences in the presence of intersymbol interference," *IEEE Trans. Inform. Theory*, vol.IT-18, pp.363-378, May, 1972.
- [15] P. Hoeher, "A statistical discrete-time model for the WSSUS multipath channel," *IEEE Trans. Veh. Technol.*, vol.41, pp.461-468, 1992.
- [16] K.W. Yip and T.S. Ng, "Efficient simulation of digital transmission over WSSUS channels," *IEEE Trans. Commun.*, vol.43, pp.2907-2913, Dec. 1995.
- [17] K.W. Yip and T.S. Ng, "Discrete-time model for digital communications over a frequency-selective Rician fading WSSUS channel," *IEE Proc.-Commun.*, vol.143, pp.37-42, Feb. 1996.
- [18] P. A. Bello, "Characterization of randomly time-variant linear channels," *IEEE Trans. Commun. Sys.*, vol.11, pp.360-393, Dec. 1963.

- [19] J.D. Parsons, *The mobile radio propagation channel*, 2nd ed. John Wiley & Sons, 2000.
- [20] R.B. Ertel, P. Cardieri, K.W. Sowerby, T.S. Rappaport, and R.H. Reed, "Overview of spatial channel models for antenna array communication systems," *IEEE Personal Commun.*, pp.10-21, Feb. 1998.
- [21] R.D. Murch and K.B. Letaief, "Antenna systems for broadband wireless access," *IEEE Communications Magazine*, Vol. 40, No. 4, pp. 76-83, April 2002.
- [22] ETSI. GSM 05.05, "Radio transmission and reception," ETSI EN 300 910 V8.5.1, Nov. 2000.
- [23] UMTS, "Selection procedure for the choice of radio transmission technologies of UMTS," *UMTS 30.03 version 3.2.0 ETSI*, Apr. 1998.
- [24] C.N. Chuah, D.N.C. Tse, J.M. Kahn, and R.A. Valenzuela, "Capacity scaling in MIMO wireless systems under correlated fading," *IEEE Trans. Info. Theory*, vol.48, pp.637-650, March 2002.
- [25] S. Loyka and A. Kouki, "New compound upper bound on MIMO channel capacity," *IEEE Commun. Lett.*, vol.6, pp.96-98, March 2002.
- [26] A. Abdi, M.Kaveh, "A space-time correlation model for multielement antenna systems in mobile fading channels," *IEEE J. Select. Areas Comm.*, vol.20, pp.550-560, April 2002.
- [27] A. Graham, *Kronecker products and matrix calculus: with applications*, John Wiley & Sons, 1981.
- [28] G.H. Golub and C.F. Van Loan, *Matrix Computation*, 3rd Ed., The Johns Hopkins University Press, 1996.
- [29] W.C. Jakes, *Microwave Mobile Communications*, IEEE Press, 1994.

- [30] J. Han, C. Mun, and H. Park, "A deterministic fading channel model with rigorous correlation characteristics," *Proc. IEEE VTC-1999 Fall*, pp.122-126, 1999.
- [31] M.F. Pop and N.C. Beaulieu, "Limitations of sum-of-sinusoids fading channel," *IEEE Trans. Commun.*, vol.49, pp.699-708, Apr. 2001.
- [32] C. Xiao, Y.R. Zheng, and N.C. Beaulieu, "Second-order statistical properties of the WSS Jakes' fading channel simulator," *IEEE Trans. Commun.*, vol.50, pp.888-891, June 2002.
- [33] Y.R. Zheng and C. Xiao, "Improved models for the generation of multiple uncorrelated Rayleigh fading waveforms," *IEEE Commun. Lett.*, vol.6, pp.256-258, June 2002.
- [34] Y.R. Zheng and C. Xiao, "Simulation models with correct statistical properties for Rayleigh fading channels," *IEEE Trans. Commun.*, vol.51, pp.920-928, June 2003.
- [35] W.H. Gerstacker and R. Schober, "Equalization concepts for EDGE," *IEEE Trans. Wireless Commun.*, vol.1, pp.190-199, Jan. 2002.
- [36] J.G. Proakis, *Digital Communications*, 4th Ed., McGraw Hill, 2001.
- [37] B.A. Bjerke and J.G. Proakis, "Equalization and decoding for multiple-input multiple-output wireless channels," *EURASIP J. Applied Signal Processing*, vol.2002, pp.249-266, March 2002.
- [38] A.F. Molisch, M. Steinbauer, M. Toeltsch, E. Bonek, and R.S. Thoma, "Capacity of MIMO systems based on measured wireless channels," *IEEE J. Select. Areas Comm.*, vol.20, pp.561-569, April 2002.
- [39] S.L. Loyka, "Channel capacity of MIMO architecture using the exponential correlation matrix," *IEEE Commun. Lett.*, vol.5, pp.369-371, 2001.
- [40] A. Grant, "Rayleigh fading multi-antenna channels," *EURASIP J. Applied Signal Processing*, vol.2002, pp.316-329, March 2002.

- [41] S. Verdu, *Multiuser Detection*, Cambridge Univ. Press, 1998.
- [42] R.M. Buehrer, N.S. Correal-Mendoza, and B.D. Woerner, "A simulation comparison of multiuser receivers for cellular CDMA," *IEEE Trans. Veh. Technol.*, vol.49, pp.1065-1085, Jul. 2000.
- [43] S.E. Bensley and B. Aazhang, "Subspace-based channel estimation for code division multiple access communication systems," *IEEE Trans. Commun.*, vol.44, pp.1009-1020, Aug. 1996.
- [44] M. Torlak, and G. Xu, "Blind multiuser channel estimation in asynchronous CDMA systems," *IEEE Trans. Signal Processing*, vol.45, pp.137-147, Jan. 1997.
- [45] X. Wang, and H.V. Poor, "Blind equalization and multiuser detection in dispersive CDMA channels," *IEEE Trans. Commun.*, vol.46, pp.91-103, Jan. 1998.
- [46] A.J. Weiss and B. Friedlander, "Channel estimation for DS-CDMA downlink with aperiodic spreading codes," *IEEE Trans. Commun.*, vol.47, pp.1561-1569, Oct. 1999.
- [47] E.G. Strom, and F. Malmsten, "A maximum likelihood approach for estimating DS-CDMA multipath fading channels," *IEEE J. Select. Areas Commun.*, vol.18, pp.132-140, Jan. 2000.
- [48] J. Namgoong, T.F. Wong, and J.S. Lehnert, "Subspace multiuser detection for multicarrier CDMA," *IEEE Trans. Commun.*, vol.48, pp.1897-1908, Nov. 2000.
- [49] S. Tsai, T.F. Wong, and J.S. Lehnert, "DS-CDMA system with joint channel estimation and MAP detection in time-selective fading channels," *IEEE J. Select. Areas Commun.*, vol.19, pp.121-131, Jan. 2001.
- [50] E. Ertin, U. Mitra, and S. Siwamogsatham, "Maximum-likelihood-based multipath channel estimation for code-division multiple-access systems," *IEEE Trans. Commun.*, vol.49, pp.290-302, Feb. 2001.

- [51] C. Sengupta, J.R. Cavallaro, and B. Aazhang, "On multipath channel estimation for CDMA systems using multiple sensors," *IEEE Trans. Commun.*, vol.49, pp.543-553, Mar. 2001.
- [52] K. Yen and L. Hanzo, "Genetic algorithm assisted joint multiuser symbol detection and fading channel estimation for synchronous CDMA systems," *IEEE J. Select. Areas Commun.*, vol.19, pp.985-998, Jun. 2001.
- [53] J.K. Tugnait and T. Li, "A multistep linear prediction approach to blind asynchronous CDMA channel estimation and equalization," *IEEE J. Select. Areas Commun.*, vol.19, pp.1090-1102, Jun. 2001.
- [54] S. Buzzi and H.V. Poor, "Channel estimation and multiuser detection in long-code DS/CDMA systems," *IEEE J. Select. Areas Commun.*, vol.19, pp.1476-1487, Aug. 2001.
- [55] G. Caire and U. Mitra, "Structured multiuser channel estimation for block-synchronous DS/CDMA," *IEEE Trans. Commun.*, vol.49, pp.1605-1617, Sept. 2001.
- [56] W.G. Phoel, and M.L. Honig, "Performance of coded DS-CDMA with pilot-assisted channel estimation and linear interference suppression," *IEEE Trans. Commun.*, vol.50, pp.822-832, May 2002.
- [57] K.J. Kim, and R.A. Iltis, "Joint detection and channel estimation algorithms for QS-CDMA signals over time-varying channels," *IEEE Trans. Commun.*, vol.50, pp.845-855, May 2002.
- [58] S. Bhashyam and B. Aazhang, "Multiuser channel estimation and tracking for long-code CDMA systems," *IEEE Trans. Commun.*, vol.50, pp.1081-1090, Jul. 2002.
- [59] Z. Xu, "Asymptotic performance of subspace methods for synchronous multirate CDMA systems," *IEEE Trans. Signal Processing*, vol.50, pp.2015-2026, Aug. 2002.

- [60] M. R. Baissas and A. M. Sayeed, "Pilot-based estimation of time-varying multipath channels for coherent CDMA receivers," *IEEE Trans. Signal Processing*, vol.50, pp.2037-2049, Aug. 2002.
- [61] TIA/EIA/IS-2000-2, "Physical Layer Standard for cdma2000 Spread Spectrum Systems," July 1999.
- [62] C. Xiao, J. Wu, S.Y. Leong, Y.R. Zheng, and K.B. Letaief, "A discrete-time model for triply selective MIMO Rayleigh fading channels," *IEEE Trans. Wireless Commun.*, vol.3, to appear, 2004.
- [63] V.M. DaSilva, and E.S. Sousa, "Multicarrier orthogonal CDMA signals for quasisynchronous communication systems," *IEEE J. Selected Areas Commun.*, vol.12, pp.842-852, Jun. 1994.
- [64] R.A. Iltis, and L. Mailaender, "Multiuser detection for quasisynchronous signals," *IEEE Trans. Commun.*, vol.44, pp.1561-1571, Nov. 1996.
- [65] J.K. Cavers, "An analysis of pilot symbol assisted modulation for Rayleigh fading channels," *IEEE trans. Veh. Technol.*, vol.40, pp. 686-693, Nov. 1991.
- [66] S. Takaoka, and F. Adachi, "Pilot-aided adaptive prediction channel estimation in a frequency nonselective fading channel," *IEICE Trans. Commun.*, vol.E85-B, pp.1552-1560, Aug. 2002.
- [67] J. Wu, C. Xiao and J.C. Olivier, "Time-varying and frequency selective channel estimation with unequally spaced pilot symbols," *Int. J. Wireless Information Networks*, vol.11, pp.93-104, Apr. 2004.
- [68] S.Y. Leong, J. Wu, J. Olivier, and C. Xiao, "Fast time-varying dispersive channel estimation and equalization for 8-PSK cellular system," in *Proc. IEEE Globecom'03*, San Francisco, CA, Dec. 2003.
- [69] S.M. Kay, *Fundamentals of Statistical Signal Processing: Estimation Theory*, Prentice Hall, 1993.

- [70] C. Xiao, and Y.R. Zheng, "Ergodic capacity, capacity distribution and outage capacity of MIMO time-varying and frequency-selective Rayleigh fading channels," submitted to *IEEE ICC'04*, Sep. 2003.
- [71] R.A. Horn, and C.R. Johnson, *Matrix Analysis*, Cambridge University Press, 1985.
- [72] J.G. Proakis, *Digital Communications*, 3rd Ed., New York: McGraw-Hill, 1995.
- [73] G.L. Stuber, *Principles of mobile communication*, Norwell, MA: Kluwer Academic Publishers, 1996.
- [74] A. Annamalai, C. Tellambura, and V.K. Bhargava, "Exact evaluation of maximal-ratio and equal-gain diversity receivers for M -ary QAM on Nakagami fading channels," *IEEE Trans. Commun.*, vol.47, pp.1335-1344, Sep. 1999.
- [75] Q.T. Zhang, "Probability of error for equal-gain combiners over rayleigh channels: some closed-form solutions," *IEEE Trans. Commun.*, vol.45, pp.270-273, Mar. 1997.
- [76] M.K. Simon, and M.-S. Alouini, *Digital communication over fading channels: a unified approach to performance analysis*, New York: John Wiley & Sons, 2000.
- [77] C. Tellambura, A. Annamalai, and V.K. Bhargava, "Unified analysis of switched diversity systems in independent and correlated fading channels," *IEEE Trans. Commun.*, vol.49, pp.1955-1965, Nov. 2001.
- [78] M.K. Simon, and M.-S. Alouini, "A unified approach to the performance analysis of digital communication over generalized fading channels," *Proc. of IEEE*, vol.86, pp.1860-1877, Sep. 1998.
- [79] N.C. Beaulieu, and A.A. Abu-Dayya, "Analysis of equal gain diversity on Nakagami fading channels," *IEEE Trans. Commun.*, vol.39, pp.225-234, Feb. 1991.
- [80] M.J. Gans, "The effect of Gaussian error in maximal ratio combiners," *IEEE Trans. Commun. Techno.*, vol. com-19, pp.492-500, Aug. 1971.

- [81] L. Cao, "Exact error rate analysis of MRC diversity with channel estimation error," M. Sc. thesis, University of Alberta, Edmonton, Alberta, Canada, 2003.
- [82] A. Aghamohammadi, and H. Meyr, "On the error probability of linearly modulated signals on Rayleigh frequency-flat fading channels," *IEEE Trans. Commun.*, vol. 38, pp.1966-1970, Nov. 1990.
- [83] M.G. Shayesteh, and A. Aghamohammadi, "On the error probability of linearly modulated signals on frequency-flat Ricean, Rayleigh, and AWGN channels," *IEEE Trans. Commun.*, vol.43, pp.1454-1466, Feb./Mar./Apr., 1995.
- [84] J.W. Craig, "A new, simple and exact result for calculating the probability of error for tow-dimensional signal constellations," in *Proc. IEEE Milit. Commun. Conf. MILCOM'91*, Mclean, VA, Oct. 1991, pp. 571-575.
- [85] A. Papoulis, S.U. Pillai, *Probability, random variables and stochastic processes*, 4th ed. New York, NY: McGraw-Hill, 2002.
- [86] S.M. Kay, *Fundamentals of statistical signal processing, vol. II, Detection theory*, Upper Saddle River, NJ: Prentice-Hall, 1998.
- [87] I. S. Gradshteyn and I. M. Ryzhik, *Table of Integrals, Series, and Products*, 6th ed. San Diego, CA: Academic, 2000.
- [88] M. Schwartz, W.R. Bennett, S. Stein, *Communication systems and techniques*, New York, NY: McGraw-Hill, 1966.
- [89] G.J. Foschini, "Performance bound for maximum-likelihood reception of digital data," *IEEE Trans. Information Theory*, vol.IT-21, pp.47-50, Jan. 1975.
- [90] A.S. Acampora, "Analysis of maximum-likelihood sequence estimation performance for quadrature amplitude modulation," *The Bell System Tech. J.*, vol.60, pp.865-885, July-Aug. 1981.

- [91] W.-H. Sheen, and G.L. Stuber, "MLSE equalization and decoding for multipath-fading channels," *IEEE Trans. Commun.*, vol.39, pp.1455-1464, Oct. 1991.
- [92] W.-H. Sheen, C-C. Tseng, and C-S. Wang, "On the diversity, bandwidth, and performance of digital transmission over frequency-selective slow fading channels," *IEEE Trans. Veh. Technol.*, vol.49, pp.835-843, May. 2000.
- [93] J.E. Mazo, "Exact matched filter bound for two-beam Rayleigh fading," *IEEE Trans. Commun.*, vol.39, pp.1027-1030, July 1991.
- [94] M.V. Clark, L.J. Greenstein, W.K. Kennedy, and M. Shafi, "Matched filter performance bounds for diversity combining receivers in digital mobile radio," *IEEE Trans. Veh. Technol.*, vol.41, pp.356-362, Nov. 1992.
- [95] V.-P. Kaasila, and A. Mammela, "Bit error probability of a matched filter in a Rayleigh fading multipath channel," *IEEE Trans. Commun.*, vol.42, pp.826-828, Feb./Mar./Apr. 1994.
- [96] T. Hunziker, and D. Dahlhaus, "Bounds on matched filter performance in doubly dispersive Gaussian WSSUS channels," *Electron. Lett.*, vol.37, pp.383-384, Mar. 2001.
- [97] N.J. Baas, and D.P. Taylor, "Matched filter bounds for wireless communication over Rayleigh fading dispersive channels," *IEEE Trans. Commun.*, vol.49, pp.1525-1528, Sep. 2001.
- [98] S.-C. Lin, "Accurate error rate estimate using moment method for optimum diversity combining and MMSE equalisation in digital cellular mobile radio," *IEE Proc. Commun.*, vol.149, pp.157-165, June 2002.
- [99] G. Ungerboeck, "Fractional tap-spacing equalizer and consequences for clock recovery in data modems," *IEEE Trans. Commun.*, vol. COM-24, pp.856-864, Aug. 1976.

- [100] S.U.H. Qureshi, "Adaptive Equalization," *Proc. IEEE*, vol.73, pp.1349-1387, Sep. 1985.
- [101] C. Xiao, J. Wu, S.Y. Leong, Y.R. Zheng, and K.B. Letaief, "A discrete-time model for spatio-temporally correlated MIMO WSSUS multipath channels," accepted for publication by *IEEE Trans. Wireless Commun.*, 2004.
- [102] S. Siwamogsatham, M.P. Fitz, and J.H. Grimm, "A new view of performance analysis of transmit diversity schemes in correlated fading," *IEEE Trans. Inform. Theory*, vol.48, pp.950-956, Apr. 2002.
- [103] G.E. Bottomley, and S. Chennakeshu, "Unification of MLSE receivers and extension to time-varying channels," *IEEE Trans. Commun.*, vol.46, pp.464-472, Apr. 1998.
- [104] K.J. Molnar, G.E. Bottomley, and R. Ramesh, "A novel fractionally-spaced MLSE receiver and channel tracking with side information," in *Proc. IEEE Vehicular Technol. Conf. VTC'98 Spring*, Vol.3, pp.2251-2255, May 1998.
- [105] K. Hamied and G.L. Stüber, "A fractionally spaced MLSE receiver," in *Proc. IEEE Intern. Conf. Commun. ICC'95*, Vol.1, pp.18-22, June,1995.
- [106] Eric W. Weisstein. "Appell hypergeometric Function," From MathWorld—A Wolfram Web Resource, <http://mathworld.wolfram.com/AppellHypergeometricFunction.html>.
- [107] J. Wu and C. Xiao, "On the error performance of linearly modulated systems with doubly selective Rayleigh fading channels", to appear in *Proc. IEEE Global Commun. Conf. GLOBECOM'04*, Dec. 2004.
- [108] H. Liu, "Error performance of a pulse amplitude and position modulated ultra-wideband system over lognormal fading channels," vol. 7, pp. 531–533, 2003.
- [109] L. F. Fenton, "The sum of lognormal probability distributions in scatter transmission systems," *IRE Trans. Commun. Syst.*, vol. CS-8, pp. 57–67, 1960.

- [110] S. Schwartz and Y. Yeh, "On the distribution function and moments of power sums with lognormal components," *Bell Syst. Tech. J.*, vol. 61, pp. 1441–1462, 1982.
- [111] R. Barakat, "Sums of independent lognormally distributed random variables," *J. Opt. Soc. Am.*, vol. 66, pp. 211–216, 1976.
- [112] N. C. Beaulieu and Q. Xie, "An optimal lognormal approximation to lognormal sum distributions," *IEEE Trans. Veh. Technol.*, vol. 53, pp. 479–489, 2004.
- [113] S. B. Slimane, "Bounds on the distribution of a sum of independent lognormal random variables," *IEEE Trans. Commun.*, vol. 49, pp. 975–978, 2001.
- [114] D. C. Schleher, "Generalized gram-charlier series with application to the sum of log-normal variates," *IEEE Trans. Inform. Theory*, pp. 275–280, 1977.
- [115] W. A. Janos, "Tail of the distributions of sums of lognormal variates," *IEEE Trans. Inform. Theory*, vol. IT-16, pp. 299–302, 1970.
- [116] N. C. Beaulieu, A. Abu-Dayya, and P. McLance, "Estimating the distribution of a sum of independent lognormal random variables," *IEEE Trans. Commun.*, vol. 43, pp. 2869–2873, 1995.
- [117] A. Papoulis, *Probability, Random Variables and Stochastic Processes*. McGraw Hill, 3rd ed., 1991.
- [118] H. R. Anderson, "Signal-to-interference ratio statistics for AM broadcast ground-wave and skywave signals in the presence of multiple skywave interferers," *IEEE Trans. Broadcasting*, vol. 34, pp. 323–330, 1988.
- [119] P. Cardieri and T. Rappaport, "Statistical analysis of co-channel interference in wireless communications systems," *Wireless Commun. Mobile Computing*, vol. 1, pp. 111–121, 2001.
- [120] M. Abramowitz and I. Stegun, *Handbook of mathematical functions with formulas, graphs, and mathematical tables*. Dover, 9 ed., 1972.

- [121] J. I. Naus, "The distribution of the logarithm of the sum of two log-normal variates," *J. Amer. Stat. Assoc.*, vol. 64, pp. 655–659, Jun. 1969.
- [122] C.-L. Ho, "Calculating the mean and variance of power sums with two log-normal components," *IEEE Trans. Veh. Technol.*, vol. 44, pp. 756–762, 1995.
- [123] M.-S. Alouini, and A.J. Goldsmith, "Area spectral efficiency of cellular mobile radio systems," *IEEE Trans. Veh. Technol.*, vol.48, pp.1047-1066, July 1999.
- [124] M.O. Hasna, M.-S. Alouini, A. Bastami, and E.S. Ebbini, "Performance analysis of cellular mobile systems with successive co-channel interference cancellation," *IEEE Trans. Wireless Commun.*, vol.2, pp.29-40, Jan. 2003.
- [125] M, Kang, M.-S. Alouini, and L. Yang, "Outage probability and spectrum efficiency of cellular mobile radio systems with smart antennas," *IEEE Trans. Commun.*, vol.50, pp.1871-1877, Dec. 2002.
- [126] S. Catreux, P.F. Driessen, and L.J. Greenstein, "Simulation results for an interference-limited multiple-input multiple-output cellular system," *IEEE Commun. Lett.*, vol.4, pp.334-336, Nov. 2000.
- [127] H. Dai, H.V. Poor, "Asymptotic spectral efficiency of multi-cell MIMO systems with frequency-flat fading," *IEEE Trans. Signal Processing*, vol.51, pp.2976-2988, Nov. 2003.
- [128] S. Catreux, P.F. Driessen, and L.J. Greenstein, "Data throughputs using multiple-input multiple-output (MIMO) techniques in a noise-limited cellular environment," *IEEE Trans. Wireless Commun.*, vol.1, pp.226-235, Apr. 2002.
- [129] J. Ramiro-Moreno, K.I. Pedersen, and P.E. Mogensen, "Network performance of transmit and receive antenna diversity in HSDPA under different packet scheduling strategies," in *Proc. IEEE Veh. Techno. Conf. VTC'03 Spring*, vol.2, pp.1454-1458, May 2003.

- [130] J. Hamalainen and R. Wichman, "Performance of multiuser diversity in the presence of feedback errors," in *Proc. IEEE Intern. Symposium Personal, Indoor and Mobile Radio Commun. PIMRC'04*, vol.1, pp.599-603, Sep. 2004.d
- [131] A. Jalali, R. Padovani, and R. Pankaj, "Data throughput of CDMA-HDR a high efficiency-high data rate personal communication wireless system," in *Proc. IEEE Veh. Techno. Conf. VTC'00 Spring*, vol.3, pp.1854-1858, May 2000.
- [132] D. Piazza and L.B. Milstein, "Multiuser diversity-mobility tradeoff: modeling and performance analysis of a proportional fair scheduling," in *Proc. IEEE Global Telecommun. Conf. GLOBECOM'02*, vol.1, pp.17-21, Nov. 2002.
- [133] A. Yamaguchi and Takeuchi, "Forward link packet scheduler for high-speed packet data system," in *Proc. IEEE Intern. Symposium Personal, Indoor and Mobile Radio Commun. PIMRC'01*, vol.2, pp.F21-F24, Sep. 2001.
- [134] A. Senst, P. Schulz-Rittich, G. Ascheid, and H. Meyr, "On the throughput of proportional fair scheduling with opportunistic beamforming for continuous fading states," in *Proc. IEEE Veh. Techno. Conf. VTC'04 Fall*, Oct. 2003.
- [135] J.M. Holtzman, "Asymptotic analysis of proportional fair algorithm," in *Proc. IEEE Intern. Symposium Personal, Indoor and Mobile Radio Commun. PIMRC'01*, vol.2, pp.F33-F37, Sep. 2001.
- [136] J.H. Rhee, T.H. Kim, and D.K. Kim, "A wireless fair scheduling algorithm for 1EV-DO system," in *Proc. IEEE Veh. Techno. Conf. VTC'01 Fall*, vol.2, pp.743-746, Oct. 2001.
- [137] H.Suzuki, "A statistical model for urban radio paopagation," *IEEE Trans. Commun.*, Vol.25, pp.673-680, July, 1977.
- [138] 3GPP:3GPP TR 25.996 v6.1.0, "Spatial channel model for multiple input multiple output (MIMO) simulations," Sep. 2003.

Appendix A

Subspace-based Channel Estimation with Pilot Symbols

In this appendix, a subspace-based channel estimation algorithm with pilot symbols is derived for systems with quasi-static fading channels. The assumption of quasi-static fading is required for the purpose of proper identification of the signal subspace and noise subspace [43]- [45], and the channel is assumed to be constant during the estimation process, which is one slot for this system. From (3.17), we will have

$$\begin{aligned}\mathbf{R}_{y_p} &= \mathbb{E}[\mathbf{y}(j_p)\mathbf{y}^H(j_p)], \\ &= \mathbf{C}\mathbf{h} \cdot \mathbf{h}^H\mathbf{C}^H + N_0\mathbf{I}_N.\end{aligned}\tag{A.1}$$

where $\mathbf{h} = \mathbf{h}(j)$, $j = 1, 2, \dots, J$, for quasi-static fading channels. Since $\mathbf{C} \cdot \mathbf{h}$ is a column vector, the rank of the matrix $\tilde{\mathbf{R}}_{y_p} = \mathbf{R}_{y_p} - N_0\mathbf{I}_N$ is 1. Therefore, an eigenvalue decomposition of $\tilde{\mathbf{R}}_{y_p}$ defines a signal subspace of dimension 1 and a noise subspace of dimension $N - 1$,

$$\tilde{\mathbf{R}}_{y_p} = \begin{bmatrix} \mathbf{u}_s & \mathcal{U}_n \end{bmatrix} \begin{bmatrix} \lambda_s & \mathbf{0} \\ \mathbf{0} & \Lambda_n \end{bmatrix} \begin{bmatrix} \mathbf{u}_s^H \\ \mathcal{U}_n^H \end{bmatrix},\tag{A.2}$$

where the scalar λ_s contains the largest eigenvalue of $\tilde{\mathbf{R}}_{y_p}$, $\mathbf{u}_s \in \mathbb{C}^{N \times 1}$ is the corresponding eigenvector defining the signal subspace, and $\mathcal{U}_n = [\mathbf{u}_2, \mathbf{u}_3, \dots, \mathbf{u}_N] \in \mathbb{C}^{N \times (N-1)}$ are the $N - 1$ orthonormal eigenvectors spanning the $(N - 1)$ -dimension noise subspace.

It follows from the analysis above that the vector $\mathbf{C} \cdot \mathbf{h}$ should be orthogonal to the noise subspace spanned by \mathcal{U}_n , *i.e.*, $(\mathbf{C} \cdot \mathbf{h})^H \cdot \mathbf{u}_k = 0$, for $k = 2, \dots, N$. Therefore, an estimation of the CIR vector \mathbf{h} can be obtained by

$$\tilde{\mathbf{h}} = \underset{\mathbf{h}}{\operatorname{argmin}} \left\{ \mathbf{h}^H \mathbf{C}^H \left(\sum_{k=2}^N \mathbf{u}_k \mathbf{u}_k^H \right) \mathbf{C} \mathbf{h} \right\}, \quad (\text{A.3})$$

and the solution under the constraint $\mathbf{h} \mathbf{h}^H = 1$ is the eigenvector corresponding to the smallest eigenvalue of the matrix $\mathbf{C}^H \left(\sum_{k=2}^N \mathbf{u}_k \mathbf{u}_k^H \right) \mathbf{C}$ up to a multiplicative factor [53], *i.e.*, the estimated CIR \mathbf{h} can be expressed as the product of $\tilde{\mathbf{h}}$ obtained from (A.3) and a complex-valued scalar ζ

$$\hat{\mathbf{h}}_{SSP} = \tilde{\mathbf{h}} \cdot \zeta. \quad (\text{A.4})$$

For blind channel estimation, the value of ζ is not attainable, and it is argued in [53] that this problem can be alleviated via differential encoding and decoding, which may result in performance degradation compared to coherent systems. To solve the ambiguity of ζ , we apply subspace-based method in systems with pilot assisted modulation, and the value of ζ can be estimated with the help of the transmitted pilot symbols.

From (3.17) and (A.4), we have

$$\frac{1}{P} \sum_{p=1}^P \mathbf{y}(j_p) = \mathbf{C} \tilde{\mathbf{h}} \cdot \zeta + \bar{\mathbf{z}}, \quad (\text{A.5})$$

where P is the number of pilot symbols within one slot, and $\bar{\mathbf{z}} = \frac{1}{P} \sum_{p=1}^P \mathbf{z}(j_p)$. This is a linear system with N equations and 1 unknown variable, and the value of ζ can be estimated as

$$\zeta = \frac{1}{P} \cdot (\mathbf{C} \tilde{\mathbf{h}})^\dagger \cdot \left[\sum_{p=1}^P \mathbf{y}(j_p) \right]. \quad (\text{A.6})$$

Combining (A.3), (A.4) and (A.6), we will have the subspace estimation of the CIR \mathbf{h} .

Appendix B

Proof of Proposition 4.1

The conditional pdf $p(\mathbf{h}_k|\hat{\mathbf{h}}_k)$ is derived in this appendix. Since both \mathbf{h}_k and \mathbf{e}_k are Gaussian distributed, the estimated CG vector $\hat{\mathbf{h}}_k = \mathbf{h}_k + \mathbf{e}_k$ and the true CG vector $\hat{\mathbf{h}}_k$ are jointly Gaussian distributed, and the pdf of the estimated CG vector $\hat{\mathbf{h}}_k$ is

$$p(\hat{\mathbf{h}}_k) = \frac{1}{\det(\pi\mathbf{R}_{\hat{h}\hat{h}})} \exp \left[-(\hat{\mathbf{h}}_k - \mathbf{u})^H \mathbf{R}_{\hat{h}\hat{h}}^{-1} (\hat{\mathbf{h}}_k - \mathbf{u}) \right], \quad (\text{B.1})$$

where $\mathbb{E}(\hat{\mathbf{h}}_k) = \mathbb{E}(\mathbf{h}_k) = \mathbf{u}$, and $\mathbf{R}_{\hat{h}\hat{h}}$ is given in (4.5b). In order to obtain the conditional pdf $p(\mathbf{h}_k|\hat{\mathbf{h}}_k)$, one needs to know the joint Gaussian pdf $p(\mathbf{h}_k, \hat{\mathbf{h}}_k)$. We define the joint channel vector $\mathbf{g}_k = [\mathbf{h}_k, \hat{\mathbf{h}}_k]^H$. Then, the joint pdf of \mathbf{h}_k and $\hat{\mathbf{h}}_k$ can be written as

$$p(\mathbf{h}_k, \hat{\mathbf{h}}_k) = \frac{1}{\det(\pi\mathbf{R}_{gg})} \exp \left[-(\mathbf{g}_k - \mathbf{v})^H \mathbf{R}_{gg}^{-1} (\mathbf{g}_k - \mathbf{v}) \right], \quad (\text{B.2})$$

where

$$\mathbf{v} = \mathbb{E}(\mathbf{g}_k) = \begin{bmatrix} \mathbf{u} \\ \mathbf{u} \end{bmatrix}, \quad \mathbf{R}_{gg} = \mathbb{E}(\mathbf{g}_k \mathbf{g}_k^H) = \begin{bmatrix} \mathbf{R}_{hh} & \mathbf{R}_{h\hat{h}} \\ \mathbf{R}_{\hat{h}h} & \mathbf{R}_{\hat{h}\hat{h}} \end{bmatrix}, \quad (\text{B.3})$$

with $\mathbf{R}_{h\hat{h}} = \mathbb{E}(\mathbf{h}_k \hat{\mathbf{h}}_k^H) = \mathbf{R}_{\hat{h}h}^H$. Using the pdf of $p(\hat{\mathbf{h}}_k)$, $p(\mathbf{h}_k, \hat{\mathbf{h}}_k)$ given in (B.1) and (B.2), one can get the conditional pdf $p(\mathbf{h}_k|\hat{\mathbf{h}}_k) = \frac{p(\mathbf{h}_k, \hat{\mathbf{h}}_k)}{p(\hat{\mathbf{h}}_k)}$ as

$$p(\mathbf{h}_k|\hat{\mathbf{h}}_k) = \frac{1}{\det[\pi(\mathbf{R}_{hh} - \mathbf{R}_{h\hat{h}} \mathbf{R}_{\hat{h}\hat{h}}^{-1} \mathbf{R}_{\hat{h}h})]} \times \exp \left[-(\mathbf{g}_k - \mathbf{v})^H \mathbf{R}_{gg}^{-1} (\mathbf{g}_k - \mathbf{v}) + (\hat{\mathbf{h}}_k - \mathbf{u})^H \mathbf{R}_{\hat{h}\hat{h}}^{-1} (\hat{\mathbf{h}}_k - \mathbf{u}) \right], \quad (\text{B.4})$$

where the equation $\det(\mathbf{R}_{gg}) = \det(\mathbf{R}_{hh} - \mathbf{R}_{h\hat{h}} \mathbf{R}_{\hat{h}\hat{h}}^{-1} \mathbf{R}_{\hat{h}h}) \det(\mathbf{R}_{\hat{h}\hat{h}})$ [86, p. 535] is used to obtain (B.4). The conditional pdf given in (B.4) can be further simplified by expanding

\mathbf{R}_{gg} of (B.3) with the following equations [86, pp. 534-535]

$$\begin{bmatrix} A & B \\ C & D \end{bmatrix}^{-1} = \begin{bmatrix} (A - BD^{-1}C)^{-1} & -(A - BD^{-1}C)^{-1}BD^{-1}, \\ -(D - CA^{-1}B)^{-1}CA^{-1} & (D - CA^{-1}B)^{-1} \end{bmatrix} \quad (\text{B.5a})$$

$$(D - CA^{-1}B)^{-1} = D^{-1} + D^{-1}C(A - BD^{-1}C)^{-1}BD^{-1}. \quad (\text{B.5b})$$

Applying (B.5) in (B.4), and after some tedious though straightforward algebraic manipulations, we obtain

$$p(\mathbf{h}_k | \hat{\mathbf{h}}_k) = \frac{1}{\det(\pi \mathbf{R}_{h|\hat{h}})} \exp \left[-(\mathbf{h}_k - \mathbf{u}_{h|\hat{h}})^H \mathbf{R}_{h|\hat{h}}^{-1} (\mathbf{h}_k - \mathbf{u}_{h|\hat{h}}) \right], \quad (\text{B.6})$$

where

$$\mathbf{u}_{h|\hat{h}} = \mathbf{u} + \mathbf{R}_{h\hat{h}} \mathbf{R}_{\hat{h}\hat{h}}^{-1} (\hat{\mathbf{h}}_k - \mathbf{u}), \quad (\text{B.7a})$$

$$\mathbf{R}_{h|\hat{h}} = \mathbf{R}_{hh} - \mathbf{R}_{h\hat{h}} \mathbf{R}_{\hat{h}\hat{h}}^{-1} \mathbf{R}_{\hat{h}h}. \quad (\text{B.7b})$$

Substituting (4.5) in (B.7) will lead to (4.6), and this completes the proof.

Appendix C

Derivation of Eqn. (5.37)

The closed-form solution of the integral $\frac{1}{\pi} \int_0^\psi \left[1 + \frac{a}{\sin^2 \theta}\right]^{-1} d\theta$, for $\psi \in [0, 2\pi]$ is derived in this Appendix. Changing the integration variable to $z = \cot(\theta)$, we will have

$$\begin{aligned} \frac{1}{\pi} \int_0^\psi \left[1 + \frac{a}{\sin^2 \theta}\right]^{-1} d\theta &= \frac{1}{\pi} \int_{\cot \psi}^{+\infty} [(z^2 + 1)(az^2 + a + 1)]^{-1} dz, \\ &= \frac{1}{\pi} \int_{\cot \psi}^{+\infty} (z^2 + 1)^{-1} dz - \frac{1}{\pi} \int_{\cot \psi}^{+\infty} \left(z^2 + \frac{a+1}{a}\right)^{-1} dz. \end{aligned} \quad (\text{C.1})$$

The first integral of (C.1) can be evaluated as

$$\frac{1}{\pi} \int_{\cot \psi}^{+\infty} (z^2 + 1)^{-1} dz = \frac{1}{2} - \frac{1}{\pi} \arctan(\cot \psi) = \frac{\psi}{\pi}, \quad (\text{C.2})$$

where the fact that $\psi \in [0, 2\pi]$ is used in the second equality, and the second integral in (C.1) can be computed as

$$\begin{aligned} \frac{1}{\pi} \int_{\cot \psi}^{+\infty} \left(z^2 + \frac{a+1}{a}\right)^{-1} dz &= \frac{1}{\pi} \sqrt{\frac{a}{1+a}} \arctan \left(\sqrt{\frac{a}{1+a}} z \right) \Big|_{\cot \psi}^{+\infty}, \\ &= \sqrt{\frac{a}{1+a}} \left[\frac{1}{2} - \frac{1}{\pi} \arctan \left(\sqrt{\frac{a}{1+a}} \cot \psi \right) \right]. \end{aligned} \quad (\text{C.3})$$

Combining (C.1)-(C.3) leads to (5.37).

VITA

Jingxian Wu was born November 25, 1975 in Qingdao, China. He received the following degrees: B.S. in Electronic Engineering from the Beijing University of Aeronautics and Astronautics at Beijing, China (1998); M.S. in Electronic Engineering from the Tsinghua University at Beijing, China (2001); Ph.D. in Electrical and Computer Engineering from the University of Missouri-Columbia, Missouri (2005). He is married to Yu Ning, and he is presently a faculty member of the Engineering Science Department of Sonoma State University, Rohnert Park, California.